Ligand binding and transmembranal signaling of the activating natural killer cell receptor NKp30

Vom Fachbereich Biologie der Technischen Universität Darmstadt

zur
Erlangung des akademischen Grades
eines Doctor rerum naturalium

genehmigte Dissertation von

Stefanie Memmer, M. Sc.
aus Darmstadt

1. Referentin: Prof. Dr. Beatrix Süß
2. Referent: Prof. Dr. Bodo Laube
3. Referent: Prof. Dr. Joachim Koch

Tag der Einreichung: 21.03.2017
Tag der mündlichen Prüfung: 12.05.2017

TECHNISCHE UNIVERSITÄT DARMSTADT

Darmstadt 2017
D17

UNIVERSITÄTSmedizin. MAINZ

GEORG SPEYER HAUS
INSTITUTE FOR TUMOR BIOLOGY AND EXPERIMENTAL THERAPY

Die vorliegende Arbeit wurde unter der Leitung von Prof. Dr. Joachim Koch in der Arbeitsgruppe „NK Cell Biology“ am Georg-Speyer-Haus, Institut für Tumorbiologie und experimentelle Therapie, Paul-Ehrlich-Straße 42-44, 60596 Frankfurt am Main und ab März 2016 in der Arbeitsgruppe „Immunobiology of Natural Killer Cells“ am Institut für Medizinische Mikrobiologie und Hygiene, Universitätsmedizin Mainz, Obere Zahlbacher Str. 67, 55131 Mainz angefertigt.

Die Betreuung seitens der Technischen Universität Darmstadt erfolgte durch Prof. Dr. Beatrix Süß am Fachbereich Biologie, Schnittspahnstraße 10, 64287 Darmstadt.

INDEX

LIST OF FIGURES **6**

LIST OF SUPPLEMENTAL FIGURES **8**

LIST OF TABLES **9**

LIST OF SUPPLEMENTAL TABLES **10**

ABBREVIATIONS **11**

SUMMARY **15**

SUMMARY (GERMAN) **18**

1. INTRODUCTION **21**

1.1 NATURAL KILLER CELLS 21
1.2 REGULATION OF NATURAL CYTOTOXICITY 22
1.3 NK CELL SIGNALING 25
1.3.1 Activating Signaling 26
1.3.2 Inhibitory Signaling 27
1.4 NATURAL CYTOTOXICITY RECEPTORS 28
1.4.1 NKp46 31
1.4.2 NKp44 33
1.4.3 NKp30 34
1.5 OBJECTIVES 37

2. MATERIAL AND METHODS **39**

2.1 MATERIAL 39
2.1.1 Instruments, Chemicals, Consumables 39
2.1.2 Enzymes, Antibiotics, Inhibitors and Additives 39
2.1.3 Antibodies, Isotype Controls and Cell Staining Reagents 40
2.1.4 Kits 42
2.1.5 Buffers and Solutions 42
2.1.6 Oligonucleotides 44
2.1.7 Plasmids 50
2.1.8 Viruses 54
2.1.9 Proteins 57
2.1.10 Bacterial Strains and Culture Media 58
2.1.11 Cell Lines and Culture Media 58
2.2 METHODS OF MICROBIOLOGY 68
2.2.1 Cultivation of Bacteria 68

2.2.2 Generation and Transformation of Chemo-Competent Bacteria 68
2.3 METHODS OF MOLECULAR BIOLOGY 68
2.3.1 Preparation of Plasmids 68
2.3.2 Isolation of genomic DNA 69
2.3.3 Polymerase Chain Reaction (PCR) 69
2.3.4 Restriction, Dephosphorylation, Purification and Ligation of DNA 70
2.3.5 Agarose Gel Electrophoresis 71
2.3.6 Isolation of DNA Fragments from Agarose Gels 72
2.3.7 Nucleic Acid Sequencing 72
2.3.8 Deep Sequencing 72
2.4 METHODS OF CELL BIOLOGY AND VIROLOGY 73
2.4.1 Cultivation of Cell Lines 73
2.4.2 Transfection of Mammalian Cells 74
2.4.3 Protein Production in Mammalian Cells 75
2.4.4 Production and Concentration of Lentiviral Particles in Mammalian Cells 75
2.4.5 Transduction of Mammalian Cells 76
2.4.6 Flow Cytometry 76
2.4.7 Immunofluorescence Microscopy 77
2.4.8 Signaling Reporter Assay 78
2.5 METHODS OF PROTEIN BIOCHEMISTRY 79
2.5.1 Protein Purification 79
2.5.2 Preparation of Cell Lysates 80
2.5.3 SDS-Polyacrylamide Gel Electrophoresis (SDS-PAGE) 80
2.5.4 Coomassie Staining of Polyacrylamide Gels 81
2.5.5 Western Blot 81
2.5.6 Enzyme-linked Immunosorbent Assay (ELISA) 82
2.5.7 Surface Plasmon Resonance (SPR) 83

3. RESULTS 85

3.1 CONTRIBUTION OF THE STALK DOMAIN OF NKP30 TO LIGAND BINDING AND SIGNALING 85
3.1.1 Analysis of NKp30/NKp46 Chimera 85
3.1.2 Contribution of Individual Amino Acids within the Stalk Domain to Ligand Binding and Signaling 90
3.1.3 Involvement of Transmembrane and Cytosolic Residues in Signaling 95
3.1.4 N-Glycosylation Scanning to Analyze the Positioning of Key Amino Acids in NKp30 and NKp46 98
3.1.5 Assembly of the NKp30/CD3ζ Complex 101

3.2 shRNA Screening to Analyze the Existence of yet Unidentified Cancer-associated Ligands of NKp30 105
3.2.1 Determination of Optimal Screening Conditions 105
3.2.2 shRNA Screening and Preparation of Deep Sequencing Libraries 107
3.2.3 Analysis of Deep Sequencing Data 110
3.2.4 Candidate Validation 111
3.3 Engineering of a Functional Mouse NKp30 Protein 115
3.3.1 Expression and Plasma Membrane Targeting of the mNKp30 Construct 116
3.3.2 Impact of N-Glycosylation on Plasma Membrane Targeting and Secretion of mNKp30 Constructs 117
3.3.3 Evidence for a Putative mNKp30-glyco Ligand on the Surface of a Mouse Mastocytoma Cell Line 119

4. DISCUSSION 121

4.1 The Stalk Domain of NKp30 Contributes to Ligand Binding and Signaling of a Pre-assembled NKp30/CD3ζ Complex 121
4.2 A Genome-wide shRNA Screening Did Not Confirm the Existence of Unknown Cellular NCR Ligands on Tumor Cell Lines 126
4.3 A Putative Mouse NKp30 Protein is Impacted by N-Glycosylation and has an Unknown Ligand on Murine Mastocytoma Cells 129
4.4 Conclusion and Perspective 132

5. REFERENCES 134

6. APPENDIX 150

6.1 Plasmid Maps 150
6.2 Protein Sequences 153
6.3 Comparison of NKp30 and NKp46 Stalk Domains 156
6.4 SPR Data 157
6.5 NKp44 Ligand and NKp46 Ligand Candidate Genes from the shRNA Screening 158

PUBLICATIONS AND PRESENTATIONS 160

CURRICULUM VITAE 161

ACKNOWLEDGEMENT 163

DECLARATION AND AFFIDAVIT 164

List of Figures

Figure 1. Human NK cell receptors and their ligands.....23
Figure 2. Regulation of NK cell responses.....24
Figure 3. Lytic and inhibitory synapse in NK cells.....25
Figure 4. Activating signaling of NK cell receptors.....26
Figure 5. Inhibitory signaling of NK cell receptors.....28
Figure 6. Natural cytotoxicity receptors.....29
Figure 7. Amino acid sequence and crystal structure of NKp46.....32
Figure 8. Amino acid sequence and crystal structure of NKp44.....33
Figure 9. Amino acid sequence and crystal structures of NKp30.....36
Figure 10. Expression of NKp30/NKp46 chimera in A5-GFP cells.....86
Figure 11. Antibody-induced signaling of NKp30/NKp46 chimera.....87
Figure 12. Ligand-induced signaling of NKp30/NKp46 chimera.....88
Figure 13. B7-H6 binding to NKp30/NKp46 chimera correlates with plasma membrane expression levels of the NCRs.....89
Figure 14. Purified soluble multivalent NKp30-Fc fusion proteins.....91
Figure 15. B7-H6-Fc-Bio is biotinylated and highly glycosylated.....92
Figure 16. Contribution of individual amino acids of the NKp30 stalk to signaling.....94
Figure 17. A positive charge at position 143 is essential and sufficient for NKp30 function.....95
Figure 18. Influence of specific amino acids within, or in the vicinity of the transmembrane domain of NKp30 on CD3ζ signaling.....96
Figure 19. Schematic representation of the N-glycosylation scanning.....99
Figure 20. Expression of N-glycosylation scanning constructs.....100
Figure 21. Glycosylation status of N-glycosylation scanning mutants.....101
Figure 22. Plasma membrane co-localization of NKp30 and NKp46 with CD3ζ in the absence of ligand.....102
Figure 23. Alanine mutations within the stalk domain have no impact on NKp30/CD3ζ co-localization.....102
Figure 24. CD3ζ impacts surface expression levels of NKp30 and NKp46 in the absence of ligand.....103
Figure 25. Workflow of the shRNA screening.....105
Figure 26. Cell lines selected for genome-wide shRNA screening.....106
Figure 27. Determination of the optimal MOI for target cell transduction.....107
Figure 28. Sorting for mCherry^{+}/NCR ligand^{low} phenotype.....108
Figure 29. Cell sorting and preparation of deep sequencing samples.....109

Figure 30. HeLa cells are negative for NCR ligands..... 111
Figure 31. Gating strategy for validation of NCR ligands..... 112
Figure 32. Sequence alignment of NKp30 in different species..... 115
Figure 33. The mNKp30 full length receptor is intracellularly retained in A5-GFP cells... 116
Figure 34. N-glycosylation impacts secretion of NKp30-Fc fusion proteins..... 117
Figure 35. N-gylcosylation is not sufficient for plasma membrane targeting of the mNKp30 full length receptor.....118
Figure 36. mNKp30-glyco-Fc has an unknown surface ligand on P815 mastocytoma cells..... 119
Figure 37. mNKp30-glyco-Fc does not bind to human B7-H6.....120
Figure 38. Model for ligand-induced activation of NKp30 and signal transduction to CD3ζ..... 125

List of Supplemental Figures

Figure S1. Sequence alignment of NKp30 isoforms..... 153
Figure S2. Sequence alignment of NKp46 isoforms..... 154
Figure S3. Sequence alignment of hNKp30 and mNKp30 forms..... 155
Figure S4. Stalk sequences of NKp30 and NKp46..... 156
Figure S5. Equilibrium binding of NKp30 variants to B7-H6..... 157

List of Tables

Table 1. Ligands of human NCRs..... 30
Table 2. Standard reaction mix and cycler protocol for Phusion® polymerase.....69
Table 3. Standard reaction mix and cycler protocol for *DreamTaq™* polymerase..... 70
Table 4. Standard reaction mix for preprarative and analytic restriction (double digestion using type II restriction endonucleases).....71
Table 5. Standard reaction mix and cycler protocol for generation of deep sequencing samples with Phusion® polymerase..... 73
Table 6. Formulation of transfection reagents for 293T/17 cells..... 75
Table 7. Primary antibodies used for flow cytometry.....77
Table 8. Secondary antibodies used for flow cytometry.....77
Table 9. Isotype controls used for flow cytometry..... 77
Table 10. Cell staining reagents used for flow cytometry.....77
Table 11. Primary antibodies used for immunofluorescence microscopy..... 78
Table 12. Secondary antibodies used for immunofluorescence microscopy.....78
Table 13. Isotype controls used for immunofluorescence microscopy.....78
Table 14. Cell staining reagents used for immunofluorescence microscopy..... 78
Table 15. Primary antibodies used for signaling reporter assays.....79
Table 16. Cell staining reagents used for signaling reporter assays.....79
Table 17. Polyacrylamide gel composition..... 81
Table 18. Antibodies used for western blot analysis..... 82
Table 19. Antibodies used for ELISA.....83
Table 20. Analyte concentrations used for SPR.....84
Table 21. Kinetic parameters (association rate constant [k_a], dissociation rate constant [k_d]) and equilibrium dissociation constants (K_D) for binding of NKp30 variants to B7-H6 as determined by SPR..... 93
Table 22. Candidate list of putative NKp30 ligands.....111
Table 23. Validation of putative NKp30 ligands.....113

List of Supplemental Tables

Table S1. Candidate list of putative NKp44 ligands..... 158
Table S2. Candidate list of putative NKp46 ligands..... 158
Table S3. Validation of putative NKp44 ligands..... 159
Table S4. Validation of putative NKp46 ligands..... 159

Abbreviations

The table of abbreviations does not contain SI (international system of units)-based or SI-derived units, the one or three letter amino acid code, or metric prefixes. Abbreviations of solutions, buffers or medium compositions are described in section 2.1 “Materials”.

aa	amino acid
ADCC	antibody-dependent cellular cytotoxicity
APCs	antigen presenting cells
APC	allophycocyanin
APS	ammonium persulfate
ATCC	American Type Culture Collection
B. taurus	*Bos taurus*
BSA	bovine serum albumin
CD	cluster of differentiation
CSF-1	colony-stimulating factor 1
CLP	common lymphoid progenitor
ClrB	C-type lectin related B
CLSM	confocal laser scanning microscopy
CMV	cytomegalovirus
Csk	C-terminal Src kinase
CTL	cytotoxic T lymphocyte
DAP10/12	DNAX-activation protein 10/12
DAPI	4’,6-diamidino-2-phenylindole dihydrochloride
DBL	Duffy-binding like
DC	dendritic cell
DNA	desoxyribonucleic acid
dNTP	desoxyribonucleoside-triphophate
DRM	detergent resistant membrane
DSMZ	Deutsche Sammlung von Mikroorganismen und Zellkulturen
DTT	dithiothreitol
E. coli	*Escherichia coli*
ELISA	enzyme-linked immunosorbent assay
ER	endoplasmic reticulum
ESR	electron spin resonance
et al.	*et alii*

FACS	fluorescence activated cell sorting
FasL	Fas ligand
FBS	fetal bovine serum
Fc	fragment crystallizable
FPKM	fragments per kilobase of exon per million fragments mapped
Gal-3	galectin 3
gDNA	genomic DNA
GFP	green fluorescent protein
GM-CSF	granulocyte macrophage colony-stimulating factor
H. sapiens	*Homo sapiens*
HA	haemagglutinin
HCMV	human cytomegalovirus
HEK	human embryonic kidney
HF	high fidelity
HLA	human leucocyte antigen
HN	haemagglutinin-neuraminidase
HRP	horseradish peroxidase
HSC	hematopoietic stem cell
IFN	interferon
IFNAR2	interferon α/β receptor subunit 2
Ig	immunoglobulin
IL	interleukin
ILC	innate lymphoid cell
ILT2	Ig-like transcript 2
ITAM	immunoreceptor tyrosine-based activation motif
ITIM	immunoreceptor tyrosine-based inhibition motif
k_a	association rate constant
k_d	dissociation rate constant
K_D	equilibrium dissociation constant
KIR	killer cell immunoglobulin-like receptor
LAIR-1	Leukocyte-associated immunoglobulin-like receptor 1
LAT	linker for activation of T cells
LB	Luria Broth
LILR	leukocyte Ig-like receptor

LLT-1	lectin-like transcript 1
LRC	leucocyte receptor complex
M. musculus/caroli/pahari	*Mus musculus/caroli/pahari*
M. mulatta/fascicularis	*Macaca mulatta/fascicularis*
MFI	median fluorescence intensity
MHC	major histocompatibility complex
MICA/B	MHC class I chain-related gene A/B
MIP1α	macrophage inflammatory protein 1α
MLL5	mixed-lineage leukemia 5
MOI	multiplicity of infection
mRNA	messenger RNA
MTOC	microtubule organizing center
MWCO	molecular weigth cut-off
NCAM	neural cell adhesion molecule
NCR	natural cytotoxicity receptor
NF-AT	nuclear factor of activated T cells
NK cell	natural killer cell
NKG2D	natural killer group 2D
NKR	natural killer cell receptor
NMR	nuclear magnetic resonance
NTAL	non-T cell activation linker
OST	oligo saccharyl transferase
P. troglodytes	*Pan troglodytes*
PCNA	proliferating cell nuclear antigen
PCR	polymerase chain reaction
PDB	protein data base
PEI	polyethyleneimine
*Pf*EMP1	*Plasmodium falciparum* erythrocyte membrane protein 1
PLC-γ	phopholipase Cγ
PMA	phorbol 12-myristate 13-acetate
PMPA	plasmamembrane protein array
R. norvegicus	*Rattus norvegicus*
RNA	ribonucleic acid
RU	response unit
SDS-PAGE	sodium dodecyl sulfate polyacrylamide gel electrophoresis

SEC	size exclusion chromatography
SH2	Src homology 2
SHIP-1	SH2 domain-containing inositol phosphatase 1
SHP-1	SH2 domain-containing phosphatase 1
shRNA	small hairpin RNA
SNP	single nucleotide polymorphism
SOCS3	suppressor of cytokine signaling 3
SPR	surface plasmon resonance
Syk	spleen tyrosine kinase
TCR	T cell receptor
TEMED	N,N,N',N'-tetramethylethylene-1,2-diamine
T_H	T helper
TLR	toll-like receptor
TMB	3,3',5,5'-tetramethylbenzidine
TNF	tumor necrosis factor
TRAIL	TNF-related apoptosis-inducing ligand
TREM	triggering receptor expressed on myeloid cells
UL16	unique-long 16
ULBP 1-6	UL16 binding protein 1-6
VSV-G	vesicular stomatitis virus glycoprotein
wt	wildtype
ZAP70	zeta chain-associated protein of 70 kDa

Summary

Natural killer cells (NK cells) are effector lymphocytes of the innate immune system, which are able to recognize and eliminate virus-infected and malignantly transformed cells. Therefore, they play an important role for the containment of pathophysiological processes. An understanding of the molecular mechanisms that lead to NK cell activation is crucial to enhance the effectivity of NK cell-based anti-cancer therapies. Effector functions are regulated by a variety of germline-encoded activating and inhibitory receptors on the surface of the NK cell. One of the major activating NK cell receptors is NKp30, belonging to the natural cytotoxicity receptors (NCRs). NKp30 is a functional receptor in humans and primates (macaques and chimpanzees) as well as on rat NK cell subsets. In contrast, it is only present as a pseudogene with two premature stop-codons in mouse. The only exception is the mouse strain *Mus caroli*, where two single nucleotide polymorphisms (SNPs) eliminate the premature stop-codons. The evolutionary reasons for the development of the murine NKp30 pseudogene are currently unknown.

For signaling, NKp30 associates with immunoreceptor tyrosine-based activation motif (ITAM)-containing adaptor proteins like CD3ζ or FcεRIγ. Until now, the mechanism how ligand binding at the ectodomain of NKp30 is communicated to the adaptor protein CD3ζ is still unknown. Therefore, the molecular details of receptor activation as well as the role of the murine NKp30 pseudogene were analyzed in this thesis.

Formerly, it was shown that the stalk domain of NKp30, a 15 amino acid sequence stretch between the immunoglobulin (Ig) domain and the transmembrane domain, is important for ligand binding and signaling. Therefore, in this thesis, mutated NKp30 variants were produced as full length receptors in A5-GFP reporter cells or NKp30::hIgG1-Fc (NKp30-Fc) fusion proteins in HEK 293T/17 cells and subsequently analyzed in binding studies (surface plasmon resonance, SPR) and signaling reporter assays. Surprisingly, analysis of NKp30/NKp46 tandem mutants showed that despite the existence of a conserved sequence motif in the membrane-proximal region, the stalk domains of NKp30 and NKp46 are not exchangeable without drastic deficiencies in folding, plasma membrane targeting and/or ligand-induced receptor signaling. Additionally, it was shown that the stalk domain of NKp30 is very sensitive to sequence alterations, as alanine substitution of any of the stalk amino acids led to impaired ligand binding and/or signaling capacity. Mutation of the arginine on amino acid position 143 to alanine (R143A) had the most drastic effect. Based on further mutational studies, N-glycosylation mapping and plasma membrane targeting studies, the existence of two interconvertible types of NKp30/CD3ζ complexes can be hypothesized: (1) a signaling incompetent structural NKp30/CD3ζ complex and (2) a ligand-induced signaling competent NKp30/CD3ζ complex. Furthermore, it can be proposed, that ligand binding at the Ig-fold of NKp30 triggers translocation of amino acid R143 of the stalk domain from the

interface between membrane and extracellular region more deeply into the lipid bilayer to enable alignment with oppositely charged aspartate residues within CD3ζ and activation of CD3ζ signaling.

Although several cellular and pathogen-derived NKp30 ligands have been identified in the last years, there is evidence for the existence of further, yet unknown cellular ligands. This assumption is based on former studies that showed binding of NKp30-Fc fusion proteins to tumor cell lines that do not express the cellular NKp30 ligands B7-H6 and BAG-6 on their surface. Therefore, in the present thesis, a screening method was established, based on transduction of ligand-bearing cell lines with a genome-wide shRNA library. After shRNA knockdown of putative ligands, cells were decorated with NKp30-Fc fusion proteins and sorted for reduced NKp30 ligand expression (fluorescence activated cell sorting, FACS). shRNA sequences were amplified from genomic DNA of the cells by PCR and subsequently analyzed via deep sequencing. The same screening method was additionally implemented for the identification of ligands of the other two NCRs, NKp44 and NKp46. Interestingly, inspite of the high number of advantages in contrast to conventional screening strategies, the existence of further cellular proteinaceous NCR ligands could not be confirmed with this screening.

There are different suggestions about the evolutionary appearance of the NCRs. Divergence from a common ancestor (at least in case of NKp30 and NKp44) might have led to an increase in complexity and fine-tuning of the immune system. Different studies suggest development of the NKp46 gene from a common NCR ancestor or from a common ancestor with the KIR genes. Interestingly, murine NKp46 is a functional protein, while NKp30 is only present as a pseudogene and NKp44 is completely lost in mouse. To shed light on the evolutionary reasons for the development of the murine NKp30 pseudogene, the two premature stop codons in the extracellular domain of the *M. musculus* NKp30 gene sequence were repaired and the protein was expressed as full length receptor in A5-GFP reporter cells and as soluble mNKp30-Fc fusion protein in HEK 293T/17 cells. Interestingly, the full length receptor as well as the mNKp30-Fc fusion protein were intracellularly retained. Repair of the three N-linked glycosylation sites in the extracellular region of mNKp30 (mNKp30-glyco) led to the secretion of the Fc fusion protein, while the full length receptor stayed intracellularly retained. As shown previously, association with CD3ζ impacts plasma membrane targeting and retention of human NKp30. Therefore, failure of mNKp30 to assemble with CD3ζ might be the reason for intracellular retention of the full length receptor. Furthermore, the mNKp30-glyco-Fc fusion protein showed specific binding to P815 murine mastocytoma cells. This speaks for the existence of a cancer- or mast cell-related mNKp30-glyco ligand. Altogether, these were the first experiments to show expression and functional analysis of a putative mNKp30 on protein level.

Based on these data, the present thesis provides deeper insight into the function of the major activating NK cell receptor NKp30. This might contribute to a better understanding of the molecular mechanisms that lead to NK cell activation, and this knowledge is crucial to enhance the effectivity of related treatments like anti-cancer and anti-viral therapies.

Summary (German)

Natürliche Killerzellen (NK-Zellen) sind Effektor-Lymphozyten des angeborenen Immunsystems. Sie zeichnen sich besonders durch die Fähigkeit aus, eine Vielzahl von Tumor- und Virus-infizierten Zellen zu erkennen und zu eliminieren. Aus diesem Grund spielen sie eine wichtige Rolle bei der Eindämmung pathophysiologischer Prozesse. Ein Verständnis der molekularen Vorgänge, die zur NK-Zell-Aktivierung führen, ist wichtig für die Verbesserung der Effektivität von NK-Zell-basierten Krebstherapien. Die Erkennung von Zielzellen durch NK-Zellen wird über spezifische Oberflächenrezeptoren vermittelt, wobei die Aktivität der NK-Zellen durch antagonistisch wirkende aktivierende und inhibierende Signale reguliert wird. Einer der wichtigsten aktivierenden NK-Zell-Rezeptoren ist NKp30, welcher zu den Natürlichen Zytotoxizitäts-Rezeptoren (*natural cytotoxicity receptors*, NCRs) gehört. NKp30 ist sowohl in Menschen und Primaten (Makaken und Schimpansen) als auch auf bestimmten NK-Zell-Untergruppen in der Ratte ein funktionaler Rezeptor. Im Gegensatz dazu ist es in der Maus nur als Pseudogen mit zwei vorzeitigen Stop-Codons vorhanden. Die einzige Ausnahme ist der Maus-Stamm *Mus caroli*, in dem zwei Einzelnukleotid-Polymorphismen (*single nucleotide polymorphisms*, SNPs) die vorzeitigen Stop-Codons eliminieren. Die Gründe für die Entwicklung des NKp30 Pseudogens in der Maus sind derzeit unbekannt. Für die Signalweiterleitung assoziiert NKp30 mit Adapter-Proteinen die intrazelluläre Immunrezeptor-Tyrosin-basierte Aktivierungsmotive (*immunoreceptor tyrosine-based activation motifs*, ITAMs) tragen (CD3ζ und FcεRIγ). Bisher sind die Ligandenbindung und die nachfolgende Rezeptor-Aktivierung, sowohl im Hinblick auf die Art der Liganden als auch auf die initialen Schritte der Signalweiterleitung an das Adapter-Protein, unzureichend verstanden. Daher sollten diese molekularen Mechanismen, sowie die Rolle des NKp30 Pseudogens in der Maus in der vorliegenden Arbeit genauer untersucht werden.

Frühere Studien haben gezeigt, dass die Stalk-Domäne von NKp30, ein 15 Aminosäuren langer Sequenzbereich zwischen der Immunglobulin (Ig) Domäne und der Transmembran-Domäne, wichtig für die Liganden-Bindung und die Signalweiterleitung ist. Deshalb wurden in der vorliegenden Arbeit mutierte Varianten des NKp30 Rezeptors als Volllängen-Proteine in A5-GFP Reporterzellen und als NKp30::hIgG1-Fc (NKp30-Fc) Fusionsproteine in HEK 293T/17 Zellen produziert und auf ihre Fähigkeit zur Liganden-Bindung (Oberflächenplasmonresonanz [*surface plasmon resonance*, SPR] Experimente) und Signalweiterleitung (Reporterassays) untersucht. Überraschenderweise zeigten Analysen von NKp30/NKp46 Tandem Mutanten, dass die Stalk Domänen beider Rezeptoren, trotz der Existenz eines konservierten Sequenz-Motivs in der Membran-nahen Region, ohne drastische Beeinträchtigungen von Faltung, Plasmamembran-Targeting und/oder Liganden-induzierter Signalweiterleitung nicht austauschbar sind. Zusätzlich zeigte sich, dass Änderungen der Aminosäure Sequenz der Stalk Domäne starke Auswirkungen auf die

Funktionalität des Rezeptors haben, da ein Aminosäure Austausch durch Alanin an jeder Stelle der Stalk Domäne zu einer Beeinträchtigung der Liganden-Bindung und/oder der Fähigkeit zur Signalweiterleitung führte. Die gravierendsten Auswirkungen hatte die Mutation von Arginin zu Alanin an Aminosäure Position 143 (R143A). Basierend auf den Ergebnissen weiterer Mutationsstudien, N-Glykosylierungskartierung (*N-glycosylation mapping*) und Ko-Expressionsstudien in HeLa Zellen kann die Existenz von zwei unterschiedlichen Typen von NKp30/CD3ζ Komplexen postuliert werden: (1) ein nicht zur Signalweiterleitung fähiger, struktureller NKp30/CD3ζ Komplex und (2) ein durch Liganden-Bindung induzierter, zur Signalweiterleitung fähiger NKp30/CD3ζ Komplex. Des Weiteren kann angenommen werden, dass die Liganden-Bindung an der Immunglobulin (Ig)-Domäne von NKp30 zu einer Translokation der Stalk-Aminosäure R143 von der Grenzfläche zwischen Membran und extrazellulärer Region zu einer tiefer in der Lipid-Doppelschicht liegenden Position führt. Dies ermöglicht eine Interaktion zwischen R143 und den entgegengesetzt geladenen Aspartat-Resten des CD3ζ-Proteins und damit die Aktivierung der Signalweiterleitung durch CD3ζ.

Obwohl in den letzten Jahren mehrere zelluläre und Pathogen-assoziierte NKp30-Liganden identifiziert wurden, ist die Existenz weiterer, bisher unbekannter zellulärer Liganden möglich. Diese Annahme basiert auf der Tatsache, dass frühere Studien die Bindung von NKp30-Fc Fusionsproteinen an Krebs-Zelllinien zeigten, die keinen der beiden bekannten zellulären NKp30-Liganden (B7-H6 und BAG-6) auf ihrer Oberfläche trugen. Auf Grund dessen sollte in der vorliegenden Arbeit die Existenz weiterer Protein-Liganden genauer untersucht werden. Hierfür wurde eine Screening-Methode etabliert, welche auf der Transduktion von Liganden-tragenden Zelllinien mit einer genom-weiten shRNA Bibliothek basiert. Nach dem *knockdown* der putativen Liganden durch die shRNAs wurden die Zellen mit NKp30-Fc Fusionsproteinen dekoriert und Zellen mit reduzierter NKp30-Liganden-Expression mittels Fluoreszenz-aktivierter Zell-Sortierung (*fluorescence activated cell sorting, FACS*) angereichert. Die shRNA Sequenzen wurden anschließend durch PCR aus der genomischen DNA der angereicherten Zellen amplifiziert und mittels *Deep sequencing* analysiert. Die selbe Screening Methode wurde auch zur Identifizierung von Liganden für die anderen beiden NCRs NKp44 und NKp46 eingesetzt. Interessanterweise konnten trotz diverser Vorteile dieser Screening Methode keine weiteren zellulären Protein-Liganden für die NCRs identifiziert werden.

Über das evolutionäre Auftreten der NCRs gibt es unterschiedliche Ansichten. Die Entwicklung aus einem gemeinsamen NCR-Vorläufer-Gen (zumindest im Fall von NKp30 und NKp44) könnte zu einer Erhöhung der Komplexität und Spezialisierung einzelner Komponenten des Immunsystems geführt haben. Studien halten sowohl die Entwicklung des NKp46 Gens aus einem gemeinsamen NCR-Vorläufer als auch aus einem gemeinsamen Vorläufer mit den KIR Genen für möglich. Interessanterweise ist murines NKp46 ein

funktionales Protein, während NKp30 nur als Pseudogen und NKp44 gar nicht in der Maus vorkommt. Um die evolutionären Gründe zu verstehen, die zur Entwicklung des murinen NKp30 (mNKp30) Pseudogens führten, wurden die zwei vorzeitigen Stop-Codons in der extrazellulären Domäne der *M. musculus* Gen-Sequenz repariert und das Protein als Volllängen-Rezeptor in A5-GFP Zellen sowie als mNKp30-Fc Fusionsprotein in HEK 293T/17 Zellen produziert. Interessanterweise wurden sowohl der Volllängen-Rezeptor als auch das mNKp30-Fc Fusionsprotein intrazellulär zurückgehalten. Eine Reparatur der drei fehlenden N-Glykosylierungsstellen in der extrazellulären Region von mNKp30 (mNKp30-glyco) führte zur Sekretion des Fc-Fusionsproteins, während der Volllängen-Rezeptor weiterhin intrazellulär zurückgehalten wurde. Wie in vorherigen Studien und auch in der vorliegenden Arbeit gezeigt wurde, beeinflusst die Assoziation mit CD3ζ die Verweilzeit des humanen NKp30 Rezeptors auf der Plasmamembran (Targeting und Retention). Daher kann die intrazelluläre Lokalisation des mNKp30 Proteins möglicherweise dadurch erklärt werden, dass der Rezeptor nicht in der Lage ist mit CD3ζ zu assoziieren. Des Weiteren zeigte das mNKp30-glyco-Fc Fusionsprotein eine spezifische Bindung an P815 Maus Mastozytom Zellen. Dies spricht für die Existenz eines Tumor- oder Mastzell-spezifischen mNKp30-glyco Liganden. Insgesamt waren dies die ersten Experimente zur Expression und Funktionsanalyse eines putativen mNKp30 Rezeptors auf Protein-Ebene.

Basierend auf diesen Daten liefert die vorliegende Arbeit tiefere Einblicke in die Funktion des aktivierenden NK Zell-Rezeptors NKp30. Dies trägt zu einem besseren Verständnis der molekularen Mechanismen bei, die zur Aktivierung von NK Zellen führen. Dieses Wissen ist wichtig für die zukünftige Entwicklung und Verbesserung von NK-Zell-basierten antiviralen und Krebs-Therapien.

1. Introduction

1.1 Natural Killer Cells

Natural killer cells (NK cells), belonging to the family of innate lymphoid cells (ILCs), play a special role in immunity, as they are part of the innate immune system, but have additional features of adaptive immune cells, like memory functions [1–5]. They were first identified as non-B/ non-T lymphocytes that are able to mediate cytotoxicity without prior antigen priming [6,7]. They arise from common lymphatic progenitors (CLPs) in the bone marrow and develop/differentiate in secondary lymphoid organs, including liver, spleen, decidua and lymph nodes [8,9]. NK cells recognize target cells via a complex interplay between germline-encoded activating and inhibitory receptors, which enables them to differentiate between healthy and infected or transformed cells [10–13]. Additionally, they are able to exert antibody-dependent cellular cytotoxicity (ADCC) via FcγRIIIα (cluster of differentiation 16 (CD 16)) [14]. Human NK cells can be divided into an immunoregulatory and a cytotoxic subset, depending on their surface expression of CD56 (neural cell adhesion molecule, NCAM) and CD16 [15]. $CD56^{bright}/CD16^{-}$ NK cells are immunoregulatory cells that produce high levels of cytokines but exert low cytotoxic activity and ADCC. In contrast, $CD56^{dim}/CD16^{+}$ NK cells are cytotoxic but produce only low levels of cytokines. $CD56^{bright}/CD16^{-}$ cells are the predominant NK cell species in secondary lymphoid tissues, while $CD56^{dim}/CD16^{+}$ NK cells are the major subset in peripheral blood, spleen and non-lymphoid tissues [15–17]. It is assumed that $CD56^{bright}/CD16^{-}$ NK cells might develop to $CD56^{dim}/CD16^{+}$ NK cells, as $CD56^{bright}/CD16^{-}$ cells appear first after hematopoietic stem cell (HSC) transplantation and in cytokine-driven models of *in vitro* differentiation, and they have longer telomeres than $CD56^{dim}/CD16^{+}$ NK cells [8,18,19].

NK cells play a major role in recognition and eradication of infected and malignantly transformed cells [20]. This is underlined by the fact that low activity of peripheral blood NK cells is linked to an increased cancer risk in adults [21]. Despite this, NK cells are involved in diverse other physiological and pathological processes.

Uterine NK cells, a special NK subpopulation, express CD94, but no CD16, and secrete cytokines like macrophage inflammatory protein 1α (MIP1α), granulocyte macrophage colony-stimulating factor (GM-CSF), colony-stimulating factor 1 (CSF1) and interferon γ (IFNγ) [22]. They play a role in controlling trophoblast invasion [23] and are important regulators of spiral artery remodeling and maintenance of decidual integrity [24]. Additionally, they regulate pathogenic T helper 17 (T_H17) cells at the maternal-fetal interface, thereby promoting immune tolerance and maintenance of pregnancy [20,25].

Furthermore, NK cells play a role in allergic asthma [26–30], autoimmune diseases [31–35], development of type I diabetes [36–41], rheumatoid arthritis [42,43] and systemic lupus erythrematosus [44–47].

NK cells in secondary lymphoid tissue like tonsils, lymph nodes and spleen secrete cytokines such as IFNγ upon activation by dendritic cells (DCs), which stimulates a more efficient killing response by T cells [48,49]. Additionally, NK cells can impair the effect of antigen presentation by antigen presenting cells (APCs), reduce T cell proliferation [50] and kill immature DCs in human and mouse [51,52]. Moreover, they can promote the maturation of DCs by secretion of IFNγ and tumor necrosis factor α (TNFα). The DCs in turn activate NK cells via interleukin 12 (IL-12) [53–55]. Furthermore, NK cells can promote priming of $CD4^+$ T helper 1 cells (T_H1) by secretion of IFNγ [56,57] and they can kill activated T cells unless these express sufficient amounts of major histocompatibility complex (MHC) class I molecules [58]. NK cells were also shown to suppress autoreactive B cells *in vitro*, and NK cell depletion *in vivo* increased the severity of autoimmunity in a Fas-deficient mouse model [59]. Moreover, human mast cells were shown to recruit NK cells via IL-8 in models of viral infection [60] and activated bone marrow-derived cultured mast cells were shown to stimulate IFNγ secretion by NK cells [61].

1.2 Regulation of Natural Cytotoxicity

NK cells are able to discriminate between target cells and healthy host cells. Their activity is regulated by a variety of activating and inhibitory cell surface receptors (Fig. 1) [62]. Inhibitory receptors detect the presence or absence of constitutively expressed self-molecules on susceptible target cells, in particular the presence of MHC class I molecules, which interact for example with the MHC class I-specific promiscuous inhibitory receptor Ig-like transcript 2 (ILT2) in humans, the lectin-like Ly49 dimers in mouse and the lectin-like CD94/NKG2A heterodimers in mouse and human [13,63–66]. Additionally, MHC class I molecules are recognized by killer cell immunoglobulin-like receptors (KIRs). These receptors are characterized by two (KIR2D) or three (KIR3D) extracellular immunoglobulin (Ig) domains and have either short (S) or long (L) intracytoplasmic tails which transduce activating or inhibitory signals, respectively [67–70]. In addition, there are other non-MHC self molecules like C-type lectin related B (ClrB), lectin-like transcript 1 (LLT-1) and CD48, which are recognized by other inhibitory NK cell receptors, like mouse natural killer cell receptor P1B (NKR-P1B), human NKR-P1A and mouse and human 2B4, respectively [71]. Interestingly, mouse and human 2B4 are able to mediate both, inhibitory and activating signals [72].

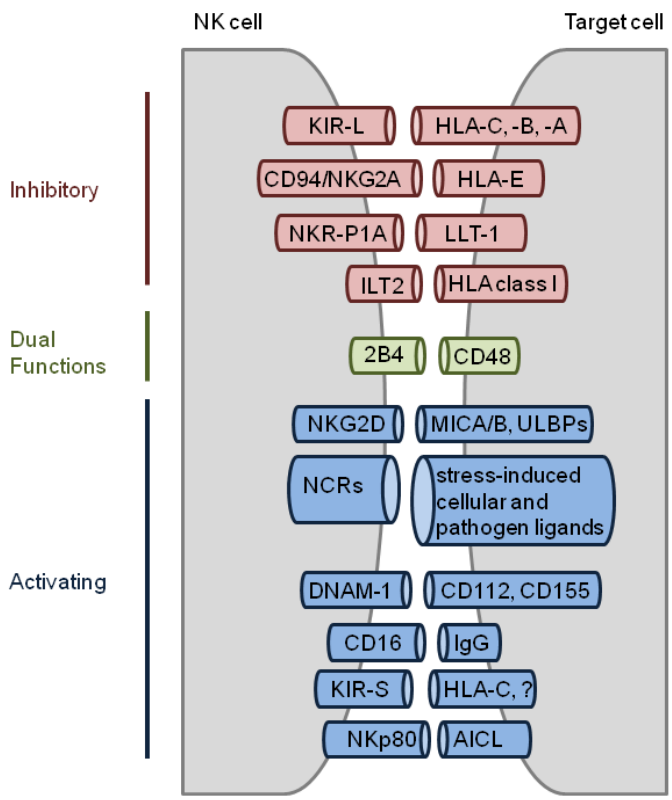

Figure 1. Human NK cell receptors and their ligands. Simplified schematic representation of a variety of human NK cell receptors and their corresponding ligands on target cells, modified after [62]. NK cell cytotoxicity is regulated by the integration of multiple activating and inhibitory signals. Inhibitory receptors are shown in red, activating receptors are shown in blue. 2B4 (green) is able to mediate both, inhibitory and activating signals.

Major activating receptors on NK cells are natural killer group 2D (NKG2D, also known as KLRK1 and CD314) [73] and the Ig-like natural cytotoxicity receptors (NCRs) NKp30 (also known as NCR3, NCTR3 and CD337) [74], NKp44 (also known as NCR2, NCTR2 and CD336) [75,76] and NKp46 (also known as NCR1, NCTR1 and CD335) [77,78]. NKG2D is a C-type lectin-like type II transmembrane protein which associates with DNAX-activation protein 10 (DAP10) for subsequent signaling. It forms a disulfide-linked homodimer, which is expressed on all mouse and human NK cells, and on several T cell subsets [79]. Human NKG2D ligands are the MHC class I chain-related genes A and B (MICA/MICB) and the UL16 binding proteins (ULBPs) [80]. Additionally, NK cells are assumed to express functional toll-like receptors (TLRs), allowing them to respond rapidly to invading pathogens [81]. Interactions of all of these receptors with their corresponding ligands on target cells regulate NK cell responses (Fig. 2). Healthy host cells are tolerated by NK cells because inhibitory signals (derived from inhibitory receptors after engagement of MHC class I molecules on target cells) overcome signals from interactions of activating receptors with their ligands [63].

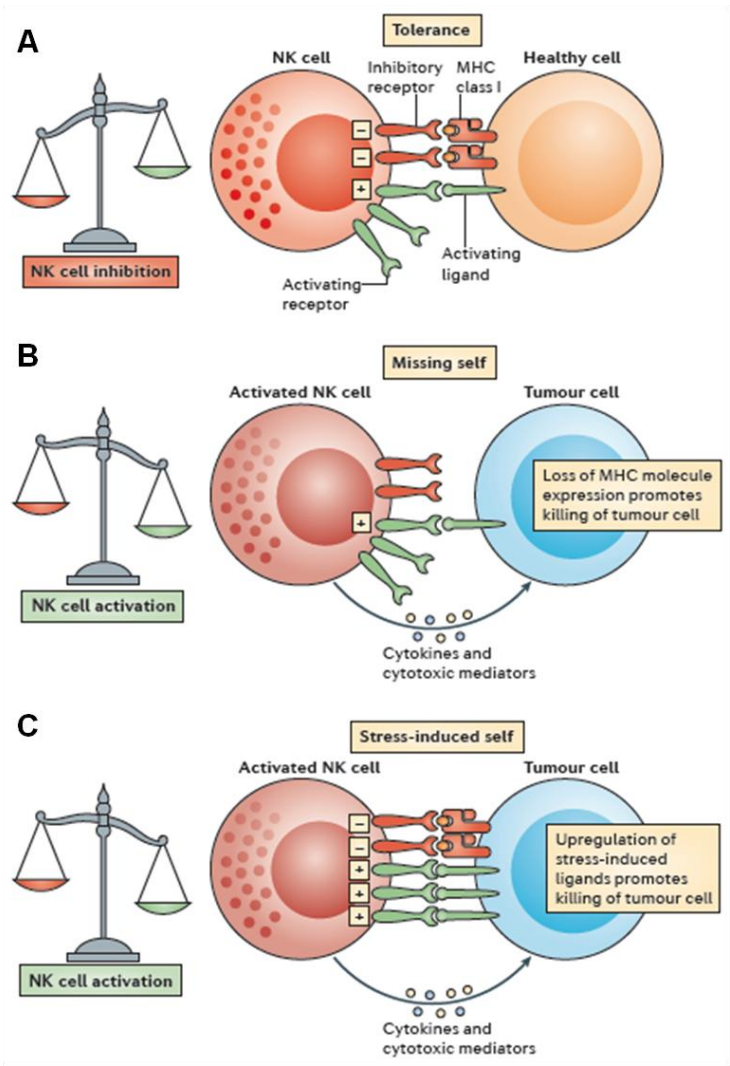

Figure 2. Regulation of NK cell responses. Schematic representation of the regulation of NK cell responses by interactions between activating and inhibitory receptors and their corresponding ligands, reprinted from [82]. (A) NK cells are tolerant to healthy host cells because activating signals are overcome by signals of inhibitory receptors. (B) Missing-self: Due to the absence of inhibitory signals NK cells become activated by cells that have lost the expression of MHC class I molecules. (C) Stress-induced self: NK cells become activated by cells that upregulate activating ligands. Due to this, activating signals overcome the inhibitory signals derived from the interaction with MHC class I molecules.

As a result of malignant transformation or viral infection, cells may lose the expression of MHC class I molecules. This leads to activation of the NK cells and is known as ‘missing-self’ triggering [10,13]. Additionally, upregulation of stress-induced ligands on target cells can activate NK cells (‘stress-induced self’) [73,79,83]. Tumor cell elimination by activated NK cells occurs directly through NK cell mediated cytotoxicity [84–87] and indirectly through the release of pro-inflammatory cytokines and chemokines [1,88].

Cytotoxicity, as well as many other NK cell effector functions, requires direct contact between the NK cell and the target cell. Upon this contact, an immunological synapse is formed, which is defined as an intentional arrangement of molecules in an immune cell at the interface with another cell [89]. Formation of the lytic (activating) NK cell synapse can be divided into different stages. First of all, a close association facilitates initial signaling and adhesion of the NK cell to its target cell. After initiation of synapse formation and in the absence of predominant inhibitory signals, effector stages proceed, including: (1) formation of a stable NK cell/target cell interface, (2) recruitment of preformed lytic granules to the synapse and (3) fusion of lytic granules with the NK cell membrane and release of contents (perforin, granzymes, Fas ligand (FasL), TNF-related apoptosis-inducing ligand (TRAIL), granulysin)

into the synaptic cleft [90]. Important for these steps is the initial actin reorganization, as well as receptor clustering, lipid raft aggregation, activating signaling and lytic granule redistribution [91–94]. Termination stages of the lytic synapse occur after secretion of the lytic granule contents and include a period of inactivity, downmodulation of accumulated activating receptors, NK cell detachment and recycling of cytolytic components (reviewed in [89]). In contrast, NK cells are also able to form an inhibitory synapse, which excludes lipid rafts [95–98], does not accumulate F-actin [99], but includes inhibitory signaling molecules like Src homology 2 domain-containing phosphatase-1 (SHP-1) [98,100]. This way, it prevents actin reorganization [101,102], blocks the recruitment of activating receptors [103,104] and promotes detachment from the target cell (Fig. 3) [105]. Altogether, the formation of inhibitory and activating synapses facilitates discrimination between healthy (self-) cells and infected, transformed or foreign cells.

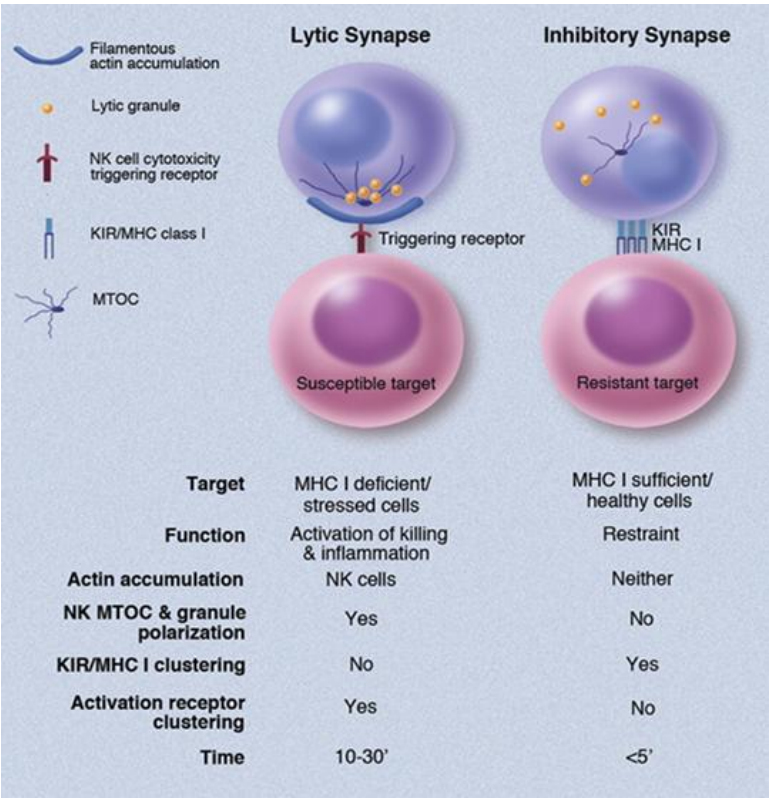

Figure 3. Lytic and inhibitory synapse in NK cells. Schematic representation of the differences between NK cell immunological synapses, adapted from [106]. KIR: killer cell immunoglobulin-like receptor, MHC I: major histocompatibility complex class I, MTOC: microtubule organizing center.

1.3 NK Cell Signaling

As stated earlier, NK cells express a large panel of receptors that allows them to discriminate between target and non-target cells. Effector functions are regulated by a dynamic interplay between multiple signaling pathways that can be simultaneously engaged [107].

1.3.1 Activating Signaling

Elimination of target cells is facilitated by activating NK cell receptors that recognize ligands on infected or transformed cells [108]. The main activation pathways are depicted in figure 4. NCRs associate with immunoreceptor tyrosine-based activation motif (ITAM, sequence: YXX(I/L)$X_{6\text{-}12}$YXX(I/L)) -bearing adaptor molecules for signaling. After receptor engagement, ITAM sequences are phosphorylated by Src family kinases. In a second step, tryrosine kinases Syk (spleen tyrosine kinase) and ZAP70 (zeta chain associated protein of 70 kDa) bind to the phosphorylated ITAMs. These kinases phosphorylate transmembrane adaptors like LAT (linker for activation of T cells) and NTAL (non-T cell activation linker), which leads to the association, phosphorylation and activation of several signaling complexes, which include signaling molecules like phospholipase Cγ (PLC-γ1, PLC-γ2) and Vav isoforms (Vav1, Vav2, Vav3) [109]. Murine and human NK cell signaling differs in the importance of different PLC-γ and Vav isoforms [110–113].

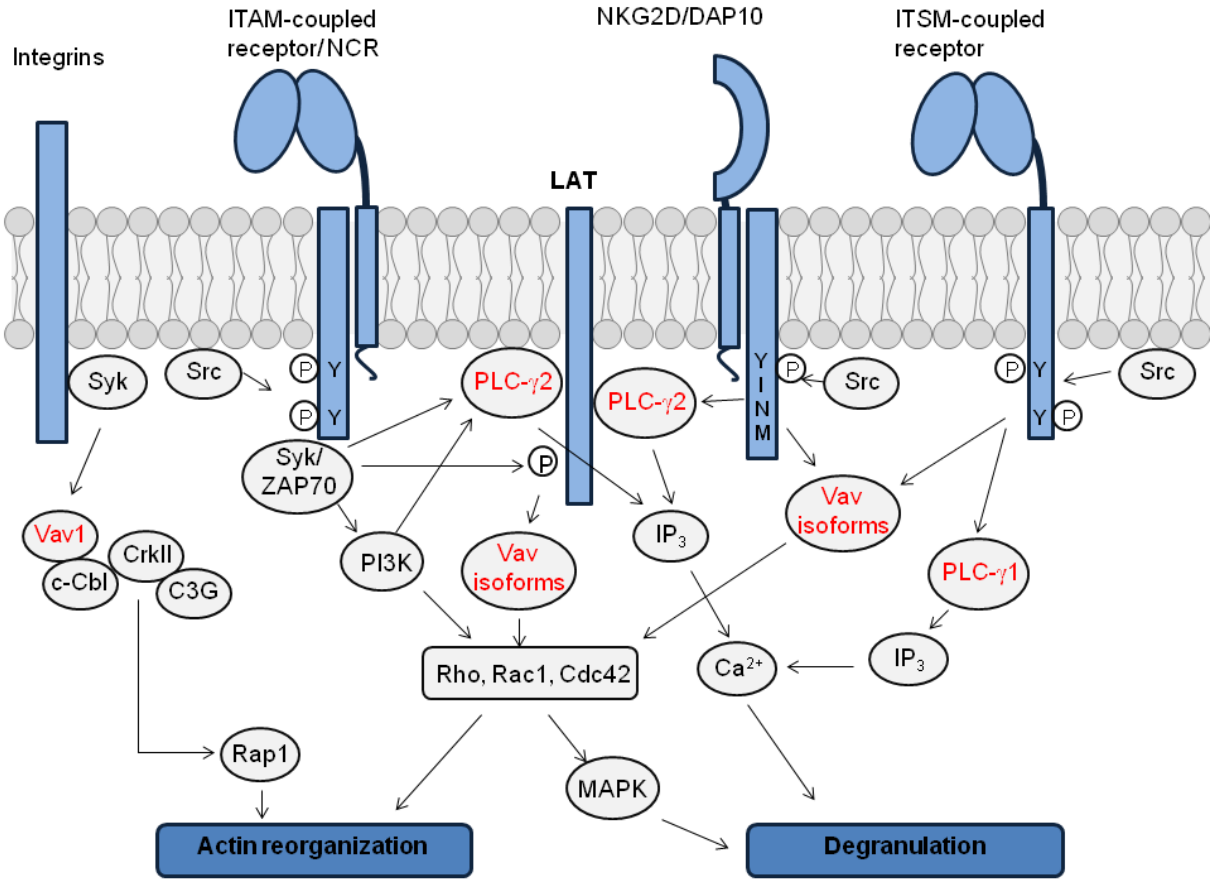

Figure 4. Activating signaling of NK cell receptors. Schematic representation of the major interactions that occur after engagement of activating receptors on NK cells, modified after [109,114]. Engagement of activating receptors leads to recruitment and activation of major signaling molecules like Vav and PLC-γ isoforms (red) and to the assembly of the c-Cbl-CrkII-C3G complex, resulting in subsequent actin reorganization and degranulation. For clarity reasons, phosphorylations are only depicted for the initial step.

Signaling of other activating NK cell receptors like integrins, DNAM-1, CD2, CD16, NKG2D and 2B4 also depends on phosphorylation of tyrosine-based signaling motifs by Src kinase family members [109]. Phosphorylation of PLC-γ isoforms during activating signaling results in subsequent mobilization of Ca^{2+} from the endoplasmic reticulum and thereby contributes to exocytosis of lytic granules [111,113,115,116]. Phosphorylation of Vav isoforms (Vav1, Vav2, Vav3) activates small GTPase proteins of the Rho family, primarily Rac1. These mediate actin reorganization. Rac1 additionally activates the PAK1-MEK-Erk pathway, which induces granule polarization and release [117]. Additionally, Vav1 associates with c-Cbl during NK cell activation [118]. c-Cbl is a scaffold protein of the cytoskeleton which forms complexes with CrkII and C3G. These complexes are able to activate Rap1 and contribute to actin reorganization and formation of lamellae [119–121].

1.3.2 Inhibitory Signaling

Although inhibitory NK cell receptors are diverse in their extracellular regions, they all share a common signaling motif in their cytoplasmic domains. This preserved sequence motif (I/L/V/S)XYXX(L/V) is called immunoreceptor tyrosine-based inhibition motif (ITIM) [122–124]. After interaction of the inhibitory receptor with its ligand, the ITIM motif becomes phosphorylated. This phosphorylation leads to the recruitment of cytoplasmic phosphatases containing a Src homology 2 (SH2) domain [125–127], like the inositol phosphatase SHIP-1 (SH2 domain-containing inositol phosphatase 1) or the tyrosine phosphatases SHP-1 and SHP-2 [128,129]. Additionally, some of the ITIM-containing receptors interact with other molecules, like Leukocyte-associated immunoglobulin-like receptor 1 (LAIR-1) and human leukocyte Ig-like receptor (LILR) with C-terminal Src kinase (Csk), Siglecs with suppressor of cytokine signaling 3 (SOCS3), CD300 with PI3K, and KIRs with β-Arrestin 2 [109]. The recruitment of tyrosine phosphatases leads to the dephosphorylation of Vav1, a key component in the signaling pathway (Fig. 5). Vav1 has a central role in promoting Rac-1 dependent actin cytoskeleton rearrangement, synapse formation and receptor clustering. Due to this, inhibition of Vav1 counteracts signaling via activating receptors [103,104,109]. Another mechanism for inhibitory signaling is used by KIR and CD94/NKG2A receptors. Here, inhibitory signaling leads to an active disassembly of the c-Cbl-CrkII-C3G complex, which is formed during NK cell activation and may contribute to the strength of LFA-1-mediated adhesion through activation of Rap1. This active disassembly is achieved by phosphorylation of CrkII and binding of the phosphorylated protein to the tyrosine kinase Abl [118].

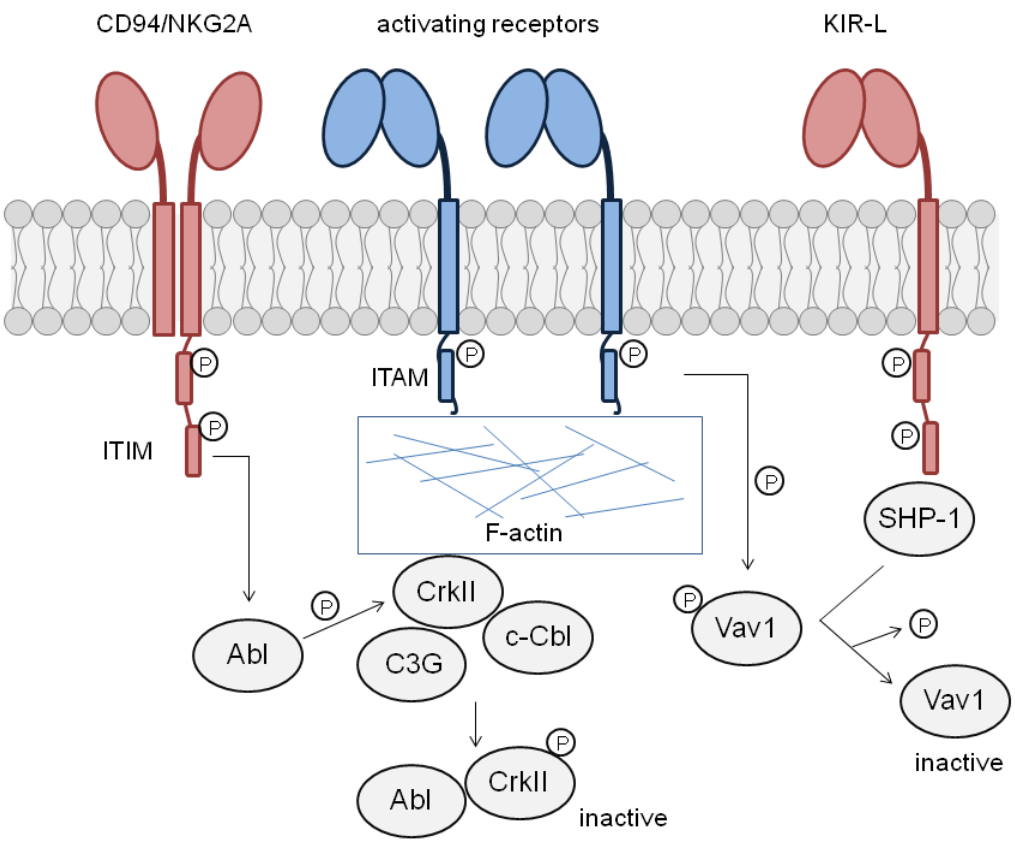

Figure 5. Inhibitory signaling of NK cell receptors. Schematic representation of the interactions that occur after engagement of inhibitory receptors on NK cells, modified after [109,114]. Signaling of activating receptors requires the c-Cbl-CrkII-C3G complex and the phosphorylated guanine nucleotide exchange factor Vav1. Phosphorylation of ITIM motifs leads to recruitment of cytoplasmic phosphatases like SHP-1 and thereby to dephosphorylation of Vav1 and its inactivation. Additionally, signaling of inhibitory receptors recruits the tyrosine kinase Abl, which binds to CrkII and phosphorylates it, thereby leading to the disassembly of the c-Cbl-CrkII-C3G complex.

1.4 Natural Cytotoxicity Receptors

The activating receptors NKp30, NKp44 and NKp46 were grouped together in the natural cytotoxicity receptor (NCR) family. They are mainly expressed on NK cells and certain ILC subsets [130–134] and all of them are specific for non-human leucocyte antigen (non-HLA) ligands. NK cell cytotoxicity is triggered by antibody crosslinking and inhibited by antibody masking of these receptors [135]. Interestingly, NKp30, NKp44 and NKp46 show no sequence homology.

The NCRs are type I transmembrane proteins that comprise an ectodomain with one (NKp30 and NKp44) or two (NKp46) Ig-like domains, that is connected to a membrane-spanning α-helix via a stalk domain, and a short cytosolic tail (Fig. 6). While NKp30 and NKp46 are constitutively expressed on NK cells, expression of NKp44 is only detected after activation [136].

For signaling, the NCRs associate with ITAM-bearing adaptor molecules like CD3ζ/FcεRIγ (NKp30 and NKp46) and DAP12 (NKp44) [74–78,137]. Signaling via the adaptor proteins is believed to be mediated by formation of an intramembrane charge contact between negatively charged amino acids of the adaptor protein and positively charged residues in the transmembrane region of the receptor [137,138].

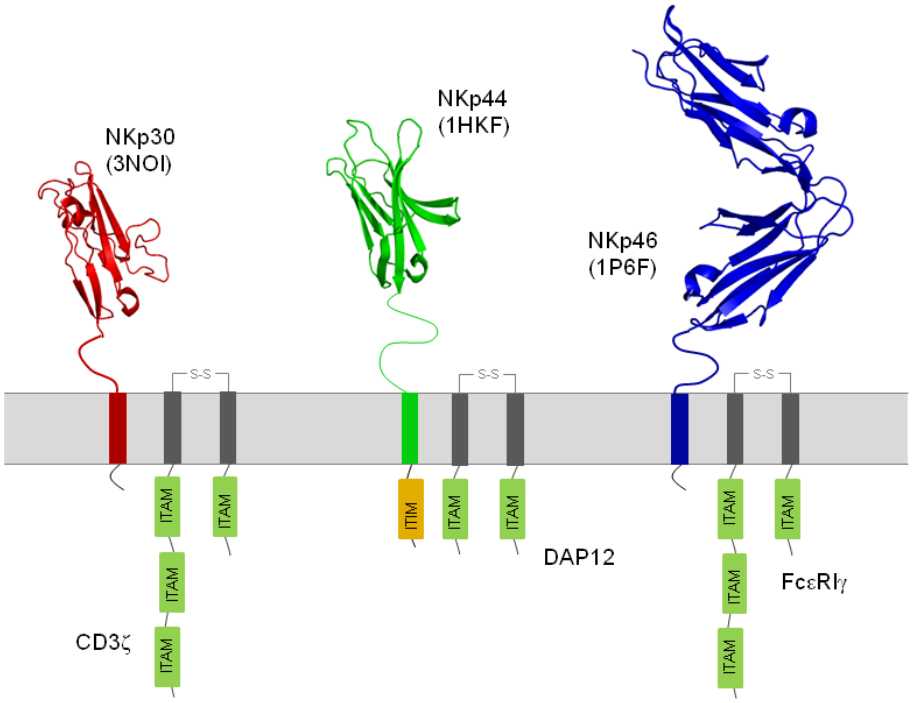

Figure 6. Natural cytotoxicity receptors. Schematic representation of the natural cytotoxicity receptors NKp30 (red; PDB: 3NOI), NKp44 (green; PDB: 1HKF) and NKp46 (blue; 1P6F). All NCRs contain either one (NKp30, NKp44) or two (NKp46) Ig-like domains, a stalk domain, a transmembrane domain and a short cytosolic tail. As the receptors themselves do not possess any intracellular ITAM motifs, they associate with ITAM (light green)-bearing adaptor proteins like CD3ζ homodimers, CD3ζ/FcεRIγ heterodimers (NKp30 and NKp46) and DAP12 (NKp44) for subsequent signaling. Notably, in contrast to the other NCRs, NKp44 contains an ITIM motif in its intracellular region (orange). Structural illustrations were made with PyMol.

There are different suggestions about the evolutional appearance of the NCRs [139–141]. Divergence from a common ancestor (at least in case of NKp30 and NKp44) might have led to an increase in complexity and fine-tuning of the immune system. This is underlined by the fact that all NCRs recognize a large panel of cellular and pathogen-derived ligands, which can lead to their activation or inhibition (Tab. 1).

Table 1. Ligands of human NCRs. HCMV: human cytomegalovirus, *Pf*EMP1: *Plasmodium falciparum* erythrocyte membrane protein 1, HA: haemagglutinin, HN: haemagglutinin-neuraminidase, PCNA: proliferating cell nuclear antigen, MLL5: mixed-lineage leukemia-5. Currently unidentified interacting molecules are not included.

Receptor	Ligand	Source	Cellular localization	Effect [activating (+)/ inhibitory (-)]	References
NKp30	B7-H6	tumor cells	plasma membrane	+	[142]
	BAG-6	stressed cells, tumor cells, DCs	nucleus, cytosol, plasma membrane, exosomes	+/-	[143–145]
	pp65	HCMV	cytosol	-	[146]
	*Pf*EMP1	*plasmodium falciparum*	plasma membrane	+	[147]
	viral HA	ectromelia virus, vaccinia virus	plasma membrane	-	[148]
	heparin, heparan sulfate	all animal cells	plasma membrane	+	[149,150]
	Gal-3	tumor cells	mainly soluble	-	[151]
NKp44	sialylated and sulfated proteo-glycans	all animal cells	plasma membrane	+	[152]
	viral HA and HN	influenza virus, sendai virus, newcastle disease virus	plasma membrane	+	[153–156]
	PCNA	tumor cells	nucleus, cytosol	-	[157]
	heparin, heparan sulfate	all animal cells	plasma membrane	+/-	[149,158, 159]

Receptor	Ligand	Source	Cellular localization	Effect [activating (+)/ inhibitory (-)]	References
NKp44	MLL5 isoform (also known as NKp44L)	tumor cells	plasma membrane	+	[160]
	viral envelope glyco-proteins	dengue virus, west nile virus	plasma membrane	+	[161]
NKp46	viral HA and HN	influenza virus, ectromelia virus, vaccinia virus, sendai virus, newcastle disease virus	plasma membrane	+	[162–164]
	heparin, heparan sulfate	all animal cells	plasma membrane	+	[149]
	Epa1, Epa6, Epa7	*C. glabrata*	plasma membrane	+	[165]
	vimentin	*M. tuberculosis* H37Ra	plasma membrane	+	[166,167]

1.4.1 NKp46

The domain organization of NKp46 is the same as in NKp30 and NKp44, with the exception that the ectodomain of NKp46 comprises two Ig-like domains that are oriented in a defined angle of 85° relative to each other and connected via a hinge region [168], which might be the ligand binding site (Fig. 7) [136]. NKp46 contains a charged arginine at the border between extracellular and transmembrane region that is assumed to be involved in subsequent signaling [76]. The receptor is expressed in a variety of mammalian species and interestingly, it is the only NCR that has an orthologue in mice [155,169,170]. This suggests that NKp46 is the major NCR involved in pathogen and tumor recognition.

A

```
  1 MSSTLPALLC VGLCLSQRIS AQQQTLPKPF IWAEPHFMVP KEKQVTICCQ
 51 GNYGAVEYQL HFEGSLFAVD RPKPPERINK VKFYIPDMNS RMAGQYSCIY
101 RVGELWSEPS NLLDLVVTEM YDTPTLSVHP GPEVISGEKV TFYCRLDTAT
151 SMFLLLKEGR SSHVQRGYGK VQAEFPLGPV TTAHRGTYRC FGSYNNHAWS
201 FPSEPVKLLV TGDIENTSLA PEDPTFPADT WGTYLLTTET GLQKDHALWD
251 HTAQNLLRMG LAFLVLVALV WFLVEDWLSR KRTRERASRA STWEGRRRLN
301 TQTL
```

B

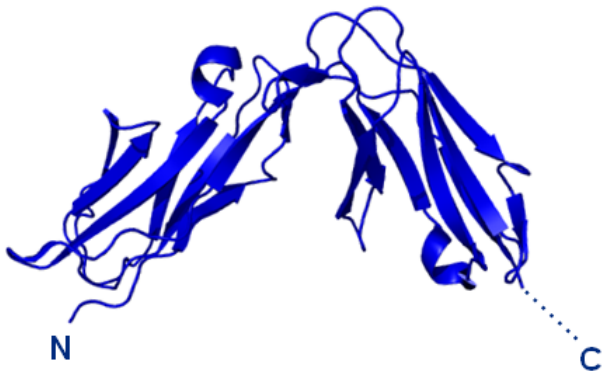

Figure 7. Amino acid sequence and crystal structure of NKp46. (A) Amino acid sequence of NKp46 isoform a. Signal peptide is shown in italics. Dark blue: Ig domains, light blue: stalk domain, green: transmembrane domain, red: cytosolic domain. (B) Crystal structure of the ectodomain of NKp46 (only Ig domain) (PDB: 1P6F). C- and N-terminus are indicated. Structural illustrations were made with PyMol.

The gene for human NKp46 is located within the leucocyte receptor complex (LRC) on chromosome 19 [77], together with the genes for FcαR, ILT/LIR, LAIRs and KIRs [171]. Interestingly, all of these genes are linked within a short region of 19q13.14 [172], which suggests the existence of a common ancestral gene [77].

Human NKp46 is expressed in four isoforms (a-d), with isoform a being the canonical form. Isoforms a and b contain two V-type Ig domains, whereas isoforms c and d contain only one V-type Ig domain. Isoforms b and d lack amino acids 228-244[a] of the stalk domain of NKp46. The intracellular domains of the NKp46 isoforms are conserved [169].

In addition to already identified ligands (Tab. 1), NKp46 recognizes unknown ligands on pancreatic β cells (leading to the development of type I diabetes) [36], and stellate cells in the liver (leading to protection from liver fibrosis) [173]. While the recognition of hepatic stellate and tumor cells seems to be independent from glycosylation, interaction with pancreatic β cells and viral HA seems to be glycosylation dependent [164,173,174]. In addition to the protein backbone, sialylation of NKp46 was shown to be necessary for HA binding [163]. Recognition of HA from several virus families (influenza virus, pox virus, newcastle disease virus) also depends on O- and N-glycosylation of NKp46 [162,164].

[a] Amino acid annotation refers to the canonical NKp46 sequence (isoform a)

Further evidence for the importance of NKp46 in elimination of virus infected and tumor cells was shown by the fact that NKp46 knockout in mice (NCR1$^{gfp/gfp}$) led to an increase in tumor metastasis and susceptibility to influenza virus infection [36,155,173,175,176].

1.4.2 NKp44

NKp44 belongs to the family of triggering receptors expressed on myeloid cells (TREM) and its sequence is encoded in the MHC class III region of human chromosome 6 [75,76]. The extracellular domain of NKp44 contains a V-type Ig-fold with a large positively charged groove on one side of the domain, suggesting an interaction with anionic ligands [177]. In contrast to NKp30 and NKp46, the cytoplasmic tail of NKp44 contains an ITIM motif (Fig. 8) [75,178], which was shown to be functional as it inhibits the release of cytotoxic agents and IFNγ [75,157,178]. NKp44 associates with ITAM containing DAP12 homodimers for signaling, which seems to be facilitated by a charged lysine in the transmembrane domain [75]. Interaction with activating ligands leads to signaling, transduced through the ITAMs of DAP12, which results in release of the cytotoxic agents TNFα and IFNγ [76,178].

A

```
  1 MAWRALHPLL LLLLLFPGSQ AQSKAQVLQS VAGQTLTVRC QYPPTGSLYE
 51 KKGWCKEASA LVCIRLVTSS KPRTMAWTSR FTIWDDPDAG FFTVTMTDLR
101 EEDSGHYWCR IYRPSDNSVS KSVRFYLVVS PASASTQTSW TPRDLVSSQT
151 QTQSCVPPTA GARQAPESPS TIPVPSQPQN STLRPGPAAP IALVPVFCGL
201 LVAKSLVLSA LLVWWGDIWW KTMMELRSLD TQKATCHLQQ VTDLPWTSVS
251 SPVEREILYH TVARTKISDD DDEHTL
```

B

Figure 8. Amino acid sequence and crystal structure of NKp44. (A) Amino acid sequence of NKp44. Signal peptide is shown in italics. Dark blue: Ig domain, light blue: stalk domain, green: transmembrane domain, red: cytosolic domain. The ITIM motif in the cytoplasmic tail is boxed. (B) Crystal structure of the ectodomain of NKp44 (only Ig domain) (PDB: 1HKF). C- and N-terminus are indicated. Structural illustrations were made with PyMol.

On circulating NK cells, NKp44 is only found upon activation. In contrast, a specialized subset of NK cells in the decidua was shown to express NKp44 constitutively, implicating that the receptor plays a role in placentation [75,179,180]. NKp44 expression was also found on a subset of interferon-producing cells located in human tonsils and ILC3s in mucosa-associated lymphoid tissues and human decidua [132,181–184]. Trophoblast cells and maternal stromal cells of the decidua both express unidentified NKp44 ligands [185]. It is suggested that PCNA could be the major NKp44 ligand in this case, as it is overexpressed in trophoblast cells during the first trimester [186] and its inhibitory character could explain the diminished ability of decidual NK cells to lyse trophoblasts despite low levels of classical HLA expression [187].
In addition to other, already identified ligands (Tab. 1), an activating NKp44 ligand was found on uninfected $CD4^+$ T cells during HIV infection, whose expression is induced by gp41 envelope protein of HIV [188].

1.4.3 NKp30

NKp30 was initially described by Pende *et al.* in 1999 [74]. It is a functional protein on human and primate (macaque and chimapanzee) [74,139,189] as well as on rat NK cell subsets [190–192]. Interestingly, in chimpanzee, NKp30 is only expressed upon NK cell activation, similar to NKp44 expression in human [189]. In contrast, NKp30 is only a pseudogene with two premature stop codons in mouse, with the exception of *M. caroli* [169,193].
The NKp30 sequence is located in the MHC class III region (human: chromosome 6, mouse: chromosome 17) [194,195]. It contains a leader sequence for plasma membrane targeting, an extracellular Ig-like domain, a short stalk domain, a single transmembrane domain and a short cytosolic tail, which does not contain any tyrosine-based phosphorylation motifs [74]. A positively charged arginine in the transmembrane region is assumed to facilitate signaling via adaptor proteins (homodimers of CD3ζ or CD3ζ/FcεRIγ heterodimers) [196,197].
In mammals, NKp30 sequences are highly conserved, except for exon 4, which encodes the intracellular region [139,169,193,195]. Human NKp30 is expressed in six splice variants (isoforms a-f) with isoforms a-c being most abundant and ubiquitously expressed. These isoforms result from alternative splicing of exon 2 (extracellular region) and exon 4 [169,194]. While isoforms a-c include the complete ectodomain sequence (V-type Ig domain), isoforms d-f are lacking amino acids 66-99[b] of the extracellular region (C-type Ig domain). Isoforms a and e contain the longest (36 amino acids (aa)) and isoforms b and d the shortest (12 aa) intracellular domain, while the length of the cytoplasmic tails of isoform c and f lies in between (25 aa; appendix, 6.2). Isoform a represents the canonical sequence of NKp30.

[b] Amino acid annotation refers to the canonical NKp30 sequence (isoform a)

According to their structural heterogeneity, the transcripts adopt different NK cell functions, with isoforms a and b stimulating the immune system and isoform c acting immunosuppressive [198].

The currently known ligands of NKp30 include: (1) the cellular proteins B7-H6 [142], BAG-6 [143–145] and Gal-3 [151], (2) the viral HCMV protein pp65 [146] and certain viral haemagglutinins [148], (3) the parasite protein *Pf*EMP1 [147] and (4) certain heparin/heparan sulfate molecules [149,150]. B7-H6, one of the cellular ligands of NKp30, is involved in immunosurveillance of malignantly transformed cells. B7-H6 is a type I transmembrane protein, which is exclusively expressed on tumor cells, and not induced by cellular stress [142]. Binding of NKp30 to B7-H6 induces NK cell activation and cytotoxicity [142,199]. In addition to its function in NK cell cytotoxicity against infected and malignantly transformed cells, NKp30 plays a role in immune regulation. In this context, it interacts with BAG-6 on the surface of immature DCs, which triggers NK cell mediated killing and facilitates the selection of a more immunogenic subset of DCs by killing immature, but tolerating mature DCs [144,200]. BAG-6 is a nuclear protein involved in p53-dependent DNA repair [201]. Interestingly, several studies showed that the protein can also be targeted to the plasma membrane of tumor cells and DCs or released on exosomes in response to stress signals [143,144]. However, the physiological role of non-nuclear BAG-6 localization is currently unknown. The third cellular NKp30 ligand Gal-3 is a β-galactoside-binding protein which is highly expressed in many types of cancer cells [151,202–204]. Tumor cells were shown to release a soluble form of Gal-3, which specifically binds to NKp30 and inhibits the NKp30-mediated cytotoxicity of NK cells [151]. In addition, NKp30 and NKp46 are able to recognize poxviral haemagglutinins on the surface of infected cells [148]. Interestingly, the NKp46/poxvirus HA interaction results in NK cell activation, while the NKp30/poxivrus HA interaction has an inhibitory effect [148]. The tegument protein pp65 of HCMV is another viral ligand of NKp30. Binding of pp65 to NKp30 leads to NK cell inhibition, which is caused by the dissociation of the NKp30/CD3ζ complex [146]. pp65 localizes to the nucleus and cytoplasm of infected cells [146,205] and could be released by lytic cells. Another pathogen derived ligand of NKp30 is *Pf*EMP1 of *Plasmodium falciparum* [147]. *Pf*EMP1 binds NKp30 via its Duffy-binding like (DBL)-1α domain, which leads to NK cell mediated killing of parasitized erythrocytes [147]. In addition, non-proteinaceous structures like heparin/heparan sulfate molecules on the surface of animal cells were shown to interact with NKp30 as well as NKp44 and NKp46 [149,150,159,206,207]. Interestingly, the currently known NKp30 ligands are unrelated in structure and sequence, and there is evidence for the existence of further yet unknown NKp30 ligands on tumor cells [137].

The structure of the Ig domain of NKp30 was resolved in an unbound (PDB: 3NOI) [136] and a B7-H6 bound state (PDB: 3PV6) [199] (Fig. 9). NKp30 and B7-H6 assemble in a 1:1

stoichiometry with a binding interface formed by the front and back β-sheets of the NKp30 C-type Ig domain and the front β-sheet of the B7-H6 V-type Ig domain. Interestingly, binding of B7-H6 leads to slight conformational changes underneath the binding interface [199].

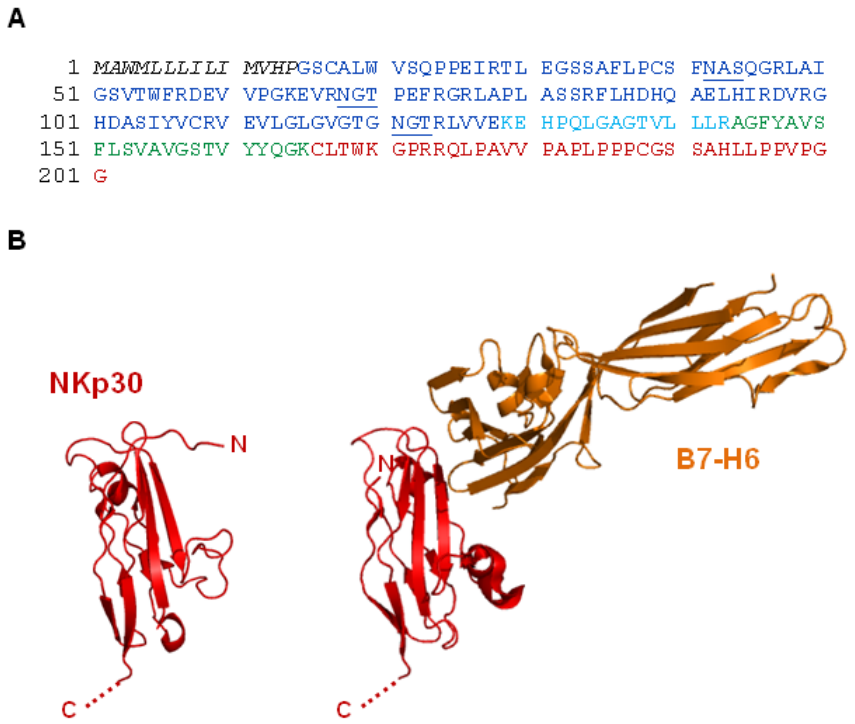

Figure 9. Amino acid sequence and crystal structures of NKp30. (A) Amino acid sequence of NKp30 isoform a. Signal peptide is shown in italics. Dark blue: Ig domain, light blue: stalk domain, green: transmembrane domain, red: cytosolic domain. Sites for N-linked glycosylation are underlined. (B) Crystal structures of the ectodomain of NKp30 (only Ig domain, C- and N-terminus are indicated) in unbound (PDB: 3NOI, left) and B7-H6 bound (PDB: 3PV6, right) state. Red: NKp30, orange: B7-H6. Structural illustrations were made with PyMol.

Interaction sites between NKp30/B7-H6 and NKp30/BAG-6 seem to be partially overlapping but not fully identical (Janina Binici, AG Koch, unpublished data). This leads to the assumption that the diversity of NKp30 ligands engages different binding pockets and not a common binding site on the receptor.

The Ig domain of NKp30 contains three N-linked glycosylation targeting sites (N42, N68, N121). Glycosylation of N42 seems to be important for B7-H6 binding, while glycosylation of N42 and N68 was shown to be essential for intracellular signaling [208]. Interestingly, all of the N-glycosylation sites are located outside of the binding pocket for B7-H6. In case of NKp30/BAG-6 binding, only glycosylation of N68 is critical, while glycosylation of N42 and N121 had less impact [208]. This additionally speaks for differences in the binding interfaces of NKp30/B7-H6 and NKp30/BAG-6.

Moreover, it was shown that the stalk domain of NKp30 influences the binding affinity for B7-H6 and BAG-6 [145,208], presumably involving stalk-dependent clustering of NKp30

[209]. C-terminal truncations of the stalk domain as well as substitution by a length-matched glycine-serine linker led to a reduced binding affinity to BAG-6 and B7-H6 and to a total loss of signaling capacity [208]. The exact mechanism, how the stalk domain of NKp30 contributes to ligand binding and signaling is still unknown.

1.5 Objectives

An important function of NK cells is the eradication of infected and malignantly transformed cells. Therefore, they play a major role in counteracting pathogenic processes and an understanding of the molecular mechanisms that lead to NK cell activation is crucial to enhance the effectivity of related treatments like anti-cancer and anti-viral therapies. One of the major activating receptors on NK cells is NKp30, belonging to the NCR family. Currently, some of the crucial steps leading from ligand binding at the ectodomain of NKp30 to activation of the NK cell are still unknown. Therefore, this thesis aimed to investigate the following points:

1. Engagement of NKp30 leads to phosphorylation of the ITAM sequence in the cytoplasmic tail of the adaptor protein CD3ζ and subsequently to actin reorganization and degranulation of the NK cell. The exact mechanism, how ligand binding at the ectodomain of NKp30 is communicated to the adaptor protein, is still unknown. It is suggested, that a positively charged arginine in the transmembrane domain of NKp30 facilitates the association and/or communication with the adaptor protein. Former studies already indicated the importance of the stalk domain of NKp30 for ligand binding and signaling [208]. Therefore, in this thesis, the function of the stalk domain, especially in signaling initiation, should be investigated in more detail by analysis of a large set of NKp30 stalk mutants for their ligand binding and signaling properties as well as for their ability to associate with the adaptor molecule CD3ζ.
2. Although a panel of cellular and pathogen-derived NKp30 ligands was identified in the last years, the existence of further, yet unknown cellular ligands of the receptor is still questionable as former studies showed binding of NKp30-Fc fusion proteins to cell lines that neither express B7-H6 nor BAG-6 on their surface. Therefore, a suitable ligand screening method should be established, based on transduction of cell lines with a genome-wide human shRNA library and subsequent deep sequencing analysis. The existence of further cellular protein-ligands of NKp30 should be analyzed by implementation of this method.
3. Phylogenetic trees of NKp30 sequences (on nucleotide as well as on protein level) showed the existence of two major clusters, one containing human and primates and the other containing rodents [169]. NKp30 was shown to be a functional receptor in human, macaque and chimpanzee, as well as on rat NK cell subsets [74,139,189–192]. In contrast, it is only a pseudogene in mouse, with the exception of *Mus caroli* [169,193]. To understand

the evolutionary reason for the development of the murine NKp30 pseudogene, the two premature stop codons in the *M. musculus* NKp30 sequence should be repaired, and the emerging protein should be analyzed for its functional properties.

2. Material and Methods

2.1 Material

2.1.1 Instruments, Chemicals, Consumables

Unless otherwise denoted, all instruments were common lab equipment. All chemicals were obtained from Applichem GmbH (Darmstadt, Germany), Biozym Scientific GmbH (Hessisch Oldendorf, Germany), Carl Roth GmbH (Karlsruhe, Germany), GE Healthcare (Buckinghamshire, UK), PAN Biotech GmbH (Aidenbach, Germany), Roche (Mannheim, Germany), Sigma-Aldrich GmbH (Saint Louis, USA; part of Merck KGaA), Thermo Fisher Scientific Inc (Waltham, USA) and all consumables were obtained from Greiner Bio-One (Kremsmünster, Austria), Merck Millipore (Darmstadt, Germany; part of Merck KGaA), Lonza (Basel, Switzerland), Sarstedt AG & Co (Nümbrecht, Germany), Bio-Rad Laboratories (Hercules, USA), BD (Becton, Dickinson and Company, Franklin Lakes, USA) and Whatmann GmbH (Dassel, Germany; part of GE Healthcare).

2.1.2 Enzymes, Antibiotics, Inhibitors and Additives

Enzyme	Supplier
DreamTaq™ Polymerase	Thermo Fisher Scientific
FastAP™ Thermo Sensitive Alkaline Phosphatase	Thermo Fisher Scientific
FastDigest® Restriction Endonucleases	Thermo Fisher Scientific
High Fidelity (HF®) Restriction Endonucleases	New England Biolabs
Phusion® Polymerase	Thermo Fisher Scientific / New England Biolabs
T4 DNA Ligase	Thermo Fisher Scientific

Antibiotic	Concentration (Application)	Supplier
Ampicillin	100 µg/ml (*E.coli*)	Applichem
Gentamicin	10 µg/ml (A5)	Gibco
Penicillin/Streptomycin	100 U/ml Penicillin, 100 µg/ml Streptomycin (mammalian cell lines)	Gibco

Antibiotic	Concentration (Application)	Supplier
Puromycin	1 μg/ml (MelJuSo, HeLa), 2 μg/ml (293T/17, DU145)	Invitrogen
Zeocin	100 μg/ml (*E.coli*), 150 μg/ml (HeLa)	Invitrogen

Inhibitor	Concentration	Supplier
cOmplete™ EDTA-free Protease Inhibitor Cocktail	1 tablet/500 ml cell culture supernatant	Roche

Additive	Concentration (in cell culture medium)	Supplier
Fetal Bovine Serum (FBS)	10% (v/v)	PAN Biotech
HEPES	10 mM	Gibco
L-Glutamine	5.4 mM (A5 cells), otherwise 2 mM	Gibco
MEM Non-Essential Amino Acids	1x	Gibco
β-Mercaptoethanol	55 μM	Gibco
Sodium Pyruvate	1 mM	Gibco

2.1.3 Antibodies, Isotype Controls and Cell Staining Reagents

Primary Antibodies (Name, Clone, Conjugation)	Species/Isotype	Supplier
anti-human BAG-6, D-1	mouse IgG	Santa Cruz Biotechnology
anti-human B7-H6, 1.45[c]	mouse IgG	A. Cerwenka
anti-human CD3ζ, 6B10.2, FITC-conjugated	mouse IgG	BioLegend/Biozol
anti-human NKp30, polyclonal	goat IgG	R&D Systems
anti-human NKp30, P30-15, APC-conjugated	mouse IgG	BioLegend/Biozol
anti-human NKp30, P30-15, hybridoma	mouse IgG	C. Watzl

[c] kindly provided by S. Textor (AG Cerwenka)

Primary Antibodies (Name, Clone, Conjugation)	Species/Isotype	Supplier
anti-human NKp30, 210845	mouse IgG	R&D Systems
anti-human NKp46, 9E2, APC-conjugated	mouse IgG	BioLegend/Biozol
anti-human NKp46, 195314	mouse IgG	R&D Systems
anti-mouse CD4, GK1.5, APC-conjugated	rat IgG	eBioscience

Secondary Antibodies/Reagents (Name, Conjugation)	Species/Isotype	Supplier
anti-human IgG-Fc, HRP-conjugated	goat IgG	Sigma-Aldrich
anti-human IgG1-Fc	mouse IgG	Jackson ImmunoResearch
Streptavidin, HRP-conjugated	streptavidin polymer	Sigma-Aldrich
anti-human IgG-Fc, Alexa647-conjugated	goat IgG	Dianova
anti-mouse IgG-Fc, Alexa647-conjugated	goat IgG	Thermo Fisher Scientific
anti-mouse IgG-Fc, Alexa546-conjugated	donkey IgG	Thermo Fisher Scientific

Isotype controls (Name, Clone, Conjugation)	Supplier
mouse IgG, MOPC-21, APC-conjugated	BioLegend/Biozol
mouse IgG, MOPC-21, FITC-conjugated	BioLegend/Biozol

Cell staining	Supplier
SYTOX Blue Dead Cell Stain	Life Technologies
DAPI	Life Technologies/ Molecular Probes
Trypan Blue Solution 0.4 %	Gibco

2.1.4 Kits

Kit	Supplier
DNA Clean & Concentrator 5 Kit	Zymo
GeneJET™ Plasmid Miniprep Kit	Thermo Fisher Scientific
GeneJET™ Gel Extraction Kit	Thermo Fisher Scientific
HRP-Juice Kit	PJK
Novex® ECL HRP Chemiluminescent Substrate Reagent Kit	Thermo Fisher Scientific
NucleoBond Xtra Midi/Maxi Kit	Macherey-Nagel
QIAamp Blood DNA Maxi Kit	QIAGEN
Qubit dsDNA BR Assay Kit	Thermo Fisher Scientific
Qubit Protein Assay Kit	Thermo Fisher Scientific

2.1.5 Buffers and Solutions

Application	Buffer/Solution	Composition
Agarose Gel Electrophoresis (2.3.5)	TAE	40 mM Tris 1 mM EDTA 1.14 % (v/v) acetic acid
	EtBr stain	0.01 % (v/v) EtBr in TAE buffer
Cultivation of Cell Lines (2.4.1)	PBS/EDTA	0.5 mM EDTA in PBS (pH 8.0)
Enzyme-linked Immunosorbent Assay (2.5.6)	5 % BSA/PBS	5 % (w/v) albumin fraction V (bovine serum albumin, BSA) in PBS
	PBS-T	0.05 % (v/v) Tween 20 in PBS
Flow Cytometry (2.4.6)	FACS buffer	2 % (v/v) FBS in PBS
	FIX-I	4 % formalin in FACS buffer

Application	Buffer/Solution	Composition
Flow Cytometry (2.4.6)	Perm buffer	0.2 % saponin 1 % BSA in FACS buffer
	FIX-II	1 % formalin in FACS buffer
Generation and Transformation of Chemo Competent Bacteria (2.2.2)	TFB I	30 mM CH_3COOK 10 mM $CaCl_2$ 50 mM $MnCl_2$ 100 mM RbCl 15 % (v/v) glycerol pH 5.8 with CH_3COOH
	TFB II	10 mM MOPS 75 mM $CaCl_2$ 10 mM RbCl 15 % (v/v) glycerol pH 6.8 with KOH
Immunofluorescence Microscopy (2.4.7)	FIX buffer	1 % formalin in PBS
	IF buffer	5 % (w/v) BSA in PBS
	IF-Perm buffer	0.2 % saponin 5 % BSA in PBS
	DAPI stain	300 nM 4′,6-Diamidine-2-phenylindole dihydrochloride (DAPI) in PBS
Protein Production in Mammalian Cells (2.4.3)	Sodium azide stock solution	25 % (w/v) sodium azide
Protein Purification (2.5.1)	Elution buffer	0.1 M glycine pH 2.7
	Regeneration buffer	20 mM NaH_2PO_4 0.05 % (v/v) sodium azide pH 7.4 with 20 mM Na_2HPO_4
	Collection buffer	1 M Tris pH 8.8
Preparation of Cell Lysates (2.5.2)	Membrane buffer	10 mM Tris-HCl pH 7.4 50 mM NaCl 5 mM $MgCl_2$ 320 mM sucrose 10 mM NaF

Application	Buffer/Solution	Composition
SDS-Polyacrylamide Gel Electrophoresis (2.5.3)	SDS running buffer	25 mM Tris 192 mM glycine 0.1 % (v/v) SDS
	3x SDS sample buffer (reducing)	180 mM Tris pH 6.8 6 % (v/v) SDS 30 % (v/v) glycerol 0.003 % (w/v) bromophenol blue 15 % (v/v) β-mercaptoethanol
	3x SDS sample buffer (non-reducing)	180 mM Tris pH 6.8 6 % (v/v) SDS 30 % (v/v) glycerol 0.003 % (w/v) bromophenol blue
Signaling Reporter Assay (2.4.8)	P/I	50 ng/ml phorbol 12-myristate 13-acetate (PMA) 750 ng/ml ionomycin in A5-GFP medium
Surface Plasmon Resonance (2.5.7)	PBS-T	0.05 % (v/v) Tween 20 in PBS
Transfection of Mammalian Cells (2.4.2)	TA-Trans	18 mM polyethyleneimine (PEI), branched, in H_2O (cell culture grade)
	Glucose solution	5 % (w/v) glucose in H_2O (cell culture grade)
Western Blot (2.5.5)	Transfer buffer	192 mM glycine 25 mM Tris 20 % (v/v) ethanol
	TBS-T	50 mM Tris 150 mM NaCl 0.1 % (v/v) Tween 20
	Blocking buffer	2.5 % (w/v) skimmed milk powder in TBS-T

2.1.6 Oligonucleotides

All oligonucleotides were purchased from Sigma-Aldrich. Nucleotides matching the annealing sequence are written in capital letters, whereas bases that were introduced by the primer are written in lower case. Endonuclease restriction sites are underlined. Barcode sequences for deep sequencing samples are written in bold.

Application	Primer	Sequence (5'→3')	T_M [°C]
Cloning of pFc-Avi-B7-H6	EcoRI BamHI B7-H6EC for	ccggaattcacgcggatccGATCTGAAAGTAGAGATGATGGC	85.8
	B7-H6EC NcoI EcoRV BglII rev	tccagatctgatatcccatggAGGCCACCAATGAATGG	83.6
Cloning of LeGO-iZ-Flag	NotI-Flag-XbaI for	cgtacgcggccgcTCAATCAGAAACTC	78.7
	NotI-Flag-XbaI rev	ccgactctagaCGGCCGTTTAAACCTTATCG	75.2
Deep Sequencing	pMK1047_bc1_for	aatgatacggcgaccaccgagatctacactctttcccta cacgacgctcttccgatct**atcacg**CTCTAGATGACTGACCCCTTG	92.4
	pMK1047_bc1_rev	caagcagaagacggcatacgagatc**gtgat**gtgactggagttcagacgtgtgctcttccgatctATGGACGAGCTGTACAAGTAA	92.6
	pMK1047_bc2_for	aatgatacggcgaccaccgagatctacactctttcccta cacgacgctcttccgatct**aaacga**CTCTAGATGACTGACCCCTTG	91.5
	pMK1047_bc2_rev	caagcagaagacggcatacgagat**tcgttt**gtgactggagttcagacgtgtgctcttccgatctATGGACGAGCTGTACAAGTAA	92.0
	pMK1047_bc3_for	aatgatacggcgaccaccgagatctacactctttcccta cacgacgctcttccgatct**aaagtc**CTCTAGATGACTGACCCCTTG	91.2
	pMK1047_bc3_rev	caagcagaagacggcatacgagat**gactttgtgactggagttcagacgtgtgctcttccgatctATGGACGAGCTGTACAAGTAA**	91.7
	pMK1047_bc4_for	aatgatacggcgaccaccgagatctacactctttcccta cacgacgctcttccgatct**aacggt**CTCTAGATGACTGACCCCTTG	92.0
	pMK1047_bc4_rev	caagcagaagacggcatacgagat**accgtt**gtgactggagttcagacgtgtgctcttccgatctATGGACGAGCTGTACAAGTAA	91.9
	pMK1047_bc5_for	aatgatacggcgaccaccgagatctacactctttcccta cacgacgctcttccgatct**aacttc**CTCTAGATGACTGACCCCTTG	91.2
	pMK1047_bc5_rev	caagcagaagacggcatacgagat**gaagtt**gtgactggagttcagacgtgtgctcttccgatctATGGACGAGCTGTACAAGTAA	91.7

Application	Primer	Sequence (5'→3')	T_M [°C]
Deep Sequencing	pMK1047_bc6_for	aatgatacggcgaccaccgagatctacactctttccct acacgacgctcttccgatct**aagaac**CTCTAGAT GACTGACCCCTTG	91.2
	pMK1047_bc6_rev	caagcagaagacggcatacgagat**gttctt**gtgactg gagttcagacgtgtgctcttccgatctATGGACGA GCTGTACAAGTAA	91.7
	pMK1047_bc7_for	aatgatacggcgaccaccgagatctacactctttccct acacgacgctcttccgatct**aatgtg**CTCTAGAT GACTGACCCCTTG	91.1
	pMK1047_bc7_rev	caagcagaagacggcatacgagat**cacatt**gtgact ggagttcagacgtgtgctcttccgatctATGGACGA GCTGTACAAGTAA	92.1
	pMK1047_bc8_for	aatgatacggcgaccaccgagatctacactctttccct acacgacgctcttccgatct**acatgt**CTCTAGAT GACTGACCCCTTG	91.6
	pMK1047_bc8_rev	caagcagaagacggcatacgagat**acatgt**gtgact ggagttcagacgtgtgctcttccgatctATGGACGA GCTGTACAAGTAA	91.5
	pMK1047_bc9_for	aatgatacggcgaccaccgagatctacactctttccct acacgacgctcttccgatct**accaaa**CTCTAGAT GACTGACCCCTTG	91.5
	pMK1047_bc9_rev	caagcagaagacggcatacgagat**tttggt**gtgactg gagttcagacgtgtgctcttccgatctATGGACGA GCTGTACAAGTAA	92.0
	pMK1047_bc10_for	aatgatacggcgaccaccgagatctacactctttccct acacgacgctcttccgatct**acgata**CTCTAGAT GACTGACCCCTTG	91.0
	pMK1047_bc10_rev	caagcagaagacggcatacgagat**tatcgt**gtgact ggagttcagacgtgtgctcttccgatctATGGACGA GCTGTACAAGTAA	91.5
	pMK1047_bc11_for	aatgatacggcgaccaccgagatctacactctttccct acacgacgctcttccgatct**acgttt**CTCTAGATG ACTGACCCCTTG	91.5
	pMK1047_bc11_rev	caagcagaagacggcatacgagat**aaacgt**gtgac tggagttcagacgtgtgctcttccgatctATGGACG AGCTGTACAAGTAA	91.4
	pMK1047_bc12_for	aatgatacggcgaccaccgagatctacactctttccct acacgacgctcttccgatct**actagg**CTCTAGAT GACTGACCCCTTG	91.2

Application	Primer	Sequence (5'→3')	T_M [°C]
Deep Sequencing	pMK1047_bc12_rev	caagcagaagacggcatacgagat**cctagt**gtgactggagttcagacgtgtgctcttccgatctATGGACGAGCTGTACAAGTAA	91.4
	pMK1047_bc13_for	aatgatacggcgaccaccgagatctacactctttccctacacgacgctcttccgatct**actcca**CTCTAGATGACTGACCCCTTG	91.8
	pMK1047_bc13_rev	caagcagaagacggcatacgagat**tggagt**gtgactggagttcagacgtgtgctcttccgatctATGGACGAGCTGTACAAGTAA	92.3
	pMK1047_bc14_for	aatgatacggcgaccaccgagatctacactctttccctacacgacgctcttccgatct**agactc**CTCTAGATGACTGACCCCTTG	91.5
	pMK1047_bc14_rev	caagcagaagacggcatacgagat**gagtct**gtgactggagttcagacgtgtgctcttccgatctATGGACGAGCTGTACAAGTAA	92.0
	pMK1047_bc15_for	aatgatacggcgaccaccgagatctacactctttccctacacgacgctcttccgatct**agcatt**CTCTAGATGACTGACCCCTTG	91.6
	pMK1047_bc15_rev	caagcagaagacggcatacgagat**aatgct**gtgactggagttcagacgtgtgctcttccgatctATGGACGAGCTGTACAAGTAA	91.5
	pMK1047_bc16_for	aatgatacggcgaccaccgagatctacactctttccctacacgacgctcttccgatct**aggaga**CTCTAGATGACTGACCCCTTG	91.5
	pMK1047_bc16_rev	caagcagaagacggcatacgagat**tctcct**gtgactggagttcagacgtgtgctcttccgatctATGGACGAGCTGTACAAGTAA	92.0
	pMK1047_bc17_for	aatgatacggcgaccaccgagatctacactctttccctacacgacgctcttccgatct**agtaag**CTCTAGATGACTGACCCCTTG	90.7
	pMK1047_bc17_rev	caagcagaagacggcatacgagat**cttact**gtgactggagttcagacgtgtgctcttccgatctATGGACGAGCTGTACAAGTAA	90.9
	pMK1047_bc18_for	aatgatacggcgaccaccgagatctacactctttccctacacgacgctcttccgatct**agtcct**CTCTAGATGACTGACCCCTTG	91.5
	pMK1047_bc18_rev	caagcagaagacggcatacgagat**aggact**gtgactggagttcagacgtgtgctcttccgatctATGGACGAGCTGTACAAGTAA	91.4

Application	Primer	Sequence (5'→3')	T_M [°C]
Deep Sequencing	pMK1047_bc19_for	aatgatacggcgaccaccgagatctacactctttccct acacgacgctcttccgatct**agttac**CTCTAGAT GACTGACCCCTTG	90.7
	pMK1047_bc19_rev	caagcagaagacggcatacgagat**gtaact**gtgact ggagttcagacgtgtgctcttccgatctATGGACGA GCTGTACAAGTAA	91.1
	pMK1047_bc20_for	aatgatacggcgaccaccgagatctacactctttccct acacgacgctcttccgatct**ataacc**CTCTAGAT GACTGACCCCTTG	91.0
	pMK1047_bc20_rev	caagcagaagacggcatacgagat**ggttat**gtgact ggagttcagacgtgtgctcttccgatctATGGACGA GCTGTACAAGTAA	91.5
	pMK1047_bc21_for	aatgatacggcgaccaccgagatctacactctttccct acacgacgctcttccgatct**gaccaa**CTCTAGAT GACTGACCCCTTG	92.6
	pMK1047_bc21_rev	caagcagaagacggcatacgagat**ttggtc**gtgact ggagttcagacgtgtgctcttccgatctATGGACGA GCTGTACAAGTAA	92.5
	pMK1047_bc22_for	aatgatacggcgaccaccgagatctacactctttccct acacgacgctcttccgatct**cctgaa**CTCTAGAT GACTGACCCCTTG	92.4
	pMK1047_bc22_rev	caagcagaagacggcatacgagat**ttcagg**gtgact ggagttcagacgtgtgctcttccgatctATGGACGA GCTGTACAAGTAA	92.2
	pMK1047_bc23_for	aatgatacggcgaccaccgagatctacactctttccct acacgacgctcttccgatct**atggag**CTCTAGAT GACTGACCCCTTG	92.1
	pMK1047_bc23_rev	caagcagaagacggcatacgagat**ctccat**gtgact ggagttcagacgtgtgctcttccgatctATGGACGA GCTGTACAAGTAA	92.3
	pMK1047_bc24_for	aatgatacggcgaccaccgagatctacactctttccct acacgacgctcttccgatct**atgtcc**CTCTAGAT GACTGACCCCTTG	92.1
	pMK1047_bc24_rev	caagcagaagacggcatacgagat**ggacat**gtgac tggagttcagacgtgtgctcttccgatctATGGACG AGCTGTACAAGTAA	92.6
	pMK1047_bc25_for	aatgatacggcgaccaccgagatctacactctttccct acacgacgctcttccgatct**caattg**CTCTAGAT GACTGACCCCTTG	92.4

Application	Primer	Sequence (5'→3')	T_M [°C]
Deep Sequencing	pMK1047_bc25_rev	caagcagaagacggcatacgagat**caattg**gtgactggagttcagacgtgtgctcttccgatctATGGACGAGCTGTACAAGTAA	92.0
	pMK1047_bc26_for	aatgatacggcgaccaccgagatctacactctttccctacacgacgctcttccgatct**cagagt**CTCTAGATGACTGACCCCTTG	92.1
	pMK1047_bc26_rev	caagcagaagacggcatacgagat**actctg**gtgactggagttcagacgtgtgctcttccgatctATGGACGAGCTGTACAAGTAA	91.4
	pMK1047_bc27_for	aatgatacggcgaccaccgagatctacactctttccctacacgacgctcttccgatct**catcag**CTCTAGATGACTGACCCCTTG	92.7
	pMK1047_bc27_rev	caagcagaagacggcatacgagat**ctgatg**gtgactggagttcagacgtgtgctcttccgatctATGGACGAGCTGTACAAGTAA	92.3
	pMK1047_bc28_for	aatgatacggcgaccaccgagatctacactctttccctacacgacgctcttccgatct**catctc**CTCTAGATGACTGACCCCTTG	92.4
	pMK1047_bc28_rev	caagcagaagacggcatacgaga**tgagatg**gtgactggagttcagacgtgtgctcttccgatctATGGACGAGCTGTACAAGTAA	92.3
	pMK1047_bc29_for	aatgatacggcgaccaccgagatctacactctttccctacacgacgctcttccgatct**ccactt**CTCTAGATGACTGACCCCTTG	92.4
	pMK1047_bc29_rev	caagcagaagacggcatacgagat**aagtgg**gtgactggagttcagacgtgtgctcttccgatctATGGACGAGCTGTACAAGTAA	91.6
	pMK1047_bc30_for	aatgatacggcgaccaccgagatctacactctttccctacacgacgctcttccgatct**cccata**CTCTAGATGACTGACCCCTTG	92.1
	pMK1047_bc30_rev	caagcagaagacggcatacgagat**tatggg**gtgactggagttcagacgtgtgctcttccgatctATGGACGAGCTGTACAAGTAA	92.0
Sequencing	45 pFUSE seq for	TGCGCCGTTACAGATCCAAG	68.3
	47 pFUSE seq rev	CGGGAGATCATGAGGGTGTC	66.9
	53 LeGO seq rev	AAGCGGCTTCGGCCAGTAAC	69.4
	61 LeGO seq for	ATGACCCTGCGCCTTATTTG	65.9

2.1.7 Plasmids

Unless otherwise denoted, plasmids were replicated in *E. coli* DH5α or *E. coli* Top10. The corresponding plasmid maps are listed in the appendix (6.1).

Mammalian expression plasmids

Protein sequences for NKp30 variants contained in mammalian expression plasmids were generated by *de novo* gene synthesis and delivered in pUC57 vectors by GenScript (sequences kindly constructed by Sandra Weil). All plasmids used in 3.1.1 to 3.1.3 and 3.1.5 were cloned in collaboration with Sandra Weil and Steffen Beyer.

Plasmid	Selection	Supplier
pDisplay-BirA-ER	amp^R	J. Hartmann
pDisplay-sBirA	amp^R	J. Hartmann
pFUSE-hIgG1-FcEQ	zeo^R	J. Hartmann [208]
pFUSE-hIgG1-FcEQ-NKp30Stalk	zeo^R	J. Hartmann [208]
pFUSE-hIgG1-FcEQ-NKp44Stalk	zeo^R	J. Hartmann
pFUSE-hIgG1-FcEQ-NKp46Stalk	zeo^R	J. Hartmann
pFUSE-hIgG1-FcEQ-IFNAR2	zeo^R	J. Hartmann [208]
pFUSE-hIgG1-FcEQ-NKp30-K129A	zeo^R	this thesis
pFUSE-hIgG1-FcEQ-NKp30-E130A	zeo^R	this thesis
pFUSE-hIgG1-FcEQ-NKp30-H131A	zeo^R	this thesis
pFUSE-hIgG1-FcEQ-NKp30-P132A	zeo^R	this thesis
pFUSE-hIgG1-FcEQ-NKp30-Q133A	zeo^R	this thesis
pFUSE-hIgG1-FcEQ-NKp30-L134A	zeo^R	this thesis
pFUSE-hIgG1-FcEQ-NKp30-G135A	zeo^R	this thesis
pFUSE-hIgG1-FcEQ-NKp30-G137A	zeo^R	this thesis
pFUSE-hIgG1-FcEQ-NKp30-T138A	zeo^R	this thesis
pFUSE-hIgG1-FcEQ-NKp30-V139A	zeo^R	this thesis
pFUSE-hIgG1-FcEQ-NKp30-L140A	zeo^R	this thesis

Plasmid	Selection	Supplier
pFUSE-hIgG1-FcEQ-NKp30-L141A	zeo^R	this thesis
pFUSE-hIgG1-FcEQ-NKp30-L142A	zeo^R	this thesis
pFUSE-hIgG1-FcEQ-NKp30-R143A	zeo^R	this thesis
pFc-Avi	zeo^R	T. Zöller
pcDNA3.1-TNFss-B7H6-hIgG1-Fc	amp^R/neo^R	A. Cohnen
pFc-Avi-B7-H6	zeo^R	this thesis
pFUSE-hIgG1-FcEQ-mNKp30	zeo^R	this thesis
pFUSE-hIgG1-FcEQ-mNKp30-glyko	zeo^R	this thesis

Lentiviral transfer plasmids

Gene sequences for NKp30 and NKp46 variants contained in lentiviral transfer plasmids were generated by *de novo* gene synthesis and delivered in pUC57 vectors by GenScript (sequences kindly constructed by Sandra Weil). All plasmids used in 3.1.1 to 3.1.3 and 3.1.5 were generated in collaboration with Sandra Weil and Steffen Beyer.

Plasmid	Selection	Supplier
LeGO-iZ	amp^R/zeo^R	J. Hartmann [208]
LeGO-iZ-NKp30FL-His	amp^R/zeo^R	J. Hartmann [208]
LeGO-iZ-NKp46FL-His	amp^R/zeo^R	this thesis
LeGO-iZ-NKp46Ig/30Stalk/30TM-His	amp^R/zeo^R	this thesis
LeGO-iZ-NKp46Ig/30Stalk/46TM-His	amp^R/zeo^R	this thesis
LeGO-iZ-NKp30Ig/46Stalk/46TM-His	amp^R/zeo^R	this thesis
LeGO-iZ-NKp30Ig/46Stalk/30TM-His	amp^R/zeo^R	this thesis
LeGO-iZ-NKp30FL-His-K129A	amp^R/zeo^R	this thesis
LeGO-iZ-NKp30FL-His-E130A	amp^R/zeo^R	this thesis
LeGO-iZ-NKp30FL-His-H131A	amp^R/zeo^R	this thesis
LeGO-iZ-NKp30FL-His-P132A	amp^R/zeo^R	this thesis
LeGO-iZ-NKp30FL-His-Q133A	amp^R/zeo^R	this thesis

Plasmid	Selection	Supplier
LeGO-iZ-NKp30FL-His-L134A	amp^R/zeo^R	this thesis
LeGO-iZ-NKp30FL-His-G135A	amp^R/zeo^R	this thesis
LeGO-iZ-NKp30FL-His-G137A	amp^R/zeo^R	this thesis
LeGO-iZ-NKp30FL-His-T138A	amp^R/zeo^R	this thesis
LeGO-iZ-NKp30FL-His-V139A	amp^R/zeo^R	this thesis
LeGO-iZ-NKp30FL-His-L140A	amp^R/zeo^R	this thesis
LeGO-iZ-NKp30FL-His-L141A	amp^R/zeo^R	this thesis
LeGO-iZ-NKp30FL-His-L142A	amp^R/zeo^R	this thesis
LeGO-iZ-NKp30FL-His-R143A	amp^R/zeo^R	this thesis
LeGO-iZ-NKp30FL-His-R143K	amp^R/zeo^R	this thesis
LeGO-iZ-NKp30FL-His-Y161F	amp^R/zeo^R	this thesis
LeGO-iZ-NKp30FL-His-Y162F	amp^R/zeo^R	this thesis
LeGO-iZ-NKp30FL-His-Y161F/Y162F	amp^R/zeo^R	this thesis
LeGO-iZ-NKp30FL-His-A144L/G145L	amp^R/zeo^R	this thesis
LeGO-iZ-NKp30FL-His-A144L/G145L/K165→161	amp^R/zeo^R	this thesis
LeGO-iZ-NKp30FL-His-V126N/E128S	amp^R/zeo^R	this thesis
LeGO-iZ-NKp30FL-His-K129N/H131S	amp^R/zeo^R	this thesis
LeGO-iZ-NKp30FL-His-Q133N/G135S	amp^R/zeo^R	this thesis
LeGO-iZ-NKp46FL-His-G241N/Q243S	amp^R/zeo^R	this thesis
LeGO-iZ-NKp46FL-His-K244N/H246S	amp^R/zeo^R	this thesis
LeGO-iZ-NKp46FL-His-L248N/W249S/D250S	amp^R/zeo^R	this thesis
LeGO-iZ-Flag	amp^R/zeo^R	this thesis
LeGO-iZ-B7-H6-Flag	amp^R/zeo^R	this thesis
LeGO-iZ-CD68-Flag	amp^R/zeo^R	this thesis
LeGO-iZ-CD74-Flag	amp^R/zeo^R	this thesis
LeGO-iZ-CD164-Flag	amp^R/zeo^R	this thesis

Plasmid	Selection	Supplier
LeGO-iZ-CD302-Flag	amp^R/zeo^R	this thesis
LeGO-iZ-CD320-Flag	amp^R/zeo^R	this thesis
LeGO-iZ-CLDN8-Flag	amp^R/zeo^R	this thesis
LeGO-iZ-CLEC6A-Flag	amp^R/zeo^R	this thesis
LeGO-iZ-CEACAM1-Flag	amp^R/zeo^R	this thesis
LeGO-iZ-CEACAM5-Flag	amp^R/zeo^R	this thesis
LeGO-iZ-FAS-Flag	amp^R/zeo^R	this thesis
LeGO-iZ-GJB5-Flag	amp^R/zeo^R	this thesis
LeGO-iZ-GPC3-Flag	amp^R/zeo^R	this thesis
LeGO-iZ-GRINA-Flag	amp^R/zeo^R	this thesis
LeGO-iZ-LIN7A-Flag	amp^R/zeo^R	this thesis
LeGO-iZ-PDZK1-Flag	amp^R/zeo^R	this thesis
LeGO-iZ-PRKCD-Flag	amp^R/zeo^R	this thesis
LeGO-iZ-RAB23-Flag	amp^R/zeo^R	T. Zöller
LeGO-iZ-ZDHHC4-Flag	amp^R/zeo^R	this thesis
LeGO-iZ-mNKp30FL-His	amp^R/zeo^R	this thesis
LeGO-iZ-Flag-mNKp30FL-His	amp^R/zeo^R	this thesis
LeGO-iZ-Flag-mNKp30FL-His-glyco	amp^R/zeo^R	this thesis

Packaging plasmids

Plasmid	Selection	Supplier
pMD2.G	amp^R	D. Trono
pCMV-ΔR8.91	amp^R	D. Trono

2.1.8 Viruses

All viruses used in this thesis were replication incompetent, self-inactivating lentiviral particles, produced with a third generation lentiviral transfer plasmid (LeGO-iZ or LeGO-iZ-Flag) packaged by a second generation packaging system (pCMV-ΔR8.91 and pMD2.G). The shRNA library was delivered in lentiviral particles pseudotyped with vesicular stomatitis virus glycoprotein (VSV-G). Viruses used in 3.1.1 to 3.1.3 were produced in collaboration with Sandra Weil and Steffen Beyer.

Application	Virus	Virus core	Supplier
chapter 3.1	[LeGO-iZ(VSV-G)] (Mock)	HIV-1	this thesis
	[LeGO-iZ-NKp30FL-His(VSV-G)]	HIV-1	this thesis
	[LeGO-iZ-NKp46FL-His(VSV-G)]	HIV-1	this thesis
	[LeGO-iZ-NKp46Ig/30Stalk/30TM-His(VSV-G)]	HIV-1	this thesis
	[LeGO-iZ-NKp46Ig/30Stalk/46TM-His(VSV-G)]	HIV-1	this thesis
	[LeGO-iZ-NKp30Ig/46Stalk/46TM-His(VSV-G)]	HIV-1	this thesis
	[LeGO-iZ-NKp30Ig/46Stalk/30TM-His(VSV-G)]	HIV-1	this thesis
	[LeGO-iZ-NKp30FL-His-K129A(VSV-G)]	HIV-1	this thesis
	[LeGO-iZ-NKp30FL-His-E130A(VSV-G)]	HIV-1	this thesis
	[LeGO-iZ-NKp30FL-His-H131A(VSV-G)]	HIV-1	this thesis
	[LeGO-iZ-NKp30FL-His-P132A(VSV-G)]	HIV-1	this thesis
	[LeGO-iZ-NKp30FL-His-Q133A(VSV-G)]	HIV-1	this thesis
	[LeGO-iZ-NKp30FL-His-L134A(VSV-G)]	HIV-1	this thesis
	[LeGO-iZ-NKp30FL-His-G135A(VSV-G)]	HIV-1	this thesis
	[LeGO-iZ-NKp30FL-His-G137A(VSV-G)]	HIV-1	this thesis
	[LeGO-iZ-NKp30FL-His-T138A(VSV-G)]	HIV-1	this thesis
	[LeGO-iZ-NKp30FL-His-V139A(VSV-G)]	HIV-1	this thesis
	[LeGO-iZ-NKp30FL-His-L140A(VSV-G)]	HIV-1	this thesis
	[LeGO-iZ-NKp30FL-His-L141A(VSV-G)]	HIV-1	this thesis

Application	Virus	Virus core	Supplier
chapter 3.1	[LeGO-iZ-NKp30FL-His-L142A(VSV-G)]	HIV-1	this thesis
	[LeGO-iZ-NKp30FL-His-R143A(VSV-G)]	HIV-1	this thesis
	[LeGO-iZ-NKp30FL-His-R143K(VSV-G)]	HIV-1	this thesis
	[LeGO-iZ-NKp30FL-His-Y161F(VSV-G)]	HIV-1	this thesis
	[LeGO-iZ-NKp30FL-His-Y162F(VSV-G)]	HIV-1	this thesis
	[LeGO-iZ-NKp30FL-His-Y161F/Y162F(VSV-G)]	HIV-1	this thesis
	[LeGO-iZ-NKp30FL-His-A144L/G145L(VSV-G)]	HIV-1	this thesis
	[LeGO-iZ-NKp30FL-His-A144L/G145L/K165→161(VSV-G)]	HIV-1	this thesis
chapter 3.2	[pMK1047(VSV-G)]	HIV-1	Viracore, UCSF
	[pMK1047-chip-a(VSV-G)]	HIV-1	Viracore, UCSF
	[pMK1047-chip-b(VSV-G)]	HIV-1	Viracore, UCSF
	[pMK1047-chip-c(VSV-G)]	HIV-1	Viracore, UCSF
	[pMK1047-chip-d(VSV-G)]	HIV-1	Viracore, UCSF
	[pMK1047-chip-e(VSV-G)]	HIV-1	Viracore, UCSF
	[pMK1047-chip-f(VSV-G)]	HIV-1	Viracore, UCSF
	[pMK1047-chip-g(VSV-G)]	HIV-1	Viracore, UCSF
	[pMK1047-chip-k(VSV-G)]	HIV-1	Viracore, UCSF
	[pMK1047-chip-l(VSV-G)]	HIV-1	Viracore, UCSF
	[pMK1047-chip-m(VSV-G)]	HIV-1	Viracore, UCSF

Application	Virus	Virus core	Supplier
chapter 3.2	[LeGO-iZ-Flag(VSV-G)] (Mock)	HIV-1	this thesis
	[LeGO-iZ-B7-H6-Flag(VSV-G)]	HIV-1	this thesis
	[LeGO-iZ-CD320-Flag(VSV-G)]	HIV-1	this thesis
	[LeGO-iZ-ZDHHC4-Flag(VSV-G)]	HIV-1	this thesis
	[LeGO-iZ-GRINA-Flag(VSV-G)]	HIV-1	this thesis
	[LeGO-iZ-RAB23-Flag(VSV-G)]	HIV-1	this thesis
	[LeGO-iZ-PDZK1-Flag(VSV-G)]	HIV-1	this thesis
	[LeGO-iZ-CLDN8-Flag(VSV-G)]	HIV-1	this thesis
	[LeGO-iZ-CLEC6A-Flag(VSV-G)]	HIV-1	this thesis
	[LeGO-iZ-CD164-Flag(VSV-G)]	HIV-1	this thesis
	[LeGO-iZ-FAS-Flag(VSV-G)]	HIV-1	this thesis
	[LeGO-iZ-GPC3-Flag(VSV-G)]	HIV-1	this thesis
	[LeGO-iZ-PRKCD-Flag(VSV-G)]	HIV-1	this thesis
	[LeGO-iZ-CD302-Flag(VSV-G)]	HIV-1	this thesis
	[LeGO-iZ-GJB5-Flag(VSV-G)]	HIV-1	this thesis
	[LeGO-iZ-CRIM1-Flag(VSV-G)]	HIV-1	this thesis
	[LeGO-iZ-CD68-Flag(VSV-G)]	HIV-1	this thesis
	[LeGO-iZ-CEACAM5-Flag(VSV-G)]	HIV-1	this thesis
	[LeGO-iZ-LIN7A-Flag(VSV-G)]	HIV-1	this thesis
	[LeGO-iZ-ABCG2-Flag(VSV-G)]	HIV-1	this thesis
	[LeGO-iZ-CEACAM1-Flag(VSV-G)]	HIV-1	this thesis
	[LeGO-iZ-CD74-Flag(VSV-G)]	HIV-1	this thesis
chapter 3.3	[LeGO-iZ-Flag-mNKp30FL-His(VSV-G)]	HIV-1	this thesis
	[LeGO-iZ-Flag-mNKp30FL-His-glyco(VSV-G)]	HIV-1	this thesis

2.1.9 Proteins

All recombinant hIgG1-Fc fusion proteins used in this thesis were produced by transient transfection of HEK 293T/17 cells.

Proteins expressed in mammalian cells

Application	Protein	Supplier
chapter 3.1 - 3.3	IFNAR2-hIgG1-FcEQ	this thesis
	NKp30-hIgG1-FcEQ	this thesis
chapter 3.1	B7-H6-hIgG1-FcEQ-Bio	this thesis
	NKp30-K129A-hIgG1-FcEQ	this thesis
	NKp30-E130A-hIgG1-FcEQ	this thesis
	NKp30-H131A-hIgG1-FcEQ	this thesis
	NKp30-P132A-hIgG1-FcEQ	this thesis
	NKp30-Q133A-hIgG1-FcEQ	this thesis
	NKp30-L134A-hIgG1-FcEQ	this thesis
	NKp30-G135A-hIgG1-FcEQ	this thesis
	NKp30-G137A-hIgG1-FcEQ	this thesis
	NKp30-T138A-hIgG1-FcEQ	this thesis
	NKp30-V139A-hIgG1-FcEQ	this thesis
	NKp30-L140A-hIgG1-FcEQ	this thesis
	NKp30-L141A-hIgG1-FcEQ	this thesis
	NKp30-L142A-hIgG1-FcEQ	this thesis
	NKp30-R143A-hIgG1-FcEQ	this thesis
chapter 3.2	NKp44-hIgG1-FcEQ	this thesis
	NKp46-hIgG1-FcEQ	this thesis
chapter 3.3	mNKp30-hIgG1-FcEQ	this thesis
	mNKp30-hIgG1-FcEQ-glyco	this thesis

2.1.10 Bacterial Strains and Culture Media

Strain	Genotype	Supplier
E. coli DH5α	F^- Φ80*lac*ZΔM15 Δ(*lac*ZYA-*arg*F) U169 *rec*A1 *end*A1 *hsd*R17 (rK–, mK+) *pho*A *sup*E44 λ– *thi*-1 *gyr*A96 *rel*A1	Invitrogen
E. coli Top10	F^- *mcr*A Δ(*mrr-hsd*RMS-*mcr*BC) φ80*lac*ZΔM15 Δ*lac*X74 *rec*A1 *ara*D139 Δ(*araleu*)7697 *gal*U *gal*K *rps*L (StrR) *end*A1 *nup*G	Invitrogen

E. coli bacteria were maintained in Luria Broth medium with the low salt formulation of Lennox (LB; trypton 1 % (w/v), yeast extract 0.5 % (w/v), NaCl 0.5 % (w/v)). Bacteria were either cultivated in liquid culture or on plates containing 1.5 % agar and the appropriate antibiotic for selection.

2.1.11 Cell Lines and Culture Media

Unmodified cell lines

Cell line	Characterization	Supplier
Ba/F3[d] (IL-3 independent subclone)	murine pro B cells	DSMZ, ACC-300
EL-4[e]	murine T cell lymphoma	ATCC, TIB-39
DU145	human prostate cancer cells	ATCC, HTB-81
HEK 293T/17	human embryonic kidney cells, highly transfectable derivative of the HEK 293T cell line	ATCC, CRL-11268
HeLa	human cervix adenocarcinoma cells	ATCC, CCL-2
MEF (CF-1)[e]	murine embryonic fibroblasts	ATCC, SCRC-1040
MelJuSo	human melanoma cells	DSMZ, ACC 74
MODE-K[e]	murine intestinal epithelial cells	[210]
NIH/3T3[e]	murine embryonic fibroblasts	ATCC, CRL-1658

[d] kindly provided by C. Watzl
[e] kindly provided by A. Steinle

Cell line	Characterization	Supplier
P815[e]	murine mastocytoma	ATCC, TIB-64
RAW 309 Cr.1[e]	murine monocytes/ macrophages	ATCC, TIB-69
YAC-1[e]	murine lymphoblasts	ATCC, TIB-160

Genetically modified cell lines

DU145, MelJuSo and 293T/17 cells used for the shRNA screening were transduced with pooled shRNAs (chip a,b,c,d,e,f,g,k,l,m; compare to 3.2). Cell lines used in 3.1.1 to 3.1.3 were generated in collaboration with Sandra Weil and Steffen Beyer.

Cell line	Modification	Supplier
A5-GFP	GFP expression under three NF-AT binding sites in the IL-2 promoter region	A. Diefenbach [211,212]
A5-GFP-NKp30FL	human NKp30 full length protein containing a C-terminal His_{10} tag; zeocin resistance	K. Oberle, J. Hartmann [208]
A5-GFP-NKp46FL	human NKp46 full length protein containing a C-terminal His_{10} tag; zeocin resistance	this thesis
A5-GFP-NKp46Ig/30Stalk/30TM	chimeric human NCR protein containing the Ig-fold of NKp46, the stalk of NKp30, the TM and cytosolic domain of NKp30, and a C-terminal His_{10} tag; zeocin resistance	this thesis
A5-GFP-NKp46Ig/30Stalk/46TM	chimeric human NCR protein containing the Ig-fold of NKp46, the stalk of NKp30, the TM and cytosolic domain of NKp46, and a C-terminal His_{10} tag; zeocin resistance	this thesis
A5-GFP-NKp30Ig/46Stalk/46TM	chimeric human NCR protein containing the Ig-fold of NKp30, the stalk of NKp46, the TM and cytosolic domain of NKp46, and a C-terminal His_{10} tag; zeocin resistance	this thesis
A5-GFP-NKp30Ig/46Stalk/30TM	chimeric human NCR protein containing the Ig-fold of NKp30, the stalk of NKp46, the TM and cytosolic domain of NKp30, and a C-terminal His_{10} tag; zeocin resistance	this thesis
A5-GFP-NKp30-K129A	human NKp30 full length protein containing an amino acid exchange from lysine to alanine at position 129 (K129A), and a C-terminal His_{10} tag; zeocin resistance	this thesis

Cell line	Modification	Supplier
A5-GFP-NKp30-E130A	human NKp30 full length protein containing an amino acid exchange from glutamic acid to alanine at position 130 (E130A), and a C-terminal His_{10} tag; zeocin resistance	this thesis
A5-GFP-NKp30-H131A	human NKp30 full length protein containing an amino acid exchange from histidine to alanine at position 131 (H131A), and a C-terminal His_{10} tag; zeocin resistance	this thesis
A5-GFP-NKp30-P132A	human NKp30 full length protein containing an amino acid exchange from proline to alanine at position 132 (P132A), and a C-terminal His_{10} tag; zeocin resistance	this thesis
A5-GFP-NKp30-Q133A	human NKp30 full length protein containing an amino acid exchange from glutamine to alanine at position 133 (Q133A), and a C-terminal His_{10} tag; zeocin resistance	this thesis
A5-GFP-NKp30-L134A	human NKp30 full length protein containing an amino acid exchange from leucine to alanine at position 134 (L134A), and a C-terminal His_{10} tag; zeocin resistance	this thesis
A5-GFP-NKp30-G135A	human NKp30 full length protein containing an amino acid exchange from glycine to alanine at position 135 (G135A), and a C-terminal His_{10} tag; zeocin resistance	this thesis
A5-GFP-NKp30-G137A	human NKp30 full length protein containing an amino acid exchange from glycine to alanine at position 137 (G137A), and a C-terminal His_{10} tag; zeocin resistance	this thesis
A5-GFP-NKp30-T138A	human NKp30 full length protein containing an amino acid exchange from threonine to alanine at position 138 (T138A), and a C-terminal His_{10} tag; zeocin resistance	this thesis
A5-GFP-NKp30-V139A	human NKp30 full length protein containing an amino acid exchange from valine to alanine at position 139 (V139A), and a C-terminal His_{10} tag; zeocin resistance	this thesis
A5-GFP-NKp30-L140A	human NKp30 full length protein containing an amino acid exchange from leucine to alanine at position 140 (L140A), and a C-terminal His_{10} tag; zeocin resistance	this thesis

Cell line	Modification	Supplier
A5-GFP-NKp30-L141A	human NKp30 full length protein containing an amino acid exchange from leucine to alanine at position 141 (L141A), and a C-terminal His_{10} tag; zeocin resistance	this thesis
A5-GFP-NKp30-L142A	human NKp30 full length protein containing an amino acid exchange from leucine to alanine at position 142 (L142A), and a C-terminal His_{10} tag; zeocin resistance	this thesis
A5-GFP-NKp30-R143A	human NKp30 full length protein containing an amino acid exchange from arginine to alanine at position 143 (R143A), and a C-terminal His_{10} tag; zeocin resistance	this thesis
A5-GFP-NKp30-Y161F	human NKp30 full length protein containing an amino acid exchange from tyrosine to phenylalanine at position 161 (Y161F), and a C-terminal His_{10} tag; zeocin resistance	this thesis
A5-GFP-NKp30-Y162F	human NKp30 full length protein containing an amino acid exchange from tyrosine to phenylalanine at position 162 (Y162F), and a C-terminal His_{10} tag; zeocin resistance	this thesis
A5-GFP-NKp30-Y161F/Y162F	human NKp30 full length protein containing two amino acid exchanges from tyrosine to phenylalanine at position 161 and 162 (Y161F/Y162F), and a C-terminal His_{10} tag; zeocin resistance	this thesis
A5-GFP-NKp30-A144L/G145L	human NKp30 full length protein containing an amino acid exchange from alanine to leucine at position 144 (A144L) and from glycine to leucine at position 145 (G145L), and a C-terminal His_{10} tag; zeocin resistance	this thesis
A5-GFP-NKp30-A144L/G145L, K165→161	human NKp30 full length protein containing an amino acid exchange from alanine to leucine at position 144 (A144L), and from glycine to leucine at position 145 (G145L), an amino acid shift from position 165 to 161 (K165→161), and a C-terminal His_{10} tag; zeocin resistance	this thesis
A5-GFP-Flag-mNKp30	*M. musculus* NKp30 containing two point mutations that change the premature stop codons TGA to TGG (Exon 2), an N-terminal Flag-tag, and a C-terminal His_{10} tag; zeocin resistance	this thesis

Cell line	Modification	Supplier
A5-GFP-Flag-mNKp30-glyco	*M. musculus* NKp30 containing two point mutations that change the premature stop codons TGA to TGG (Exon 2), three point mutations that transfer three glycosylation sites NAS, NVT and NRT in the extracellular domain, an N-terminal Flag-tag, and a C-terminal His_{10} tag; zeocin resistance	this thesis
Ba/F3-mock[f]	mock transduced Ba/F3 cells; puromycin resistance; intracellular GFP-expression; IL-3 independent subclone	A. Cohnen, J. Hartmann [208]
Ba/F3-B7-H6[f]	human B7-H6 full length protein; puromycin resistance; intracellular GFP-expression; IL-3 independent subclone	A. Cohnen, J. Hartmann [208]
HeLa-ABCG2-Flag	human ABCG2 containing a C-terminal Flag tag; zeocin resistance	this thesis
HeLa-B7-H6-Flag	human B7-H6 containing a C-terminal Flag tag; zeocin resistance	this thesis
HeLa-CD3ζ	human CD3ζ full length protein; puromycin resistance	E. Peters
HeLa-CD68-Flag	human CD68 containing a C-terminal Flag tag; zeocin resistance	this thesis
HeLa-CD74-Flag	human CD74 containing a C-terminal Flag tag; zeocin resistance	this thesis
HeLa-CD164-Flag	human CD164 containing a C-terminal Flag tag; zeocin resistance	this thesis
HeLa-CD302-Flag	human CD302 containing a C-terminal Flag tag; zeocin resistance	this thesis
HeLa-CD320-Flag	human CD320 containing a C-terminal Flag tag; zeocin resistance	this thesis
HeLa-CLDN8-Flag	human CLDN8 containing a C-terminal Flag tag; zeocin resistance	this thesis
HeLa-CLEC6A-Flag	human CLEC6A containing a C-terminal Flag tag; zeocin resistance	this thesis
HeLa-CEACAM1-Flag	human CEACAM1 containing a C-terminal Flag tag; zeocin resistance	this thesis

[f] generated and kindly provided by A. Cohnen

Cell line	Modification	Supplier
HeLa-CEACAM5-Flag	human CEACAM5 containing a C-terminal Flag tag; zeocin resistance	this thesis
HeLa-CRIM1-Flag	human CRIM1 containing a C-terminal Flag tag; zeocin resistance	this thesis
HeLa-FAS-Flag	human FAS containing a C-terminal Flag tag; zeocin resistance	this thesis
HeLa-GJB5-Flag	human GJB5 containing a C-terminal Flag tag; zeocin resistance	this thesis
HeLa-GBC3-Flag	human GPC3 containing a C-terminal Flag tag; zeocin resistance	this thesis
HeLa-GRINA-Flag	human GRINA containing a C-terminal Flag tag; zeocin resistance	this thesis
HeLa-LIN7A-Flag	human LIN7A containing a C-terminal Flag tag; zeocin resistance	this thesis
HeLa-Mock (LeGO-iZ-Flag)	zeocin resistance	this thesis
HeLa-PDZK1-Flag	human PDZK1 containing a C-terminal Flag tag; zeocin resistance	this thesis
HeLa-PRKCD-Flag	human PRKCD containing a C-terminal Flag tag; zeocin resistance	this thesis
HeLa-RAB23-Flag	human RAB23 containing a C-terminal Flag tag; zeocin resistance	this thesis
HeLa-ZDHHC4-Flag	human ZDHHC4 containing a C-terminal Flag tag; zeocin resistance	this thesis
HeLa-NKp30FL	human NKp30 full length protein containing a C-terminal His_{10} tag; zeocin resistance	this thesis
HeLa-NKp46FL	human NKp46 full length protein containing a C-terminal His_{10} tag; zeocin resistance	this thesis
HeLa-CD3ζ-NKp30FL	human CD3ζ full length protein; puromycin resistance; human NKp30 full length protein containing a C-terminal His_{10} tag; zeocin resistance	this thesis
HeLa-CD3ζ-NKp46FL	human CD3ζ full length protein; puromycin resistance; human NKp46 full length protein containing a C-terminal His_{10} tag; zeocin resistance	this thesis

Cell line	Modification	Supplier
HeLa-CD3ζ-NKp30-K129A	human CD3ζ full length protein; puromycin resistance; human NKp30 full length protein containing an amino acid exchange from lysine to alanine at position 129 (K129A), and a C-terminal His_{10} tag; zeocin resistance	this thesis
HeLa-CD3ζ-NKp30-E130A	human CD3ζ full length protein; puromycin resistance; human NKp30 full length protein containing an amino acid exchange from glutamic acid to alanine at position 130 (E130A), and a C-terminal His_{10} tag; zeocin resistance	this thesis
HeLa-CD3ζ-NKp30-H131A	human CD3ζ full length protein; puromycin resistance; human NKp30 full length protein containing an amino acid exchange from histidine to alanine at position 131 (H131A), and a C-terminal His_{10} tag; zeocin resistance	this thesis
HeLa-CD3ζ-NKp30-P132A	human CD3ζ full length protein; puromycin resistance; human NKp30 full length protein containing an amino acid exchange from proline to alanine at position 132 (P132A), and a C-terminal His_{10} tag; zeocin resistance	this thesis
HeLa-CD3ζ-NKp30-Q133A	human CD3ζ full length protein; puromycin resistance; human NKp30 full length protein containing an amino acid exchange from glutamine to alanine at position 133 (Q133A), and a C-terminal His_{10} tag; zeocin resistance	this thesis
HeLa-CD3ζ-NKp30-L134A	human CD3ζ full length protein; puromycin resistance; human NKp30 full length protein containing an amino acid exchange from leucine to alanine at position 134 (L134A), and a C-terminal His_{10} tag; zeocin resistance	this thesis
HeLa-CD3ζ-NKp30-G135A	human CD3ζ full length protein; puromycin resistance; human NKp30 full length protein containing an amino acid exchange from glycine to alanine at position 135 (G135A), and a C-terminal His_{10} tag; zeocin resistance	this thesis
HeLa-CD3ζ-NKp30-G137A	human CD3ζ full length protein; puromycin resistance; human NKp30 full length protein containing an amino acid exchange from glycine to alanine at position 137 (G137A), and a C-terminal His_{10} tag; zeocin resistance	this thesis

Cell line	Modification	Supplier
HeLa-CD3ζ-NKp30-T138A	human CD3ζ full length protein; puromycin resistance; human NKp30 full length protein containing an amino acid exchange from threonine to alanine at position 138 (T138A), and a C-terminal His_{10} tag; zeocin resistance	this thesis
HeLa-CD3ζ-NKp30-V139A	human CD3ζ full length protein; puromycin resistance; human NKp30 full length protein containing an amino acid exchange from valine to alanine at position 139 (V139A), and a C-terminal His_{10} tag; zeocin resistance	this thesis
HeLa-CD3ζ-NKp30-L140A	human CD3ζ full length protein; puromycin resistance; human NKp30 full length protein containing an amino acid exchange from leucine to alanine at position 140 (L140A), and a C-terminal His_{10} tag; zeocin resistance	this thesis
HeLa-CD3ζ-NKp30-L141A	human CD3ζ full length protein; puromycin resistance; human NKp30 full length protein containing an amino acid exchange from leucine to alanine at position 141 (L141A), and a C-terminal His_{10} tag; zeocin resistance	this thesis
HeLa-CD3ζ-NKp30-L142A	human CD3ζ full length protein; puromycin resistance; human NKp30 full length protein containing an amino acid exchange from leucine to alanine at position 142 (L142A), and a C-terminal His_{10} tag; zeocin resistance	this thesis
HeLa-CD3ζ-NKp30-R143A	human CD3ζ full length protein; puromycin resistance; human NKp30 full length protein containing an amino acid exchange from arginine to alanine at position 143 (R143A), and a C-terminal His_{10} tag; zeocin resistance	this thesis
p30-15	murine B cells, spleen, hybridoma producing the anti-NKp30 antibody clone p30-15	C. Watzl
RMA neo^e	murine T cell lymphoma	A. Steinle

Culture Media

A5-GFP (and modified subclones)

DMEM + 10 % FBS
+ 5.4 mM L-glutamine
+ 100 U/ml penicillin
+ 100 μg/ml streptomycin
+ 10 mM HEPES
+ 1x MEM non-essential amino acids
+ 10 μg/ml gentamicin
+ 55 μM β-mercaptoethanol

Ba/F3 (and modified subclones)

RPMI + 10 % FBS
+ 2 mM L-glutamine
+ 100 U/ml penicillin
+ 100 μg/ml streptomycin
+ 55 μM β-mercaptoethanol

DU145, 293T/17, HeLa, MelJuSo (and modified subclones)

DMEM + 10 % FBS
+ 2 mM L-glutamine
+ 100 U/ml penicillin
+ 100 μg/ml streptomycin

EL-4, P815, YAC-1

RPMI + 10 % FBS
+ 2 mM L-glutamine
+ 100 U/ml penicillin
+ 100 μg/ml streptomycin
+ 1 mM sodium pyruvate

HeLa-CD3ζ (and modified subclones)

DMEM + 10 % FBS
+ 2 mM L-glutamine
+ 100 U/ml penicillin
+ 100 μg/ml streptomycin
+ 1 μg/ml puromycin

MEF, NIH/3T3, RAW 309

DMEM + 10 % FBS
+ 2 mM L-glutamine
+ 100 U/ml penicillin
+ 100 μg/ml streptomycin
+ 1 mM sodium pyruvate

MODE-K

RPMI + 10 % FBS
+ 2 mM L-glutamine
+ 100 U/ml penicillin
+ 100 μg/ml streptomycin
+ 1 mM sodium pyruvate
+ 1x MEM non-essential amino acids
+ 55 μM β-mercaptoethanol

RMA neo

RPMI + 10 % FBS
+ 2 mM L-glutamine
+ 100 U/ml penicillin
+ 100 μg/ml streptomycin
+ 1 mM sodium pyruvate
+ 1 mg/ml G418

2.2 Methods of Microbiology

2.2.1 Cultivation of Bacteria

E. coli bacteria were grown in LB medium with the respective antibiotic for selection over night at 37°C. Bacteria were either cultivated in liquid culture on a bacteria shaker, or on plates containing 1.5 % agar.

2.2.2 Generation and Transformation of Chemo-Competent Bacteria

Chemo-competent bacteria were generated by implementation of the $CaCl_2$/RbCl method [213]. Therefore, 100 ml of LB medium were inoculated with 2 ml of an overnight *E. coli* culture (DH5α or TOP10) and incubated at 37°C and 120 rpm until an OD_{600} of 0.4-0.6 was reached. Afterwards, bacteria were incubated on ice for 10 minutes and pelleted by centrifugation (2000xg, 10 min, 0°C). The pellet was resuspended in 7.5 ml TFB I buffer (sterile filtrated, ice-cold) and incubated on ice for one hour. After that, bacteria were pelleted (2000xg, 10 min, 0°C) and resuspended in 2 ml TBF II buffer (sterile filtrated, ice-cold). The bacteria suspension was frozen in 50 µl aliquots and stored at -80°C.
For transformation of chemo-competent bacteria, either 50 ng plasmid DNA or 5-10 µl ligation reaction (2.3.4) were mixed with 50 µl bacteria suspension and incubated on ice for 20 min. Afterwards, bacteria were heat-shocked at 42°C for 45 seconds and again incubated on ice for 2 min. After addition of 800 µl LB medium, bacteria were incubated at 37°C and 600 rpm for 30-60 min. Finally, the bacteria suspension was either applied to LB plates or liquid LB medium containing the respective antibiotic for selection (2.1.2).

2.3 Methods of Molecular Biology

2.3.1 Preparation of Plasmids

Plasmids were isolated from transformed bacteria using either the GeneJET™ Plasmid Miniprep kit or the NucleoBond® Xtra Midi/Maxi kit according to manufacturers' instructions. Small amounts of DNA (plasmid mini preparation) were isolated from 5 ml and larger amounts of DNA (plasmid midi or maxi preparation) from 100-500 ml liquid cultures. Precipitated and dried DNA was reconstituted with 50-1000 µl (depending on the amount of DNA) nuclease-free water. The DNA concentration was determined either spectrophotometrically (NanoDrop ND 1000, PeqLab) or fluorometrically (Qubit® Fluorometer, Thermo Fisher Scientific). For spectrophotometric determination, 1 µl of DNA (aqueous solution) was measured at the UV absorbance spectrum (220-300 nm). H_2O served as blank.

For fluorometric determination the Qubit dsDNA BR assay kit was used according to manufacturers' instructions. 1 µl of DNA (aqueous solution) was applied to the analysis.

2.3.2 Isolation of genomic DNA

Genomic DNA was isolated from approximately $5*10^6$ mammalian cells using QIAamp blood DNA maxi kit (QIAGEN) according to manufacturers' instructions. DNA was eluted with 600 µl of nuclease-free water.

2.3.3 Polymerase Chain Reaction (PCR)

To amplify specific DNA sequences from either plasmid DNA or bacteria colonies, the polymerase chain reaction (PCR) [214,215] was applied. DNA was amplified either using *DreamTaq*™ (no proof-reading activity) or Phusion® (3'-5' exonuclease activity) polymerase (both Thermo Fisher Scientific). Annealing temperatures and elongation times were dependent on the melting temperature of the primers (T_M), length of the DNA fragment to be amplified, and elongation time of the polymerase. Standard reaction mixes and cycler protocols are represented in table 2 and 3. PCR reactions were afterwards analyzed via agarose gel electrophoresis (2.3.5), and DNA fragments of interest were isolated from agarose gels (2.3.6) for subsequent cloning.

Table 2. Standard reaction mix and cycler protocol for Phusion® polymerase.

Reaction Mix		PCR protocol			
20 ng	template DNA	**1.**	98°C	30 s	initial denaturation
0.5 µM	Primer (forward)				
0.5 µM	Primer (reverse)	**2.**	98°C	15 s	denaturation
0.2 mM	dNTPs				
3 % (v/v)	DMSO	**3.**	5°C below melting temperature (T_M) of the primers	15 s	annealing
1x	Phusion® GC- or HF-buffer				
1 U	Phusion® Polymerase	**4.**	72°C	15-30 s/kB	elongation
	to 50 µl H_2O				
		5.	72°C	5 min	final elongation
		6.	4°C	∞	storage
			step 2-4 are repeated in 25-35 cycles		

Table 3. Standard reaction mix and cycler protocol for *DreamTaq*™ polymerase.

Reaction Mix		PCR protocol			
20 ng	template DNA or	**1.**	98°C	30 s	initial denaturation
1	bacterial colony	**2.**	98°C	15 s	denaturation
0.5 µM	Primer (forward)	**3.**	5°C below melting temperature (T_M) of the primers	15 s	annealing
0.5 µM	Primer (reverse)	**4.**	72°C	60 s/kB	elongation
0.2 mM	dNTPs	**5.**	72°C	5 min	final elongation
3 % (v/v)	DMSO	**6.**	4°C	∞	storage
1x	*DreamTaq*™ green buffer		step 2-4 are repeated in 25-35 cycles		
0.625 U	*DreamTaq*™ Polymerase				
	to 50 µl H_2O				

2.3.4 Restriction, Dephosphorylation, Purification and Ligation of DNA

Unless otherwise denoted, DNA restrictions were performed using FastDigest® restriction endonucleases (Thermo Fisher Scientific) or High fidelity (HF®) restriction endonucleases (New England Biolabs) according to manufacturers' instructions. Either 1 µg (analytic restriction) or up to 4 µg (preparative restriction) DNA were incubated with the corresponding enzymes at 37°C for 30 min. A standard reaction mixture for double digestion is listed in table 4. If necessary, enzymes were inactivated at 80°C for 10 min. Afterwards, samples were either directly purified using the GeneJET™ Gel Extraction kit (Thermo Fisher Scientific) or applied to agarose gel electrophoresis (2.3.5).

Table 4. Standard reaction mix for preprarative and analytic restriction (double digestion using type II restriction endonucleases).

Component	Preparative Restriction	Analytic Restriction
DNA	4 µg	1 µg
10x buffer (*FastDigest* or *CutSmart*)	5 µl	2 µl
Enzyme 1	2 µl	0.5 µl
Enzyme 2	2 µl	0.5 µl
H_2O	to 50 µl	to 20 µl

To prevent self-ligation, the phosphorylated 5'-end of the linearized vector DNA was dephosphorylated prior to ligation. For this, 1-5 µg vector DNA were incubated with *Fast*AP™ thermo sensitive alkaline phosphatase (Thermo Fisher Scientific) in FastAP buffer for 10 min at 37°C, followed by enzyme inactivation for 5 min at 75°C. Dephosphorylated DNA was purified using the GeneJET™ Gel Extraction Kit (Thermo Fisher Scientific).
For ligation, insert and vector DNA were applied at a molar ratio of 3:1 with the overall DNA amount of the mixture limited to 100 ng. Appropriate amounts of DNA were calculated with the following equation:

$$insert\ DNA\ [ng] = \frac{molar\ ratio \times insert\ DNA\ [bp] \times vector\ DNA\ \ [ng]}{vector\ DNA\ [bp]}$$

The DNA was incubated either 60-120 min at room temperature or over night at 4°C with T4 DNA ligase (Thermo Fisher Scientific) in the appropriate buffer and used directly for transformation or stored at -20°C.

2.3.5 Agarose Gel Electrophoresis

Agarose gel electrophoresis was used to separate DNA molecules by their size. Agarose concentrations were adjusted to the size of the DNA. For larger molecules (>500 bp) 0.8 % agarose gels were used, whereas fragments ≤ 500 bp were separated on 2 % agarose gels. Unless the buffer of the DNA samples did not already contain a density reagent and tracking dyes (DreamTaq™ green or FastDigest® green buffer), DNA samples were mixed with 6x loading dye (Thermo Fisher Scientific). GeneRuler™ 1 kb Plus DNA ladder or GeneRuler™ 100 bp Plus DNA ladder (Thermo Fisher Scientific) were applied to the agarose gels as size standard together with the DNA samples. TAE buffer was used as running buffer and for

production of agarose gels. The electrophoresis was performed at 120 V for approximately 50 min, depending on the size of the DNA molecules. Afterwards, gels were stained with EtBr stain (5-15 min) and DNA fragments were detected and photographically documented under UV light using a Gel Doc 2000 gel documentation system.

2.3.6 Isolation of DNA Fragments from Agarose Gels

For subsequent cloning, DNA fragments had to be isolated from agarose gels. For this purpose, the fragment of interest was cut from the gel under low intensity UV light and isolated using the GeneJET™ Gel Extraction kit (Thermo Fisher Scientific) according to manufacturers' instructions. DNA was eluted with 30 µl of prewarmed nuclease-free water. Concentrations of the purified DNA samples were determined either spectrophotometrically (NanoDrop ND 1000, PeqLab) or fluorometrically (Qubit® Fluorometer, Thermo Fisher Scientific).

2.3.7 Nucleic Acid Sequencing

Nucleic acid sequencing (*Lightrun* sequencing) was performed by GATC Biotech using the chain-termination method [216]. Sequencing samples consisted of 5 µl template DNA (concentration: 80-100 ng/µl) and 5 µl primer (concentration: 5 µM).

2.3.8 Deep Sequencing

Deep sequencing samples were generated from genomic DNA by PCR using primers that introduce adaptor sequences suitable for Illumina sequencing and barcodes to distinguish between the samples (2.1.6). Phusion® polymerase was used to amplify the DNA fragments, as its 3'-5' exonuclease activity is critical for the high quality needed for deep sequencing experiments. Standard reaction mix and cycler protocol are listed in table 5.

Table 5. Standard reaction mix and cycler protocol for generation of deep sequencing samples with Phusion® polymerase.

Reaction Mix		PCR protocol			
195 µl	gDNA	**1.**	98°C	30 s	initial denaturation
9.75 µl	Primer (forward, 100 µM)	**2.**	98°C	15 s	denaturation
9.75 µl	Primer (reverse, 100 µM)	**3.**	56°C	15 s	annealing
39 µl	dNTPs (10 mM)	**4.**	72°C	15 s	elongation
58.5 µl	DMSO	**5.**	72°C	10 min	final elongation
390 µl	Phusion® HF-buffer	**6.**	4°C	∞	storage
11.7 µl	Phusion® Polymerase		step 2-4 are repeated in 25 cycles		
	to 1950 µl H_2O				

DNA fragments were extracted from agarose gels after electrophoresis using GeneJET™ Gel Extraction kit (Thermo Fisher Scientific). Afterwards, DNA was concentrated using the DNA Clean & Concentrator 5 kit (Zymo). All samples (30) for one cell line were barcoded differently and thus could be analyzed on the same Illumina lane. Therefor, 2000 ng of each sample (30) were pooled and again concentrated (Zymo DNA Celan & Concentrator 5 kit). The final concentrations of the three samples (293T/17, DU145, MelJuSo) were determined by Qubit assay and ranged between 50-80 ng/µl. Deep sequencing was done by Beckman Coulter Genomics using single end 100 base reads on Illumina HiSeq 2500 machines.

2.4 Methods of Cell Biology and Virology

2.4.1 Cultivation of Cell Lines

All used cell lines were cultured according to suppliers' recommendations in the appropriate medium (2.1.11). Cells were passaged 2-3 times a week, depending on cell density. Adherent cells were washed one time with PBS and detached using PBS/EDTA (incubation time cell line dependent). Suspension cells and detached adherent cells were counted in a Neubauer counting chamber and the appropriate fraction of cells was pelleted, resuspended in fresh medium and cultured in a cell culture incubator at 37°C, 5 % CO_2 and saturated water atmosphere.

For long term storage, cells were kept in liquid nitrogen as cryo cultures. For this purpose, detached cells or suspension cells were pelleted (300xg, 3 min, 4°C) and resuspended in

freezing medium (either fresh medium or FBS containing 10 % (v/v) DMSO). The cell suspension was aliquoted in cryogenic vials, transferred to a freezing container (Mr. Frosty, Nalgene®) and stored at -80°C for 24 h. Afterwards, cryo cultures were stored in the gas phase of liquid nitrogen.

To reconstitute cells from long term storage, cryo cultures were thawed at 37°C and resuspended in 5 ml fresh medium. Afterwards, cells were pelleted (300xg, 3 min, 4°C), resuspended in fresh medium and seeded into a cell culture flask.

2.4.2 Transfection of Mammalian Cells

Mammalian cells were transfected using the polyethyleneimine (PEI) method [217,218]. For this purpose, cells were seeded into T175 flasks ($2*10^7$ cells/T175) one day before the experiment. Immediately before transfection, medium was exchanged to DMEM containing no FBS (DMEM -FBS). The transfection reagent consisted of two solutions (A and B). Solution A contained the appropriate amount of DNA in 5 % glucose and solution B contained the appropriate amount of TA-Trans (PEI) in 5 % glucose. Both solutions were mixed independently and incubated for at least 10 min at room temperature. Afterwards, both solutions were combined, mixed properly and again incubated for at least 10 min at room temperature. Then, the transfection reagent was mixed with DMEM -FBS and added drop wise to the cells. After gentle shaking of the flask to suspend the transfection reagent properly, cells were incubated at 37°C for 4-6 h. Then, DMEM containing 12.5 % FBS was added to achieve a final FBS concentration of 5 % in the medium. In case of *in vivo* biotinylated Fc fusion proteins, a slightly different transfection protocol was used. Solution A contained two plasmids carrying the genes for ER-tagged and soluble *E. coli* biotin ligase (pDisplay-BirA-ER, pDisplay-sBirA) in addition to the expression plasmid, and solutions A and B contained DMEM -FBS instead of 5 % glucose solution. Incubation times were the same as for non-biotinylated proteins. After 4-6 hours, medium was exchanged to DMEM-Bio (DMEM + 2 mM L-glutamine, 5 % (v/v) Panexin-NTA, 20 μM biotin). Amounts of components used for transfection in T175 flasks are depicted in table 6.

Table 6. Formulation of transfection reagents for 293T/17 cells. Amounts were calculated for transfection in a T175 flask.

Ingredient	Non-Biotinylated Fc Fusion Proteins		Biotinylated Fc Fusion Proteins	
	Solution A	Solution B	Solution A	Solution B
mammalian expression plasmid	65 µg		7 µg	
pDisplay-BirA-ER			14 µg	
pDisplay-sBirA			14 µg	
TA-trans		65 µl		140 µl
5 % glucose	310 µl	310 µl		
DMEM -FBS			2.3 ml	2.2 ml

2.4.3 Protein Production in Mammalian Cells

Fusion proteins of the extracellular domain of the different NCR mutants, the extracellular domain of interferon α/β receptor subunit 2 (IFNAR2) or B7-H6 were produced by transient transfection of 293T/17 cells with the different pFUSE-hIgG1-FcEQ or pFc-Avi constructs, using the polyethyleneimine (PEI) transfection method (2.4.2). One protein production contained 10-80 T175 flasks. Cell culture supernatant containing the soluble receptor-hIgG1-Fc fusion proteins was collected two days after transfection. The supernatant was sterile filtered (0.22 µm) and supplemented with 0.01 % sodium azide, 1x cOmplete™ EDTA-free protease inhibitor cocktail (Roche) and protein A sepharose® 4B conjugate (Life Technologies).

2.4.4 Production and Concentration of Lentiviral Particles in Mammalian Cells

All viruses used in this thesis were replication incompetent, self-inactivating lentiviral particles produced by transfection of 293T/17 cells (2.4.2) with a third generation lentiviral transfer plasmid (LeGO-iZ or LeGO-iZ-Flag) packaged by a second generation packaging system (pCMV-ΔR8.91 and pMD2.G). The DNA was applied at a ratio of 2.8 : 1.84 : 1 (transfer : packaging : envelope). This led to the formation of lentiviral particles consisting of the HIV-1 core and pseudotyped with VSV-G. Virus-containing supernatant was collected and sterile filtered (0.45 µm) 2-3 days after transfection. Afterwards, supernatant (two T175 flasks/virus) was concentrated either by low speed (2,000xg, 24h, 4°C) or ultracentrifugation (50,000xg,

3h, 4°C). The virus pellet was resuspended in 1 ml of the respective cell culture medium (over night, 4°C).

2.4.5 Transduction of Mammalian Cells

For transduction, cells were passaged either one day (adherent cells) or directly (suspension cells) before the experiment (cell numbers depending on cell line; shRNA screening: $3.1*10^6$ cells/T75 [293T/17, DU145 or MelJuSo], all other transductions: A5: $2.5*10^5$ cells/well [24-well-plate], HeLa: $5*10^4$ cells [12-well-plate]). Immediately before transduction, medium was exchanged to basal medium containing no additives. Afterwards, 8 μg/ml protamine sulfate and virus at a suitable multiplicity of infection (MOI; depending on cell line and experiment) were added and cells were incubated 5-7 h at 37°C. After incubation, medium was exchanged to fresh culture medium and cells were cultured 2-3 days before selection or analysis.

2.4.6 Flow Cytometry

For flow cytometry, $1\text{-}5*10^5$ cells/sample were subjected to the respective staining procedures. Surface staining of cells was done with either the respective primary antibodies or recombinant Fc fusion proteins, diluted in FACS buffer (1 h, 4°C, dilutions are shown in tab. 7). Afterwards, cells were stained with the respective fluorochrome-conjugated secondary antibodies (30 min, 4°C, protected from light, dilutions are shown in tab. 8). Viability of cells was determined with SytoxBlue stain, according to manufacturers' instructions. Samples incubated with the respective isotype control or secondary antibody alone served as negative control. Between all staining steps, cells were washed twice with FACS buffer (centrifugation 300xg, 3 min, 4°C). For intracellular staining, the cells were first fixed with FIX-I buffer and afterwards permeabilized and stained with Perm buffer and the respective staining agents (incubation conditions were equal to the surface staining procedure). In the end, cells were resuspended in FACS buffer (surface staining) or FIX-II buffer (intracellular staining) and analyzed on a BD FACSCanto II instrument using the BD FACSDiva software. For fluorescence activated cell sorting (FACS), cells were stained with the respective antibody under sterile conditions without fixation and sorted using the BD FACSAria sorter with the BD FACSDiva software. Data obtained by flow cytometry was further analyzed with FlowJo software.

Table 7. Primary antibodies used for flow cytometry.

Primary Antibodies (Name, Clone, Conjugation) and Recombinant Proteins	Species/Isotype	Dilution
anti-human BAG-6, D-1	mouse IgG	1 μg/ml
anti-human B7-H6, 1.45	mouse IgG	4 μg/ml
anti-human NKp30, P30-15, APC-conjugated	mouse IgG	1.25 μg/ml
anti-human NKp46, 9E2, APC-conjugated	mouse IgG	2.5 μg/ml
anti-mouse CD4, GK1.5, APC-conjugated	rat IgG	0.2 μg/ml
IgG1-FcEQ fusion proteins	human IgG	75 μg/ml

Table 8. Secondary antibodies used for flow cytometry.

Secondary Antibodies (Name, Clone, Conjugation)	Species/Isotype	Dilution
anti-human IgG-Fc, Alexa647-conjugated	goat IgG	15 μg/ml
anti-mouse IgG-Fc, Alexa546-conjugated	donkey IgG	10 μg/ml

Table 9. Isotype controls used for flow cytometry.

Isotype controls	Dilution
mouse IgG, MOPC-21, APC-conjugated	1.25-2.5 μg/ml

Table 10. Cell staining reagents used for flow cytometry.

Cell staining	Dilution
SYTOX Blue dead cell stain	1 μM

2.4.7 Immunofluorescence Microscopy

For immunofluorescence microscopy, $2*10^5$ adherent cells were seeded on Polysine® slides (Thermo Fisher Scientific) and incubated at 37°C for 16 h. Afterwards, cells were washed with PBS, fixed with FIX buffer for 10 min at room temperature, and blocked with IF buffer for 30 min at room temperature. For surface staining, cells were incubated with specific antibodies in IF buffer for 1 h. For intracellular staining, cells were permeabilized with IF-Perm buffer for 30 min and afterwards incubated with specific antibodies for 1 h at room temperature. Subsequently, cells were stained with DAPI solution (300 nM) and covered with

mounting medium. Brightfield and fluorescence images were obtained with a TCS-SP5 laser scanning microscope (Leica) using a HCX PL APO Lbd.Bl 63x/1.4-0.6 oil objective. Images were analyzed using LAS-AF lite 2.0 and ImageJ software.

Table 11. Primary antibodies used for immunofluorescence microscopy.

Primary Antibodies (Name, Clone, Conjugation)	Species/Isotype	Dilution
anti-human CD3ζ, 6B10.2, FITC-conjugated	mouse IgG	10 µg/ml
anti-human NKp30, P30-15, hybridoma	mouse IgG	0.73 µg/ml
anti-human NKp46, 195314	mouse IgG	5 µg/ml

Table 12. Secondary antibodies used for immunofluorescence microscopy.

Secondary Antibodies (Name, Clone, Conjugation)	Species/Isotype	Dilution
anti-mouse IgG-Fc, Alexa647-conjugated	goat IgG	10 µg/ml

Table 13. Isotype controls used for immunofluorescence microscopy.

Isotype controls (Name, Clone, Conjugation)	Dilution
mouse IgG, MOPC-21, FITC-conjugated	10 µg/ml

Table 14. Cell staining reagents used for immunofluorescence microscopy.

Cell staining	Dilution
DAPI	300 nM

2.4.8 Signaling Reporter Assay

Signaling reporter assays were carried out in two different settings. Reporter cells were mixed with equal amounts of Ba/F3 Mock or Ba/F3 B7-H6 cells or incubated in plates coated with the respective antibody against the receptor expressed on the reporter cell surface. For the first setting, reporter and target cells were washed with PBS and resuspended in A5-GFP medium. $5*10^4$ target cells were mixed with $5*10^4$ reporter cells in a final volume of 200 µl. For the second setting, plates were coated with 100 µl of anti-NKp30 or anti-NKp46 solution (5 µg/ml) for 2 h. Afterwards, $5*10^4$ reporter cells/well were added. In both cases, treatment of reporter cells with PMA and ionomycin (P/I) served as positive control and treatment of

reporter cells with A5-GFP medium alone served as negative control. After overnight incubation at 37°C, cells were stained with a CD4-specific antibody in FACS buffer to distinguish between reporter and target cells. Additionally, cells were incubated with SytoxBlue solution to exclude dead cells. GFP expression of the reporter cells was determined by flow cytometry (2.4.6). Reporter assays with Ba/F3 Mock or Ba/F3 B7-H6 cells, used in chapter 3.1.1 - 3.1.3 were performed by Sandra Weil.

Table 15. Primary antibodies used for signaling reporter assays.

Primary Antibodies (Name, Clone, Conjugation)	Species/Isotype	Dilution
anti-human NKp30, 210845	mouse IgG	5 μg/ml
anti-human NKp46, 195314	mouse IgG	5 μg/ml
anti-mouse CD4, GK1.5, APC-conjugated	rat IgG	0.2 μg/ml

Table 16. Cell staining reagents used for signaling reporter assays.

Cell staining	Dilution
SYTOX Blue dead cell stain	1 μM

2.5 Methods of Protein Biochemistry

2.5.1 Protein Purification

Soluble multivalent NCR::hIgG1-Fc (NCR-Fc) fusion proteins were produced in HEK 293T/17 cells. The Fc part of the fusion proteins contained two amino acid substitutions that reduce background binding to Fc receptors (L118E, N180Q, FcEQ) [208]. Proteins were purified from cell culture supernatant by protein A purification. All purification steps were performed on ice and with ice cold buffers. Proteins were produced as mentioned in 2.4.2 and 2.4.3, and the supernatant containing 0.01 % sodium azide, 1x cOmplete™ EDTA-free protease inhibitor cocktail (Roche) and 1 ml/L protein A sepharose® 4B conjugate (Life Technologies) was incubated on a tilt/roller mixer over night at 4°C. To purify the proteins, the suspension was applied onto an Econo-Pac column (Bio-Rad) including a bed support frit (30 μm, polyethylene) and the flow through was stored at 4°C until further analysis. Afterwards, protein A beads were washed with 40 column volumes of PBS. After washing, proteins were eluted with 20 column volumes of elution puffer by pH shift. To neutralize the pH of the eluted proteins, collection buffer (1/10 of the volume of the elution fraction) was added to the collection tube prior to elution. To concentrate the purified protein, the elution fraction was

applied to an Amicon Ultra-4 centrifugal filter unit (Merck Millipore) with the appropriate molecular weight cut-off (MWCO). The elution fraction was washed three times with PBS to exchange the buffer and concentrated ~ 20-fold. Protein concentration was either determined fluorometrically using the Qubit® 2.0 fluorometer and the Qubit Protein Assay kit according to manufacturers' instructions, or by enzyme-linked immunosorbent assay (ELISA; 2.5.6). Proteins were either short term stored at 4°C or frozen at -20°C. Repeated freezing and thawing was avoided. Samples of the whole purification process were taken for subsequent sodium dodecyl sulfate polyacrylamide gel electrophoresis (SDS-PAGE) and western blot analysis (2.5.3-2.5.5). Protein A beads were regenerated by adding 10 column volumes of regeneration buffer. Afterwards, beads were washed once, transferred to a reaction tube and stored in PBS.

2.5.2 Preparation of Cell Lysates

For preparation of membrane proteins from cell lysates, cells were detached and resuspended in membrane buffer containing 1x cOmplete™ EDTA-free protease inhibitor cocktail (300 µl buffer/90 mg cell pellet). The cell suspension was sonicated for 5 min at high power in a Bioruptor® (Diagenode Inc.) and centrifuged (21,255xg, 10 min, 4°C) to separate crude membranes from cytosolic proteins. The membrane pellet was resuspended in 1x SDS sample buffer, incubated at 37°C for 30 min and centrifuged. The supernatant was applied to SDS-PAGE (2.5.3).

2.5.3 SDS-Polyacrylamide Gel Electrophoresis (SDS-PAGE)

To prepare samples for SDS-PAGE, the protein solutions were mixed with either reducing or non-reducing SDS sample buffer. In case of reducing buffer, 200-300 mM dithiothreitol (DTT) was additionally added to the samples. Samples for reducing SDS-PAGE were heated for 10 min at 95°C in case of purified proteins (2.5.1) or for 30 min at 37°C in case of membrane protein samples (2.5.2).
Polyacrylamide gels were prepared according to table 17. The polyacrylamide concentration in the gels was dependent on the molecular weight of the proteins to be separated.

Table 17. Polyacrylamide gel composition. The specifications refer to the preparation of two gels (100 mm x 100 mm x 1 mm). TEMED: N, N, N', N'-tetramethylethylene-1,2-diamine, APS: ammonium persulfate.

Ingredients	Resolving Gel			Stacking Gel
	10 %	12 %	15 %	5 %
30 % acrylamide	3.3 ml	4.0 ml	5.0 ml	1.0 ml
H_2O	4.0 ml	3.3 ml	2.3 ml	4.0 ml
1.5 M Tris pH 8.8	2.5 ml	2.5 ml	2.5 ml	----
1.5 M Tris pH 6.8	----	----	----	750 µl
20 % SDS	50 µl	50 µl	50 µl	30 µl
10 % APS	100 µl	100 µl	100 µl	60 µl
TEMED	4 µl	4 µl	4 µl	6 µl

Electrophoresis was performed at 200 V in a Mini-PROTEAN® II electrophoresis cell (Bio-Rad) with SDS running buffer according to Laemmli [219]. Duration of the electrophoresis was dependent on the molecular weight of the proteins and the acrylamide concentration of the gel.

2.5.4 Coomassie Staining of Polyacrylamide Gels

Coomassie staining was used to visualize proteins on polyacrylamide gels. For this purpose, gels were stained with Instant*Blue*™ (Expedeon) for one to three hours at room temperature. Afterwards, gels were washed twice with water, to reduce background staining.

2.5.5 Western Blot

To specifically visualize proteins by immunostaining, western blot analysis was applied. In a first step, proteins were transferred from polyacrylamide gels onto nitrocellulose membranes. Therefor, a Trans-Blot® SD Semi-Dry transfer cell (Bio-Rad) was used according to manufacturers' instructions. In brief, one piece of blotting paper, the nitrocellulose membrane, the polyacrylamide gel, and another piece of blotting paper were stacked and every component was soaked with transfer buffer beforehand. Blotting was performed at 10 V for 20 min. To avoid unspecific antibody binding, membranes were then incubated in blocking buffer for at least one hour at room temperature. Afterwards, membranes were stained with the appropriate antibody (diluted in blocking buffer) for one hour. In case of

Strep-HRP, the staining reagent was diluted in TBS-T without skimmed milk powder to avoid background staining. After washing (3 times, TBS-T, 5-10 min, room temperature), antibodies bound to the membrane were detected using the Novex® ECL HRP Chemiluminescent Substrate Reagent kit (Thermo Fisher Scientific) or HRP-Juice kit (PJK) according to manufacturers' instructions. Chemiluminescence signals were detected using the FUSION FX system (Vilber Lourmat).

Table 18. Antibodies used for western blot analysis.

Antibody (Name, Clone, Conjugation)	Species/Isotype	Dilution
anti-human NKp30, polyclonal	goat IgG	1:1,000
anti-human NKp46, 195314	mouse IgG	1:500
anti-goat IgG-Fc, HRP-conjugated	donkey IgG	1:20,000
anti-human IgG-Fc, HRP-conjugated	goat IgG	1:10,000
anti-mouse IgG-Fc, HRP-conjugated	goat IgG	1:20,000
Streptavidin-HRP	streptavidin-polymer	1:1,000

2.5.6 Enzyme-linked Immunosorbent Assay (ELISA)

To determine concentrations of the Fc fusion proteins for surface plasmon resonance (SPR), ELISA plates were coated with 5 µg/ml mouse anti-human IgG over night at room temperature, blocked with 5 % BSA/PBS and incubated with ULBP2-Fc (R&D Systems) in 1:1 dilutions (250 ng/ml - 0.12 ng/ml, standard curve), or the Fc fusion protein solutions in duplicates. Every incubation step was performed for one hour. Wells were washed once with PBS-T between all incubation steps. The amount of bound Fc fusion protein was quantified using a goat anti-human IgG-HRP antibody and 3,3',5,5'-tetramethylbenzidine substrate (1-Step™ Ultra TMB-ELISA, Pierce) in a microtiter plate reader (λ = 450 nm). To stop the reaction, 50 µl of 1 N sulfuric acid were added per well. A standard curve was created from A_{450} values and concentrations of the ULBP2-Fc standard (R&D Systems). Concentrations of the samples were determined by comparison of A_{450} values of the samples to this standard curve.

Table 19. Antibodies used for ELISA.

Antibody (Name, Conjugation)	Species/Isotype	Diution
anti-human IgG-Fc, HRP-conjugated	goat IgG	1:50,000
anti-human IgG1-Fc	mouse IgG	5 µg/ml

2.5.7 Surface Plasmon Resonance (SPR)

To determine kinetic parameters (k_a, k_d) and equilibrium dissociation constants (K_D) for the interaction of the different NKp30-Fc mutants with the cellular ligand B7-H6, the Biotin CAPture kit (GE Healthcare) and the Biacore T200 system (GE Healthcare) were used according to manufacturers' instructions. Proteins were diluted in running buffer (PBS-T). 150-200 response units (RU) of biotinylated B7-H6-Fc protein were immobilized on a Sensor Chip CAP (GE Healthcare). Different analyte concentrations of the NKp30-Fc mutants were sequentially injected over the flow cells at 25°C and a flow rate of 30 µl/min in the single cycle kinetics model. To substract background, the analyte was additionally injected over a second flow cell which was only activated with Biotin CAPture Reagent. Sensograms were analyzed using Biacore T200 Evaluation Software version 2.0 (GE Healthcare). Reference surface data was subtracted from sample data and K_D values for the initial NKp30/B7-H6 interaction were determined by bivalent analyte fit. In this model, one analyte molecule (A) can bind to one or two ligand molecules (B) and both analyte binding sites are assumed to be equivalent.

$$A + B \underset{k_{d1}}{\overset{k_{a1}}{\rightleftharpoons}} AB$$

$$AB + B \underset{k_{d2}}{\overset{k_{a2}}{\rightleftharpoons}} AB_2$$

Kinetic parameters: k_{a1}: association rate constant for formation of AB
k_{a2}: association rate constant for formation of AB_2
k_{d1}: dissociation rate constant for complex AB
k_{d2}: dissociation rate constant for complex AB_2

K_D values were determined from the initial NKp30/B7-H6 interaction, as binding to the second site does not change the refractive index and therefore does not give rise to a response.

$$K_D = \frac{K_{d1}}{K_{a1}}$$

Table 20. Analyte concentrations used for SPR.

Protein	Concentrations [nM]
IFNAR2-hIgG1-FcEQ	512, 256, 128, 64, 32
NKp30-hIgG1-FcEQ	64, 32, 16, 8, 4
NKp30-K129A-hIgG1-FcEQ	512, 256, 128, 64, 32
NKp30-E130A-hIgG1-FcEQ	512, 256, 128, 64, 32
NKp30-H131A-hIgG1-FcEQ	512, 256, 128, 64, 32
NKp30-P132A-hIgG1-FcEQ	512, 256, 128, 64, 32
NKp30-Q133A-hIgG1-FcEQ	256, 128, 64, 32, 16
NKp30-L134A-hIgG1-FcEQ	256, 128, 64, 32, 16
NKp30-G135A-hIgG1-FcEQ	256, 128, 64, 32, 16
NKp30-G137A-hIgG1-FcEQ	256, 128, 64, 32, 16
NKp30-T138A-hIgG1-FcEQ	256, 128, 64, 32, 16
NKp30-V139A-hIgG1-FcEQ	64, 32, 16, 8, 4
NKp30-L140A-hIgG1-FcEQ	64, 32, 16, 8, 4
NKp30-L141A-hIgG1-FcEQ	64, 32, 16, 8, 4
NKp30-L142A-hIgG1-FcEQ	64, 32, 16, 8, 4
NKp30-R143A-hIgG1-FcEQ	64, 32, 16, 8, 4

3. Results

The NKp30 receptor on NK cells plays an important role for the recognition of target cells. Like other immunoreceptors, it associates with adaptor proteins for intracellular signaling [135,137,220]. The mechanism, how ligand binding at the ectodomain of NKp30 is communicated to the adaptor protein is still unknown. Formerly, it was shown that the stalk domain of the NKp30 protein contributes to ligand binding and signaling [208]. Based on these results, this thesis aimed to investigate the influence of the stalk domain on NKp30 function in more detail. Furthermore, as knowledge about cancer-associated NKp30 ligands is still scarce, the existence of other, yet unknown cellular NKp30 ligands was examined by implementation of a genome-wide shRNA screening. Additionally, the evolutionary role of the NKp30 protein was analyzed on the example of *M. musculus*, where NKp30 is only present as a non-expressed pseudogene. Parts of this thesis are published in Memmer *et al.* (2016) [221].

3.1 Contribution of the Stalk Domain of NKp30 to Ligand Binding and Signaling

Signaling of the NCRs is mediated by the association with ITAM bearing adaptor molecules like CD3ζ/FcεRIγ (NKp30 and NKp46) or DAP12 (NKp44) [135,137,220]. The functional importance of this interaction is illustrated by the finding that NK cells from knockout mice lacking CD3ζ and FcεRIγ showed reduced cytotoxic activity against a large number of tumor cell lines [222]. Moreover, previous studies showed a reduced number of T cell receptor (TCR) molecules on the surface of T cells, due to intracellular TCR retention in the absence of CD3ζ [223–225]. The nuclear magnetic resonance (NMR) structure of a disulfide-stabilized transmembrane helix dimer of CD3ζ shows two aspartate residues in the proximity of the outer membrane leaflet (PDB: 2HAC) [226]. These amino acids are believed to form an intramembrane charge contact with positively charged residues in the transmembrane region of the TCR α chain, NKp30 and NKp46 [137,227]. Previous studies from our group showed that the stalk domain of NKp30 increases the affinity for binding of its cognate ligands B7-H6 and BAG-6 and the signaling capacity of the receptor [145,208]. Despite this, not much is known about the interaction of immunoreceptor and adaptor protein that initiates signaling.

3.1.1 Analysis of NKp30/NKp46 Chimera

To shed more light on the initial steps of NKp30 signaling, and especially on the role of the stalk domain in this process, chimeric NKp30/NKp46 receptors were constructed and analyzed. Even though NKp30 and NKp46 differ in their number of Ig domains and the sequence and length of their stalk domains, they both signal via the same adaptor proteins.

Although the stalk domain of NKp46 is much longer than the stalk domain of NKp30, there is a conserved sequence motif in the membrane-proximal regions of both receptors [$K^{129/244}$(-)$HX_9LLR^{143/258}$, (-) indicates a negatively charged amino acid; appendix, 6.3]. To analyze if the extracellular domains (Ig-fold and stalk) of NKp30 and NKp46 represent individual functional entities or if sequence stretches are interchangeable, A5-GFP reporter cells were transduced with chimeric receptors containing exchanged Ig domains or exchanged stalk domains in the NKp30 and NKp46 extracellular regions (Fig. 10 A). Notably, the N-terminal end of the stalk domain was determined by the C-terminal end of the Ig-fold (resolved in the crystal structure), and the border between stalk and TM domain was predicted using TMpred [208,228]. Expression and plasma membrane targeting of the NCR chimera or their wildtype counterparts was analyzed by flow cytometry (Fig. 10 B).

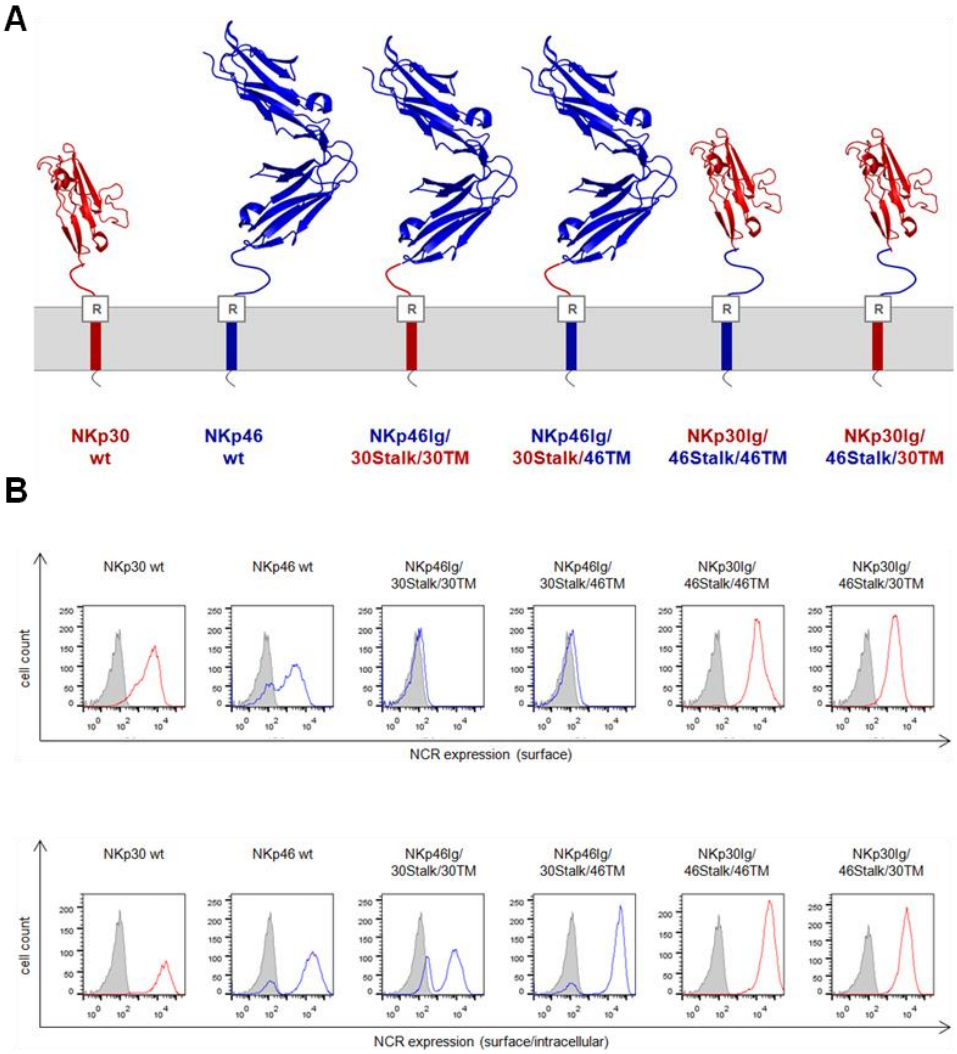

Figure 10. Expression of NKp30/NKp46 chimera in A5-GFP cells. (A) Schematic representation of NKp30 wildtype (wt) (red, PDB: 3NOI), NKp46 wt (blue, PDB: 1P6F) and NKp30/NKp46 chimera (NKp30 domains in red, NKp46 domains in blue) in the plasma membrane (grey). (B) Surface and intracellular expression of the receptors and corresponding NKp30/NKp46 chimera in transduced A5-GFP cells, analyzed by flow cytometry. Grey: Mock control, red: anti-NKp30, blue: anti-NKp46. One representative experiment out of three is shown.

Even though all of the NCR constructs were detectable intracellularly, only the wildtype NCRs and chimera containing the Ig domain of NKp30 and the stalk of NKp46 (NKp30Ig/46Stalk/46TM and NKp30Ig/46Stalk/30TM) were targeted to the plasma membrane, while chimera containing the Ig domain of NKp46 and the stalk of NKp30 (NKp46Ig/30Stalk/30TM and NKp46Ig/30Stalk/46TM) were intracellularly retained. This shows that the stalk domain of NKp46 is compatible with NKp30 maturation, whereas the stalk domain of NKp30 is unable to maintain folding, plasma membrane targeting and retention of NKp46.

In a next step, the NCR chimera and their wildtype counterparts were analyzed for their signaling capacity in signaling reporter assays. A5-GFP reporter cells are murine T cells that were transduced with a reporter cassette and carry the genetic information for GFP under the IL-2 promoter. Signaling via the CD3ζ chain activates the transcription factor NF-AT, which binds to three NF-AT binding sites in the IL-2 promoter region and initiates GFP expression [211,212]. In a first setting, reporter cells transduced with NCR variants were incubated in plates coated with either anti-NKp30- or anti-NKp46-specific antibodies and subsequently analyzed by flow cytometry. In this setting, signaling of the constructs could be analyzed in a ligand-independent way via antibody crosslinking and therefore independent of the receptors affinity for their corresponding ligands (Fig. 11).

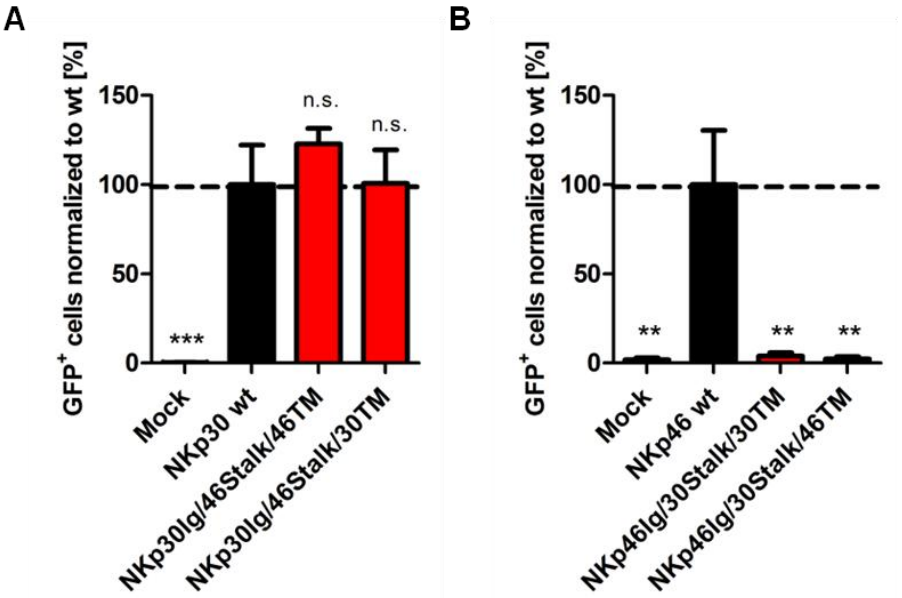

Figure 11. Antibody-induced signaling of NKp30/NKp46 chimera. Signaling reporter assays of transduced A5-GFP cells after stimulation with plate-bound NKp30-specific (A) or NKp46-specific (B) antibodies (antibody epitopes are located in the Ig-fold of the respective NCR). GFP expression was analyzed by flow cytometry of $CD4^+$/$SytoxBlue^-$ A5-GFP cells. The percentage of GFP-positive cells normalized to NKp30 wt is indicated as mean ± SEM of 3 independent experiments measured in duplicates. Statistical significance of flow cytometry experiments was assessed by one-way ANOVA and Dunnett's multiple comparisons test with Prism 6 software. n.s., not significant, $p>0.05$; **, $p=0.001-0.01$; ***, $p=0.0001-0.001$.

Interestingly, both chimera containing the Ig domain of NKp30 and the stalk domain of NKp46 (NKp30Ig/46Stalk/46TM and NKp30Ig/46Stalk/30TM) showed receptor signaling comparable to NKp30 wt (Fig. 11 A). Signaling capacity after antibody crosslinking demonstrates principal functionality of these chimera with respect to signaling via CD3ζ. As expected, no signaling was observed for A5 cells expressing NKp46Ig/30Stalk/30TM or NKp46Ig/30Stalk/46TM (Fig. 11 B), which were both retained intracellularly and thus not present on the plasma membrane.

The next question was, if the NCR chimera containing the Ig domain of NKp30 and the stalk domain of NKp46 are able to perform ligand-induced signaling. Therefore, NCR-transduced A5-GFP cells were co-cultured with Ba/F3 target cells either transduced with the NKp30 ligand B7-H6 or Mock virus as negative control, which was described elsewhere [145,208]. Surprisingly, B7-H6 was unable to induce CD3ζ signaling and proportional GFP expression of the two chimera containing the Ig domain of NKp30 and the stalk of NKp46 (Fig. 12). Notably, none of the NCR transduced reporter cell lines showed signaling after co-incubation with Mock transduced Ba/F3 cells.

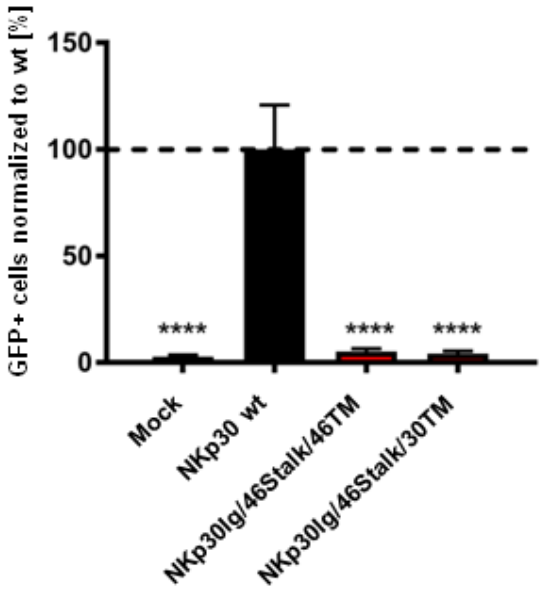

Figure 12. Ligand-induced signaling of NKp30/NKp46 chimera. Signaling reporter assays of transduced A5-GFP cells after co-incubation with Ba/F3 B7-H6 cells. GFP expression was analyzed by flow cytometry of $CD4^+$/$SytoxBlue^-$ A5-GFP cells. The percentage of GFP-positive cells normalized to NKp30 wt is indicated as mean ± SEM of 3 independent experiments measured in duplicates. Statistical significance of flow cytometry experiments was assessed by one-way ANOVA and Dunnett's multiple comparisons test with Prism 6 software. ****, $p<0.0001$.

Due to these results, it was questionable if the impaired capacity for ligand-induced signaling might result from a reduced binding affinity for B7-H6. To exclude this, cells carrying the chimera or wildtype NKp30 were decorated with soluble B7-H6-Fc fusion proteins (Fig. 13). Interestingly, surface expression of the NKp30Ig/46Stalk/46TM mutant was much higher while surface expression of the NKp30Ig/46Stalk/30TM mutant was much lower than surface expression of wildtype NKp30 (red bars). These differences are also visible in total protein expression levels (surface and intracellular, compare to Fig. 10) and therefore do not result from differences in plasma membrane targeting. In all of the constructs, a correlation of

NKp30 expression and B7-H6 binding (red and black bars) was visible, indicating that signaling of the mutants is not influenced by impaired ligand binding.

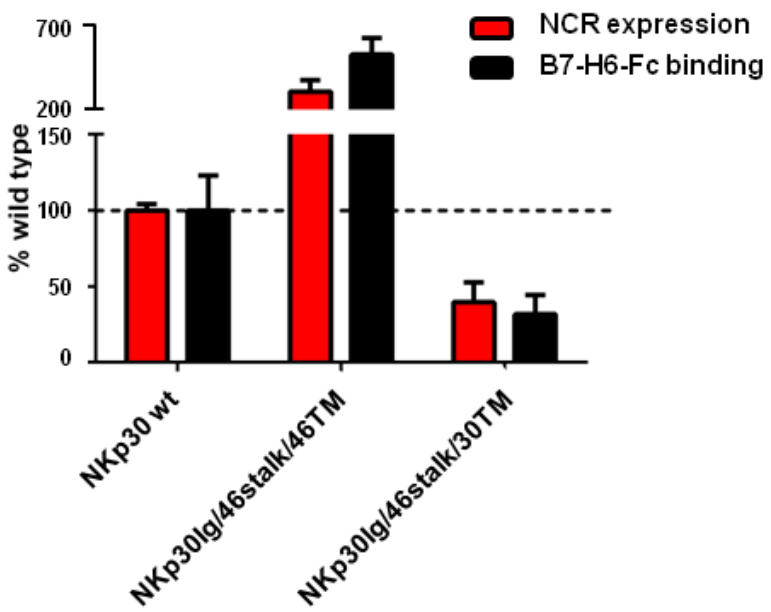

Figure 13. B7-H6 binding to NKp30/NKp46 chimera correlates with plasma membrane expression levels of the NCRs. Surface expression of NCR variants on transduced A5-GFP cells and binding of B7-H6-Fc fusion protein to these A5-GFP cells were analyzed by flow cytometry and related to plasma membrane expression levels and B7-H6-Fc binding capacity of NKp30 wt. Red bars: NCR expression based on NKp30-specific antibodies, black bars: B7-H6-Fc binding after detection with hIgG1-Fc-specific antibodies. Results are shown as mean ± SEM of one representative experiment measured in duplicates.

Altogether, this indicates that the Ig domain and the stalk domain of NKp30 and presumably NKp46 are a functional entity, mediating ligand-induced conformational changes required for CD3ζ signaling. In contrast, signaling capacity does not seem to depend on a cognate TM domain as no differences in signaling are visible between NKp30Ig/46Stalk/46TM and NKp30Ig/46Stalk/30TM. Moreover, as the stalk domain of NKp46 can substitute for the stalk domain of NKp30 during antibody crosslinking, but not during ligand-induced signaling, it seems that both stalk domains contain a sequence motif needed for signaling in general but not sufficient for ligand-induced signaling. This might be the above mentioned membrane-proximal $K^{129/244}$(-)$HX_9LLR^{143/258}$ motif, which is preserved in NKp30 and NKp46. Additionally, these results show that the mechanism of signaling after antibody mediated crosslinking is different from the mechanism of ligand-induced signaling and can not picture the physiological interaction.

3.1.2 Contribution of Individual Amino Acids within the Stalk Domain to Ligand Binding and Signaling

Data from the NKp30/NKp46 chimera implicated the existence of specific sequence motifs in the stalk domain of NKp30 that are required for receptor function. Therefore, in a next step the specific contribution of individual stalk amino acids to ligand binding and signaling was analyzed by systematic alanine scanning mutagenesis. In this approach, the amino acids to be analyzed are sequentially replaced by alanine. Replacement by alanine eliminates the side chain at the β carbon but does not alter the main chain conformation, as replacement by glycine or proline would. Additionally, it does not lead to extreme electrostatic or steric effects [229]. In this approach, wildtype NKp30 and 14 NKp30 alanine mutants were produced as soluble NKp30-Fc fusion proteins and as full length receptor constructs.

To analyze the effects of the different alanine substitutions on B7-H6 binding, fusion proteins of the NKp30 ectodomain and the Fc part of human IgG1 were used. Similar soluble multivalent Fc fusion proteins were shown to be valuable tools to study receptor/ligand interactions *in vitro* [146,153,230]. The Fc parts of the fusion proteins contained two amino acid substitutions (FcEQ: L118E, N180Q) for reduced background binding to Fc receptors [208]. For the production, 293T/17 cells were transiently transfected with the different constructs and the secreted Fc fusion proteins were purified from cell culture supernatants via protein A sepharose. The predicted molecular weight of the proteins was 39.8 kDa, but due to N-linked glycosylation, the apparent molecular weight in SDS-PAGE was around 50-55 kDa. Fusion proteins of the different NKp30 alanine mutants as well as wildtype NKp30 displayed comparable apparent molecular weight as expected (Fig. 14 A). Assembly of an intermolecular disulfide bridge between the Fc parts of two Fc fusion proteins led to the formation of homodimers as seen by comparison of reducing and non-reducing SDS-PAGE (Fig. 14 A/B). Under non-reducing conditions, a second signal was visible with approximately twice the size of the homodimer, which might be an aggregated form of the protein. Interestingly, the R143A mutant showed a bigger portion of putatively aggregated protein compared to the other mutants.

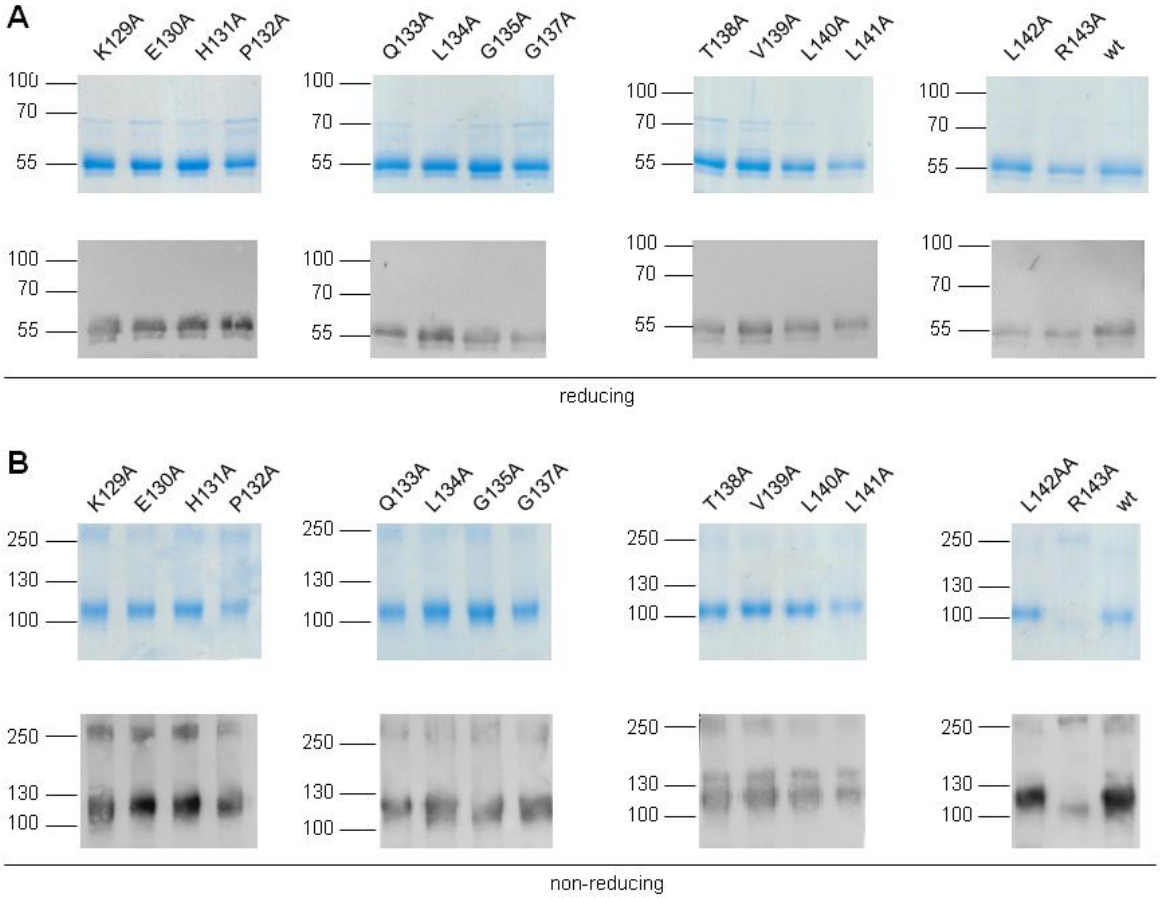

Figure 14. Purified soluble multivalent NKp30-Fc fusion proteins. (A) Reducing (+DTT) and (B) non-reducing (-DTT) coomassie-stained SDS-PAGE and corresponding western blots of mutant NKp30-Fc fusion proteins. 2 µg of Fc fusion protein were used for coomassie-stained SDS-PAGE and 0.5 µg were used for western blot analysis. Blots were detected using an HRP-conjugated anti-human IgG1-Fc antibody.

To determine kinetic parameters (k_a and k_d) and equilibrium dissociation constants (K_D) for binding of NKp30 wt and the different alanine mutants to B7-H6, surface plasmon resonance (SPR) was applied. For this purpose, a biotinylated fusion protein of the B7-H6 ectodomain fused to human IgG1-Fc (B7-H6-Fc-Bio) was produced (Fig. 15). The protein was detectable in coomassie-stained SDS-PAGE and presence of the human IgG1-Fc part (anti-human IgG1-Fc-HRP) as well as presence of the biotinylation (streptavidin-HRP) was verified by western blot analysis. As visible under reducing conditions, B7-H6-Fc-Bio has an apparent molecular weight of 80-100 kDa whereas the predicted molecular weight is 56 kDa. This indicates that the protein is present in a highly glycosylated form, which is in accordance with the fact that the ectodomain of B7-H6 is reported to contain nine potential N-glycosylation sites [142]. In addition, assembly of homodimers was verified under non-reducing conditions, where the protein showed an apparent molecular weight of roughly 200-250 kDa.

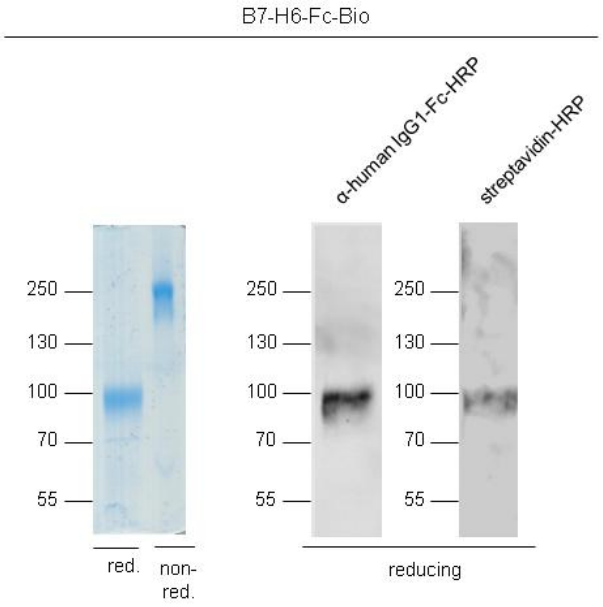

Figure 15. B7-H6-Fc-Bio is biotinylated and highly glycosylated. Reducing (+DTT) and non-reducing (-DTT) coomassie-stained SDS-PAGE and corresponding western blot detection of B7-H6-Fc-Bio fusion proteins. 2 µg of Fc fusion protein were used for coomassie-stained SDS-PAGE and 0.5 µg were used for western blot analysis. Blots were detected using an HRP-conjugated anti-human IgG1-Fc antibody and HRP-conjugated streptavidin. red.: reducing.

For SPR measurements, the biotinylated B7-H6-Fc fusion protein (ligand) was immobilized on the sensor chip via a biotin-streptavidin interaction. Afterwards, different concentrations of the NKp30-Fc mutants (analyte) were sequentially injected over the flow cells. As both, NKp30 and B7-H6 were present as Fc fusion proteins, data was fitted with the bivalent analyte model. According to Chi^2 values, bivalent analyte fit was sufficient for all sensograms (Tab. 21). A K_D value of 84.8 nM was obtained for NKp30 wt (Tab. 21 and appendix, 6.4), which was in accordance with previous measurements of NKp30-Fc fusion proteins [208]. Comparison of the alanine mutants showed that mutation of the amino acids close to the Ig-fold had the most drastic effect, leading to K_D values in the micromolar range (K129A: 2.6 µM, E130A: 2.4 µM, H131A: 1.7 µM). The greater the distance between the alanine mutation and the Ig-fold, the less prominent was the effect on K_D values. Alanine mutations of the membrane-proximal amino acids showed K_D values similar to NKp30 wt (V139A: 36.3 nM, L140A: 39.1 nM, L141A: 79.7 nM, L142A: 44.5 nM) except for the R143A mutant, which displayed a slightly higher K_D value (253.9 nM). Altogether, this is in line with the fact that B7-H6 binds to the Ig-fold of NKp30 and influence of the mutations decreases with increasing distance from the binding pocket.

Table 21. Kinetic parameters (association rate constant [k_a], dissociation rate constant [k_d]) and equilibrium dissociation constants (K_D) for binding of NKp30 variants to B7-H6 as determined by SPR.

NKp30 variant	k_{a1}[1/Ms]	k_{d1}[1/s]	K_D	k_{a2}[1/RUs]	k_{d2}[1/s]	R_{max}[RU]	Chi^2
wt	$1.848x10^5$	0.01568	84.8 nM	$1.695x10^{-4}$	$4.747x10^{-4}$	29.51	0.0450
K129A	$3.983x10^3$	0.01024	2.6 µM	$1.010x10^{-4}$	$3.565x10^{-4}$	82.87	0.200
E130A	$1.067x10^{-4}$	0.02601	2.4 µM	$2.819x10^{-4}$	$1.754x10^{-4}$	151.4	0.266
H131A	$4.317x10^3$	0.007382	1.7 µM	$1.251x10^{-4}$	$2.043x10^{-4}$	92.42	0.141
P132A	$2.239x10^5$	0.01715	76.6 nM	$2.038x10^{-4}$	$7.947x10^{-4}$	79.02	0.819
Q133A	$2.672x10^3$	0.02109	7.9 µM	$2.927x10^{-4}$	$2.683x10^{-4}$	36.05	0.0672
L134A	$1.854x10^5$	0.02435	131.3 nM	$2.622x10^{-4}$	$6.582x10^{-4}$	82.98	1.5
G135A	$7.102x10^3$	0.005343	752.3 nM	$3.222x10^{-4}$	$2.295x10^{-4}$	178.6	0.0825
G137A	$8.123x10^4$	0.005512	67.9 nM	0.002121	0.004202	71.58	3.16
T138A	$9.709x10^3$	0.006610	680.8 nM	$4.297x10^{-4}$	$4.354x10^{-4}$	13.13	0.274
V139A	$4.008x10^5$	0.01453	36.3 nM	$1.432x10^{-4}$	0.001044	68.01	0.414
L140A	$4.527x10^5$	0.01768	39.1 nM	$2.254x10^{-4}$	0.001179	19.99	0.0296
L141A	$1.930x10^5$	0.01538	79.7 nM	$1.855x10^{-4}$	$5.017x10^{-4}$	25.05	0.0224
L142A	$3.830x10^5$	0.01705	44.5 nM	$1.894x10^{-4}$	$5.507x10^{-4}$	23.29	0.0466
R143A	$3.622x10^4$	0.009299	253.9 nM	$2.068x10^{-4}$	$3.115x10^{-4}$	46.95	0.0075

To investigate whether ligand binding of the individual NKp30 alanine mutants is correlated with their capacity to promote CD3ζ signaling, A5-GFP cells were transduced with the respective full length receptor constructs, and signaling reporter assays were performed by stimulation with plate-bound NKp30-specific antibodies or Ba/F3 B7-H6 cells. Ligand-induced signaling of NKp30 after stimulation with Ba/F3 B7-H6 cells was significantly reduced by alanine mutation at any of the amino acid positions within the stalk domain (Fig. 16 A). Most drastic loss of function was visible for the two amino acids at the transition of the N-terminal Ig domain and the stalk domain of NKp30 (K129A: 27.6 % and E130A: 37.0 % GFP^+ cells normalized to wildtype) and two of the three C-terminal leucine residues at the transition between the stalk domain and the transmembrane domain (L140A: 30.0 % and L141A: 36.3 % GFP^+ cells normalized to wildtype). Mutation of R143, which is believed to mediate an intramembrane charge contact with CD3ζ, and mutation of L142 led to a complete loss of

signaling capacity (R143A: 2.5 % and L142A: 11.1 % compared to Mock control: 8.0 % GFP$^+$ cells normalized to wildtype; Fig. 16 A).

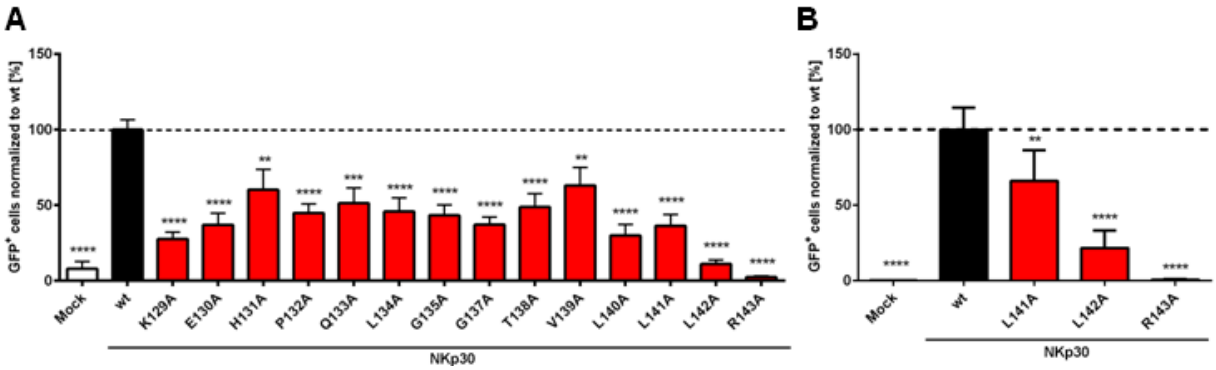

Figure 16. Contribution of individual amino acids of the NKp30 stalk to signaling. A5-GFP cells transduced with the different NKp30 alanine mutants were analyzed for their signaling capacity after co-incubation with Ba/F3 B7-H6 cells (A) or after stimulation with plate-bound NKp30-specific antibodies (B). GFP expression was analyzed by flow cytometry of CD4$^+$/SytoxBlue$^-$ A5-GFP cells. The percentage of GFP-positive cells normalized to wildtype is indicated as mean ± SEM of 3 independent experiments measured in duplicates. Statistical significance of flow cytometry experiments was assessed by one-way ANOVA and Dunnett's multiple comparisons test with Prism 6 software. **, p=0.001-0.01; ***, p=0.0001-0.001; ****, p<0.0001.

Notably, signaling reporter assays were performed at saturating conditions for more than 12 hours, therefore excluding that slight differences in expression levels of the NKp30 variants might affect determination of their signaling capacity. Impaired signaling of the mutants can be due to (1) a failure to mediate ligand-induced conformational changes, needed for signaling, or (2) a lack of specific motifs that are generally needed for communication with CD3ζ. To evaluate this, signaling reporter assays were performed after receptor stimulation with plate-bound NKp30-specific antibodies (Fig. 16 B). Interestingly, also in this setting, the L141A and L142A mutants showed reduced signaling capacity (L141A: 66.0 % and L142A: 21.6 % GFP$^+$ cells normalized to wildtype) and the NKp30 variant devoid of R143 showed no CD3ζ signaling (R143A: 0.6 % compared to Mock: 0.1 % GFP$^+$ cells normalized to wildtype). This demonstrates that the impaired signaling of L141A, L142A and R143A is due to a loss in signaling capacity in general. This again speaks for the importance of the conserved $K^{129/244}$(-)$HX_9LLR^{143/258}$ motif in the stalk domains of NKp30 and NKp46. Notably, L141, L142 and R143 in the NKp30 stalk are also highly conserved among species (compare to Fig. 32).

In order to investigate whether ligand-induced NKp30 signaling requires the side chain of R143 or only a positively charged residue at position 143, another NKp30 variant was produced, where R143 was substituted by a lysine (R143K). Surprisingly, the signaling capacity of the R143K mutant was maintained or even improved when compared to NKp30 wt after stimulation with Ba/F3 B7-H6 cells (Mock: 2.8 %, and R143K: 132.9 % GFP$^+$ cells normalized to wildtype; Fig. 17). This demonstrates that a positive charge at position 143 is essential and sufficient for NKp30 function. The evolutionary reason why NKp30, as

well as other immunoreceptors, contain a charged arginine instead of a lysine for interaction with CD3ζ is unknown. Even though lysine seems to be advantageous for signaling capacity, there might be other effects, like decreased protein stability, that negatively influence the receptor and that are not visible in overexpression experiments.

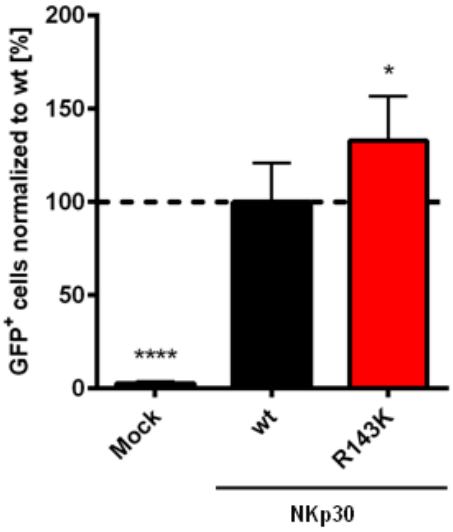

Figure 17. A positive charge at position 143 is essential and sufficient for NKp30 function. A5-GFP cells transduced with a lysine mutant of R143 (R143K) were analyzed for their signaling capacity after co-incubation with Ba/F3 B7-H6 cells. GFP expression was analyzed by flow cytometry of $CD4^+$/$SytoxBlue^-$ A5-GFP cells. The percentage of GFP-positive cells normalized to wildtype is indicated as mean ± SEM of 3 independent experiments measured in duplicates. Statistical significance of flow cytometry experiments was assessed by one-way ANOVA and Dunnett's multiple comparisons test with Prism 6 software. *, p=0.01-0.05; ****, p<0.0001.

3.1.3 Involvement of Transmembrane and Cytosolic Residues in Signaling

Based on the results from NKp30/NKp46 chimera and NKp30 alanine scanning mutants, it became obvious that a conserved sequence motif in the stalk domain of NKp30 (and the membrane-proximal stalk region of NKp46) is important for signaling capacity. Moreover, a positive charge on amino acid position 143 was shown to be essential for signaling. As TMpred analysis predicts R143 to be located outside of the membrane, it was hypothesized that ligand binding initiates a stalk-dependent shift of the transmembrane region of NKp30 in order to burry R143 more deeply into the membrane, thereby facilitating the association with CD3ζ. Presumably, such a register shift might expose residues from the lipid interface to secondary effector molecules in the cytoplasm. Therefore, signaling contributions of amino acids in the proximity of R143 and at the transition of transmembrane domain and cytosolic domain of NKp30 were investigated (Fig. 18).

First, it was analyzed whether the tyrosine residues Y161 and Y162, which are located near the border between transmembrane and cytosolic region of NKp30, contribute to signaling. It was assumed that a ligand-induced conformational change in NKp30 might expose the two tyrosines to the cytoplasm, facilitate their potential phosphorylation and thereby start signaling cascades. To analyze if this was the case, either one or both of the tyrosines were substituted by phenylalanine (Y161F, Y162F, Y161F/Y162F; Fig. 18 A). As phenylalanine has a similar aromatic side chain as tyrosine but lacks the hydroxyl group, this kind of mutation prevents phosphorylation and can be used to analyze the contribution of tyrosine phosphorylation in signaling cascades. Surface expression of the mutants was analyzed by

flow cytometry, confirming similar expression levels (Fig. 18 B). Interestingly, the mutations even slightly enhanced signaling capacity of the receptor in reporter assays with Ba/F3 B7-H6 target cells (Mock: 2.8 %, Y161F: 133.0 %, Y162F: 143.3 % and Y161F/Y162F: 137.1 % GFP$^+$ cells normalized to wildtype; Fig. 18 C). This shows that Y161 and Y162 do not contribute to NKp30/CD3ζ signaling.

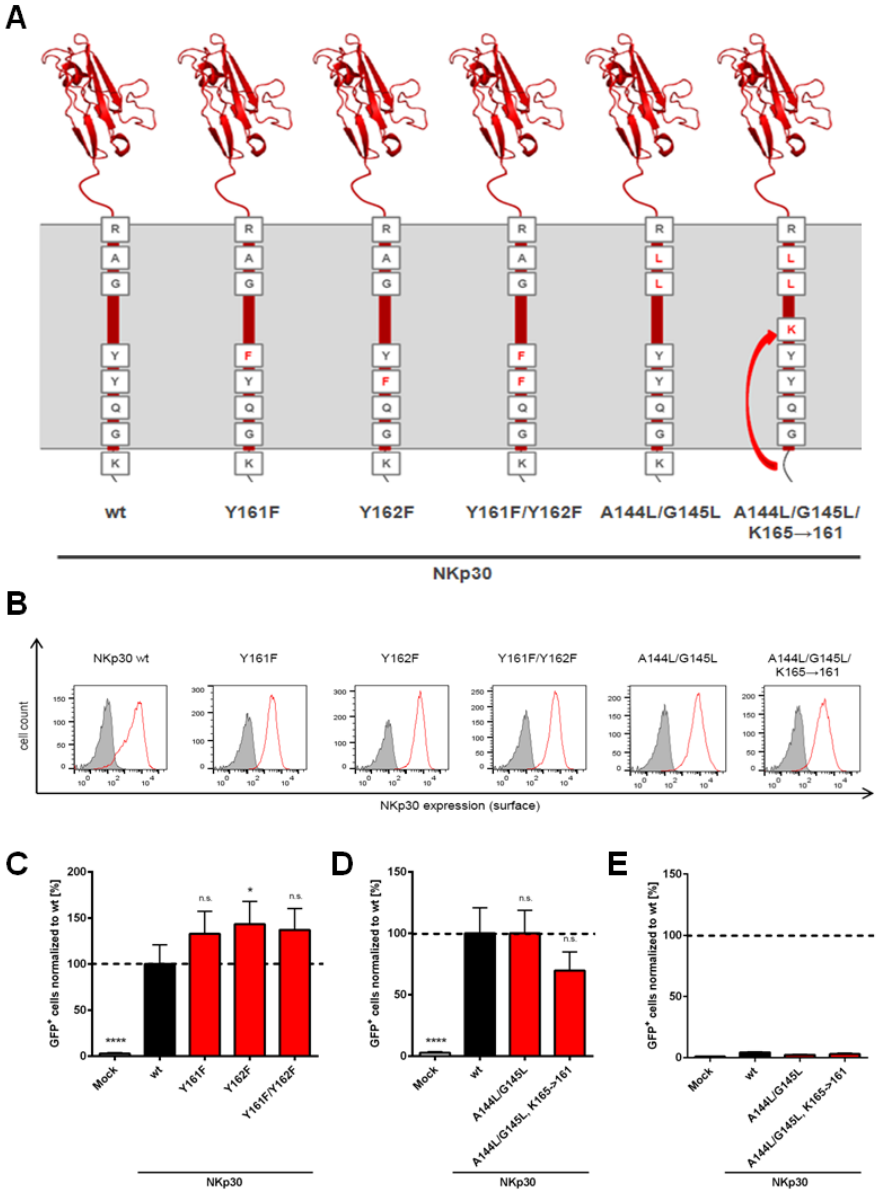

Figure 18. Influence of specific amino acids within, or in the vicinity of the transmembrane domain of NKp30 on CD3ζ signaling. (A) Schematic representation of NKp30 wt (PDB: 3NOI) and NKp30 mutants in the plasma membrane. Wildtype amino acids are shown in black, mutated amino acids are shown in red. (B) Surface expression of the receptor mutants in A5-GFP cells analyzed by flow cytometry. Grey: isotype control, red: anti-NKp30. One representative experiment out of three is shown. (C/D) A5-GFP cells transduced with the different receptor mutants were analyzed for their signaling capacity after co-incubation with Ba/F3 B7-H6 cells. GFP expression was analyzed by flow cytometry of CD4$^+$/SytoxBlue$^-$ A5-GFP cells. The percentage of GFP-positive cells normalized to wildtype is indicated as mean ± SEM of 3 independent experiments measured in duplicates. Statistical significance of flow cytometry experiments was assessed by one-way ANOVA and Dunnett's multiple comparisons test with Prism 6 software. (E) Same experiment as in D, A5-GFP cells were co-incubated with Ba/F3 Mock cells. GFP expression was analyzed by flow cytometry of CD4$^+$/SytoxBlue$^-$ A5-GFP cells and normalized to the percentage of GFP-positive NKp30 wildtype cells after co-incubation with Ba/F3 B7-H6 cells. n.s., not significant, p>0.05; *, p=0.01-0.05; ****, p<0.0001.

As the leucine residues preceding R143 (L140, L141 and L142) were found to be intolerant to alanine substitution (compare to Fig. 16), it was suggested that these residues might play a role for the relocation of R143 after ligand binding. A shift of R143 more deeply into the membrane might require strong forces to overcome charge repellence of the hydrophobic membrane interface. This might be achieved by ligand-induced receptor oligomerization [209,231] and an unpolar “lid” generated by L140, L141 and L142, that shields the positive charge of R143 from the hydrophobic transmembrane region. To verify this, it was tested if substitution of the two amino acids succeeding R143 by leucine could reduce charge repellence of R143 and thereby render NKp30 signaling independent from ligand binding (A144L/G145L; Fig. 18 A). This would lead to constitutive GFP expression of the reporter cells even in the absence of a stimulating ligand. Wildtype NKp30 and the A144L/G145L mutant were expressed equally well in A5-GFP reporter cells (Fig. 18 B). Interestingly, the double mutant showed no increase in signaling capacity after co-incubation with Ba/F3 B7-H6 target cells (A144L/G145L: 100.1 % GFP^+ cells normalized to wildtype; Fig. 18 D) and no GFP expression (signaling) without ligand stimulation (after co-incubation with Ba/F3 Mock target cells; Fig. 18 E).

Prediction of NKp30’s transmembrane region based on TMpred [228] suggests that the transmembrane domain is anchored between two flanking positive charges (R143 and K165). Therefore, it was analyzed if a combined mutation of A144 and G145 to leucine and a shift of K165 to amino acid position 161 (A144L/G145L/K165→161; Fig 18 A) uncouples signaling from ligand binding and forces R143 into the inner core of the membrane for permanent contact with CD3ζ. While expression of the A144L/G145L/K165→161 construct was preserved (Fig. 18 B), only moderate reduction of signaling capacity after co-incubation with Ba/F3 B7-H6 cells (A144L/G145L/K165→161 69.7 % GFP^+ cells normalized to wildtype; Fig. 18 D) and no signaling without ligand stimulation (Fig. 18 E) were observed. Interestingly, in addition it was not possible to uncouple receptor signaling from ligand binding by systematically shifting R143 towards the C-terminus of NKp30 while simultaneously preserving the sequence order of the transmembrane domain, as none of the mutants was targeted to the plasma membrane (experiments performed by Sandra Weil, AG Koch). This demonstrates that a positive charge might not be permanently tolerated within the inner core of NKp30’s transmembrane domain.

Altogether, these data argue for a strong charge repellence, which keeps the side chain of R143 at the transition interface between extracellular region and membrane. Alignment of R143 with the aspartate of CD3ζ to enable signaling might be achieved by ligand-induced receptor clustering and/or stalk-dependent conformational changes.

3.1.4 N-Glycosylation Scanning to Analyze the Positioning of Key Amino Acids in NKp30 and NKp46

To investigate if a stalk-dependent conformational change might occur that leads to a temporary alignment of R143 with the aspartate of CD3ζ, it was necessary to analyze the positioning of R143 in ground state. For this purpose, N-glycosylation scanning was performed. N-glycosylation of eukaryotic membrane proteins is catalyzed by a membrane-associated oligo saccharyl transferase (OST) complex in the lumen of the endoplasmic reticulum (ER). The OST complex transfers an oligosaccharide to the side chain of an asparagine (N) acceptor in the N-X-S/T motif (where X can be every amino acid except for proline). According to the 12+14 rule, such an acceptor site must be placed a minimum of 14 amino acids N-terminal or 12 amino acids C-terminal from the membrane surface to be N-glycosylated, as the active site of the OST complex is positioned a certain distance away from the ER membrane [232]. This minimal distance can be used to map the ends of TM segments of membrane proteins [233–235]. Therefore, N-glycosylation scanning introduces N-glycosylation acceptor sites 14 amino acids N-terminal or 12 amino acids C-terminal from the amino acid to be analyzed. The addition of an oligosaccharide adds about 2 kDa to the protein and is visible as motility shift in SDS-PAGE. While the presence of glycosylation indicates that the amino acid to be analyzed is located outside of the plasma membrane, the absence of glycosylation is not that conclusive as it might be due to the fact that the used N-X-S/T motif is an inefficient acceptor site or is located too close to the membrane [233].

In this thesis, the N-glycosylation scanning method was used to analyze the positioning of key amino acids that were assumed to be located near the interface between extracellular and membrane region of NKp30 (L140, R143, Y147) and the corresponding region of NKp46 (N255, R258, A262). Therefor, N-gylcosylation acceptor sites were introduced 14 amino acid positions N-terminal from each residue to be analyzed (Fig. 19).

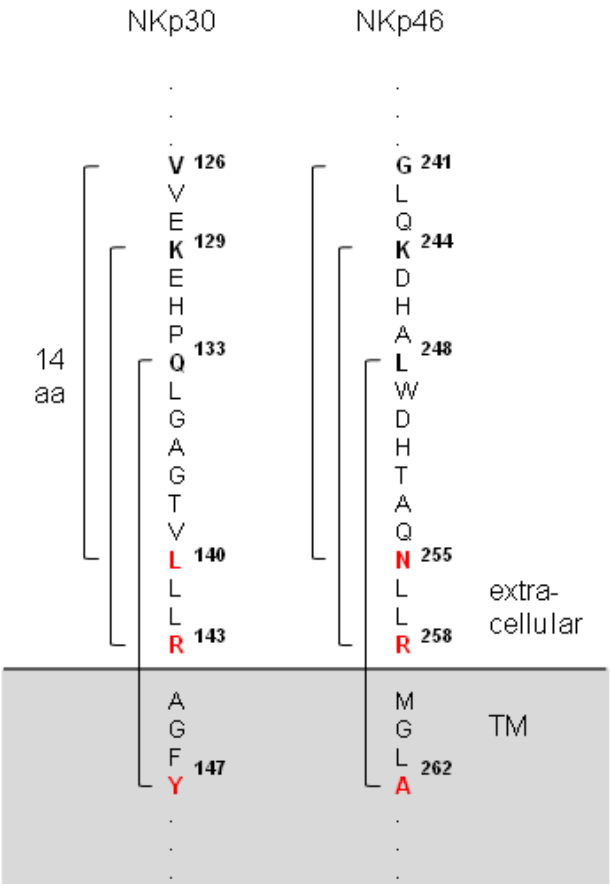

Figure 19. Schematic representation of the N-glycosylation scanning. Amino acids mutated to N-glycosylation acceptor sites are shown in bold black, amino acids to be analyzed at the membrane transition interface are shown in bold red. Brackets indicate the 14 amino acid distance between N-glycosylation sites and the amino acids to be analyzed.

293T/17 cells were lentivirally transduced with the different NKp30 and NKp46 constructs and analyzed for receptor expression by flow cytometry (Fig. 20). All constructs were expressed and incorporated into the plasma membrane, thereby indicating that the introduction of N-glycosylation sites did not affect membrane targeting. Due to this, artifacts caused by glycosylation of constructs that were not inserted into the membrane correctly, could be excluded.

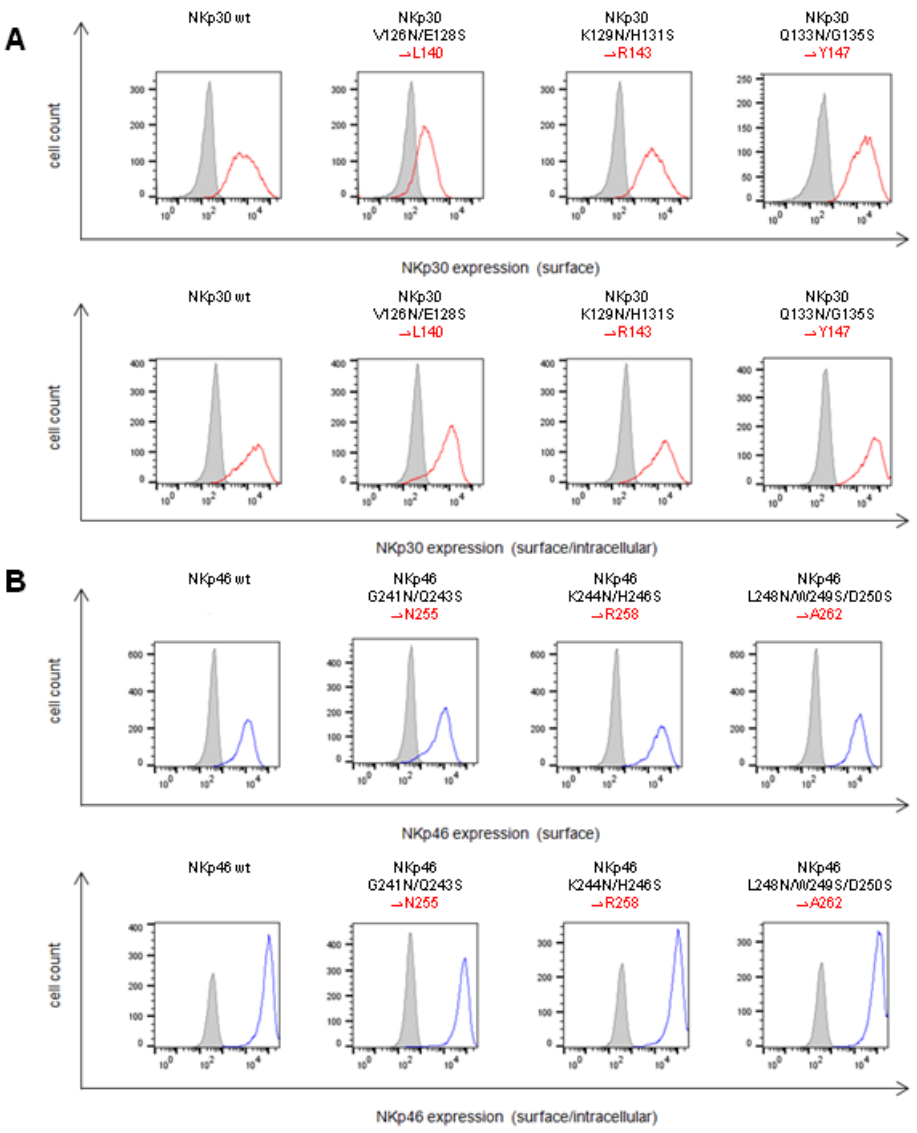

Figure 20. Expression of N-glycosylation scanning constructs. Plasma membrane and intracellular expression of the NKp30 (A) and NKp46 (B) mutants in transduced 293T/17 cells, analyzed by flow cytometry. Grey: isotype control, red: anti-NKp30, blue: anti-NKp46. One representative experiment out of three is shown.

Glycosylation of the different mutants was analyzed by western blot, showing that in case of NKp30, only the V126N/E128S mutant (showing the positioning of L140) is additionally glycosylated. This speaks for the fact that L140 is positioned outside of the membrane. In contrast, the absence of glycosylation of K129N/H131S and Q133N/G135S indicates that R143 and Y147 are located in the membrane region. Due to the fact that L140 lies outside of the transmembrane region, R143 can only be located a maximum of three amino acids inside of the membrane and therefore it is likely that its side chain does not align with the aspartate of CD3ζ in ground state. In contrast to that, glycosylation of all three N-glycosylation scanning mutants was detectable in case of NKp46, showing not only that R258 is located

outside of the membrane, but also that it is positioned at least four amino acids away from the border between extracellular and membrane region (Fig. 21 B).

This shows that a ligand induced conformational change that leads to charge alignment between immunoreceptor and CD3ζ in the transmembrane region is possible. It is likely that slight differences in this mechanism exist between NKp30 and NKp46, as the positioning of the transmembrane domains of both receptors does not seem to be equal.

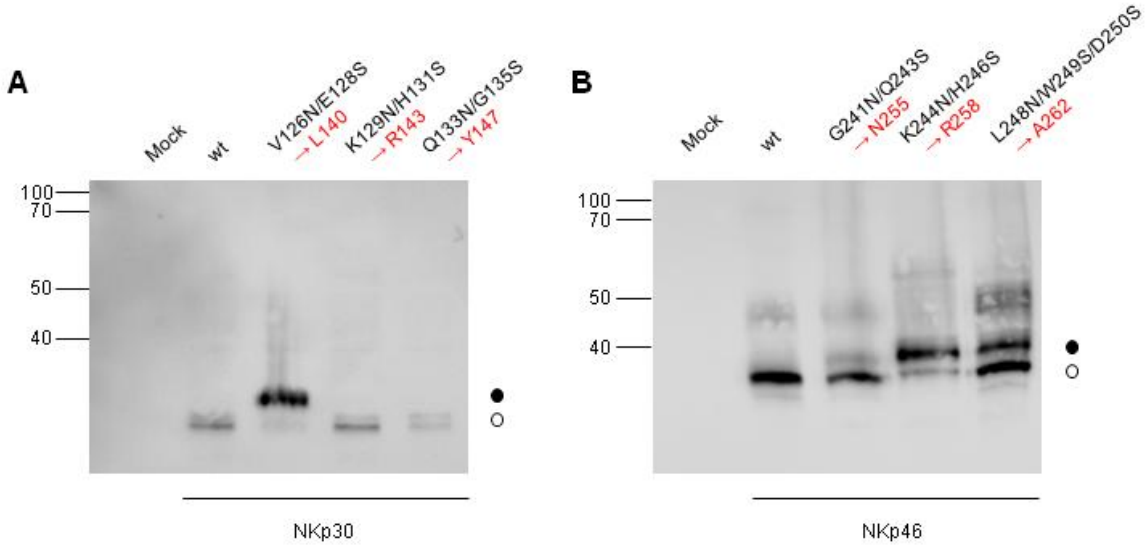

Figure 21. Glycosylation status of N-glycosylation scanning mutants. Western blot analysis of NKp30 (A) and NKp46 (B) mutants detected with NKp30- or NKp46-specific antibodies, respectively. Solid circles: glycosylated sites, open circles: non-glycosylated sites. One representative experiment out of three is shown.

3.1.5 Assembly of the NKp30/CD3ζ Complex

Results from the former experiments revealed several stalk amino acids to be critical for NKp30 signaling and led to the assumption that signaling via CD3ζ might be facilitated by a conformational change in the receptor that is induced by ligand binding. However, at this stage it was unclear whether this might be essential to activate a pre-existing NKp30/CD3ζ complex or whether it enables recruitment of CD3ζ to a pre-activated receptor/ligand complex. To analyze this, the interaction of NKp30 and NKp46 with CD3ζ was investigated in non-lymphoid cells. Therefor, HeLa cells were transduced with CD3ζ and the different receptor variants. Expression of NKp30, NKp46 and CD3ζ was confirmed by confocal laser scanning microscopy (CLSM) after detection with specific antibodies (Fig. 22). Interestingly, NKp30 and NK46 co-localized with CD3ζ at the plasma membrane of the cells, speaking for a tight interaction of both proteins even in the absence of ligand.

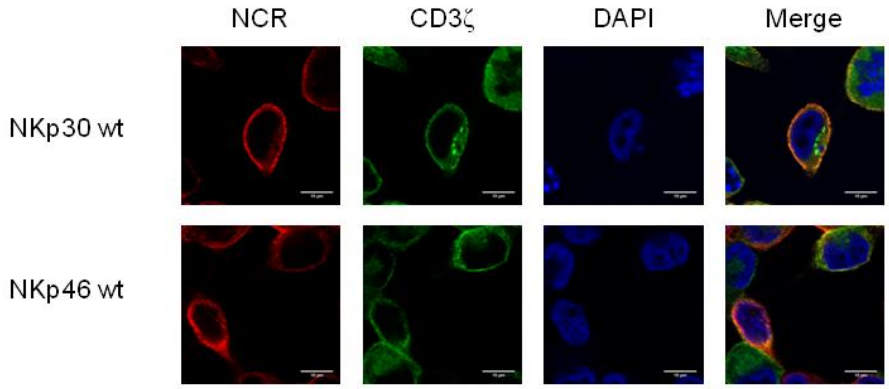

Figure 22. Plasma membrane co-localization of NKp30 and NKp46 with CD3ζ in the absence of ligand. Immunofluorescence staining of CD3ζ-transduced HeLa cells additionally transduced with either NKp30 or NKp46. Red: surface staining of the NCRs with specific antibodies, green: intracellular staining of CD3ζ with specific antibodies, blue: DAPI, size bar: 10 µm. One representative picture out of at least five is shown.

Additionally, CLSM analysis of the NKp30 alanine mutants showed co-localization of all the different receptor variants, including L141A, L142A and R143A, with CD3ζ (Fig. 23). This indicates that the membrane proximal amino acids are involved in signal transduction at the NKp30/CD3ζ interface rather than in assembly of the NKp30/CD3ζ complex itself.

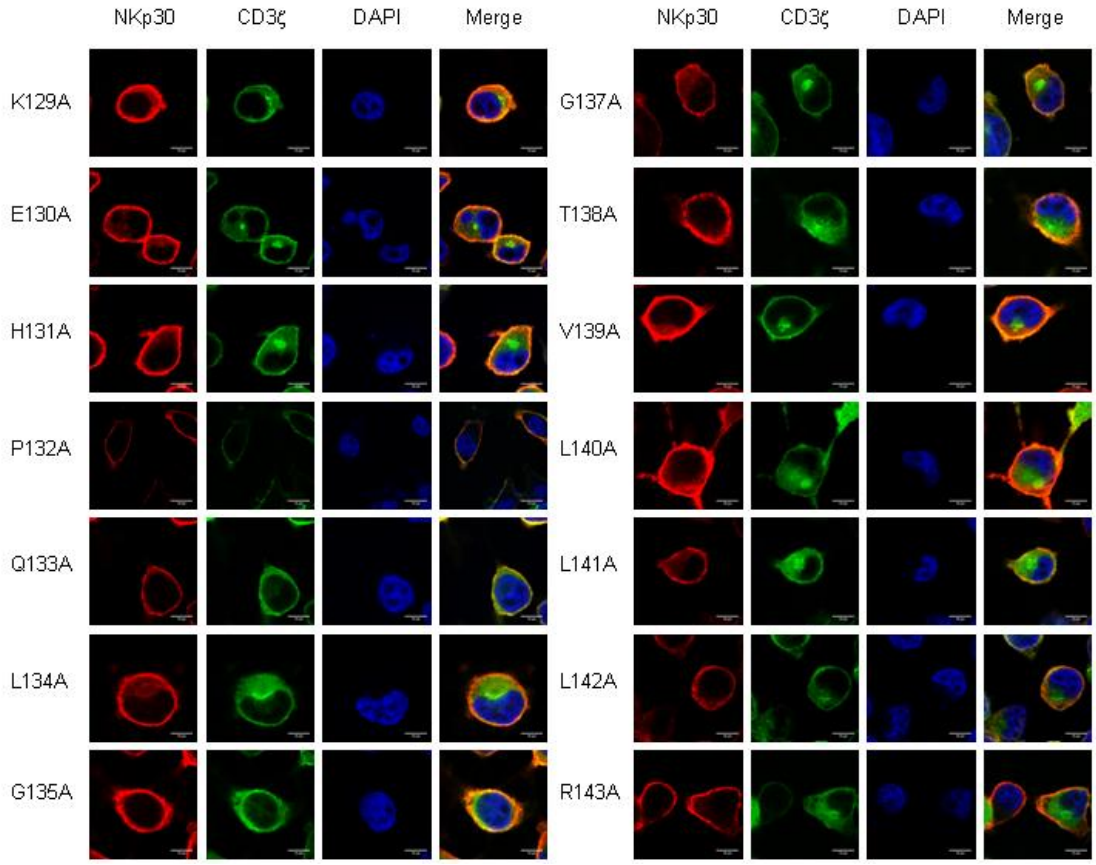

Figure 23. Alanine mutations within the stalk domain have no impact on NKp30/CD3ζ co-localization. Immunofluorescence microscopy of CD3ζ-transduced HeLa cells additionally transduced with NKp30 receptor mutants. Red: plasma membrane staining of NKp30 with specific antibodies, green: intracellular staining of CD3ζ with specific antibodies, blue: DAPI, size bar: 10 µm. One representative picture out of at least five is shown.

Furthermore, expression levels of NKp30 and NKp46 alone and in combination with CD3ζ were analyzed in comparative immunofluorescence and flow cytometry studies (Fig. 24).

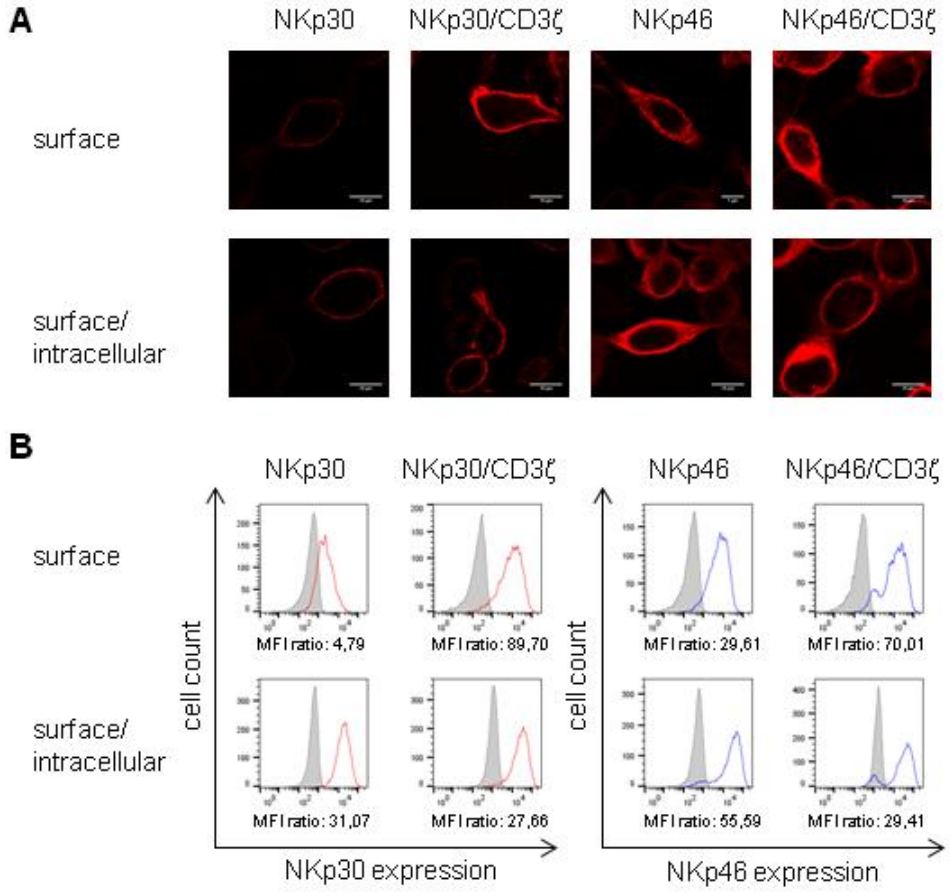

Figure 24. CD3ζ impacts surface expression levels of NKp30 and NKp46 in the absence of ligand. (A) Immunofluorescence microscopy analysis of NKp30 and NKp46 expression (plasma membrane and intracellular) in HeLa cells with or without CD3ζ. Red: staining of the NCRs with specific antibodies, size bar: 10 μm. One representative picture out of at least five is shown. (B) Flow cytometry analysis of NKp30 and NKp46 expression (plasma membrane and intracellular) in HeLa cells with or without CD3ζ. Grey: isotype control, red: anti-NKp30, blue: anti-NKp46. MFI ratios (median fluorescence intensity of NCR staining normalized to median fluorescence intensity of isotype control staining) are indicated. One representative experiment out of three is shown.

Each one of the experimental setups showed higher NCR expression levels in the presence of CD3ζ, indicating that both, NKp30 and NKp46, require CD3ζ for efficient plasma membrane targeting and/or retention. Additionally, these results support the hypothesis of pre-existing NKp30/CD3ζ and NKp46/CD3ζ complexes, as they clearly show that CD3ζ influences NCR expression levels in the absence of ligand, which can only be achieved if both proteins are able to interact without the need of prior ligand binding to the receptor.

Taken together, these results speak for the formation of structural NKp30/CD3ζ and NKp46/CD3ζ complexes without the requirement of auxiliary factors specific for lymphoid

cells and without requiring a pre-activated receptor ligand complex. Therefore, ligand-induced conformational changes, that lead to charge alignment between receptor and CD3ζ in the transmembrane region, might enable activation of pre-formed NKp30/CD3ζ and NKp46/CD3ζ complexes, respectively.

3.2 shRNA Screening to Analyze the Existence of yet Unidentified Cancer-associated Ligands of NKp30

Up to now, only a few cellular ligands have been identified for NKp30. The receptor binds to B7-H6, a cell surface protein selectively expressed on cancer cells [142,236]. Additionally, two other cellular proteins were shown to bind to NKp30, BAG-6 (also known as BAT-3) and Gal-3. BAG-6 is a mainly nuclear protein, which is present in various tissues, on the plasma membrane of immune cells, tumor cells and on exosomes. Additionally, a soluble form of the protein can be secreted upon cellular stress [143–145]. Gal-3 is a mainly soluble ligand of NKp30, which is expressed and released by many types of tumor cells [151]. Previous experiments led to the assumption that other cancer-associated NKp30 ligands might exist, implicated by NKp30-Fc binding to tumor cell lines that neither express B7-H6 nor BAG-6 on their surface (as Gal-3 is a soluble ligand). Therefore, the existence of other, yet unknown, cellular NKp30 ligands (and NKp44/ NKp46 ligands) was analyzed using a genome-wide shRNA screening.

3.2.1 Determination of Optimal Screening Conditions

Since conventional strategies such as co-immunoprecipitation have mostly failed, a novel approach based on a genome-wide shRNA knockdown was established to identify yet unknown NCR ligands (Fig. 25). In this setting, cell lines were transduced with a lentiviral shRNA library, and transduced cells (mCherry^{+}) were enriched by puromycin selection and sorted for decreased NCR ligand expression (NCRL^{low} phenotype). Afterwards, genomic DNA (gDNA) was isolated from sorted cells and sublibraries were generated and subjected to deep sequencing. Candidate lists were obtained from deep sequencing raw data by *in silico* analysis.

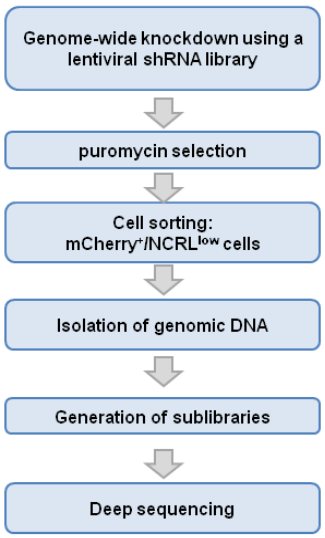

Figure 25. Workflow of the shRNA screening.

The first goal was to identify suitable cell lines that express high amounts of NCR ligands and are easy to transduce with lentiviral vectors. Therefor, a large panel of cell lines was screened for their surface expression of NCR ligands using NCR-Fc fusion proteins. From this panel, three cell lines were selected for the shRNA screening. All of them expressed different levels of NCR ligands, as shown by differential decoration patterns with NCR-Fc fusion proteins. In all cases IFNAR2-Fc served as negative control to exclude background binding of the hIgG1-Fc part (Fig. 26). All selected cell lines were human cells from different origin. DU145 is a prostate cancer cell line, 293T/17 cell are embryonic kidney cells, and MelJuSo is a melanoma cell line. Interestingly, BAG-6 was not detectable on the surface of any of these cell lines, while B7-H6 was only expressed on the surface of 293T/17 cells. This demonstrates the existence of an unknown interaction partner of NKp30-Fc on the surface of DU145 and MelJuSo cells, which should be identified in this screening. In contrast, the B7-H6 expressing 293T/17 cells served as positive control.

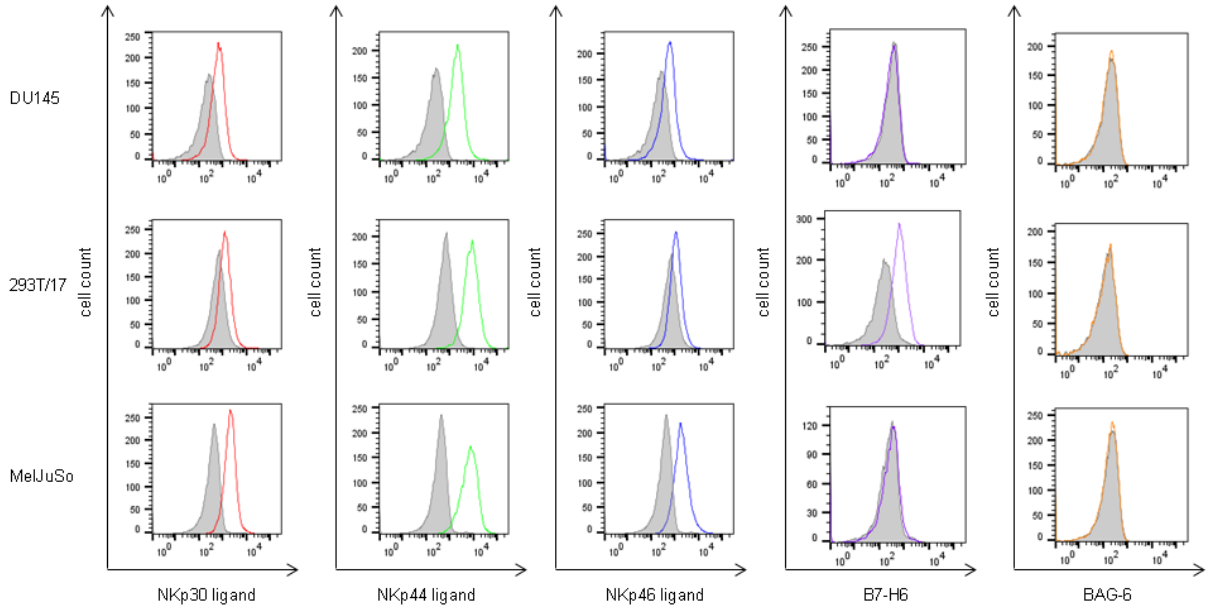

Figure 26. Cell lines selected for genome-wide shRNA screening. DU145, 293T/17 and MelJuSo cells were decorated with recombinant NCR-Fc fusion proteins or a specific antibody against the NKp30 ligands B7-H6 or BAG-6, respectively, and analyzed by flow cytometry. IFNAR2-Fc staining served as background control for NCR-Fc staining and secondary antibody staining served as control for BAG-6 and B7-H6 stainings (grey). One representative experiment out of three is shown.

A genome-wide human shRNA library (kindly provided by Michael McManus and Sergio Covarrubias, University of California in San Francisco, UCSF) was used for the knockdown-screening. This library contained 550,000 shRNAs with roughly 25 shRNAs targeting one gene. Due to the complexity of the library, the shRNAs were divided into 10 chips. shRNAs were delivered in lentiviral particles, pseudotyped with VSV-G by the Viracore core facility of the UCSF. Particles conferred an additional puromycin resistance and an mCherry fluorescence marker for selection. Such high-coverage shRNA libraries were shown to be a valuable tool for RNAi screenings [237,238].

Before starting the screening, transduction efficacy of the shRNA library was determined on the selected cell lines. Therefor, cells were transduced with control virus [pMK1047(VSV-G)], which did only contain the selection markers but no shRNAs. The optimal MOI was determined by flow cytometry analysis of the mCherry selection marker (Fig. 27). Based on mathematical considerations and empirical observations, 30-40 % of the cells should be transduced in order to avoid multiple integrations and to maintain the complexity of the library (Sergio Covarrubias, personal communication). For DU145 and 293T/17 cells, an MOI of 0.5 resulted in an optimal transduction rate (DU145: 35.2 % and 293T/17: 38.0 % of transduced cells). As transduction efficacy was slightly higher in MelJuSo cells (66.3 % of transduced cells at an MOI of 0.5), in this cell line an MOI of 0.3 was used for the screening.

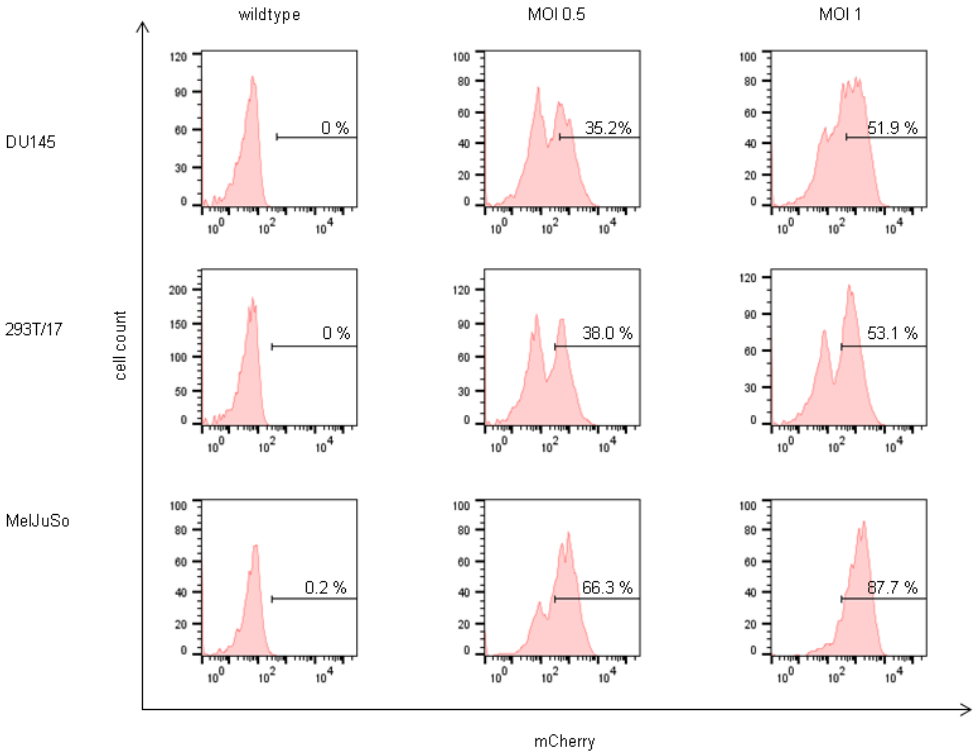

Figure 27. Determination of the optimal MOI for target cell transduction. DU145, 293T/17 and MelJuSo cells were transduced with [pMK1047(VSV-G)] control virus and analyzed for expression of the transduction marker (mCherry) by flow cytometry. Percentages of mCherry-positive cells are indicated.

3.2.2 shRNA Screening and Preparation of Deep Sequencing Libraries

The screening was carried out by implementation of the optimized transduction parameters. After three to four days, puromycin was added to the culture medium for enrichment of transduced cells (MelJuSo: 1 µg/ml, 293T/17 and DU145: 2 µg/ml puromycin in cell culture medium). Cell sorting was carried out after another three to four days of puromycin selection. Cells were decorated with NCR-Fc fusion proteins and sorted for high mCherry expression

(transduction marker) and reduced decoration with NCR-Fc fusion proteins (Fig. 28). This sorting strategy was assumed to enrich cells carring shRNAs against NCR ligands.

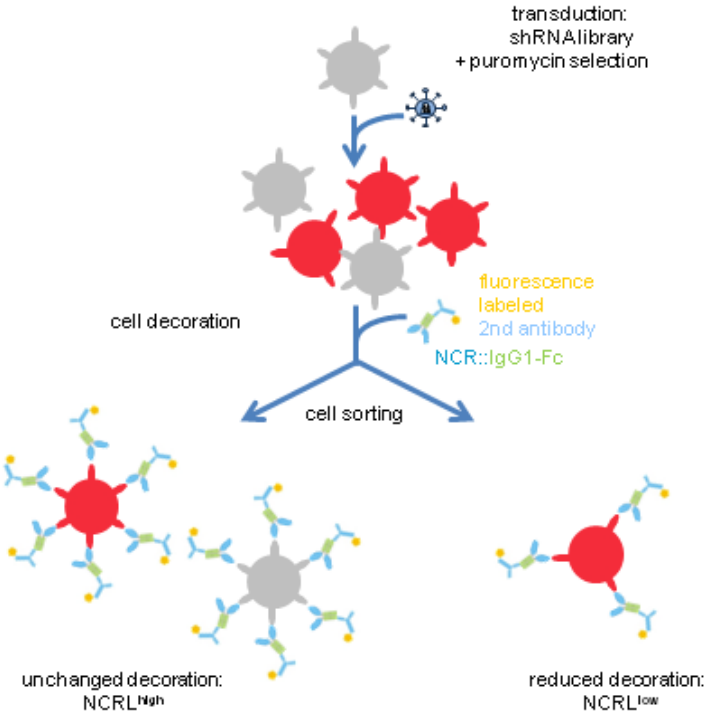

Figure 28. Sorting for mCherry^{+}/NCR ligand^{low} phenotype. Schematic representation of the sorting progress. mCherry-posititve (transduced) cells are shown in red, untransduced cells are shown in grey.

Altogether, 30 cell sorts (one sort for each chip and every NCR-Fc fusion protein) were performed per cell line (90 sorts altogether, Fig. 29 A-C). The sorting gate (mCherry^{+}/NCR ligand^{low}) was roughly 5 % of 10^{7} cells. gDNA was isolated from sorted cells and subjected to PCR for generation of deep sequencing sublibraries (collaboration with Zoltán Ivics and Csaba Miskey, Paul-Ehrlich-Institut, Langen). Adaptor sequences to attach the fragment to an Illumina flow cell and barcodes to distinguish the different samples from each other, were introduced by the respective primers (Fig. 29 D). As deep sequencing of the 90 samples was carried out in three lanes, no more than 30 different barcodes were needed to differentiate between the samples.

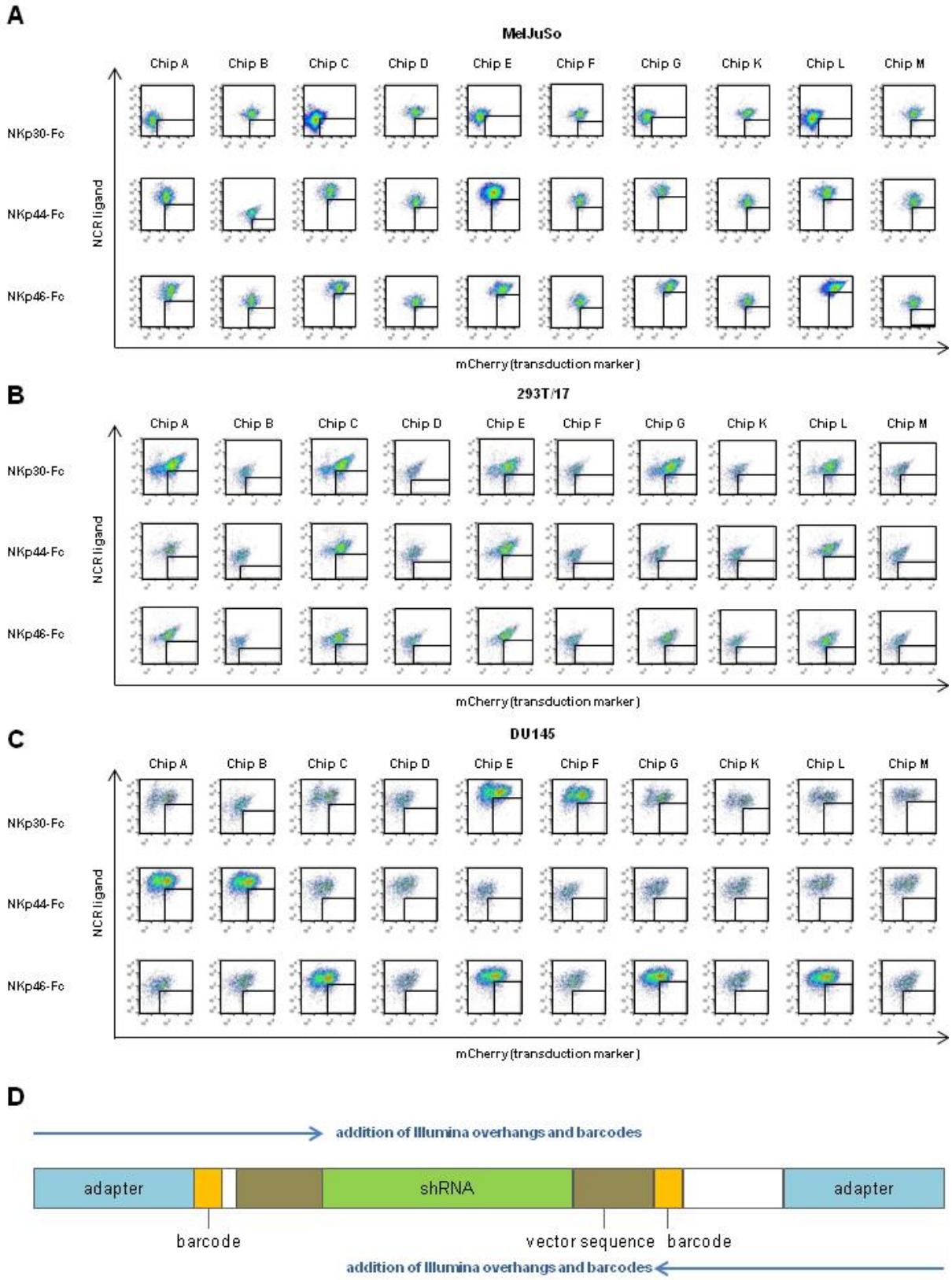

Figure 29. Cell sorting and preparation of deep sequencing samples. (A-C) Sorting gates for mCherry^{+}/NCR ligand^{low} cells in the screening cell lines MelJuSo (A), 293T/17 (B) and DU145 (C) 7 days post transduction. (D) Schematic representation of PCR fragment preparation for Illumina sequencing. Blue arrows indicate sequences that were introduced by PCR, white regions indicate spacer sequences.

3.2.3 Analysis of Deep Sequencing Data

To identify putative NKp30 ligands, deep sequencing raw data had to be further processed and narrowed down. Trimming of the raw data, association of sequences to samples (barcoding) and to genes (NM accession numbers) was done in collaboration with Alexander Williams (Gladstone Bioinformatics Core, Gladstone Institutes, UCSF). Data was further processed according to the following quality parameters (collaboration with Csaba Miskey, Paul-Ehrlich-Institut, Langen): (1) To be included, the cumulative read numbers for a particular shRNA had to be more than 100 for all three NCR samples in the respective cell line. This led to the reduction of background. (2) For each receptor, only shRNAs were included, which displayed a log2-fold change above two when compared to samples from the other two NCR-Fc fusion protein decorations in the same cell line. This led to the exclusion of shRNAs with minor effects. (3) Candidate genes for which less than 8 independent shRNA sequences were detected, were regarded as non-specific hits and thus removed from the list. (4) Data sets were merged to a protein localization data set from Uniprot and only proteins that can be localized on the cell membrane were included in the candidate lists. This analysis led to 9 data sets (one for each receptor in each cell line), containing between 20-200 candidate genes each. These data sets were further narrowed by (1) filtering for expression levels of the candidate genes in the screening cell lines, based on publicly available expression data (The Human Protein Atlas, RefExA, and EMBL Expression Atlas) and (2) documented association of the candidate with cancer and/or immunity. Additionally, candidate genes involved in the expression and plasma membrane targeting of membrane proteins were excluded from the final lists as they were likely to contribute to the surface expression of the putative ligand but not to be the NCR interaction partner itself. As such proteins are highly involved in shaping the cell surfaces, it was not surprising that they were present in high numbers in the initial candidate lists. Overall, this speaks for the fact that such a screening method is suitable to identify interacting membrane proteins. The final analysis resulted in candidate lists comprising 8 candidate genes for NKp30 (Tab. 22), 4 candidate genes for NKp44 (appendix, 6.5) and 11 candidate genes for NKp46 (appendix, 6.5).

Table 22. Candidate list of putative NKp30 ligands. FPKM: fragments per kilobase of exon per million fragments mapped.

Nr.	UniProt entry	Accession numbers	Gene names	Protein name	Expression (FPKM) screening cell line	Chromosome	Localization/type	Relation to	
								cancer	immunity
1	CD320_HUMAN (Q9NPF0)	NM_001165895, NM_016579	CD320_8D6A_UNQ198/PRO224	CD320 antigen	Mel-JuSo (45)	19	Membrane/ single-pass type I membrane protein	-	+
2	ZDHC4_HUMAN (Q9NPG8)	NM_001134387, NM_001134388, NM_001134389, NM_018106	ZDHHC4_ZNF374_DC1_UNQ5787/PRO19576	Probable palmitoyltransferase ZDHHC4	Mel-JuSo (12), DU145 (13)	7	Membrane/ multi-pass membrane protein	-	-
3	LFG1_HUMAN (Q7Z429)	NM_000837, NM_001009184	GRINA_LFG1_NMDARA1_TMBIM3	Protein lifeguard 1	Mel-JuSo (55), DU145 (36)	8	Membrane/ multi-pass membrane protein	-	-
4	RAB23_HUMAN (Q9ULC3)	NM_001278666, NM_001278667, NM_001278668, NM_016277, NM_183227	RAB23_HSPC137	Ras-related protein Rab-23	Mel-JuSo (3), DU145 (6)	6	Cell membrane, cytoplasmic vesicle, autophagosome, endosome membrane / lipid-anchor	-	-
5	NHRF3_HUMAN (Q5T2W1)	NM_001201325, NM_001201326, NM_002614	PDZK1_CAP70_NHERF3_PDZD1	Na(+)/H(+) exchange regulatory cofactor NHE-RF3	293T (1-11.3)	1	Cell membrane, cytoplasm/ peripheral membrane protein	+	-
6	CLD8_HUMAN (P56748)	NM_199328	CLDN8_UNQ779/PRO1573	Claudin-8	DU145 (na),	21	Cell junction, tight junction, cell membrane/ multi-pass membrane protein	+	-
7	CLC6A_HUMAN (Q6EIG7)	NM_001007033	CLEC6A_CLECSF10_DECTIN2	C-type lectin domain family 6 member A	DU145 (na)	12	Membrane/ single-pass type II membrane protein	-	+
8	MUC24_HUMAN (Q04900)	NM_001142401, NM_001142402, NM_001142403, NM_001142404, NM_006016	CD164	Sialomucin core protein 24	DU145 (22)	6	Lysosome membrane, endosome membrane, cell membrane, isoform 2: secreted, isoform 1: expressed by prostate cancer tumors and prostate cancer cell lines/ single-pass type I membrane protein	+	-

3.2.4 Candidate Validation

For validation of the candidates obtained in the shRNA screening, the respective proteins were expressed in HeLa cells. This cell line was chosen for validation experiments as it does not express any NCR ligands on its surface (Fig. 30).

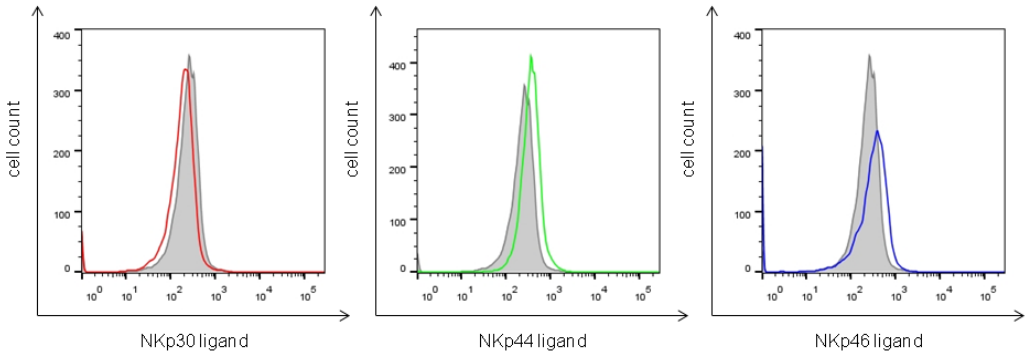

Figure 30. HeLa cells are negative for NCR ligands. HeLa cells were decorated with recombinant NCR-Fc fusion proteins and analyzed by flow cytometry. Grey: IFNAR2-Fc (background control), red: NKp30-Fc, green: NKp44-Fc, blue: NKp46-Fc. One representative experiment out of three is shown.

For this purpose, commercially available cDNA clones (Origene) were purchased and the cDNA sequences were cloned into a lentiviral vector containing a zeocin resistance and a C-terminal Flag® tag (LeGO-iZ-Flag). Constructs were packaged into lentiviral particles, pseudotyped with VSV-G. Transient transfection of HeLa cells with the commercially available plasmids was not possible as the constructs conferred protein expression under a cytomegalovirus (CMV) promoter, which was rapidly silenced in HeLa cells. Three days after

transduction, cells were selected with zeocin. After two weeks of selection, cells were analyzed for expression of the candidate protein (Flag$^+$) and decoration with the respective NCR-Fc fusion protein. Mock transduced cells served as negative control and B7-H6 transduced cells served as positive control for putative NKp30 ligands (Fig. 31).

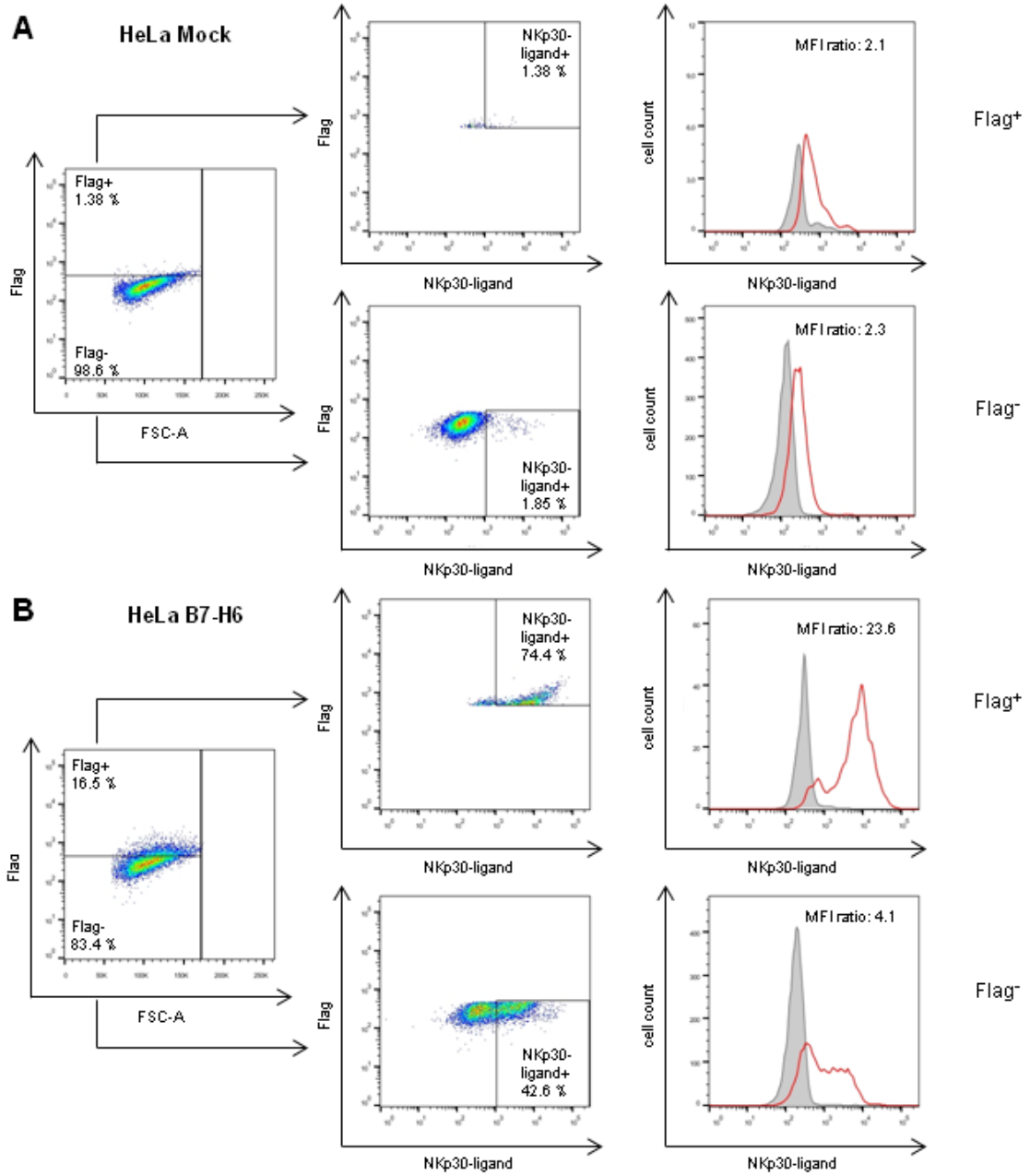

Figure 31. Gating strategy for validation of NCR ligands. HeLa cells, stably transduced with empty vector (Mock, A) or B7-H6 (B) were stained for surface expression of NKp30 ligands with recombinant NKp30-Fc fusion proteins, and for intracellular expression of the Flag® tagged protein with anti-Flag® M2 antibody. Flag-positive and Flag-negative populations were analyzed for the amount of NKp30-Fc decoration. MFI ratios (median fluorescence intensity of NKp30-Fc staining normalized to median fluorescence intensity of IRNAR2-Fc control staining) are indicated. One representative experiment out of three is shown.

Mock transduced HeLa cells showed only low background staining with anti-Flag® M2 antibody (1.38 % Flag$^+$ cells) and no differences in the amounts of NCR ligand$^+$ cells were visible in both populations (Flag$^+$: 1.38 % and Flag$^-$: 1.85 %). In contrast, the NKp30 ligand

B7-H6 led to a clear shift in NKp30-Fc decoration (Flag$^+$: 74.4 % NCR ligand$^+$ cells and Flag$^-$: 42.6 % NCR ligand$^+$ cells). Additionally, it was clearly visible that in the Flag$^+$ (B7-H6$^+$) population the NKp30-Fc/IFNAR2-Fc MFI ratio was much higher than in the Flag$^-$ (B7-H6$^-$) population (Flag$^+$: 23.6 compared to Flag$^-$: 9.2), showing that introduction of the Flag tagged protein is the reason for increased NKp30-Fc decoration. This indicates the specific interaction of NKp30 and B7-H6 and shows that the experimental setup is suitable for candidate validation.

In a next step, the 8 putative NKp30 ligands found in the shRNA screening (compare to Tab. 22) were analyzed according to the developed validation protocol (Tab. 23).

Table 23. Validation of putative NKp30 ligands.

Candidate	Population [%]		Amount of NKp30-ligand$^+$ cells [%]		MFI ratio NKp30-Fc/IFNAR2-Fc	
	Flag$^+$	Flag$^-$	Flag$^+$	Flag$^-$	Flag$^+$	Flag$^-$
CD320	12.7	87.3	9.3	2.3	2.0	2.2
ZDHHC4	4.9	95.1	1.8	1.1	1.5	1.6
GRINA	0.4	99.6	5.7	0.8	1.0	1.3
RAB23	13.6	86.4	3.3	0.4	1.4	1.4
PDZK1	0.4	99.6	35.7	1.6	2.4	2.1
CLDN8	4.6	95.4	6.5	2.7	1.8	1.6
CLEC6A	2.6	97.4	2.1	0.6	1.5	1.5
CD164	23.4	76.6	1.9	1.5	1.5	1.6

Over all, it was clearly visible that all of the candidates behaved like the negative control, showing no shift in NKp30-Fc decoration and no differences in MFI ratios of the Flag-positive and Flag-negative population. Expression of GRINA (0.4 % Flag$^+$) and PDZK1 (0.4 % Flag$^+$) was very low, suggesting that overexpression of these proteins might have negative effects on the cells. Therefore, the higher amount of NKp30-ligand$^+$ cells (35.7 %) in the Flag$^+$ population of PDZK1-transduced cells is assumed to be an artifact of the low expression rate, as underlined by the fact that the NKp30-Fc/IFNAR2-Fc MFI ratios of the Flag$^+$ and Flag$^-$ populations were in the same range (2.4 and 2.1). In summary, this data indicates that none of the candidate proteins directly influences NKp30-Fc binding to the surface of HeLa cells. The same validation procedure was applied for the putative NKp44 and NKp46 ligands,

also with no hint for interaction with the respective NCR (appendix, 6.5). Altogether, no yet unknown NCR ligand could be identified with the established screening method.

3.3 Engineering of a Functional Mouse NKp30 Protein

Human NKp30 was shown to be a highly potent receptor, involved in immune regulation and NK cell cytotoxicity against infected and malignantly transformed cells. Additionally, it was found as a functional protein in macaque and chimpanzee [74,139,189] as well as on rat NK cell subsets [190–192]. Interestingly, while the receptor is constitutively expressed in all the other species, in chimpanzee, NKp30 expression depends on NK cell activation [189]. Moreover, NKp30 is only a non-expressed pseudogene in a large number of inbred and wild mouse strains, due to the existence of two premature stop codons at the beginning of exon 2. The only exception is *M. caroli*, where two single nucleotide polymorphisms eliminate the premature stop codons [169,193,195].

A

```
H.sapiens_isoform_a      MAWMLLLILIMVHPGSCALWVSQPPEIRTLEGSSAFLPCSFNASQGRLAIGSVTWFRDEV        60
M.mulatta                MAWMLLLILIMVYPGSCALWVSQPPEIRTLEGSSAFLPCSFNASQGRLAIGSVTWFRDEV        60
M.fascicularis           MAWMLLLILIMVYPGSCALWVSQPPEIRTLEGSSAFLPCSFNASQGRLAIGSVTWFRDEV        60
P.troglodytes            MAWMLLLILIMVHPGSCALWVSQPPEIRTLEGSSAFLPCSFNASQGRLAIGSVTWFRDEV        60
B.taurus                 MAQMLLFIFIIIRPGSCVLWVSQPPEIRTQEGSPAFLPCSFNASQGSLAIGSVTWYRDKV        60
R.norvegicus             MAKVLLIVFIMVYAGSCAIWVSQPPEIRAQEGTTASLPCSFNASRGKAAIGSATWYQDKV        60
M.caroli                 MAKVLLVIFIMVYPGSCALWVSQPPETPVQKDTTASLPCPFNAIRGKPATGSVTWYQDKV        60
                         ** :**.::*::  ***.:*******  . :.: * *** *** :*  * **.**::*:*
H.sapiens_isoform_a      VPGKEVRNGTPEFRGRLAPLASSRFLHDHQAELHIRDVRGHDASIYVCRVEVLGLGVGTG        120
M.mulatta                APGKEVRNGTPEFRGRLAPLSSSRFLRDHQAELHIWDVRGHDAGIYVCRVEVLGLGVGTG        120
M.fascicularis           APGKEVRNGTPEFRGRLAPLSSSRFLRDHQAELHIWDVRGHDAGIYVCRVEVLGLGVGTG        120
P.troglodytes            VPGKEVRNETPEFRGRLAPLASSRFLHDHQAELHIRDVRGHDASIYVCRVEVLGLGVGTG        120
B.taurus                 APGMEVRNETAEFQGRLAPLPSSRFLCDHQAELHIWDTRGRDTGVYVCRVEVLGLGVGTG        120
R.norvegicus             APGMELSNVTPGFRGRVASFSASQFIRGHKAGLLIQDIQSHDARIYVCRVEVLGLGVGTG        120
M.caroli                 TLGMELSNVTPGFGGRLVSFSVSQFIRDHKAGLLIQDTQSYDAGIYVCRVEVLGLGVRTG        120
                         . * *: * *  * **:. :  *:*: .*:* * * * :. *: :************ **
H.sapiens_isoform_a      NGTRLVVEKEHPQLG--------AGTVLLLRAGFYAVSFLSVAVGSTVYYQG---KCLTW        169
M.mulatta                NGTRLVVEKEYPQLG--------AGTVLLLRAGFYAVSFLSVAMGSTLYYQG---KCLTW        169
M.fascicularis           NGTRLVVEKEYPQLG--------AGTVLLLRAGFYAVSFLSVAVGSTLYYQG---KCHCH        169
P.troglodytes            NGTRLVVEKEHPQLG--------AGTVLLLRAGFYAVSFLSVAVGSTVYYQG---KCLTW        169
B.taurus                 NGTLLVVEEGPPQLA--------AGTVLLLRAGFYAFSFLSVAMGSSMYYQG---KYHCH        169
R.norvegicus             NGTRLVVEKEPPQQASNAEPERAAYTSLLLRAGVYALSFLSVATGSVIYYQG---KCLCH        177
M.caroli                 DGTWLLVEKGPPQQASNTEQE--AHTSILLRAGFYALSFLSVATGSTIYYQGGSHKCPCH        178
                         :** *:**:  ** .        * * :*****.**.****** ** :****   *
H.sapiens_isoform_a      KGPRRQLPAVVPAPLPPPCGSSAHLLPPVPGG          201
M.mulatta                KGPRRQLPAVVPGPLPPPCGSSAHLLPPVPGG          201
M.fascicularis           MGTHCHS-------------------------          176
P.troglodytes            KGPRRQLPAVVPAPLPPPCGSSAQLLPPVPGG          201
B.taurus                 KGTPCHSLDGL---------------------          180
R.norvegicus             VGNTATPPTASEERF-----------------          192
M.caroli                 MENMDTPPAASEK-------------------          191
```

B

Percent Identity Matrix

1: H.sapiens_isoform_a	100.00	95.02	90.34	99.00	73.89	63.04	58.24
2: M.mulatta	95.02	100.00	94.32	94.03	76.11	65.22	60.44
3: M.fascicularis	90.34	94.32	100.00	89.77	80.68	68.18	63.07
4: P.troglodytes	99.00	94.03	89.77	100.00	74.44	63.04	58.24
5: B.taurus	73.89	76.11	80.68	74.44	100.00	62.22	59.44
6: R.norvegicus	63.04	65.22	68.18	63.04	62.22	100.00	77.66
7: M.caroli	58.24	60.44	63.07	58.24	59.44	77.66	100.00

Figure 32. Sequence alignment of NKp30 in different species. (A) Multiple sequence alignment (created by Clustal Omega) of NKp30 from *H. sapiens* (canonical sequence, isoform a), *M. mulatta*, *M. fascicularis*, *P. troglodytes, B. taurus, R. norvegicus* and *M. caroli*. (*) positions which have a single, fully conserved residue; (:) conservation between groups of strongly similar properties; (.) conservation between groups of weakly similar properties. (B) Percent identity matrix of NKp30 sequences from vertebrate species (created by Clustal2.1).

Sequence alignment of NKp30 from different species showed that the protein is highly conserved in human and primates. In contrast to that, NKp30 sequences in rodents differ markedly in their extracellular and intracellular domains (Fig. 32). In addition, phylogenetic trees showed that at the nucleotide level as well as on protein level, the species are separated into two major clusters, one containing human and primates and the other containing rodents [169]. Currently, not much is known about the evolutionary role of this separation and the consequences for NKp30 function in rodents.

3.3.1 Expression and Plasma Membrane Targeting of the mNKp30 Construct

In order to decipher the evolutionary role and biological function of the NKp30 protein in mouse, the premature stop codons in exon 2 of the *M. musculus* NKp30 sequence were removed to generate a putative mouse NKp30 (mNKp30, appendix 6.2) full length receptor and an N-terminal Flag® tag was introduced to the sequence to facilitate antibody detection. A5-GFP reporter cells were transduced with the mNKp30 construct and expression as well as plasma membrane targeting of the full length receptor were analyzed by flow cytometry in comparison to mock transduced cells (Fig. 33). Interestingly, while intracellular detection of the protein was possible, no surface expression of the mNKp30 full length receptor was observed, indicating the absence of certain motifs within the mNKp30 sequence, that are required for plasma membrane targeting of the receptor.

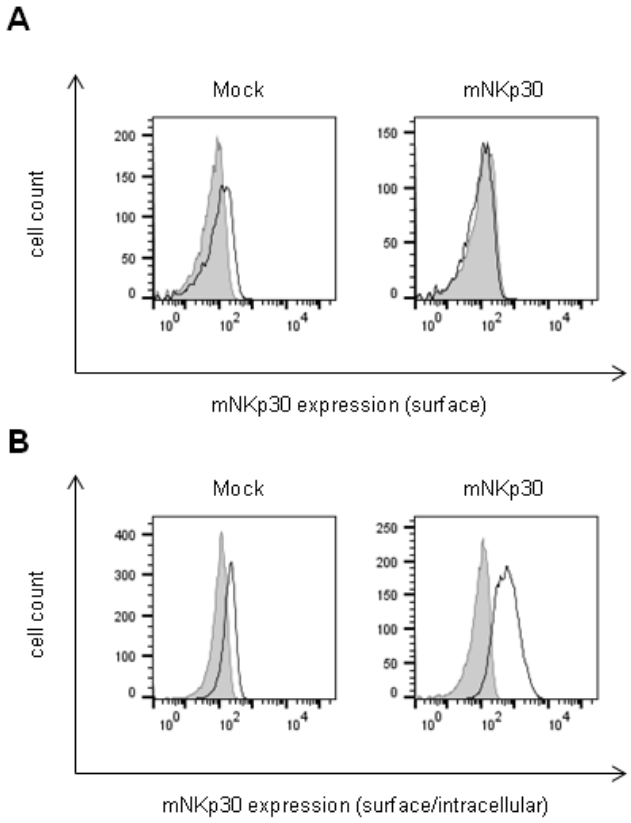

Figure 33. The mNKp30 full length receptor is intracellularly retained in A5-GFP cells. (A) Surface and (B) intracellular expression of full length mNKp30 in transduced A5-GFP cells, analyzed by flow cytometry. Mock transduced A5-GFP cells served as control. Grey = isotype control; black = anti-FLAG® M2 antibody.

3.3.2 Impact of N-Glycosylation on Plasma Membrane Targeting and Secretion of mNKp30 Constructs

To find out more about the reasons for intracellular retention of the full length mNKp30 receptor in A5-GFP cells, sequence differences between human (canonical) and murine NKp30 were analyzed in more detail. Interestingly, it was found that the putative mNKp30 sequence additionally contains mutations that eliminate the three consensus N-glycosylation sites in the extracellular domain of the receptor. Since N-glycosylation is important for plasma membrane targeting and ligand binding of NKp30 in human [208], in a second step these three N-linked glycosylation motifs in the mNKp30 gene sequence were repaired (mNKp30-glyco, appendix 6.2). To analyze the impact of the N-glycosylation site mutations in detail, soluble mNKp30-Fc fusion proteins were produced in HEK 293T/17 cells and the secreted proteins were purified from cell culture supernatant via protein A sepharose. In contrast to the purified hNKp30-Fc, which could be detected with an apparent molecular weight of roughly 50 kDa under reducing conditions (~ 100kDa under non-reducing conditions), the mNKp30-Fc fusion protein which contained no N-linked glycosylations, was not detectable after purification (Fig. 34 A). Interestingly, the mNKp30-Fc construct with repaired N-glycosylation sites (mNKp30-glyco-Fc) could be purified from cell culture supernatant via protein A and showed the same behavior as hNKp30-Fc, speaking for an influence of N-glycosylation on Fc protein secretion in 293T/17 cells.

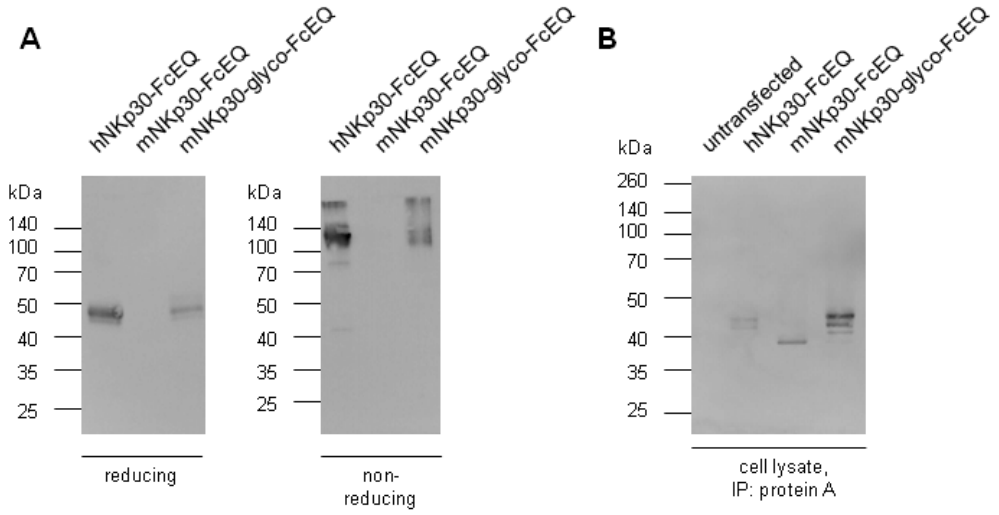

Figure 34. N-glycosylation impacts secretion of NKp30-Fc fusion proteins. (A) Western blot analysis of hNKp30-, mNKp30- and mNKp30-glyco-Fc fusion proteins under reducing (left) and non-reducing (right) conditions after protein A purification from HEK 293T/17 supernatants. (B) Western blot analysis of hNKp30-, mNKp30- and mNKp30-glyco-Fc fusion proteins after protein A pull-down from HEK 293T/17 cell lysates. Cell lysates of untransfected HEK 293T/17 cells served as negative control. Proteins were detected with an HRP-conjugated anti-human IgG1-Fc antibody.

To analyze if mNKp30-Fc was not expressed, or intracellularly retained like the mNKp30 full length receptor, cell lysates of transiently transfected HEK 293T/17 cells were generated and analyzed for the presence of NKp30-Fc (Fig. 34 B). Interestingly, all three NKp30-Fc variants were detectable in the lysates. While hNKp30-Fc and mNKp30-glyco-Fc were present in differently glycosylated forms (mono-, di-, tri-glycosylated), mNKp30-Fc was only detected as unglycosylated protein (each N-glycosylation leads to an increase of roughly 2 kDa in protein size; Fig. 34 B). This clearly shows that the absence of N-gylcosylation sites in the extracellular domain of mNKp30-Fc leads to intracellular retention of the protein in 293T/17 cells. In contrast to that, an N-glycosylated full length mNKp30 receptor (mNKp30-glyco) was also intracellularly retained in A5-GFP cells (Fig. 35), speaking for the absence of additional transmembrane or intracellular motifs that are required for plasma membrane targeting and/or retention of the full length receptor in these cells.

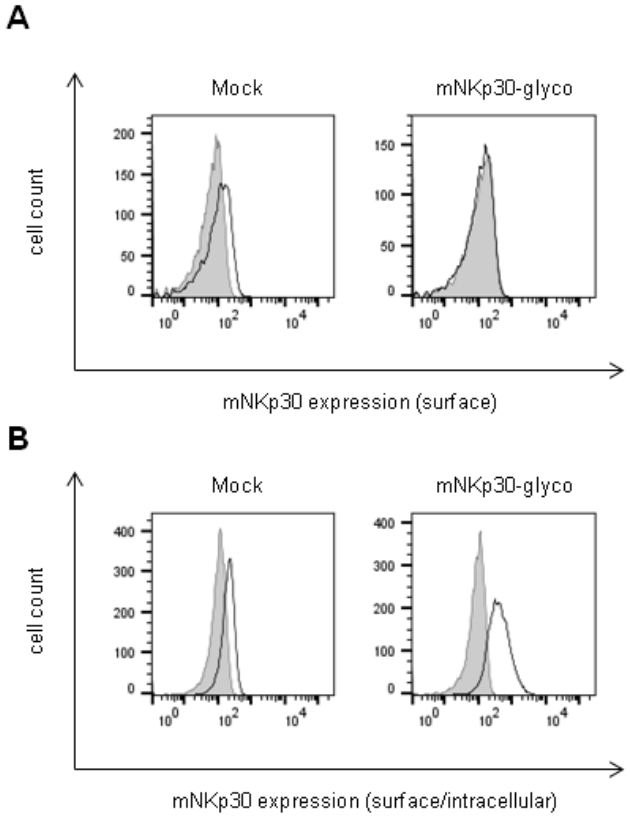

Figure 35. N-gylcosylation is not sufficient for plasma membrane targeting of the mNKp30 full length receptor. (A) Surface and (B) intracellular expression of full length mNKp30-glyco in transduced A5-GFP cells analyzed by flow cytometry. Mock transduced A5-GFP cells served as control. Grey = isotype control; black = anti-FLAG® M2 antibody.

3.3.3 Evidence for a Putative mNKp30-glyco Ligand on the Surface of a Mouse Mastocytoma Cell Line

In a second step, the N-glycosylated putative mNKp30 protein should be analyzed for its functionality. As the full length mNKp30-glyco receptor was intracellularly retained in A5-GFP cells, reporter assays to analyze activation and signaling capacity of the receptor could not be performed. However, mNKp30-glyco's ability to bind cellular ligands was analyzed by decoration of nine different mouse cell lines with hNKp30-Fc and mNKp30-glyco-Fc fusion proteins. IFNAR2-Fc fusion proteins served as background control (Fig. 36).

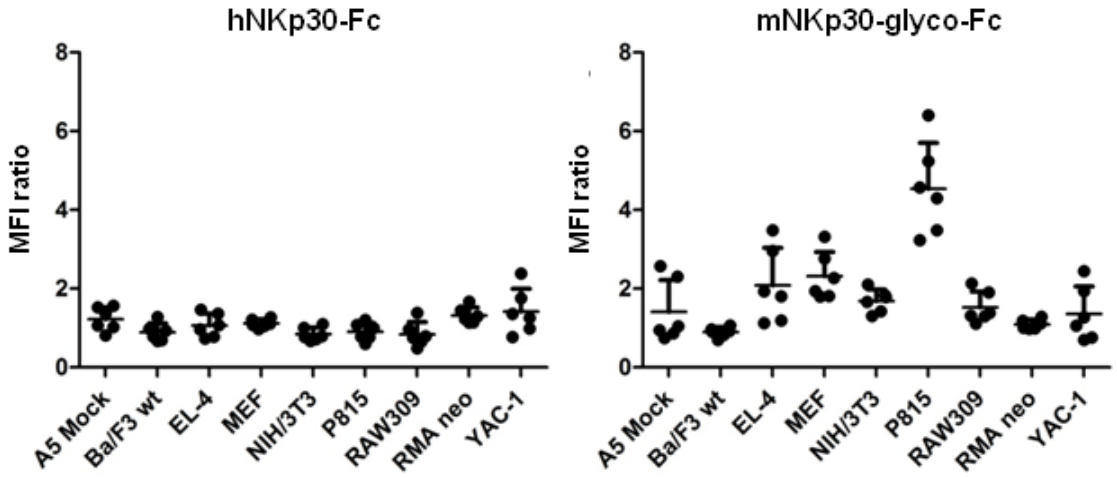

Figure 36. mNKp30-glyco-Fc has an unknown surface ligand on P815 mastocytoma cells. Binding of hNKp30-Fc and mNKp30-glyco-Fc to nine murine cell lines was analyzed by flow cytomtery. Median fluorescence intensity (MFI) ratios (MFI of NKp30-Fc fusion protein staining normalized to MFI of IFNAR2-Fc control staining) are indicated with mean ± SEM. Each dot represents an independent staining.

As expected, hNKp30-Fc did not bind to any of the cell lines (mean MFI ratio < 2), showing that human NKp30 does not interact with surface structures on mouse cells. In contrast, mNKp30-glyco-Fc bound with varying extent to the different mouse cell lines. Low binding was observed on EL-4 (T lymphocytes) and MEF (embryonic fibroblasts) cells (EL-4: mean MFI ratio 2.1 and MEF: mean MFI ratio 2.3). In contrast, no binding was observed on other T lymphocyte (A5 Mock, RMA neo) or embryonic fibroblast (NIH/3T3) cell lines (mean MFI ratios < 2). This does not speak for the existence of a specific surface ligand of mNKp30-glyco on mouse T lymphocytes or embryonic fibroblasts. The most prominent binding was observed on P815 cells, showing a mean MFI ratio 4.5, which is comparable with values obtained for hNKp30-Fc staining of human B7-H6-expressing K562 cells [208]. This indicates that mNKp30-glyco-Fc is able to interact with an unknown surface structure on mouse mastocytoma cells, which could either be mast cell derived or of cancerous origin.

Notably, P815 is the only mastocytoma cell line tested in this setting. To verify this finding, mNKp30-glyco-Fc should be analyzed for binding to other murine mastocytoma cell lines.
Additionally, mNKp30-glyco-Fc binding to the human NKp30 ligand B7-H6 was analyzed in comparison to hNKp30-Fc (Fig. 37). Therefor, Mock transduced or B7-H6 transduced Ba/F3 cells were decorated with the different Fc fusion proteins in comparison to IFNAR2-Fc staining as background control.

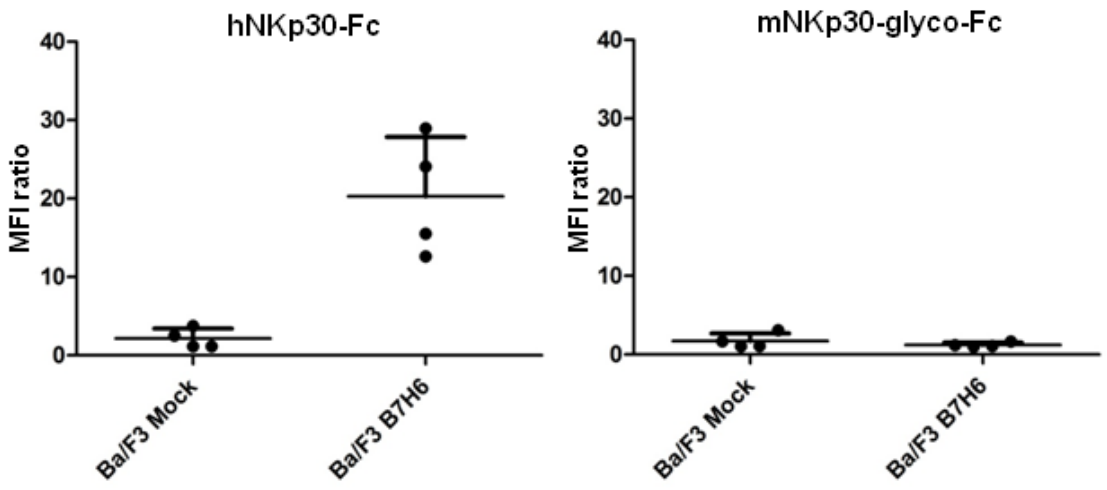

Figure 37. mNKp30-glyco-Fc does not bind to human B7-H6. Binding of hNKp30-Fc and mNKp30-glyco-Fc to murine Ba/F3 Mock cells (transduced with an empty vector) and Ba/F3 cells transduced with human B7-H6 (Ba/F3 B7-H6), analyzed by flow cytometry. Median fluorescence intensity (MFI) ratios (MFI of NKp30-Fc fusion protein staining normalized to MFI of IFNAR2-Fc control staining) are indicated with mean ± SEM. Each dot represents an independent staining.

As expected, hNKp30-Fc bound to a high degree to Ba/F3 B7-H6 cells (Ba/F3 B7-H6: mean MFI ratio 20.3, compared to Mock: mean MFI ratio: 2.2). In contrast, binding of mNKp30-glyco-Fc to Ba/F3 B7-H6 cells was not observed (Ba/F3 B7-H6: mean MFI ratio 1.2, compared to Mock: mean MFI ratio: 1.7). The absence of such an interaction is not surprising as hNKp30 and mNKp30-glyco only share a sequence homology of 62 % (appendix, 6.2). Additionally, the B7-H6 full length sequence is not present in mice [142].
Altogether, these results show that binding patterns of hNKp30 and the putative mNKp30-glyco protein differ. While hNKp30-Fc showed no binding to surface structures on mouse cells, mNKp30-glyco-Fc seems to recognize a putative ligand of murine origin.

4. Discussion

NKp30 is one of the major activating receptors on NK cells mediating cytotoxicity against virally infected and tumor cells. An understanding of the molecular mechanisms, leading from ligand binding at the ectodomain of NKp30 to activation of the NK cell, is crucial to enhance the effectivity of NK cell-based cancer therapies. The results of this thesis demonstrated, that the Ig and stalk domain of NKp30 are a functional entity for signaling via CD3ζ. Moreover, they indicated that the NKp30/CD3ζ complex is pre-assembled, but signaling incompetent in ground state and switches to a signaling competent conformation after ligand binding.
Furthermore, while a few proteinaceous ligands, like the tumor antigens B7-H6 [142,236], BAG-6 [143,145] and Gal-3 [151], the parasite protein *Pf*EMP1 [147] and the viral ligands pp65 [146] and certain haemagglutinins [148], were identified for NKp30 in the last years, the existence of other, yet unknown ligands of the receptor is still questionable and could not be confirmed by implementation of a genome-wide shRNA screening in this thesis.
Interestingly, in mouse, the major NKp30 ligand B7-H6 is absent [142], and NKp30 is only present as a non-expressed pseudogene, due to two premature stop codons in the beginning of exon 2 [169,193,195]. As the evolutionary reason for this is still unknown, a putative mouse NKp30 protein with repaired stop codons and repaired N-glycosylation sites was constructed. Analysis of this protein indicated the existence of an unknown murine cellular mNKp30 ligand on mastocytoma cells. This was the first time, expression and functional analysis of a putative mouse NKp30 receptor could be shown on protein level.

4.1 The Stalk Domain of NKp30 Contributes to Ligand Binding and Signaling of a Pre-assembled NKp30/CD3ζ Complex

The importance of the stalk domain was already shown for all NCRs. While sialic acid moieties attached to the stalk domains of NKp44 [153,154] and NKp46 [163,239] mediate binding of the receptors to certain viral haemagglutinins, the amino acids of the NKp30 stalk domain were shown to contribute directly to receptor function, as truncation of the stalk domain or substitution by a length-matched GS-linker led to a significant reduction in ligand binding and a complete loss of CD3ζ signaling [208]. Interestingly, the stalk domain of NKp30 has no influence on the physiological role of the receptor, as all NKp30 isoforms posses the complete stalk domain but some act stimulative while others act immunosuppressive [198]. The fact that the stalk sequence is preserved in all isoforms additionally speaks for the importance of this domain for the functionality of the receptor. Formerly, the NKp30 stalk was assumed to be a flexible region, as it was not resolved in the crystal structure of the NKp30/B7-H6 complex. Notably, the amino acid sequence used for crystallization contained

aa 19-135 of the extracellular NKp30 domain and therefore lacked 8 stalk aa compared to our predictions [199,208].

In this thesis, analysis of NKp30/NKp46 chimera showed that the ectodomains of both proteins form functional entities of an Ig domain and a cognate stalk domain, as indicated by the fact that the NKp30 stalk was incompatible with folding and plasma membrane targeting of NKp46 and the stalk of NKp46 was unable to facilitate ligand-induced signaling of NKp30. Intracellular retention of the chimera containing the Ig domain of NKp46 and the stalk of NKp30 might be explained by length differences of the two stalk domains. The stalk of NKp30 (15 aa) is much shorter than the stalk of NKp46 (47 aa), and NKp30 contains only one Ig domain while NKp46 contains two. Therefore, the short stalk of NKp30 together with the Ig domains of NKp46 might lead to sterical hindrance, thereby preventing membrane incorporation of the chimera. Notably, even though the stalk domain of NKp30 was indispensable for interconnecting ligand binding to signaling, the stalk domain of NKp46 was sufficient to maintain principal signaling capacity of NKp30 as demonstrated by retained signaling of the NKp30Ig/46stalk/46TM and NKp30Ig/46stalk/30TM chimera after antibody-crosslinking. This phenotype might be partially explained by the existence of a preserved sequence motif in the NKp30 and NKp46 stalk [$K^{129/244}$(-)$HX_9LLR^{143/258}$, where (-) indicates a negatively charged amino acid; appendix, 6.3]. The membrane-proximal LLR motif as well as the lysine on position 129 of the NKp30 stalk are additionally highly conserved among species (Fig. 32). This sequence motif seems to confer principal signaling capacity, independent of the stalk length. In this context, $K^{129/244}$(-)H might be important for the integrity of the Ig domain (at least in case of NKp30) and $LLR^{143/258}$ might be needed for signal transduction. Cell decoration experiments additionally showed that the inability of the NKp30Ig/46stalk/46TM and NKp30Ig/46stalk/30TM chimera to exert ligand induced signaling is not caused by impaired ligand binding to the constructs.

A more detailed insight into the contribution of individual stalk amino acids to ligand binding and signaling was obtained by alanine scanning mutagenesis. Amino acid alterations close to the Ig-fold were shown to have the most drastic effect on ligand binding, whereas alanine mutations of the membrane-proximal stalk amino acids showed K_D values similar to wildtype NKp30 (compare to 3.1.2). The only exception was the R143A mutant, which displayed a slightly higher K_D value. In western blot analysis, under non-reducing conditions, apart from the signal of the homodimer, a second signal with approximately twice the size was visible for all NKp30-Fc fusion proteins. The R143A mutant showed an elevated amount of this higher molecular weight signal compared to the other mutants. It might be speculated that in this case the substitution of the positive charge led to a longer hydrophobic region that causes clustering of the proteins, which might be connected to differences in K_D values. However, this was not addressed further.

Every alanine mutant showed impaired signaling capacity in reporter assays with Ba/F3 B7-H6 cells, when compared to wildtype (3.1.2). As expected, signaling capacity was completely lost when R143, which is believed to enable an intramembrane charge interaction with aspartate residues of CD3ζ [226], was mutated to alanine. In contrast, signaling was maintained when R143 was substituted by lysine (R143K), showing that a positive charge on position 143 is essential and sufficient for signaling. In addition to R143, the two preceding leucine residues, which are conserved in NKp30 and NKp46, were shown to be of particular importance for NKp30 signaling. This suggested a similar mechanism for signal transduction to CD3ζ for both NCRs. Moreover, the presence of several leucine residues in front of the aspartic acid in the transmembrane domain of CD3ζ [226] further indicates the importance of such residues for the signaling interface and presumably for compensation of charge repellence within the hydrophobic membrane environment. In addition, the stalk domain is a highly hydrophobic region, which might induce the formation of NKp30 oligomers. An impact of the stalk on NKp30 ectodomain self-assembly was formerly shown by size exclusion chromatography (SEC) of soluble NKp30 ectodomain proteins produced in insect cells. NKp30 proteins containing the stalk domain (30Stalk-His) showed a higher amount of oligomers when compared to NKp30 proteins without stalk domain (30LBD-His) [209]. Ligand-induced receptor clustering is a common mechanism for receptor-mediated signaling in immune responses [240–242]. However, until now, this mechanism was not assured for NKp30 in *in vivo* settings.

Surprisingly, insertion of additional leucine residues in the vicinity of R143 in order to increase local hydrophobicity had no effect on signaling capacity. Moreover, attempts to displace R143 towards the C-terminus of NKp30, in order to bury it more deeply into the membrane and to uncouple ligand binding and CD3ζ signaling, showed an incompatibility with folding and plasma membrane targeting of NKp30 (experiments performed by Sandra Weil, AG Koch). This suggests that R143 might require additional conformational changes for translocation of the charged side chain into the membrane.

Formation of the NK cell immunological synapse generates a synaptic cleft of roughly 8 nm, which resembles the length of an NKG2D/MICA pair [89,243]. The length of the NKp30/B7-H6 complex is approximately the same as for KIR/HLA-C and NKG2D/MICA complexes [199]. This suggests that all receptor/ligand pairs within the immunological synapse must have a certain length to facilitate interactions. Additionally, the restricted space could cause conformational changes of the receptor after ligand binding, to adjust the receptor/ligand complex to the synaptic cleft. This could induce the conformational change needed to translocate the charged side chain of R143 into the membrane for signaling. Taken together, these data indicate that efficient ligand binding and its communication to

CD3ζ require a highly defined stalk domain with respect to length, sequence, conformational properties and charge.

N-glycosylation mapping showed that R143 of NKp30 is located in close proximity to the interface between membrane and extracellular region, as shown by the fact that L140 is located outside and R143 inside, or directly at the border of the membrane (3.1.4). As, due to these results, R143 could only be located a maximum of three amino acids into the membrane region, the charged side-chain is likely to snorkle to the extracellular region [244–248]. This suggests that in ground state, the positively charged side chain of R143 is not aligned with the negatively charged aspartate side chain of CD3ζ, which is located six amino acids into the membrane [226]. Interestingly, for NKp46, the location of R258 was mapped to be at least four amino acids away from the lipid bilayer, in the extracellular region. This speaks for slight differences in the conformational changes that lead to activation of NKp30 and NKp46. These differences might also explain the fact that the stalk domain of NKp46 is not able to mediate ligand-induced signaling of NKp30, while principal signaling capacity is preserved.

Until now, the mechanisms that induce signaling via adaptor proteins after ligand binding to immunoreceptors are largely unknown. For T cells it is suggested that both, TCR aggregation and conformational changes after ligand binding may play a role for signaling (reviewed in Smith-Garvin *et al.* [249]). As results from this thesis indicated that a translocation of R143 from the interface between membrane and extracellular region to the inner core of the membrane might induce signaling, it was questionable if this translocation facilitates the assembly of the receptor/CD3ζ complex or leads to its activation. Immunofluorescence and flow cytometry experiments showed that the presence of CD3ζ clearly increases the plasma membrane expression of NKp30 and NKp46 even in the absence of ligand (3.1.5). This argues for the existence of pre-assembled NKp30/CD3ζ and NKp46/CD3ζ complexes on the plasma membrane of inactive cells. Therefore, R143 is more likely to provide a switch to induce CD3ζ signaling than to promote assembly of the NKp30/CD3ζ complex. This idea is compatible with previous reports showing that CD3ζ is essential for plasma membrane expression of the TCR [224,250] and that the TCR/CD3ζ complex is loosely associated in the absence of ligand [251]. Previous studies demonstrated that in the presence of lipid, the cytoplasmic tail of CD3ζ is folded, thereby preventing ITAM phosphorylation, whereas in aqueous solution, it loses its conformation and can be phosphorylated. This indicates, that without activation, the cytoplasmic tail of CD3ζ might be associated with the plasma membrane and therefore be inaccessible to phosphorylation. After activation via receptor-crosslinking, it could be released from the membrane, leading to phosphorylation of the ITAM motifs [252]. Additionally, a piston-like movement of the TCR complex upon ligand binding is possible, which could be mediated by the transmembrane domain of CD3εγ [253]. Similar

mechanisms might be relevant for signal transduction of the NKp30/CD3ζ and NKp46/CD3ζ complex.

Based on these data, two interconvertible types of NKp30/CD3ζ assemblies can be proposed: (1) a signaling-incompetent structural NKp30/CD3ζ complex and (2) a ligand-induced signaling-competent NKp30/CD3ζ complex. Moreover, it can be suggested that ligand binding to the ectodomain of NKp30 (and presumably NKp46) induces translocation of R143 (R258 in NKp46) more deeply into the membrane for alignment with the aspartate of CD3ζ and activation of CD3ζ signaling. This conformational change might lead to the release of the previously membrane-associated cytoplasmic tail of CD3ζ, and thereby facilitate phosphorylation of the ITAM motifs (Fig. 38). Involvement of snorkeling residues in control of membrane signaling was already shown for integrins, where substitution of the snorkeling to a non-snorkeling amino acid leads to spontaneous integrin activation [254–256]. Interestingly, in the present study, substitution of R143 with a non-snorkeling amino acid had the opposite effect, leading to a complete loss of signaling capacity of NKp30, while substitution with a snorkeling-competent lysine did not impair signaling. This shows the mechanism of signaling control of NKp30 to be different from the mechanism found in integrins. Further studies are needed to elucidate the proposed contribution of R143 to signaling of NKp30 in more detail.

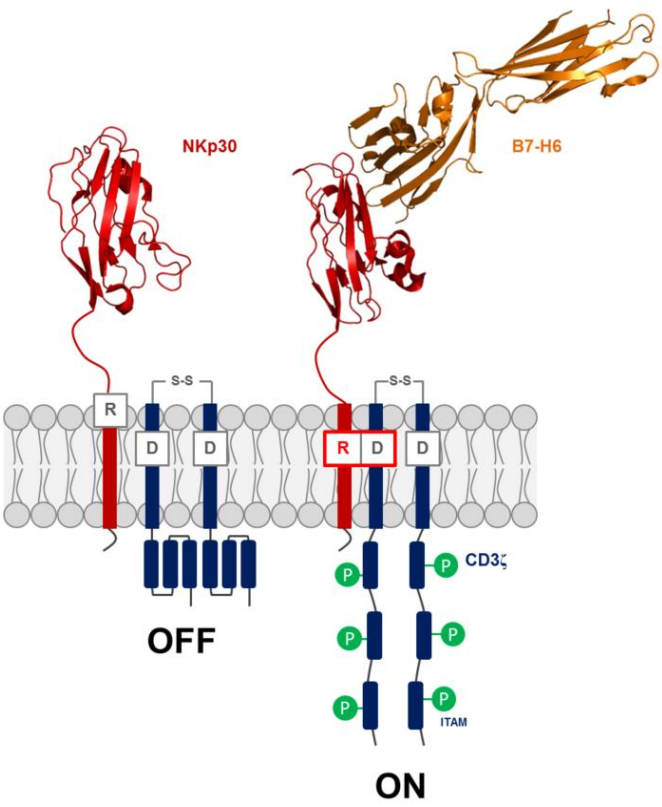

Figure 38. Model for ligand-induced activation of NKp30 and signal transduction to CD3ζ. In ground-state (OFF), NKp30 (PDB: 3NOI) and CD3ζ form a signaling incompetent structural complex (NKp30/CD3ζ) with R143 placed directly at the plasma membrane interface. Upon ligand binding (NKp30/B7-H6, PDB: 3PV6), conformational changes within NKp30 enable translocation of R143 more deeply into the plasma membrane for alignment with aspartate residues of CD3ζ. Consequently, the structural NKp30/CD3ζ complex is converted into a signaling competent complex (ON), which releases the formerly membrane-associated cytoplasmic tail of CD3ζ and mediates CD3ζ-dependent cellular signaling.

4.2 A Genome-wide shRNA Screening Did Not Confirm the Existence of Unknown Cellular NCR Ligands on Tumor Cell Lines

Analysis of the existence of yet unknown NCR ligands has been shown to be a big challenge. Attempts to co-purify NCR ligands with their corresponding receptors have mostly failed or led to low recovery rates, thereby preventing subsequent identification. This might be caused by different reasons like low affinity or problems in solubilization of single-pass and multi-pass transmembrane proteins [257–259]. As observed in this thesis, solubilization of NCRs themselves is indeed critical and highly depends on lipid composition of the host cell membrane and characteristics of the detergent. In addition, NCRs are likely to be recruited to lipid rafts upon formation of the activating NK cell synapse, which might lead to a close interaction with other activating NK cell receptors and to solubilization problems. Lipid rafts, also called detergent resistant membranes (DRM), are plasma membrane microdomains, which are assumed to be important for cell signaling and membrane trafficking due to co-localization of certain surface receptors and signaling molecules [260,261]. They are rich in sphingolipids with saturated acyl chains and cholesterol in the outer leaflet [262]. It has been demonstrated that lipid rafts accumulate in the immunological synapse of cytotoxic T lymphocytes (CTL) [263–265] and NK cells [266]. Lipid rafts cluster at the contact site of NK cell and target cell upon formation of the activating NK cell synapse [266]. In contrast, clustering of lipid rafts does not appear upon formation of the inhibitory NK cell synapse [267,268]. Other activating NK cell receptors, like 2B4 and NKG2D were already shown to be associated with lipid rafts upon ligation [104,269]. For NCRs, recruitment to lipid rafts is assumed, but was not yet proven.

Additionally, properties of the NCR ligands are unknown and the binding interfaces might depend on secondary modifications. Moreover, a stable NCR/ligand interaction might require additional actions on the cell surface, like complex formation with other receptors, which is a suggested mechanism for NCRs [270]. This can only be reflected by analysis of NCR ligands on living cells, and not for example in a co-purification setting with soluble NCR-Fc fusion proteins. Finally, NCRs have been shown to recognize non-proteinaceous ligands like heparan sulfate proteoglycans, which are not likely to be identified in conventional approaches [137].

Soluble NKp30-Fc fusion proteins can bind to tumor cell lines that neither express B7-H6 nor BAG-6 on their surface (Fig. 26 and [271]). For NKp46, no tumor cell surface ligands have been identified so far. However, also soluble NKp44- and NKp46-Fc fusion proteins were able to bind to tumor cell lines (Fig. 26). Other groups obtained identical results with NCR-Fc fusion proteins and NCR-ILZ fusion proteins [142,160,272,273]. This indicated a possible existence of yet unknown NCR ligands on tumor cells, which was further analyzed in this

thesis. As stated earlier, analysis of the existence of such ligands is critical. An shRNA screening like the one implemented in this thesis has the advantage that it allows for analysis of NCR ligands on living cells. Therefore, the chosen cell lines were transduced with a genome-wide shRNA library and afterwards selected for impaired NCR ligand expression by decoration with NCR-Fc fusion proteins and cell sorting. In this setting, failures due to low solubility of NCR ligands or NCRs themselves can be excluded. Additionally, secondary modifications of the binding interface and synergistic actions such as complex formation with other factors (like co-ligands) on the cell surface should be preserved, as long as they originate from the ligand and not from the NCR itself.

Interestingly, even though this screening approach has a lot of advantages, no tumor cell surface ligands could be identified for the NCRs, which might be caused by different reasons. The NCR-Fc fusion proteins used in this study contained the complete ectodomain of the receptors and showed reduced background binding to Fc-gamma receptors (FcγR) and neonatal Fc receptor (FcRn) [208]. But apart from these advantages, the use of Fc fusion proteins is critical to identify yet unknown NCR ligands. For one, the Fc fusion proteins show a reduced background binding to Fc receptors, but no complete loss of it. Background binding might therefore hinder the identification of unknown ligands in this setting, especially if they are expressed in low levels. Additionally, it was shown, that the glycosylation pattern of NKp30-Fc fusion proteins is critical to mediate binding affinity to heparan sulfate and seems to depend on the cell line used for expression [150]. Glycosylation of NKp30-Fc proteins produced in 293T cells seems to differ from glycosylation of NKp30-Fc proteins produced in NK-92 cells [208]. This might negatively affect the outcome of a ligand screening. Furthermore, additional requirements like complex formation with other receptors on the NK cell surface or homo-oligomerization can not contribute to ligand binding in this setting. On the basis of their structure, monovalent receptor/ligand interactions are expected for all of the NCRs. In case of NKp30, the crystallization of the receptor bound to its ligand B7-H6 showed a 1:1 stoichiometry [199]. Dimerization or homo-oligomerization, as formerly shown for NKp30 ectodomains [209] might provide a mechanism how the receptors are able to interact with sequencially and structurally unrelated ligands. In T cells, ligand-induced receptor clustering is a common mechanism for receptor-mediated signaling [240–242]. A selective cross-talk between the NCRs could be another explanation [270]. Ligands recognized by the NCRs via one of these scenarios could not be found with the screening method implemented here, as NCR-Fc fusion proteins are not suitable to picture such physiological interactions. Ideally, such a screening should be carried out using NK cells instead of NCR-Fc fusion proteins for selection of cells with reduced ligand expression. This way, all additional requirements for receptor/ligand interactions would be fulfilled, as the interaction would be similar to the native process. In such a positive selection, cells with

reduced NCR-ligand expression after shRNA knockdown would be ideally resistant to NK cell-mediated killing while cells in which shRNA knockdown did not lead to reduced ligand expression would be killed. Therefore, cells containing shRNAs against potential NCR ligands would be enriched and shRNA sequences could be subsequently analyzed from this cell cohort. Problematically, this approach is not usable, due to the variety of different receptors mediating cytotoxicity on NK cells. Reduced expression of one NCR ligand on a cell is likely to be overcome by other receptor/ligand interactions, thereby preventing a positive selection of cells. Knockout approaches leaving just one functional receptor on the surface of the NK cell are not applicable due to the high number of different receptors (activating as well as inhibitory) and the amount of genetic modifications that would be needed.

Many of the proteins found in the initial candidate lists were intracellular components involved in transport of membrane proteins. As these proteins are not present on the cell surface and can therefore not act as primary ligands of the NCRs, they were excluded from the final lists. Either way, they are likely to contribute to membrane targeting and/or retention of putative NCR ligands and could therefore play a role in recognition of tumor cells by NK cells.

Furthermore, an autocrine influence of a secreted protein of the target cell is possible, which could act like a soluble adaptor molecule between the membrane-bound ligand protein and the receptor. As the final candidate lists only contained proteins that can be targeted to the plasma membrane, such secreted factors would not be identified in this screening. The requirement of such soluble proteins to facilitate the NCR/ligand interaction would also explain the difficulties in the identification of NCR ligands with other screening methods like pull-down, knock-in or bait-and-prey screenings.

In addition, proteins that are essential for the survival of the cell are unlikely to be identified as ligands in this screening approach. This is caused by the fact that knockdown of an essential protein could lead to severely impaired viability of the cell, causing early cell death or decreased proliferation. In contrast, as implementation of shRNAs leads to knockdown but not knockout of the putative ligands, the remaining amount of protein could still be sufficient for an interaction with the Fc fusion protein and thereby lead to a false negative result. Furthermore, abnormal behavior of NCR ligands, like retargeting to the plasma membrane upon cellular stress (as it was shown for BAG-6)[143,144] could negatively influence the outcome of the established method.

Validation might be another critical step in the identification of unknown NCR ligands. In case of complex formation between different proteins on the cell surface to form an NCR ligand, knockdown of a single component could be sufficient to lead to impaired NCR-Fc binding visible in the screening. But knock-in of this single component in a validation experiment

might not lead to increased NCR-Fc binding as other essential components could be missing. Therefore, other validation approaches might be needed to exclude the putative ligands.

Finally, the existence of yet unknown NCR ligands on tumor cells could not be verified in this screening. It is possible that no yet unknown proteinaceous NCR ligands exist on tumor cells and NCR-Fc fusion proteins might bind to other surface structures like carbohydrates, which can not be found directly in such screenings.

4.3 A Putative Mouse NKp30 Protein is Impacted by N-Glycosylation and has an Unknown Ligand on Murine Mastocytoma Cells

On human NK cells, NKp30 is a major activating receptor that plays an important role mediating cytotoxicity against virally infected and malignantly transformed cells [142,143,146,148,236]. Additionally, it participates in maturation and killing of immature DCs [144,200,274]. Human NKp30 is expressed in six different splice forms. From an evolutionary point, the existence of these splice forms with different tissue distribution and function might reflect an increase in complexity and fine tuning of the innate immune response [139]. Alignment of NKp30 protein sequences from different species showed a high sequence similarity between human and monkey and between rat and mouse NKp30 (Fig. 32). Sequence similarity of NKp30 in human and chimpanzee (*P. troglodytes*) is 99%, while it is 95% and 90% in human and macaques (*M. mulatta* and *M. fascicularis*, respectively, Fig. 32). This is in accordance with the fact that chimpanzees and humans diverged approximately 5-6 million years ago, whereas macaques and humans diverged approximately 20 million years ago [275]. While NKp30 is expressed as a functional receptor on rat splenic NK cell subsets, it is only a pseudogene in mice, with exception of *M. caroli* [169,193]. The term “pseudogene” describes gene copies with coding-sequence deficiencies like frameshifts and premature stop codons, that have close similarities to orthologous genes but are nonfunctional [276,277]. In case of murine NKp30, the gene sequence is an unprocessed pseudogene that contains two premature stop codons and would encode a severely truncated and nonfunctional protein [169]. Such unprocessed pseudogenes emerge via gene duplication and have introns and regulatory sequences, only their expression is prevented [278,279]. Duplicated genes can either obtain new adaptive functions, can be maintained as they were at the time of duplication or can be silenced and become pseudogenes [280–284]. It is suggested that pseudogenes develop because the gene they arose of did not lead to a selection advantage or even conferred a selection disadvantage for the organism in evolutionary terms [277]. The murine NKp30 pseudogene might have developed from an ancestral *NCR* gene. Formerly, it was suggested that the NCRs

evolutionary appeared in the following progression: NKp46-NKp30-NKp44 [139]. Interestingly, newer studies suggest that NKp44 and NKp30 are evolutionary older than NKp46. NKp46 is only found in mammalian species, while NKp44 is also present in carp and NKp30 is present in almost all jawed vertebrate species (including cartilaginous fish). From this, NKp30 seems to be the most conserved and evolutionary oldest NK cell receptor (NKR) [140,141]. Additionally, it is suggested that NKp46 does not share the same ancestor than NKp30 and NKp44, but has a common ancestor with KIRs, as it maps to the LRC on human chromosome 19q13 near the KIR genes [140]. Both suggestions are in line with the fact that NKp46 is a functional protein in mouse, while NKp30 is only present as a pseudogene and NKp44 is completely lost. Interestingly, *M. caroli* is the only mouse strain that expresses NKp30 on mRNA level. Analysis of NKp30 mRNAs revealed the presence of two different transcripts, one of them containing an additional exon between exon 1 and 2, which leads to a frameshift and to generation of a new premature stop codon in the Ig domain. In the other transcript, a small intron between exon 2 and 3 is retained, which could lead to the production of a soluble NKp30 protein without transmembrane region. Soluble NKp30 can also be detected in rat, but not in any other mammals [169].

To shed light on the evolutionary role of the murine NKp30 pseudogene, the two premature stop codons in the extracellular domain of the *M. musculus* NKp30 gene sequence were repaired and the protein was expressed as full length receptor and as soluble mNKp30-Fc fusion protein. Interestingly, both mNKp30 constructs were expressed but intracellularly retained in A5-GFP and HEK 293T/17 cells, respectively. Failure of plasma membrane targeting due to mutations in the signal peptide could be excluded, since both constructs contained different signal peptides (full length receptor: mouse NKp30 signal peptide, Fc fusion protein: IL-2 secretion sequence) and the signal peptides of mouse and rat NKp30 proteins are homologue. Interestingly, sequence comparison showed that the three N-linked glycosylation motifs in the extracellular domain of NKp30 are conserved between human and rat, but are missing in the murine sequence. Previous work showed that N-glycosylation at these sides is important for plasma membrane targeting, ligand binding and signaling of human NKp30 [208]. A triple mutant that lacks all N-glycosylation sides (N42Q/N68Q/N121Q) was not targeted to the cell surface of A5-GFP cells and only small amounts could be detected in membrane fractions of transduced 293T cells. B7-H6 binding of NKp30 was shown to depend on glycosylation of N42, while glycosylation of N42 and N68 was important for intracellular signaling upon B7-H6 binding. In contrast, glycosylation of N68 was critical for NKp30/BAG-6 binding [208]. Altogether this speaks for the high impact of N-glycosylation on NKp30 function. As the three N-glycosylation sites are also present in rat and dog (and two of them are present in cow), it is likely that the ancestral NKp30 gene contained the three N-glycosylation sites. In the present study, N-glycosylation facilitated

secretion of the mNKp30-Fc fusion protein (mNKp30-glyco-Fc), while the full length receptor (mNKp30-glyco) was still intracellularly retained. This indicates the existence of additional sequence motifs outside of the extracellular region, which lead to intracellular retention independent from N-glycosylation. The sequence identity of rat and mouse NKp30 transmembrane domains leads to the assumption, that this sequence motif might be located in the cytosolic region of the NKp30 receptor. This is in line with the fact that the intracellular regions of NKp30 differ among species and might activate different signaling pathways [139,169,193,195]. As shown in this thesis, human NKp30 forms a pre-assembled complex with the signaling adaptor protein CD3ζ. This facilitates plasma membrane targeting and retention of the receptor. Therefore, it can be assumed that intracellular retention of the full length mNKp30 and mNKp30-glyco receptors might be due to an inability to assemble with CD3ζ, which is constitutively expressed in A5-GFP cells. While the intracellularly retained full length mNKp30-glyco receptor could not serve for investigation of ligand binding and signaling, mNKp30-glyco-Fc fusion proteins could be used to investigate a potential mNKp30-glyco/B7-H6 interaction and to screen different mouse cell lines for expression of potential mNKp30-glyco ligands. Binding of mNKp30-glyco-Fc to Ba/F3 B7-H6 cells was not observed. The absence of such an interaction is not surprising as the B7-H6 full length sequence is not present in mice [142] and the NKp30/B7-H6 system shows a clear co-evolving receptor/ligand relationship [141]. Interestingly, hNKp30-Fc showed no binding to the different mouse cell lines analyzed in a cell decoration screening, while mNKp30-glyco-Fc was able to bind to P815 cells (Fig. 36). Thus, mNKp30-glyco-Fc recognizes an unknown cellular ligand on murine mastocytoma cells. This unknown ligand might be of mast cell origin or emerge from cancerous cell transformation. Thus, it remains elusive, if a putative murine NKp30 receptor might be related to an immunoregulatory NK cell response or to the NK cell-mediated recognition and elimination of transformed cells. Mouse bone marrow-derived cultured mast cells, activated with lipopolysaccharide, polyinosinic-polycytidylic acid, or CpG can stimulate NK cells to secrete IFNγ. This stimulation is cell contact-dependent and seems to be partly mediated by the OX40 ligand on mast cells. However, this interaction appears to be influenced by additional mediators, which were not yet determined [61]. Interestingly, mast cell/NK cell interactions seem to affect cytokine release by NK cells while their cytotoxicity is not affected. Differentially regulated cytotoxicity and cytokine production of NK cells have been shown for the human [16,285] as well as for the murine system [286,287]. Additionally, mast cell/NK cell interactions based on soluble mediators were shown to play a role in early virus infections. In dengue infection, immune surveillance by mast cells is important for NK cell recruitment and viral clearance [288], and human cord blood-derived mast cells, stimulated with virus-associated TLR3 agonist, can recruit NK cells via the CXCL8 (IL-8)/CXCR1 axis [289]. This data indicates a role of mast cells in recruitment and

cytokine release of NK cells. Therefore, it is possible that an interaction of an ancient NKp30 receptor with a surface ligand on mast cells might have played a role for immunoregulation of NK cells. However, this interaction got lost in mouse. In *M. caroli*, NKp30 is not likely to mediate a mast cell/NK cell interaction, due to its putative soluble character. An interaction of NKp30 with surface ligands on mast cells should be further investigated in other species, especially in human.

4.4 Conclusion and Perspective

Altogether, it was shown that the stalk domain of NKp30 contributes to signaling of a pre-assembled NKp30/CD3ζ complex. Moreover, regulation of NKp30 signaling seems to depend on two interconvertible types of NKp30/CD3ζ assemblies: (1) a signaling-incompetent structural NKp30/CD3ζ complex and (2) a ligand-induced signaling-competent NKp30/CD3ζ complex. Presumably, the same is true in case of NKp46. To further verify the proposed model, pull-down experiments could be used to analyze the assembly of the NKp30/CD3ζ complex in the presence and absence of ligand. However, NCR solubilization for pulldown experiments is critical, due to low solubility. Conformational changes that bring R143 into closer contact with the aspartate of CD3ζ after ligand binding could be confirmed by either solution NMR (nuclear magnetic resonance) in micelle environments or solid-state NMR in bilayer environments. Additionally, the model could be verified by electron spin resonance (ESR) spectroscopy of lipids that are spin-labeled close to the terminal methyl end of the acyl chains. Such spectra can resolve between lipids directly contacting the protein and those in the fluid bilayer regions of the membrane [290]. Moreover, this method can be used to detect oligomer formation [291–294] from the stoichiometry of the protein-associated lipid, which is related to intramembrane structure and assembly of integral membrane proteins [295,296]. The possibility of conformational change mechanisms to facilitate signal transduction between receptor and adaptor molecule via repositioning of oppositely charged residues should be further analyzed for other immunoreceptors, especially for the T cell receptor.
Despite the fact that tumor cell lines which neither express B7-H6 nor BAG-6 on their surface were shown to be stainable with NKp30-Fc fusion proteins, no yet unknown ligand could be identified by implementation of a genome-wide shRNA screening. The same was true in case of NKp44-Fc and NKp46-Fc. Anyway, as stated earlier, further validation approaches like a specific shRNA knockdown of the putative candidate could be needed to finally exclude or confirm the ligands. Additionally, negative selection by decoration with NCR-Fc fusion proteins and subsequent cell sorting might not be a perfect way to screen for ligands. Ideally, selection would be carried out by implementation of a cell line similar to the A5-GFP reporter cells, which only expresses one functional receptor on the surface. But receptor activation in

this cell line should not lead to GFP expression but to cytotoxic activity against the interaction partner mediated by release of perforin and granzymes. However, generation of such a cell line might be difficult due to the amount of genetic alterations that would be needed. Another possible approach to identify yet unknown proteinaceous ligands of the NCRs would be the plasmamembrane protein array (PMPA) technique as provided by Retrogenix. Here, NCR-Fc fusion proteins, produced in NK-92 cells, could be screenend for binding to ~ 4,500 human plasmamembrane proteins overexpressed in a ligand-negative cell line like HeLa. This approach has already successfully implemented to identify receptors for protein ligands, peptides and viruses [297–301].

In the present thesis, it was shown for the first time that a full length mNKp30 receptor, derived from the *M. musculus* NKp30 sequence by removal of the premature stop codons, would be intracellularly retained and that in case of receptor-Fc fusion proteins, glycosylation of the mNKp30 ectodomain is sufficient to counteract intracellular retention. Interestingly, the full length receptor stays intracellular despite glycosylation of the ectodomain. Additionally, it was shown that mNKp30-glyco is able to bind to an unknown surface molecule on P815 mouse mastocytoma cells. However, it is interesting that in mouse, expression of a conventional NKp30 membrane protein is prevented in so many ways, even in the two mouse strains that contain single nucleotide polymorphisms (SNPs) that remove the premature stop codons. As stated earlier, in *M. caroli*, analysis of mRNA expression revealed the presence of two different transcripts, one of them containing an additional exon between exon 1 and 2, which leads to a frameshift and to the generation of a new premature stop codon in the Ig domain. In the other transcript, a small intron between exon 2 and 3 is retained, and the mRNA would encode a soluble protein which misses the transmembrane domain when expressed. In *M. pahari*, a base insertion leads to a frameshift and to the generation of an additional premature stop codon in the middle of the Ig domain [169]. This speaks for an evolutionary high pressure against the NKp30 protein, which indicates that NKp30 expression in mice might not be beneficial or even confers an evolutionary disadvantage. To find the reason for this, it would be interesting to identify the interaction partner of the putative mNKp30 receptor, which could shed light on the evolutionary disadvantage caused by this interaction. In a first step, mNKp30-glyco should be analyzed for its binding to murine BAG-6, Gal-3 and OX40L by implementation of SPR measurements. Furthermore, different screening approaches like co-immunoprecipitation should be carried out to find the unknown ligand. Additionally, the exact intracellular localization of mNKp30-glyco should be analyzed by immunofluorescence with an antibody generated against the protein. Finally, it would be interesting to characterize mNKp30 proteins derived from other mouse strains like *M. caroli* and *M. pahari* in comparison to the one derived from *M. musculus*, to look for similarities in their behavior.

5. References

[1] Moretta A., Marcenaro E., Parolini S., Ferlazzo G., Moretta L.: NK cells at the interface between innate and adaptive immunity. *Cell Death Differ.* **2008**; 15(2):226–33.

[2] Sun J.C., Beilke J.N., Lanier L.L.: Adaptive immune features of natural killer cells. *Nature* **2009**; 457(7229):557–61.

[3] Sun J.C., Lanier L.L.: NK cell development, homeostasis and function: parallels with $CD8^+$ T cells. *Nat. Rev. Immunol.* **2011**; 11(10):645–57.

[4] O'Leary J.G., Goodarzi M., Drayton D.L., Andrian U.H. von: T cell- and B cell-independent adaptive immunity mediated by natural killer cells. *Nat. Immunol.* **2006**; 7(5):507–16.

[5] Paust S., Gill H.S., Wang B.Z., Flynn M.P., Moseman E.A., Senman B., *et al.*: Critical role for CXCR6 in NK cell-mediated antigen-specific memory to haptens and viruses. *Nat. Immunol.* **2010**; 11(12):1127–35.

[6] Herberman R.B., Nunn M.E., Lavrin D.H.: Natural cytotoxic reactivity of mouse lymphoid cells against syngeneic acid allogeneic tumors. I. Distribution of reactivity and specificity. *Int. J. Cancer* **1975**; 16(2):216–29.

[7] Kiessling R., Klein E., Wigzell H.: "Natural" killer cells in the mouse. I. Cytotoxic cells with specificity for mouse Moloney leukemia cells. Specificity and distribution according to genotype. *Eur. J. Immunol.* **1975**; 5(2):112–7.

[8] Freud A.G., Caligiuri M.A.: Human natural killer cell development. *Immunol. Rev.* **2006**; 214:56–72.

[9] Di Santo J.P.: Natural killer cells: diversity in search of a niche. *Nat. Immunol.* **2008**; 9(5):473–5.

[10] Ljunggren H.G., Karre K.: In search of the 'missing self': MHC molecules and NK cell recognition. *Immunol. Today* **1990**; 11(7):237–44.

[11] Tortorella D., Gewurz B.E., Furman M.H., Schust D.J., Ploegh H.L.: Viral subversion of the immune system. *Annu. Rev. Immunol.* **2000**; 18:861–926.

[12] Hewitt E.W.: The MHC class I antigen presentation pathway: Strategies for viral immune evasion. *Immunology* **2003**; 110(2):163–9.

[13] Kärre K., Ljunggren H.G., Piontek G., Kiessling R.: Selective rejection of H-2-deficient lymphoma variants suggests alternative immune defence strategy. *Nature* **1986**; 319(6055):675–8.

[14] Trinchieri G.: Biology of natural killer cells. *Adv. Immunol.* **1989**; 47:187–376.

[15] Cooper M.A., Fehniger T.A., Caligiuri M.A.: The biology of human natural killer-cell subsets. *Trends Immunol.* **2001**; 22(11):633–40.

[16] Cooper M.A., Fehniger T.A., Turner S.C., Chen K.S., Ghaheri B.A., Ghayur T., *et al.*: Human natural killer cells: a unique innate immunoregulatory role for the $CD56^{bright}$ subset. *Blood* **2001**; 97(10):3146–51.

[17] Baume D.M., Robertson M.J., Levine H., Manley T.J., Schow P.W., Ritz J.: Differential responses to interleukin 2 define functionally distinct subsets of human natural killer cells. *Eur. J. Immunol.* **1992**; 22(1):1–6.

[18] Sivori S., Cantoni C., Parolini S., Marcenaro E., Conte R., Moretta L., *et al.*: IL-21 induces both rapid maturation of human $CD34^+$ cell precursors towards NK cells and acquisition of surface killer Ig-like receptors. *Eur. J. Immunol.* **2003**; 33(12):3439–47.

[19] Romagnani C., Juelke K., Falco M., Morandi B., D'Agostino A., Costa R., *et al.*: $CD56^{bright}CD16^-$ killer Ig-like $receptor^-$ NK cells display longer telomeres and acquire features of $CD56^{dim}$ NK cells upon activation. *J. Immunol.* **2007**; 178(8):4947–55.

[20] Mandal A., Viswanathan C.: Natural killer cells: In health and disease. *Hematol. Oncol. Stem Cell Ther.* **2015**; 8(2):47–55.

[21] Imai K., Matsuyama S., Miyake S., Suga K., Nakachi K.: Natural cytotoxic activity of peripheral-blood lymphocytes and cancer incidence: an 11-year follow-up study of a general population. *The Lancet* **2000**; 356(9244):1795–9.

[22] Moffett-King A.: Natural killer cells and pregnancy. *Nat. Rev. Immunol.* **2002**; 2(9):656–63.
[23] Moffett-King A., Entrican G., Ellis S., Hutchinson J., Bainbridge D.: Natural killer cells and reproduction. *Trends Immunol.* **2002**; 23(7):332–3.
[24] Tirado-Gonzalez I., Barrientos G., Freitag N., Otto T., Thijssen V.L.J.L., Moschansky P., *et al.*: Uterine NK cells are critical in shaping DC immunogenic functions compatible with pregnancy progression. *PLoS ONE* **2012**; 7(10):e46755.
[25] Fu B., Li X., Sun R., Tong X., Ling B., Tian Z., *et al.*: Natural killer cells promote immune tolerance by regulating inflammatory TH_{17} cells at the human maternal-fetal interface. *PNAS* **2013**; 110(3):E231-40.
[26] Wingett D., Nielson C.P.: Divergence in NK cell and cyclic AMP regulation of T cell CD40L expression in asthmatic subjects. *J. Leukoc. Biol.* **2003**; 74(4):531–41.
[27] Ple C., Barrier M., Amniai L., Marquillies P., Bertout J., Tsicopoulos A., *et al.*: Natural killer cells accumulate in lung-draining lymph nodes and regulate airway eosinophilia in a murine model of asthma. *Scand. J. Immunol.* **2010**; 72(2):118–27.
[28] Haworth O., Cernadas M., Levy B.D.: NK cells are effectors for resolvin E1 in the timely resolution of allergic airway inflammation. *J. Immunol.* **2011**; 186(11):6129–35.
[29] Jira M., Antosova E., Vondra V., Strejcek J., Mazakova H., Prazakova J.: Natural killer and interleukin-2 induced cytotoxicity in asthmatics. *Allergy* **1988**; 43(4):294–8.
[30] Culley F.J.: Natural killer cells in infection and inflammation of the lung. *Immunology* **2009**; 128(2):151–63.
[31] Yabuhara A., Yang F.C., Nakazawa T., Iwasaki Y., Mori T., Koike K., *et al.*: A killing defect of natural killer cells as an underlying immunologic abnormality in childhood systemic lupus erythematosus. *J. Rheumatol.* **1996**; 23(1):171–7.
[32] Aramaki T., Ida H., Izumi Y., Fujikawa K., Huang M., Arima K., *et al.*: A significantly impaired natural killer cell activity due to a low activity on a per-cell basis in rheumatoid arthritis. *Mod. Rheumatol.* **2009**; 19(3):245–52.
[33] Zhang B., Yamamura T., Kondo T., Fujiwara M., Tabira T.: Regulation of experimental autoimmune encephalomyelitis by natural killer (NK) cells. *J. Exp. Med.* **1997**; 186(10):1677–87.
[34] Xu W., Fazekas G., Hara H., Tabira T.: Mechanism of natural killer (NK) cell regulatory role in experimental autoimmune encephalomyelitis. *J. Neuroimmunol.* **2005**; 163(1-2):24–30.
[35] Hao J., Liu R., Piao W., Zhou Q., Vollmer T.L., Campagnolo D.I., *et al.*: Central nervous system (CNS)-resident natural killer cells suppress Th_{17} responses and CNS autoimmune pathology. *J. Exp. Med.* **2010**; 207(9):1907–21.
[36] Gur C., Porgador A., Elboim M., Gazit R., Mizrahi S., Stern-Ginossar N., *et al.*: The activating receptor NKp46 is essential for the development of type 1 diabetes. *Nat. Immunol.* **2010**; 11(2):121–8.
[37] Maruyama T., Watanabe K., Takei I., Kasuga A., Shimada A., Yanagawa T., *et al.*: Anti-asialo GM1 antibody suppression of cyclophosphamide-induced diabetes in NOD mice. *Diabetes Res.* **1991**; 17(1):37–41.
[38] Maruyama T., Watanabe K., Yanagawa T., Kasatani T., Kasuga A., Shimada A., *et al.*: The suppressive effect of anti-asialo GM1 antibody on low-dose streptozotocin-induced diabetes in CD-1 mice. *Diabetes Res.* **1991**; 16(4):171–5.
[39] Gur C., Enk J., Kassem S.A., Suissa Y., Magenheim J., Stolovich-Rain M., *et al.*: Recognition and killing of human and murine pancreatic beta cells by the NK receptor NKp46. *J. Immunol.* **2011**; 187(6):3096–103.
[40] Brauner H., Elemans M., Lemos S., Broberger C., Holmberg D., Flodstrom-Tullberg M., *et al.*: Distinct phenotype and function of NK cells in the pancreas of nonobese diabetic mice. *J. Immunol.* **2010**; 184(5):2272–80.
[41] Poulton L.D., Smyth M.J., Hawke C.G., Silveira P., Shepherd D., Naidenko O.V., *et al.*: Cytometric and functional analyses of NK and NKT cell deficiencies in NOD mice. *Int. Immunol.* **2001**; 13(7):887–96.

[42] Pazmany L.: Do NK cells regulate human autoimmunity? *Cytokine* **2005**; 32(2):76–80.
[43] Dalbeth N., Callan M.F.C.: A subset of natural killer cells is greatly expanded within inflamed joints. *Arthritis Rheum.* **2002**; 46(7):1763–72.
[44] Erkeller-Yuksel F.M., Lydyard P.M., Isenberg D.A.: Lack of NK cells in lupus patients with renal involvement. *Lupus* **1997**; 6(9):708–12.
[45] Hervier B., Beziat V., Haroche J., Mathian A., Lebon P., Ghillani-Dalbin P., *et al.*: Phenotype and function of natural killer cells in systemic lupus erythematosus: excess interferon-gamma production in patients with active disease. *Arthritis. Rheum.* **2011**; 63(6):1698–706.
[46] Schepis D., Gunnarsson I., Eloranta M.L., Lampa J., Jacobson S.H., Kärre K., *et al.*: Increased proportion of $CD56^{bright}$ natural killer cells in active and inactive systemic lupus erythematosus. *Immunology* **2009**; 126(1):140–6.
[47] Park Y.W., Kee S.J., Cho Y.N., Lee E.H., Lee H.Y., Kim E.M., *et al.*: Impaired differentiation and cytotoxicity of natural killer cells in systemic lupus erythematosus. *Arthritis Rheum.* **2009**; 60(6):1753–63.
[48] Ferlazzo G., Pack M., Thomas D., Paludan C., Schmid D., Strowig T., *et al.*: Distinct roles of IL-12 and IL-15 in human natural killer cell activation by dendritic cells from secondary lymphoid organs. *PNAS* **2004**; 101(47):16606–11.
[49] Vitale M., Della Chiesa M., Carlomagno S., Romagnani C., Thiel A., Moretta L., *et al.*: The small subset of $CD56^{bright}CD16^{-}$ natural killer cells is selectively responsible for both cell proliferation and interferon-gamma production upon interaction with dendritic cells. *Eur. J. Immunol.* **2004**; 34(6):1715–22.
[50] Deniz G., Erten G., Kucuksezer U.C., Kocacik D., Karagiannidis C., Aktas E., *et al.*: Regulatory NK cells suppress antigen-specific T cell responses. *J. Immunol.* **2008**; 180(2):850–7.
[51] Piccioli D., Sbrana S., Melandri E., Valiante N.M.: Contact-dependent stimulation and inhibition of dendritic cells by natural killer cells. *J. Exp. Med.* **2002**; 195(3):335–41.
[52] Hayakawa Y., Screpanti V., Yagita H., Grandien A., Ljunggren H.G., Smyth M.J., *et al.*: NK cell TRAIL eliminates immature dendritic cells in vivo and limits dendritic cell vaccination efficacy. *J. Immunol.* **2004**; 172(1):123–9.
[53] Walzer T., Dalod M., Robbins S.H., Zitvogel L., Vivier E.: Natural-killer cells and dendritic cells: "l'union fait la force". *Blood* **2005**; 106(7):2252–8.
[54] Moretta L., Ferlazzo G., Bottino C., Vitale M., Pende D., Mingari M.C., *et al.*: Effector and regulatory events during natural killer-dendritic cell interactions. *Immunol. Rev.* **2006**; 214:219–28.
[55] Degli-Esposti M.A., Smyth M.J.: Close encounters of different kinds: dendritic cells and NK cells take centre stage. *Nat. Rev. Immunol.* **2005**; 5(2):112–24.
[56] Martin-Fontecha A., Thomsen L.L., Brett S., Gerard C., Lipp M., Lanzavecchia A., *et al.*: Induced recruitment of NK cells to lymph nodes provides IFN-gamma for T(H)1 priming. *Nat. Immunol.* **2004**; 5(12):1260–5.
[57] Morandi B., Bougras G., Muller W.A., Ferlazzo G., Munz C.: NK cells of human secondary lymphoid tissues enhance T cell polarization via IFN-gamma secretion. *Eur. J. Immunol.* **2006**; 36(9):2394–400.
[58] Lu L., Ikizawa K., Hu D., Werneck M.B.F., Wucherpfennig K.W., Cantor H.: Regulation of activated $CD4^{+}$ T cells by NK cells via the Qa-1-NKG2A inhibitory pathway. *Immunity* **2007**; 26(5):593–604.
[59] Takeda K., Dennert G.: The development of autoimmunity in C57BL/6 lpr mice correlates with the disappearance of natural killer type 1-positive cells: evidence for their suppressive action on bone marrow stem cell proliferation, B cell immunoglobulin secretion, and autoimmune symptoms. *J. Exp. Med.* **1993**; 177(1):155–64.
[60] Portales-Cervantes L., Haidl I., Lee P., Marshall J.: Virus-infected human mast cells enhance Natural Killer cell functions. *J. Immunol.* **2015**; 9(1):94-108.

[61] Vosskuhl K., Greten T.F., Manns M.P., Korangy F., Wedemeyer J.: Lipopolysaccharide-mediated mast cell activation induces IFN-gamma secretion by NK cells. *J. Immunol.* **2010**; 185(1):119–25.

[62] Vivier E., Tomasello E., Baratin M., Walzer T., Ugolini S.: Functions of natural killer cells. *Nat. Immunol.* **2008**; 9(5):503–10.

[63] Biassoni R.: Human Natural Killer Receptors, Co-Receptors, and Their Ligands. In: Coligan J.E., Bierer B.E., Margulies D.H., Shevach E.M., Strober W., editors. *Current Protocols in Immunology*. Hoboken, NJ, USA: John Wiley & Sons, Inc; **2009**.

[64] Parham P.: MHC class I molecules and KIRs in human history, health and survival. *Nat. Rev. Immunol.* **2005**; 5(3):201–14.

[65] Vilches C., Parham P.: KIR: Diverse, Rapidly Evolving Receptors of Innate and Adaptive Immunity. *Annu. Rev. Immunol.* **2002**; 20(1):217–51.

[66] Karlhofer F.M., Ribaudo R.K., Yokoyama W.M.: MHC class I alloantigen specificity of Ly-49^{+} IL-2-activated natural killer cells. *Nature* **1992**; 358(6381):66–70.

[67] Moretta A., Sivori S., Vitale M., Pende D., Morelli L., Augugliaro R., *et al.*: Existence of both inhibitory (p58) and activatory (p50) receptors for HLA-C molecules in human natural killer cells. *J. Exp. Med*. **1995**; 182(3):875–84.

[68] Biassoni R., Cantoni C., Falco M., Verdiani S., Bottino C., Vitale M., *et al.*: The human leukocyte antigen (HLA)-C-specific "activatory" or "inhibitory" natural killer cell receptors display highly homologous extracellular domains but differ in their transmembrane and intracytoplasmic portions. *J. Exp. Med.* **1996**; 183(2):645–50.

[69] Colonna M., Samaridis J.: Cloning of immunoglobulin-superfamily members associated with HLA-C and HLA-B recognition by human natural killer cells. *Science* **1995**; 268(5209):405–8.

[70] Wagtmann N., Biassoni R., Cantoni C., Verdiani S., Malnati M.S., Vitale M., *et al.*: Molecular clones of the p58 NK cell receptor reveal immunoglobulin-related molecules with diversity in both the extra- and intracellular domains. *Immunity* **1995**; 2(5):439–49.

[71] Kumar V., McNerney M.E.: A new self: MHC-class-I-independent Natural-killer-cell self-tolerance. *Nat. Rev. Immunol.* **2005**; 5(5):363–74.

[72] Chlewicki L.K., Velikovsky C.A., Balakrishnan V., Mariuzza R.A., Kumar V.: Molecular Basis of the Dual Functions of 2B4 (CD244). *J. Immunol.* **2008**; 180(12):8159–67.

[73] Bauer S.: Activation of NK Cells and T Cells by NKG2D, a Receptor for Stress-Inducible MICA. *Science* **1999**; 285(5428):727–9.

[74] Pende D., Parolini S., Pessino A., Sivori S., Augugliaro R., Morelli L., *et al.*: Identification and molecular characterization of NKp30, a novel triggering receptor involved in natural cytotoxicity mediated by human natural killer cells. *J. Exp. Med.* **1999**; 190(10):1505–16.

[75] Cantoni C., Bottino C., Vitale M., Pessino A., Augugliaro R., Malaspina A., *et al.*: NKp44, A triggering receptor involved in tumor cell lysis by activated human natural killer cells, is a novel member of the immunoglobulin superfamily. *J. Exp. Med.* **1999**; 189(5):787–96.

[76] Vitale M., Bottino C., Sivori S., Sanseverino L., Castriconi R., Marcenaro E., *et al.*: NKp44, a novel triggering surface molecule specifically expressed by activated natural killer cells, is involved in non-major histocompatibility complex-restricted tumor cell lysis. *J. Exp. Med.* **1998**; 187(12):2065–72.

[77] Pessino A., Sivori S., Bottino C., Malaspina A., Morelli L., Moretta L., *et al.*: Molecular cloning of NKp46: A novel member of the immunoglobulin superfamily involved in triggering of natural cytotoxicity. *J. Exp. Med.* **1998**; 188(5):953–60.

[78] Sivori S., Vitale M., Morelli L., Sanseverino L., Augugliaro R., Bottino C., *et al.*: p46, a novel natural killer cell-specific surface molecule that mediates cell activation. *J. Exp. Med.* **1997**; 186(7):1129–36.

[79] Raulet D.H.: Roles of the NKG2D immunoreceptor and its ligands. *Nat. Rev. Immunol.* **2003**; 3(10):781–90.

[80] Obeidy P., Sharland A.F.: NKG2D and its ligands. *Int. J. Biochem. Cell Biol.* **2009**; 41(12):2364–7.
[81] Lauzon N.M., Mian F., Ashkar A.A.: Toll-like Receptors, Natural Killer Cells and Innate Immunity. In: Lambris JD, editor. *Current Topics in Innate Immunity.* New York, NY: Springer New York; **2007**, p. 1–11.
[82] Vivier E., Ugolini S., Blaise D., Chabannon C., Brossay L.: Targeting natural killer cells and natural killer T cells in cancer. *Nat. Rev. Immunol.* **2012**; 12(4):239–52.
[83] Raulet D.H., Guerra N.: Oncogenic stress sensed by the immune system: role of natural killer cell receptors. *Nat. Rev. Immunol.* **2009**; 9(8):568–80.
[84] Zamai L., Ahmad M., Bennett I.M., Azzoni L., Alnemri E.S., Perussia B.: Natural Killer (NK) Cell–mediated Cytotoxicity: Differential Use of TRAIL and Fas Ligand by Immature and Mature Primary Human NK Cells. *J. Exp. Med.* **1998**; 188(12):2375–80.
[85] Montel A.H., Bochan M.R., Goebel W.S., Brahmi Z.: Fas-mediated cytotoxicity remains intact in perforin and granzyme B antisense transfectants of a human NK-like cell line. *Cell Immunol.* **1995**; 165(2):312–7.
[86] Lee R.K., Spielman J., Zhao D.Y., Olsen K.J., Podack E.R.: Perforin, Fas ligand, and tumor necrosis factor are the major cytotoxic molecules used by lymphokine-activated killer cells. *J. Immunol.* **1996**; 157(5):1919–25.
[87] Topham N.J., Hewitt E.W.: Natural killer cell cytotoxicity: how do they pull the trigger? *Immunology* **2009**; 128(1):7–15.
[88] Wehner R., Dietze K., Bachmann M., Schmitz M.: The bidirectional crosstalk between human dendritic cells and natural killer cells. *J. Innate Immun.* **2011**; 3(3):258–63.
[89] Orange J.S.: Formation and function of the lytic NK-cell immunological synapse. *Nat. Rev. Immunol.* **2008**; 8(9):713–25.
[90] Krzewski K., Coligan J.E.: Human NK cell lytic granules and regulation of their exocytosis. *Front. Immunol.* **2012**; 3:335.
[91] Carpen O., Virtanen I., Lehto V.P., Saksela E.: Polarization of NK cell cytoskeleton upon conjugation with sensitive target cells. *J. Immunol.* **1983**; 131(6):2695–8.
[92] Orange J.S., Harris K.E., Andzelm M.M., Valter M.M., Geha R.S., Strominger J.L.: The mature activating natural killer cell immunologic synapse is formed in distinct stages. *PNAS* **2003**; 100(24):14151–6.
[93] Orange J.S., Ramesh N., Remold-O'Donnell E., Sasahara Y., Koopman L., Byrne M., *et al.*: Wiskott-Aldrich syndrome protein is required for NK cell cytotoxicity and colocalizes with actin to NK cell-activating immunologic synapses. *PNAS* **2002**; 99(17):11351–6.
[94] Gismondi A., Jacobelli J., Mainiero F., Paolini R., Piccoli M., Frati L., *et al.*: Cutting edge: functional role for proline-rich tyrosine kinase 2 in NK cell-mediated natural cytotoxicity. *J. Immunol.* **2000**; 164(5):2272–6.
[95] Lou Z., Jevremovic D., Billadeau D.D., Leibson P.J.: A balance between positive and negative signals in cytotoxic lymphocytes regulates the polarization of lipid rafts during the development of cell-mediated killing. *J. Exp. Med.* **2000**; 191(2):347–54.
[96] Fassett M.S., Davis D.M., Valter M.M., Cohen G.B., Strominger J.L.: Signaling at the inhibitory natural killer cell immune synapse regulates lipid raft polarization but not class I MHC clustering. *PNAS* **2001**; 98(25):14547–52.
[97] Sanni T.B., Masilamani M., Kabat J., Coligan J.E., Borrego F.: Exclusion of lipid rafts and decreased mobility of CD94/NKG2A receptors at the inhibitory NK cell synapse. *Mol. Biol. Cell* **2004**; 15(7):3210–23.
[98] Vyas Y.M., Maniar H., Lyddane C.E., Sadelain M., Dupont B.: Ligand binding to inhibitory killer cell Ig-like receptors induce colocalization with Src homology domain 2-containing protein tyrosine phosphatase 1 and interruption of ongoing activation signals. *J. Immunol.* **2004**; 173(3):1571–8.

[99] McCann F.E., Vanherberghen B., Eleme K., Carlin L.M., Newsam R.J., Goulding D., *et al.*: The size of the synaptic cleft and distinct distributions of filamentous actin, ezrin, CD43, and CD45 at activating and inhibitory human NK cell immune synapses. *J. Immunol.* **2003**; 170(6):2862–70.

[100] Vyas Y.M., Maniar H., Dupont B.: Cutting edge: differential segregation of the SRC homology 2-containing protein tyrosine phosphatase-1 within the early NK cell immune synapse distinguishes noncytolytic from cytolytic interactions. *J. Immunol.* **2002**; 168(7):3150–4.

[101] Dietrich J., Cella M., Colonna M.: Ig-like transcript 2 (ILT2)/leukocyte Ig-like receptor 1 (LIR1) inhibits TCR signaling and actin cytoskeleton reorganization. *J. Immunol.* **2001**; 166(4):2514–21.

[102] Masilamani M., Nguyen C., Kabat J., Borrego F., Coligan J.E.: CD94/NKG2A inhibits NK cell activation by disrupting the actin network at the immunological synapse. *J. Immunol.* **2006**; 177(6):3590–6.

[103] Endt J., McCann F.E., Almeida C.R., Urlaub D., Leung R., Pende D., *et al.*: Inhibitory receptor signals suppress ligation-induced recruitment of NKG2D to GM1-rich membrane domains at the human NK cell immune synapse. *J. Immunol.* **2007**; 178(9):5606–11.

[104] Watzl C., Long E.O.: Natural killer cell inhibitory receptors block actin cytoskeleton-dependent recruitment of 2B4 (CD244) to lipid rafts. *J. Exp. Med.* **2003**; 197(1):77–85.

[105] Burshtyn D.N., Shin J., Stebbins C., Long E.O.: Adhesion to target cells is disrupted by the killer cell inhibitory receptor. *Curr. Biol.* **2000**; 10(13):777–80.

[106] Mace E.M., Orange J.S.: Multiple distinct NK-cell synapses. *Blood* **2011**; 118(25):6475–6.

[107] Vivier E.: Natural Killer Cell Signaling Pathways. *Science* **2004**; 306(5701):1517–9.

[108] Bottino C., Castriconi R., Moretta L., Moretta A.: Cellular ligands of activating NK receptors. *Trends Immunol.* **2005**; 26(4):221–6.

[109] Watzl C., Long E.O.: Signal transduction during activation and inhibition of natural killer cells. *Curr. Protoc. Immunol.* **2010**; Chapter 11:Unit 11.9B.

[110] Billadeau D.D., Brumbaugh K.M., Dick C.J., Schoon R.A., Bustelo X.R., Leibson P.J.: The Vav-Rac1 pathway in cytotoxic lymphocytes regulates the generation of cell-mediated killing. *J. Exp. Med.* **1998**; 188(3):549–59.

[111] Tassi I., Colonna M.: The cytotoxicity receptor CRACC (CS-1) recruits EAT-2 and activates the PI3K and phospholipase Cgamma signaling pathways in human NK cells. *J. Immunol.* **2005**; 175(12):7996–8002.

[112] Ting A.T., Karnitz L.M., Schoon R.A., Abraham R.T., Leibson P.J.: Fc gamma receptor activation induces the tyrosine phosphorylation of both phospholipase C (PLC)-gamma 1 and PLC-gamma 2 in natural killer cells. *J. Exp. Med.* **1992**; 176(6):1751–5.

[113] Upshaw J.L., Schoon R.A., Dick C.J., Billadeau D.D., Leibson P.J.: The isoforms of phospholipase C-gamma are differentially used by distinct human NK activating receptors. *J. Immunol.* **2005**; 175(1):213–8.

[114] Long E.O., Kim H.S., Liu D., Peterson M.E., Rajagopalan S.: Controlling natural killer cell responses: integration of signals for activation and inhibition. *Annu. Rev. Immunol.* **2013**; 31:227–58.

[115] Caraux A., Kim N., Bell S.E., Zompi S., Ranson T., Lesjean-Pottier S., *et al.*: Phospholipase C-gamma2 is essential for NK cell cytotoxicity and innate immunity to malignant and virally infected cells. *Blood* **2006**; 107(3):994–1002.

[116] Regunathan J., Chen Y., Kutlesa S., Dai X., Bai L., Wen R., *et al.*: Differential and nonredundant roles of phospholipase Cgamma2 and phospholipase Cgamma1 in the terminal maturation of NK cells. *J. Immunol.* **2006**; 177(8):5365–76.

[117] Jiang K., Zhong B., Gilvary D.L., Corliss B.C., Hong-Geller E., Wei S., *et al.*: Pivotal role of phosphoinositide-3 kinase in regulation of cytotoxicity in natural killer cells. *Nat. Immunol.* **2000**; 1(5):419–25.

[118] Peterson M.E., Long E.O.: Inhibitory receptor signaling via tyrosine phosphorylation of the adaptor Crk. *Immunity* **2008**; 29(4):578–88.
[119] Abassi Y.A., Vuori K.: Tyrosine 221 in Crk regulates adhesion-dependent membrane localization of Crk and Rac and activation of Rac signaling. *EMBO J.* **2002**; 21(17):4571–82.
[120] Bouton A.H., Riggins R.B., Bruce-Staskal P.J.: Functions of the adapter protein Cas: signal convergence and the determination of cellular responses. *Oncogene* **2001**; 20(44):6448–58.
[121] Scaife R.M., Langdon W.Y.: c-Cbl localizes to actin lamellae and regulates lamellipodia formation and cell morphology. *J. Cell Sci.* **2000**; 113 Pt 2:215–26.
[122] Bolland S., Ravetch J.V.: Inhibitory pathways triggered by ITIM-containing receptors. *Adv. Immunol.* **1999**; 72:149–77.
[123] Vely F., Vivier E.: Conservation of structural features reveals the existence of a large family of inhibitory cell surface receptors and noninhibitory/activatory counterparts. *J. Immunol.* **1997**; 159(5):2075–7.
[124] Burshtyn D.N., Scharenberg A.M., Wagtmann N., Rajagopalan S., Berrada K., Yi T., *et al.*: Recruitment of tyrosine phosphatase HCP by the killer cell inhibitor receptor. *Immunity* **1996**; 4(1):77–85.
[125] Malbec O., Fong D.C., Turner M., Tybulewicz V.L., Cambier J.C., Fridman W.H., *et al.*: Fc epsilon receptor I-associated lyn-dependent phosphorylation of Fc gamma receptor IIB during negative regulation of mast cell activation. *J. Immunol.* **1998**; 160(4):1647–58.
[126] Smith K.G., Tarlinton D.M., Doody G.M., Hibbs M.L., Fearon D.T.: Inhibition of the B cell by CD22: a requirement for Lyn. *J. Exp. Med.* **1998**; 187(5):807–11.
[127] Maeda A., Scharenberg A.M., Tsukada S., Bolen J.B., Kinet, J.P., Kurosaki, T.: Paired immunoglobulin-like receptor B (PIR-B) inhibits BCR-induced activation of Syk and Btk by SHP-1. *Oncogene* **1999**; 18(14).
[128] Tamir I., Dal Porto J.M., Cambier J.C.: Cytoplasmic protein tyrosine phosphatases SHP-1 and SHP-2: regulators of B cell signal transduction. *Curr. Opin. Immunol.* **2000**; 12(3):307–15.
[129] Rohrschneider L.R., Fuller J.F., Wolf I., Liu Y., Lucas D.M.: Structure, function, and biology of SHIP proteins. *Genes Dev.* **2000**; 14(5):505–20.
[130] Tang Q., Grzywacz B., Wang H., Kataria N., Cao Q., Wagner J.E., *et al.*: Umbilical cord blood T cells express multiple natural cytotoxicity receptors after IL-15 stimulation, but only NKp30 is functional. *J. Immunol.* **2008**; 181(7):4507–15.
[131] Juelke K., Romagnani C.: Differentiation of human innate lymphoid cells (ILCs). *Curr. Opin.Immunol.* **2016**; 38:75–85.
[132] Spits H., Artis D., Colonna M., Diefenbach A., Di Santo J.P., Eberl G., *et al.*: Innate lymphoid cells — a proposal for uniform nomenclature. *Nat. Rev. Immunol.* **2013**; 13(2):145–9.
[133] Hudspeth K., Silva-Santos B., Mavilio D.: Natural cytotoxicity receptors: broader expression patterns and functions in innate and adaptive immune cells. *Front. Immunol.* **2013**; 4:69.
[134] Correia D.V., Fogli M., Hudspeth K., da Silva M.G., Mavilio D., Silva-Santos B.: Differentiation of human peripheral blood Vdelta1+ T cells expressing the natural cytotoxicity receptor NKp30 for recognition of lymphoid leukemia cells. *Blood* **2011**; 118(4):992–1001.
[135] Moretta A., Biassoni R., Bottino C., Mingari M.C., Moretta L.: Natural cytotoxicity receptors that trigger human NK-cell-mediated cytolysis. *Immunol. Today* **2000**; 21(5):228–34.
[136] Joyce M.G., Sun P.D.: The structural basis of ligand recognition by natural killer cell receptors. *J. Biomed. Biotechnol.* **2011**; 2011:203628.
[137] Koch J., Steinle A., Watzl C., Mandelboim O.: Activating natural cytotoxicity receptors of natural killer cells in cancer and infection. *Trends Immunol.* **2013**; 34(4):182–91.
[138] Lanier LL. NK cell recognition. *Annu. Rev. Immunol.* **2005**; 23(1):225–74.

[139] Maria A. de, Biassoni R., Fogli M., Rizzi M., Cantoni C., Costa P., *et al.*: Identification, molecular cloning and functional characterization of NKp46 and NKp30 natural cytotoxicity receptors in *Macaca fascicularis* NK cells. *Eur. J. Immunol.* **2001**; 31(12):3546–56.

[140] Ohta Y., Flajnik M.F.: Coevolution of MHC genes (LMP/TAP/class Ia, NKT-class Ib, NKp30-B7H6): lessons from cold-blooded vertebrates. *Immunol. Rev.* **2015**; 267(1):6–15.

[141] Flajnik M.F., Tlapakova T., Criscitiello M.F., Krylov V., Ohta Y.: Evolution of the B7 family: co-evolution of B7H6 and NKp30, identification of a new B7 family member, B7H7, and of B7's historical relationship with the MHC. *Immunogenetics* **2012**; 64(8):571–90.

[142] Brandt C.S., Baratin M., Yi E.C., Kennedy J., Gao Z., Fox B., *et al.*: The B7 family member B7-H6 is a tumor cell ligand for the activating natural killer cell receptor NKp30 in humans. *J. Exp. Med.* **2009**; 206(7):1495–503.

[143] Pogge von Strandmann E., Simhadri V.R., Tresckow B. von, Sasse S., Reiners K.S., Hansen H.P., *et al.*: Human leukocyte antigen-B-associated transcript 3 is released from tumor cells and engages the NKp30 receptor on natural killer cells. *Immunity* **2007**; 27(6):965–74.

[144] Simhadri V.R., Reiners K.S., Hansen H.P., Topolar D., Simhadri V.L., Nohroudi K., *et al.*: Dendritic cells release HLA-B-associated transcript-3 positive exosomes to regulate natural killer function. *PLoS ONE* **2008**; 3(10):e3377.

[145] Binici J., Hartmann J., Herrmann J., Schreiber C., Beyer S., Güler G., *et al.*: A soluble fragment of the tumor antigen BCL2-associated athanogene 6 (BAG-6) is essential and sufficient for inhibition of NKp30 receptor-dependent cytotoxicity of natural killer cells. *J. Biol. Chem.* **2013**; 288(48):34295–303.

[146] Arnon T.I., Achdout H., Levi O., Markel G., Saleh N., Katz G., *et al.*: Inhibition of the NKp30 activating receptor by pp65 of human cytomegalovirus. *Nat. Immunol.* **2005**; 6(5):515–23.

[147] Mavoungou E., Held J., Mewono L., Kremsner P.G.: A Duffy binding-like domain is involved in the NKp30-mediated recognition of *Plasmodium falciparum*-parasitized erythrocytes by natural killer cells. *J. Infect. Dis.* **2007**; 195(10):1521–31.

[148] Jarahian M., Fiedler M., Cohnen A., Djandji D., Hammerling G.J., Gati C., *et al.*: Modulation of NKp30- and NKp46-mediated natural killer cell responses by poxviral hemagglutinin. *PLoS Pathog.* **2011**; 7(8):e1002195.

[149] Hecht M.L., Rosental B., Horlacher T., Hershkovitz O., Paz J.L. de, Noti C., *et al.*: Natural cytotoxicity receptors NKp30, NKp44 and NKp46 bind to different heparan sulfate/heparin sequences. *J. Proteome Res.* **2009**; 8(2):712–20.

[150] Hershkovitz O., Jarahian M., Zilka A., Bar-Ilan A., Landau G., Jivov S., *et al.*: Altered glycosylation of recombinant NKp30 hampers binding to heparan sulfate: a lesson for the use of recombinant immunoreceptors as an immunological tool. *Glycobiology* **2007**; 18(1):28–41.

[151] Wang W., Guo H., Geng J., Zheng X., Wei H., Sun R., *et al.*: Tumor-released Galectin-3, a soluble inhibitory ligand of human NKp30, plays an important role in tumor escape from NK cell attack. *J. Biol. Chem.* **2014**; 289(48):33311–9.

[152] Ito K., Higai K., Shinoda C., Sakurai M., Yanai K., Azuma Y., *et al.*: Unlike natural killer (NK) p30, natural cytotoxicity receptor NKp44 binds to multimeric alpha2,3-NeuNAc-containing N-glycans. *Biol. Pharm. Bull.* **2012**; 35(4):594–600.

[153] Arnon T.I., Lev M., Katz G., Chernobrov Y., Porgador A., Mandelboim O.: Recognition of viral hemagglutinins by NKp44 but not by NKp30. *Eur. J. Immunol.* **2001**; 31(9):2680–9.

[154] Jarahian M., Watzl C., Fournier P., Arnold A., Djandji D., Zahedi S., *et al.*: Activation of natural killer cells by newcastle disease virus hemagglutinin-neuraminidase. *J. Virol.* **2009**; 83(16):8108–21.

[155] Gazit R., Gruda R., Elboim M., Arnon T.I., Katz G., Achdout H., *et al.*: Lethal influenza infection in the absence of the natural killer cell receptor gene Ncr1. *Nat. Immunol.* **2006**; 7(5):517–23.

[156] Ho J.W., Hershkovitz O., Peiris M., Zilka A., Bar-Ilan A., Nal B., *et al.*: H5-type influenza virus hemagglutinin is functionally recognized by the natural killer-activating receptor NKp44. *J. Virol.* **2008**; 82(4):2028–32.
[157] Rosental B., Brusilovsky M., Hadad U., Oz D., Appel M.Y., Afergan F., *et al.*: Proliferating cell nuclear antigen is a novel inhibitory ligand for the natural cytotoxicity receptor NKp44. *J. Immunol.* **2011**; 187(11):5693–702.
[158] Brusilovsky M., Radinsky O., Cohen L., Yossef R., Shemesh A., Braiman A., *et al.*: Regulation of natural cytotoxicity receptors by heparan sulfate proteoglycans in -cis: A lesson from NKp44. *Eur. J. Immunol.* **2015**; 45(4):1180–91.
[159] Hershkovitz O., Jivov S., Bloushtain N., Zilka A., Landau G., Bar-Ilan A., *et al.*: Characterization of the recognition of tumor cells by the natural cytotoxicity receptor, NKp44. *Biochemistry* **2007**; 46(25):7426–36.
[160] Baychelier F., Sennepin A., Ermonval M., Dorgham K., Debre P., Vieillard V.: Identification of a cellular ligand for the natural cytotoxicity receptor NKp44. *Blood* **2013**; 122(17):2935–42.
[161] Hershkovitz O., Rosental B., Rosenberg L.A., Navarro-Sanchez M.E., Jivov S., Zilka A., *et al.*: NKp44 receptor mediates interaction of the envelope glycoproteins from the West Nile and dengue viruses with NK cells. *J. Immunol.* **2009**; 183(4):2610–21.
[162] Arnon T.I., Achdout H., Lieberman N., Gazit R., Gonen-Gross T., Katz G., *et al.*: The mechanisms controlling the recognition of tumor- and virus-infected cells by NKp46. *Blood* **2004**; 103(2):664–72.
[163] Mandelboim O., Lieberman N., Lev M., Paul L., Arnon T.I., Bushkin Y., *et al.*: Recognition of haemagglutinins on virus-infected cells by NKp46 activates lysis by human NK cells. *Nature* **2001**; 409(6823):1055–60.
[164] Glasner A., Zurunic A., Meningher T., Lenac Rovis T., Tsukerman P., Bar-On Y., *et al.*: Elucidating the mechanisms of influenza virus recognition by Ncr1. *PLoS ONE* **2012**; 7(5):e36837.
[165] Vitenshtein A., Charpak-Amikam Y., Yamin R., Bauman Y., Isaacson B., Stein N., *et al.*: NK Cell Recognition of *Candida glabrata* through Binding of NKp46 and NCR1 to Fungal Ligands Epa1, Epa6, and Epa7. *Cell Host Microbe* **2016**; 20(4):527–34.
[166] Garg A., Barnes P.F., Porgador A., Roy S., Wu S., Nanda J.S., *et al.*: Vimentin Expressed on Mycobacterium tuberculosis-Infected Human Monocytes Is Involved in Binding to the NKp46 Receptor. *J. Immunol.* **2006**; 177(9):6192–8.
[167] Vankayalapati R., Wizel B., Weis S.E., Safi H., Lakey D.L., Mandelboim O., *et al.*: The NKp46 receptor contributes to NK cell lysis of mononuclear phagocytes infected with an intracellular bacterium. *J. Immunol.* **2002**; 168(7):3451–7.
[168] Foster C.E., Colonna M., Sun P.D.: Crystal structure of the human natural killer (NK) cell activating receptor NKp46 reveals structural relationship to other leukocyte receptor complex immunoreceptors. *J. Biol. Chem.* **2003**; 278(46):46081–6.
[169] Hollyoake M., Campbell R.D., Aguado B.: NKp30 (NCR3) is a pseudogene in 12 inbred and wild mouse strains, but an expressed gene in *Mus caroli*. *Mol. Biol. Evol.* 2005; 22(8):1661–72.
[170] Narni-Mancinelli E., Jaeger B.N., Bernat C., Fenis A., Kung S., Gassart A. de, *et al.*: Tuning of natural killer cell reactivity by NKp46 and Helios calibrates T cell responses. *Science* **2012**; 335(6066):344–8.
[171] Wende H., Colonna M., Ziegler A., Volz A.: Organization of the leukocyte receptor cluster (LRC) on human chromosome 19q13.4. *Mamm. Genome* **1999**; 10(2):154–60.
[172] Wagtmann N., Rojo S., Eichler E., Mohrenweiser H., Long E.O.: A new human gene complex encoding the killer cell inhibitory receptors and related monocyte/macrophage receptors. *Curr. Biol.* **1997**; 7(8):615–8.
[173] Gur C., Doron S., Kfir-Erenfeld S., Horwitz E., Abu-Tair L., Safadi R., *et al.*: NKp46-mediated killing of human and mouse hepatic stellate cells attenuates liver fibrosis. *Gut* **2012**; 61(6):885–93.

[174] Costello R.T., Sivori S., Marcenaro E., Lafage-Pochitaloff M., Mozziconacci M.J., Reviron D., *et al.*: Defective expression and function of natural killer cell-triggering receptors in patients with acute myeloid leukemia. *Blood* **2002**; 99(10):3661–7.
[175] Glasner A., Ghadially H., Gur C., Stanietsky N., Tsukerman P., Enk J., *et al.*: Recognition and prevention of tumor metastasis by the NK receptor NKp46/NCR1. *J. Immunol.* **2012**; 188(6):2509–15.
[176] Lakshmikanth T., Burke S., Ali T.H., Kimpfler S., Ursini F., Ruggeri L., *et al.*: NCRs and DNAM-1 mediate NK cell recognition and lysis of human and mouse melanoma cell lines in vitro and in vivo. *J. Clin. Invest.* **2009**; 119(5):1251–63.
[177] Cantoni C., Ponassi M., Biassoni R., Conte R., Spallarossa A., Moretta A., *et al.*: The three-dimensional structure of the human NK cell receptor NKp44, a triggering partner in natural cytotoxicity. *Structure* **2003**; 11(6):725–34.
[178] Campbell K.S., Yusa S., Kikuchi-Maki A., Catina T.L.: NKp44 triggers NK cell activation through DAP12 association that is not influenced by a putative cytoplasmic inhibitory sequence. *J. Immunol.* **2004**; 172(2):899–906.
[179] Manaster I., Mandelboim O.: The unique properties of uterine NK cells. *Am. J. Reprod. Immunol.* **2010**; 63(6):434–44.
[180] Rham C. de, Ferrari-Lacraz S., Jendly S., Schneiter G., Dayer J.M., Villard J.: The proinflammatory cytokines IL-2, IL-15 and IL-21 modulate the repertoire of mature human natural killer cell receptors. *Arthritis Res. Ther.* **2007**; 9(6):R125.
[181] Cella M., Fuchs A., Vermi W., Facchetti F., Otero K., Lennerz J.K.M., *et al.*: A human natural killer cell subset provides an innate source of IL-22 for mucosal immunity. *Nature* **2008**; 457(7230):722–5.
[182] Cella M., Otero K., Colonna M.: Expansion of human NK-22 cells with IL-7, IL-2, and IL-1beta reveals intrinsic functional plasticity. *PNAS* **2010**; 107(24):10961–6.
[183] Fuchs A., Cella M., Kondo T., Colonna M.: Paradoxic inhibition of human natural interferon-producing cells by the activating receptor NKp44. *Blood* **2005**; 106(6):2076–82.
[184] Vacca P., Montaldo E., Croxatto D., Loiacono F., Canegallo F., Venturini P.L., *et al.*: Identification of diverse innate lymphoid cells in human decidua. *Mucosal Immunol.* **2015**; 8(2):254–64.
[185] Hanna J., Goldman-Wohl D., Hamani Y., Avraham I., Greenfield C., Natanson-Yaron S., *et al.*: Decidual NK cells regulate key developmental processes at the human fetal-maternal interface. *Nat. Med.* **2006**; 12(9):1065–74.
[186] Korgun E.T., Celik-Ozenci C., Acar N., Cayli S., Desoye G., Demir R.: Location of cell cycle regulators cyclin B1, cyclin A, PCNA, Ki67 and cell cycle inhibitors p21, p27 and p57 in human first trimester placenta and deciduas. *Histochem. Cell Biol.* **2006**; 125(6):615–24.
[187] Vacca P., Cantoni C., Prato C., Fulcheri E., Moretta A., Moretta L., *et al.*: Regulatory role of NKp44, NKp46, DNAM-1 and NKG2D receptors in the interaction between NK cells and trophoblast cells. Evidence for divergent functional profiles of decidual versus peripheral NK cells. *Int. Immunol.* **2008**; 20(11):1395–405.
[188] Vieillard V., Strominger J.L., Debre P.: NK cytotoxicity against $CD4^+$ T cells during HIV-1 infection: a gp41 peptide induces the expression of an NKp44 ligand. *PNAS* **2005**; 102(31):10981–6.
[189] Rutjens E., Mazza S., Biassoni R., Koopman G., Radic L., Fogli M., *et al.*: Differential NKp30 inducibility in chimpanzee NK cells and conserved NK cell phenotype and function in long-term HIV-1-infected animals. *J. Immunol.* **2007**; 179(2):1389.
[190] Backman-Petersson E., Miller J.R., Hollyoake M., Aguado B., Butcher G.W.: Molecular characterization of the novel rat NK receptor 1C7. *Eur. J. Immunol.* **2003**; 33(2):342–51.
[191] Hsieh C.L., Nagasaki K., Martinez O.M., Krams S.M.: NKp30 is a functional activation receptor on a subset of rat natural killer cells. *Eur. J. Immunol.* **2006**; 36(8):2170–80.

[192] Hsieh C.L., Ogura Y., Obara H., Ali U.A., Rodriguez G.M., Nepomuceno R.R., *et al.*: Identification, cloning, and characterization of a novel rat natural killer receptor, RNKP30: a molecule expressed in liver allografts. *Transplantation* **2004**; 77(1):121–8.

[193] Sivakamasundari R., Raghunathan A., Zhang C.Y., Chowdhury R.R., Weissman S.M.: Expression and cellular localization of the protein encoded by the 1C7 gene: a recently described component of the MHC. *Immunogenetics* **2000**; 51(8-9):723–32.

[194] Neville M.J., Campbell R.D.: A new member of the Ig superfamily and a V-ATPase G subunit are among the predicted products of novel genes close to the TNF locus in the human MHC. *J. Immunol.* **1999**; 162(8):4745–54.

[195] Xie T., Rowen L., Aguado B., Ahearn M.E., Madan A., Qin S., *et al.*: Analysis of the gene-dense major histocompatibility complex class III region and its comparison to mouse. *Genome Res.* **2003**; 13(12):2621–36.

[196] Seidel E., Glasner A., Mandelboim O.: Virus-mediated inhibition of natural cytotoxicity receptor recognition. *Cell. Mol. Life Sci.* **2012**; 69(23):3911–20.

[197] Lanier L.L.: Natural killer cell receptor signaling. *Curr. Opin. Immunol.* **2003**; 15(3):308–14.

[198] Delahaye N.F., Rusakiewicz S., Martins I., Menard C., Roux S., Lyonnet L., *et al.*: Alternatively spliced NKp30 isoforms affect the prognosis of gastrointestinal stromal tumors. *Nat. Med.* **2011**; 17(6):700–7.

[199] Li Y., Wang Q., Mariuzza R.A.: Structure of the human activating natural cytotoxicity receptor NKp30 bound to its tumor cell ligand B7-H6. *J. Exp. Med.* **2011**; 208(4):703–14.

[200] Vitale M., Della Chiesa M., Carlomagno S., Pende D., Arico M., Moretta L., *et al.*: NK-dependent DC maturation is mediated by TNFalpha and IFNgamma released upon engagement of the NKp30 triggering receptor. *Blood* **2005**; 106(2):566–71.

[201] Sasaki T., Gan E.C., Wakeham A., Kornbluth S., Mak T.W., Okada H.: HLA-B-associated transcript 3 (Bat3)/Scythe is essential for p300-mediated acetylation of p53. *Genes Dev.* **2007**; 21(7):848–61.

[202] Lahm H., Andre S., Hoeflich A., Fischer J.R., Sordat B., Kaltner H., *et al.*: Comprehensive galectin fingerprinting in a panel of 61 human tumor cell lines by RT-PCR and its implications for diagnostic and therapeutic procedures. *J. Cancer Res. Clin. Oncol.* **2001**; 127(6):375–86.

[203] Lotan R., Matsushita Y., Ohannesian D., Carralero D., Ota D.M., Cleary K.R., *et al.*: Lactose-binding lectin expression in human colorectal carcinomas. Relation to tumor progression. *Carbohydr. Res.* **1991**; 213:47–57.

[204] Miyazaki J., Hokari R., Kato S., Tsuzuki Y., Kawaguchi A., Nagao S., *et al.*: Increased expression of galectin-3 in primary gastric cancer and the metastatic lymph nodes. *Oncol. Rep.* **2002**; 9(6):1307–12.

[205] Schmolke S., Drescher P., Jahn G., Plachter B.: Nuclear targeting of the tegument protein pp65 (UL83) of human cytomegalovirus: an unusual bipartite nuclear localization signal functions with other portions of the protein to mediate its efficient nuclear transport. *J. Virol.* **1995**; 69(2):1071–8.

[206] Bloushtain N., Qimron U., Bar-Ilan A., Hershkovitz O., Gazit R., Fima E., *et al.*: Membrane-associated heparan sulfate proteoglycans are involved in the recognition of cellular targets by NKp30 and NKp46. *J. Immunol.* **2004**; 173(4):2392–401.

[207] Zilka A., Landau G., Hershkovitz O., Bloushtain N., Bar-Ilan A., Benchetrit F., *et al.*: Characterization of the heparin/heparan sulfate binding site of the natural cytotoxicity receptor NKp46. *Biochemistry* **2005**; 44(44):14477–85.

[208] Hartmann J., Tran T.V., Kaudeer J., Oberle K., Herrmann J., Quagliano I., *et al.*: The stalk domain and the glycosylation status of the activating natural killer cell receptor NKp30 are important for ligand binding. *J. Biol. Chem.* **2012**; 287(37):31527–39.

[209] Herrmann J., Berberich H., Hartmann J., Beyer S., Davies K., Koch J.: Homo-oligomerization of the activating natural killer cell receptor NKp30 ectodomain increases its binding affinity for cellular ligands. *J. Biol. Chem.* **2014**; 289(2):765–77.

[210] Vidal K., Grosjean I., Revillard J.P., Gespach C., Kaiserlian D.: Immortalization of mouse intestinal epithelial cells by the SV40-large T gene. *J.Immunol. Methods* **1993**; 166(1):63–73.
[211] Andersen P.S., Menne C., Mariuzza R.A., Geisler C., Karjalainen K.: A Response Calculus for Immobilized T Cell Receptor Ligands. *J.Biol. Chem.* **2001**; 276(52):49125–32.
[212] Fiering S., Northrop J.P., Nolan G.P., Mattila P.S., Crabtree G.R., Herzenberg L.A.: Single cell assay of a transcription factor reveals a threshold in transcription activated by signals emanating from the T-cell antigen receptor. *Genes Dev.* **1990**; 4(10):1823–34.
[213] Hanahan D.: Techniques for transformation of E. coli. In: Glover, D.M., (ed.): *DNA Cloning. A Practical Approach*, p. 109–136.
[214] Mullis K.B., Faloona FA (eds.). *Recombinant DNA Part F*. Elsevier; *1987*.
[215] Saiki R., Scharf S., Faloona F., Mullis K., Horn G., Erlich H., *et al.*: Enzymatic amplification of beta-globin genomic sequences and restriction site analysis for diagnosis of sickle cell anemia. *Science* **1985**; 230(4732):1350–4.
[216] Sanger F., Nicklen S., Coulson A.R.: DNA sequencing with chain-terminating inhibitors. *PNAS* **1977**; 74(12):5463–7.
[217] Rudolph C., Lausier J., Naundorf S., Müller R.H., Rosenecker J.: In vivo gene delivery to the lung using polyethylenimine and fractured polyamidoamine dendrimers. *J. Gene Med.* **2000**; 2(4):269–78.
[218] Akinc A., Thomas M., Klibanov A.M., Langer R.: Exploring polyethylenimine-mediated DNA transfection and the proton sponge hypothesis. *J. Gene Med.* **2005**; 7(5):657–63.
[219] Laemmli U.K.: Cleavage of Structural Proteins during the Assembly of the Head of Bacteriophage T4. *Nature* **1970**; 227(5259):680–5.
[220] Moretta A., Bottino C., Vitale M., Pende D., Cantoni C., Mingari M.C., *et al.*: Activating receptors and coreceptors involved in human natural killer cell-mediated cytolysis. *Annu. Rev. Immunol.* **2001**; 19(1):197–223.
[221] Memmer S., Weil S., Beyer S., Zöller T., Peters E., Hartmann J., *et al.*: The stalk domain of NKp30 contributes to ligand binding and signaling of a pre-assembled NKp30/CD3zeta complex. *J. Biol. Chem.* **2016**; 291(49):25427–25438.
[222] Tomasello E., Desmoulins P.O., Chemin K., Guia S., Cremer H., Ortaldo J., *et al.*: Combined natural killer cell and dendritic cell functional deficiency in KARAP/DAP12 loss-of-function mutant mice. *Immunity* **2000**; 13(3):355–64.
[223] Hall C., Berkhout B., Alarcon B., Sancho J., Wileman T., Terhorst C.: Requirements for cell surface expression of the human TCR/CD3 complex in non-T cells. *Int. Immunol.* **1991**; 3(4):359–68.
[224] Kappes D., Tonegawa S.: Surface expression of alternative forms of the TCR/CD3 complex. *PNAS* **1991**; 88(23):10619–23.
[225] Sussman J., Bonifacino J., Lippincott-Schwartz J., Weissman A., Saito T., Klausner R., *et al.*: Failure to synthesize the T Cell CD3-zeta chain: Structure and function of a partial T cell receptor complex. *Cell* **1988**; 52(1):85–95.
[226] Call M.E., Schnell J.R., Xu C., Lutz R.A., Chou J.J., Wucherpfennig K.W.: The structure of the zetazeta transmembrane dimer reveals features essential for its assembly with the T cell receptor. *Cell* **2006**; 127(2):355–68.
[227] Arnaud J., Chenu C., Huchenq A., Gouaillard C., Kuhlmann J., Rubin B.: Defective interactions between TCR chains and CD3 heterodimers prevent membrane expression of TCR-alpha beta in human T cells. *J. Immunol.* **1996**; 156(6):2155–62.
[228] Hofmann K.: TMbase - A database of membrane spanning proteins segments. *Biol. Chem. Hoppe-Seyler* **1993**; 374:166.
[229] Cunningham B.C., Wells J.A.: High-resolution epitope mapping of hGH-receptor interactions by alanine-scanning mutagenesis. *Science* **1989**; 244(4908):1081–5.
[230] Mandelboim O., Malik P., Davis D.M., Jo C.H., Boyson J.E., Strominger J.L.: Human CD16 as a lysis receptor mediating direct natural killer cell cytotoxicity. *PNAS* **1999**; 96(10):5640–4.

[231] Chung I., Akita R., Vandlen R., Toomre D., Schlessinger J., Mellman I.: Spatial control of EGF receptor activation by reversible dimerization on living cells. *Nature* **2010**; 464(7289):783–7.
[232] Nilsson I.M., Heijne G. von: Determination of the distance between the oligosaccharyltransferase active site and the endoplasmic reticulum membrane. *J. Biol. Chem.* **1993**; 268(8):5798–801.
[233] Cheung J.C., Reithmeier R.A.: Membrane integration and topology of the first transmembrane segment in normal and Southeast Asian ovalocytosis human erythrocyte anion exchanger 1. *Mol. Membr. Biol.* **2005**; 22(3):203–14.
[234] Popov M., Li J., Reithmeier R.A.: Transmembrane folding of the human erythrocyte anion exchanger (AE1, Band 3) determined by scanning and insertional N-glycosylation mutagenesis. *Biochem. J.* **1999**; 339 (Pt 2):269–79.
[235] Popov M., Tam L.Y., Li J., Reithmeier R.A.: Mapping the ends of transmembrane segments in a polytopic membrane protein. Scanning N-glycosylation mutagenesis of extracytosolic loops in the anion exchanger, band 3. *J. Biol. Chem.* **1997**; 272(29):18325–32.
[236] Kaifu T., Escaliere B., Gastinel L.N., Vivier E., Baratin M.: B7-H6/NKp30 interaction: a mechanism of alerting NK cells against tumors. *Cell. Mol. Life Sci.* **2011**; 68(21):3531–9.
[237] Bassik M.C., Lebbink R.J., Churchman L.S., Ingolia N.T., Patena W., Leproust E.M., *et al.*: Rapid creation and quantitative monitoring of high coverage shRNA libraries. *Nat. Methods* **2009**; 6(6):443–5.
[238] Bassik M.C., Kampmann M., Lebbink R.J., Wang S., Hein M.Y., Poser I., *et al.*: A systematic mammalian genetic interaction map reveals pathways underlying ricin susceptibility. *Cell* **2013**; 152(4):909–22.
[239] Mendelson M., Tekoah Y., Zilka A., Gershoni-Yahalom O., Gazit R., Achdout H., *et al.*: NKp46 O-glycan sequences that are involved in the interaction with hemagglutinin type 1 of influenza virus. *J. Virol.* **2010**; 84(8):3789–97.
[240] Germain R.N.: T-cell signaling: the importance of receptor clustering. *Curr. Biol.* **1997**; 7(10):R640-4.
[241] Qian D., Weiss A.: T cell antigen receptor signal transduction. *Curr. Opin. Cell Biol.* **1997**; 9(2):205–12.
[242] Faure M., Barber D.F., Takahashi S.M., Jin T., Long E.O.: Spontaneous clustering and tyrosine phosphorylation of NK cell inhibitory receptor induced by ligand binding. *J. Immunol.* **2003**; 170(12):6107–14.
[243] McCann F.E., Suhling K., Carlin L.M., Eleme K., Taner S.B., Yanagi K., *et al.*: Imaging immune surveillance by T cells and NK cells. *Immunol. Rev.* **2002**; 189(1):179–92.
[244] Krishnakumar S.S., London E.: The control of transmembrane helix transverse position in membranes by hydrophilic residues. *J. Mol. Biol.* **2007**; 374(5):1251–69.
[245] Strandberg E., Killian J.A.: Snorkeling of lysine side chains in transmembrane helices: how easy can it get? *FEBS Lett.* **2003**; 544(1-3):69–73.
[246] Strandberg E., Morein S., Rijkers D.T., Liskamp R.M., van der Wel, P.C., Killian J.A.: Lipid dependence of membrane anchoring properties and snorkeling behavior of aromatic and charged residues in transmembrane peptides. *Biochemistry* **2002**; 41(23):7190–8.
[247] Segrest J.P., Loof H. de, Dohlman J.G., Brouillette C.G., Anantharamaiah G.M.: Amphipathic helix motif: classes and properties. *Proteins* **1990**; 8(2):103–17.
[248] Mishra V.K., Palgunachari M.N., Segrest J.P., Anantharamaiah G.M.: Interactions of synthetic peptide analogs of the class A amphipathic helix with lipids. Evidence for the snorkel hypothesis. *J. Biol. Chem.* **1994**; 269(10):7185–91.
[249] Smith-Garvin J.E., Koretzky G.A., Jordan M.S.: T cell activation. *Annu. Rev. Immunol.* **2009**; 27:591–619.
[250] John S., Banting G.S., Goodfellow P.N., Owen M.J.: Surface expression of the T cell receptor complex requires charged residues within the alpha chain transmembrane region. *Eur. J. Immunol.* **1989**; 19(2):335–9.

[251] Bolliger L., Johansson B., Palmer E.: The short extracellular domain of the T cell receptor zeta chain is involved in assembly and signal transduction. *Mol. Immunol.* **1997**; 34(12-13):819–27.
[252] Aivazian D., Stern L.J.: Phosphorylation of T cell receptor zeta is regulated by a lipid dependent folding transition. *Nat. Struct. Biol.* **2000**; 7(11):1023–6.
[253] Sun Z.J., Kim K.S., Wagner G., Reinherz E.L.: Mechanisms contributing to T cell receptor signaling and assembly revealed by the solution structure of an ectodomain fragment of the CD3$\epsilon\gamma$ heterodimer. *Cell* **2001**; 105(7):913–23.
[254] Arnaout M.A., Mahalingam B., Xiong J.P.: Integrin structure, allostery, and bidirectional signaling. *Annu. Rev. Cell Dev. Biol.* **2005**; 21:381–410.
[255] Shattil S.J., Kim C., Ginsberg M.H.: The final steps of integrin activation: the end game. *Nat. Rev. Mol. Cell Biol.* **2010**; 11(4):288–300.
[256] Hynes R.O.: Integrins: bidirectional, allosteric signaling machines. *Cell* **2002**; 110(6):673–87.
[257] Kalipatnapu S., Chattopadhyay A.: Membrane Protein Solubilization: Recent Advances and Challenges in Solubilization of Serotonin1A Receptors. *IUBMB Life* **2005**; 57(7):505–12.
[258] Thomas T.C., McNamee M.G.: Purification of membrane proteins. *Methods Enzymol.* **1990**; 182:499–520.
[259] Seddon A.M., Curnow P., Booth P.J.: Membrane proteins, lipids and detergents: not just a soap opera. *Biochim. Biophys. Acta* **2004**; 1666(1-2):105–17.
[260] Dykstra M., Cherukuri A., Sohn H.W., Tzeng S.J., Pierce S.K.: Location is everything: lipid rafts and immune cell signaling. *Annu. Rev. Immunol.* **2003**; 21:457–81.
[261] Marwali M.R., MacLeod M.A., Muzia D.N., Takei F.: Lipid Rafts Mediate Association of LFA-1 and CD3 and Formation of the Immunological Synapse of CTL. *J. Immunol.* **2004**; 173(5):2960–7.
[262] Simons K., Ehehalt R.: Cholesterol, lipid rafts, and disease. *J. Clin. Invest.* **2002**; 110(5):597–603.
[263] Burack W.R., Lee K.H., Holdorf A.D., Dustin M.L., Shaw A.S.: Cutting Edge: Quantitative Imaging of Raft Accumulation in the Immunological Synapse. *J. Immunol.* **2002**; 169(6):2837–41.
[264] Dupre L., Aiuti A., Trifari S., Martino S., Saracco P., Bordignon C., *et al.*: Wiskott-Aldrich syndrome protein regulates lipid raft dynamics during immunological synapse formation. *Immunity* **2002**; 17(2):157–66.
[265] Viola A., Schroeder S., Sakakibara Y., Lanzavecchia A.: T lymphocyte costimulation mediated by reorganization of membrane microdomains. *Science* **1999**; 283(5402):680–2.
[266] Lou Z., Jevremovic D., Billadeau D.D., Leibson P.J.: A balance between positive and negative signals in cytotoxic lymphocytes regulates the polarization of lipid rafts during the development of cell-mediated killing. *J.Exp. Med.* **2000**; 191(2):347–54.
[267] Fassett M.S., Davis D.M., Valter M.M., Cohen G.B., Strominger J.L.: Signaling at the inhibitory natural killer cell immune synapse regulates lipid raft polarization but not class I MHC clustering. *PNAS* **2001**; 98(25):14547–52.
[268] Masilamani M., Nguyen C., Kabat J., Borrego F., Coligan J.E.: CD94/NKG2A inhibits NK cell activation by disrupting the actin network at the immunological synapse. *J. Immunol.* **2006**; 177(6):3590–6.
[269] Endt J., McCann F.E., Almeida C.R., Urlaub D., Leung R., Pende D., *et al.*: Inhibitory receptor signals suppress ligation-induced recruitment of NKG2D to GM1-rich membrane domains at the human NK cell immune synapse. *J. Immunol.* **2007**; 178(9):5606–11.
[270] Augugliaro R., Parolini S., Castriconi R., Marcenaro E., Cantoni C., Nanni M., *et al.*: Selective cross-talk among natural cytotoxicity receptors in human natural killer cells. *Eur. J. Immunol.* **2003**; 33(5):1235–41.

[271] Hartmann J.: Influence of the stalk domain and the glycosylation status of the human activating nautral killer cell receptor NKp30 on ligand binding [Ph. D. thesis]. Frankfurt am Main: *Goethe Universität*; **2012**.

[272] Byrd A., Hoffmann S.C., Jarahian M., Momburg F., Watzl C.: Expression Analysis of the Ligands for the Natural Killer Cell Receptors NKp30 and NKp44. *PLoS ONE* **2007**; 2(12):e1339.

[273] Cagnano E., Hershkovitz O., Zilka A., Bar-Ilan A., Golder A., Sion-Vardy N., *et al.*: Expression of ligands to NKp46 in benign and malignant melanocytes. *J. Invest. Dermatol.* **2008**; 128(4):972–9.

[274] Spaggiari G.M., Carosio R., Pende D., Marcenaro S., Rivera P., Zocchi M.R., *et al.*: NK cell-mediated lysis of autologous antigen-presenting cells is triggered by the engagement of the phosphatidylinositol 3-kinase upon ligation of the natural cytotoxicity receptors NKp30 and NKp46. *Eur. J. Immunol.* **2001**; 31(6):1656–65.

[275] Kumar S., Hedges S.B.: A molecular timescale for vertebrate evolution. *Nature* **1998**; 392(6679):917–20.

[276] Tutar Y.: Pseudogenes. *Comp. Funct. Genomics* **2012**; 2012:424526.

[277] Mighell A.J., Smith N.R., Robinson P.A., Markham A.F.: Vertebrate pseudogenes. *FEBS Lett.* **2000**; 468(2-3):109–14.

[278] Pink R.C., Wicks K., Caley D.P., Punch E.K., Jacobs L., Carter D.R.: Pseudogenes: pseudo-functional or key regulators in health and disease? *RNA* **2011**; 17(5):792–8.

[279] Zhang Z.D., Frankish A., Hunt T., Harrow J., Gerstein M.: Identification and analysis of unitary pseudogenes: historic and contemporary gene losses in humans and other primates. *Genome Biol.* **2010**; 11(3):R26.

[280] Cooke J., Nowak M.A., Boerlijst M., Maynard-Smith J.: Evolutionary origins and maintenance of redundant gene expression during metazoan development. *Trends Genet.* **1997**; 13(9):360–4.

[281] Tachida H., Kuboyama T.: Evolution of Multigene Families by Gene Duplication: A Haploid Model. *Genetics* **1998**; 149(4):2147.

[282] Wagner K.U., Dierisseau P., Rucker E.B., Robinson G.W., Hennighausen L.: Genomic architecture and transcriptional activation of the mouse and human tumor susceptibility gene TSG101: common types of shorter transcripts are true alternative splice variants. *Oncogene* **1998**; 17(21):2761–70.

[283] Force A., Lynch M., Pickett F.B., Amores A., Yan Y.L., Postlethwait J.: Preservation of duplicate genes by complementary, degenerative mutations. *Genetics* **1999**; 151(4):1531–45.

[284] Ganfornina M.D., Sánchez D.: Generation of evolutionary novelty by functional shift. *Bioessays* **1999**; 21(5):432–9.

[285] Wendt K., Wilk E., Buyny S., Buer J., Schmidt R.E., Jacobs R.: Gene and protein characteristics reflect functional diversity of $CD56^{dim}$ and $CD56^{bright}$ NK cells. *J. Leukoc. Biol.* **2006**; 80(6):1529–41.

[286] Hayakawa Y., Smyth M.J.: CD27 dissects mature NK cells into two subsets with distinct responsiveness and migratory capacity. *J. Immunol.* **2006**; 176(3):1517–24.

[287] Vahlne G., Becker S., Brodin P., Johansson M.H.: IFN-gamma production and degranulation are differentially regulated in response to stimulation in murine natural killer cells. *Scand. J. Immunol.* **2008**; 67(1):1–11.

[288] St. John A.L., Rathore A.P., Yap H., Ng M.L., Metcalfe D.D., Vasudevan S.G., *et al.*: Immune surveillance by mast cells during dengue infection promotes natural killer (NK) and NKT-cell recruitment and viral clearance. *PNAS* **2011**; 108(22):9190–5.

[289] Burke S.M., Issekutz T.B., Mohan K., Lee P.W., Shmulevitz M., Marshall J.S.: Human mast cell activation with virus-associated stimuli leads to the selective chemotaxis of natural killer cells by a CXCL8-dependent mechanism. *Blood* **2008**; 111(12):5467–76.

[290] Marsh D.: Electron spin resonance in membrane research: protein-lipid interactions from challenging beginnings to state of the art. *Eur. Biophys. J.* **2010**; 39(4):513–25.

[291] Arora A., Williamson I.M., Lee A.G., Marsh D.: Lipid-protein interactions with cardiac phospholamban studied by spin-label electron spin resonance. *Biochemistry* **2003**; 42(17):5151–8.

[292] Ryba N.J., Hoon M.A., Findlay J.B., Saibil H.R., Wilkinson J.R., Heimburg T., *et al.*: Rhodopsin mobility, structure, and lipid-protein interaction in squid photoreceptor membranes. *Biochemistry* **1993**; 32(13):3298–305.

[293] Kota Z., Pali T., Dixon N., Kee T.P., Harrison M.A., Findlay J.B., *et al.*: Incorporation of transmembrane peptides from the vacuolar H^+-ATPase in phospholipid membranes: spin-label electron paramagnetic resonance and polarized infrared spectroscopy. *Biochemistry* **2008**; 47(12):3937–49.

[294] Marsh D.: Orientation and peptide-lipid interactions of alamethicin incorporated in phospholipid membranes: polarized infrared and spin-label EPR spectroscopy. *Biochemistry* **2009**; 48(4):729–37.

[295] Pali T., Bashtovyy D., Marsh D.: Stoichiometry of lipid interactions with transmembrane proteins--Deduced from the 3D structures. *Protein Sci.* **2006**; 15(5):1153–61.

[296] Marsh D.: Stoichiometry of lipid-protein interaction and integral membrane protein structure. *Eur. Biophys. J.* **1997**; 26(2):203–8.

[297] Turner L., Lavstsen T., Berger S.S., Wang C.W., Petersen J.E., Avril M., *et al.*: Severe malaria is associated with parasite binding to endothelial protein C receptor. *Nature* **2013**; 498(7455):502–5.

[298] Salanti A., Clausen T.M., Agerbaek M.O., Al Nakouzi N., Dahlback M., Oo H.Z., *et al.*: Targeting Human Cancer by a Glycosaminoglycan Binding Malaria Protein. *Cancer Cell* **2015**; 28(4):500–14.

[299] Sandercock A.M., Rust S., Guillard S., Sachsenmeier K.F., Holoweckyj N., Hay C., *et al.*: Identification of anti-tumour biologics using primary tumour models, 3-D phenotypic screening and image-based multi-parametric profiling. *Mol. Cancer* **2015**; 14:147.

[300] Williams G.S., Mistry B., Guillard S., Ulrichsen J.C., Sandercock A.M., Wang J., *et al.*: Phenotypic screening reveals TNFR2 as a promising target for cancer immunotherapy. *Oncotarget* **2016**; 7(42):68278–91.

[301] Sosnovtsev S.V., Sandoval-Jaime C., Parra G.I., Tin C.M., Jones R.W., Soden J., *et al.*: Identification of Human Junctional Adhesion Molecule 1 as a Functional Receptor for the Hom-1 Calicivirus on Human Cells. *MBio* **2017**; 8(1).

6. Appendix

6.1 Plasmid Maps

pDisplay-BirA-ER

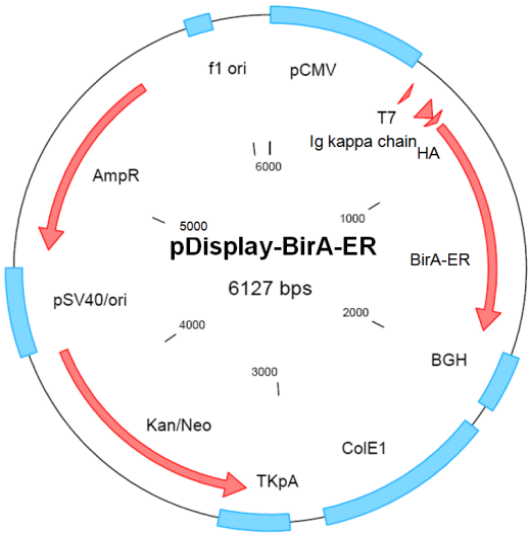

pDisplay-sBirA

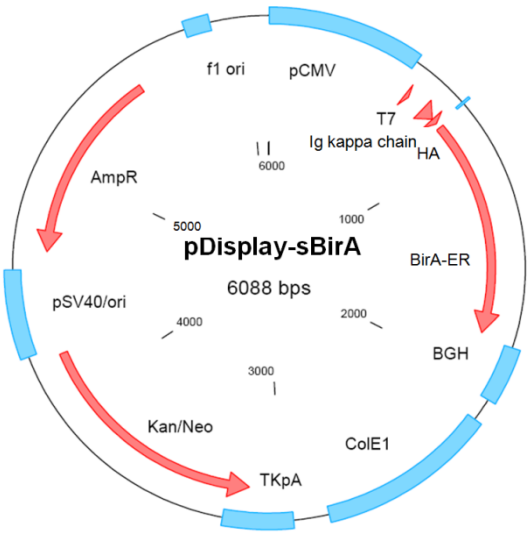

pUC57 and variants

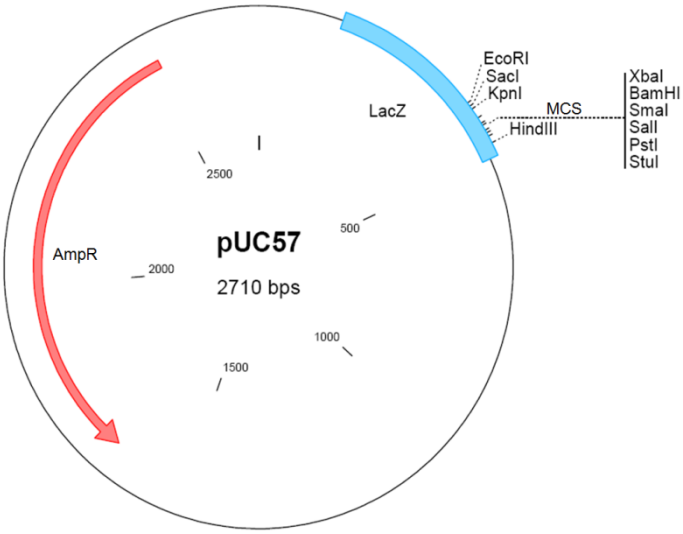

pcDNA3.1-TNFss-B7H6-hIgG1-Fc

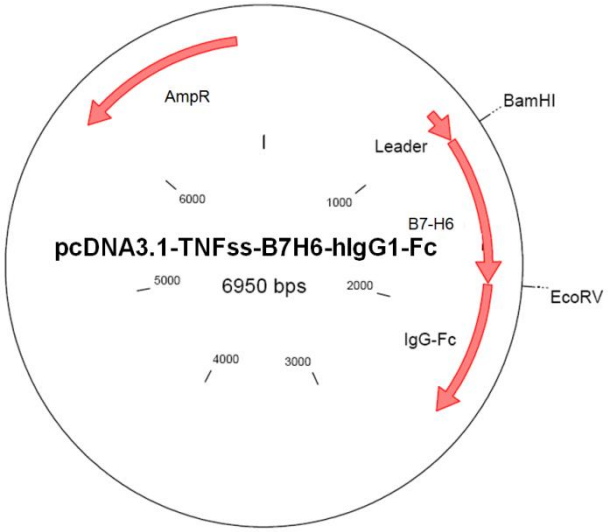

pFUSE-hIgG1-FcEQ and variants

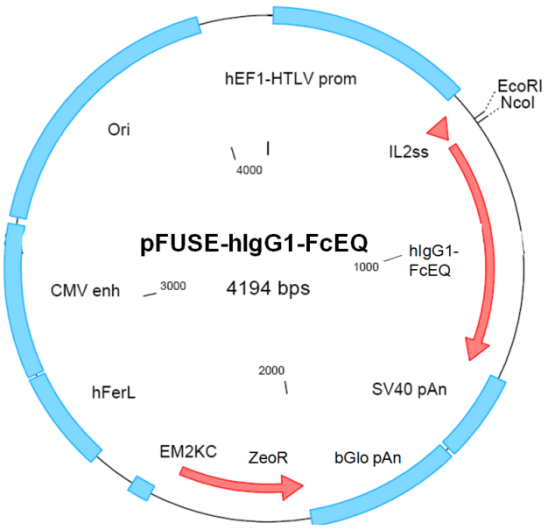

Inserts were introduced via *Eco*RI/*Nco*I restriction sites

pFc-Avi and variants

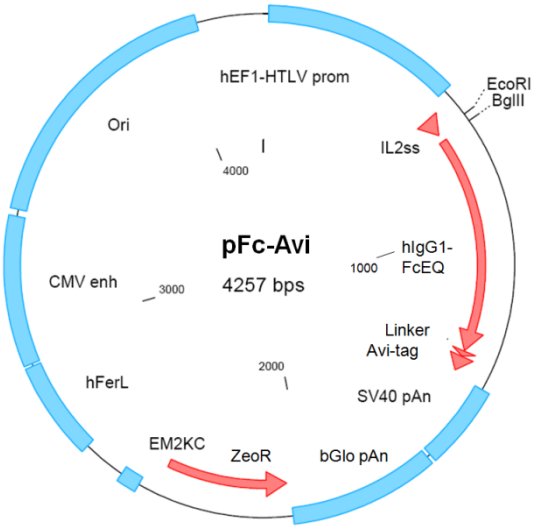

Insert was introduced via *Eco*RI/*Bgl*II restriction sites

LeGO-iZ and variants

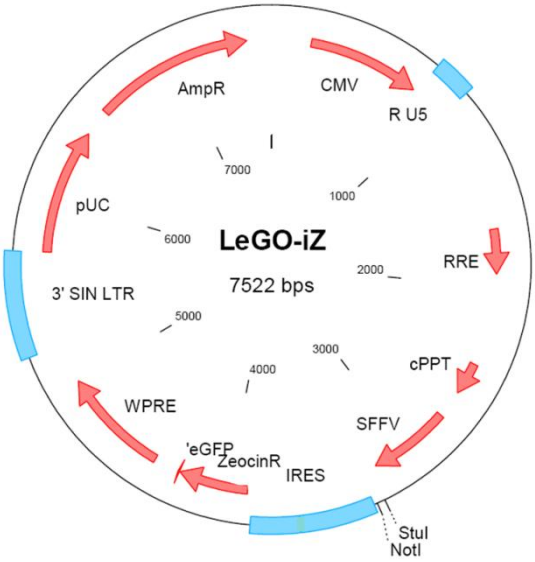

Inserts were introduced via *Stu*I/*Not*I restriction sites

LeGO-iZ-Flag and variants

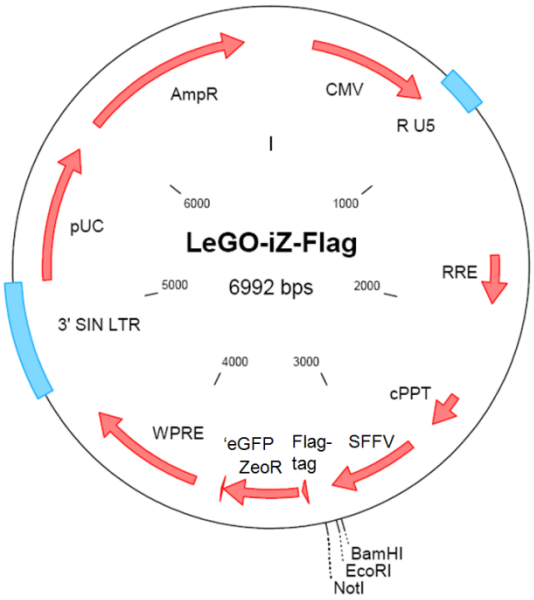

Inserts were introduced via *Bam*HI/*Not*I or *Eco*RI/*Not*I restriction sites

pCMV-Δ8.91

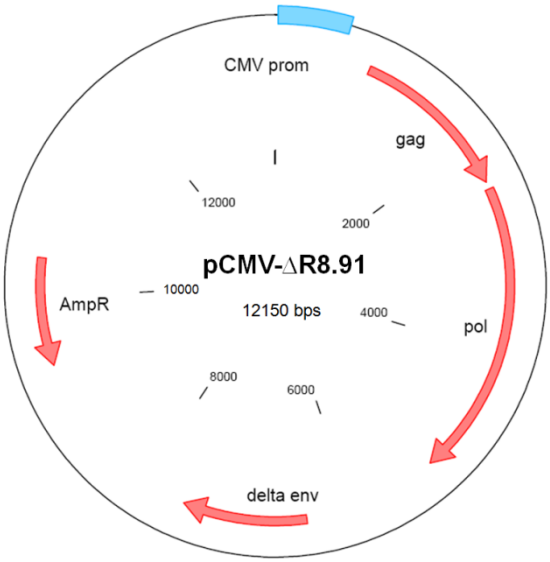

pMD2.G

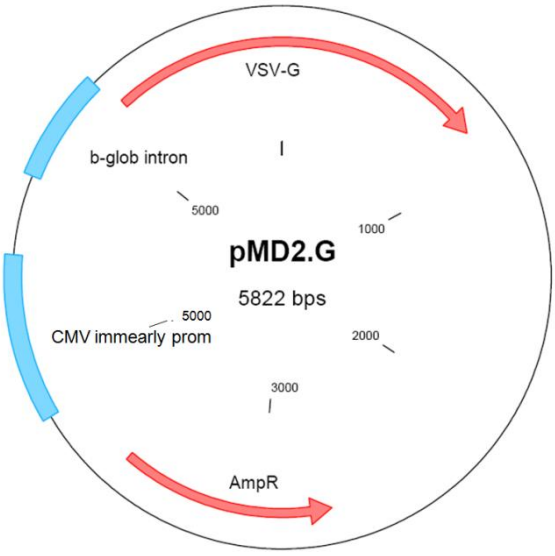

6.2 Protein Sequences

Human NKp30 (isoform a-f)

A

```
NKp30_isoform_a      MAWMLLLILIMVHPGSCALWVSQPPEIRTLEGSSAFLPCSFNASQGRLAIGSVTWFRDEV   60
NKp30_isoform_b      MAWMLLLILIMVHPGSCALWVSQPPEIRTLEGSSAFLPCSFNASQGRLAIGSVTWFRDEV   60
NKp30_isoform_c      MAWMLLLILIMVHPGSCALWVSQPPEIRTLEGSSAFLPCSFNASQGRLAIGSVTWFRDEV   60
NKp30_isoform_d      MAWMLLLILIMVHPGSCALWVSQPPEIRTLEGSSAFLPCSFNASQGRLAIGSVTWFRDEV   60
NKp30_isoform_e      MAWMLLLILIMVHPGSCALWVSQPPEIRTLEGSSAFLPCSFNASQGRLAIGSVTWFRDEV   60
NKp30_isoform_f      MAWMLLLILIMVHPGSCALWVSQPPEIRTLEGSSAFLPCSFNASQGRLAIGSVTWFRDEV   60
                     ************************************************************

NKp30_isoform_a      VPGKEVRNGTPEFRGRLAPLASSRFLHDHQAELHIRDVRGHDASIYVCRVEVLGLGVGTG   120
NKp30_isoform_b      VPGKEVRNGTPEFRGRLAPLASSRFLHDHQAELHIRDVRGHDASIYVCRVEVLGLGVGTG   120
NKp30_isoform_c      VPGKEVRNGTPEFRGRLAPLASSRFLHDHQAELHIRDVRGHDASIYVCRVEVLGLGVGTG   120
NKp30_isoform_d      VPGKE--------------------------AELHIRDVRGHDASIYVCRVEVLGLGVGTG   95
NKp30_isoform_e      VPGKE--------------------------AELHIRDVRGHDASIYVCRVEVLGLGVGTG   95
NKp30_isoform_f      VPGKE--------------------------AELHIRDVRGHDASIYVCRVEVLGLGVGTG   95
                     *****                           ******************************

NKp30_isoform_a      NGTRLVVEKEHPQLGAGTVLLLRAGFYAVSFLSVAVGSTVYYQGKCLTWKGPRRQLP---   177
NKp30_isoform_b      NGTRLVVEKEHPQLGAGTVLLLRAGFYAVSFLSVAVGSTVYYQGKYAKSTL--SGFP---   175
NKp30_isoform_c      NGTRLVVEKEHPQLGAGTVLLLRAGFYAVSFLSVAVGSTVYYQGKCHCHMGTHCHSSDGP   180
NKp30_isoform_d      NGTRLVVEKEHPQLGAGTVLLLRAGFYAVSFLSVAVGSTVYYQGKYAKSTL--SGFP---   150
NKp30_isoform_e      NGTRLVVEKEHPQLGAGTVLLLRAGFYAVSFLSVAVGSTVYYQGKCLTWKGPRRQLP---   152
NKp30_isoform_f      NGTRLVVEKEHPQLGAGTVLLLRAGFYAVSFLSVAVGSTVYYQGKCHCHMGTHCHSSDGP   155
                     *******************************************

NKp30_isoform_a      -AVVPAPLPPPCGSSAHLLPPVPGG  201
NKp30_isoform_b      -QL----------------------  177
NKp30_isoform_c      RGVIPEPRCP---------------  190
NKp30_isoform_d      -QL----------------------  152
NKp30_isoform_e      -AVVPAPLPPPCGSSAHLLPPVPGG  176
NKp30_isoform_f      RGVIPEPRCP---------------  165
                       :
```

B

```
Percent Identity Matrix

1: NKp30_isoform_a  100.00   93.79   91.94   92.76  100.00   90.68
2: NKp30_isoform_b   93.79  100.00   93.22  100.00   92.76   92.11
3: NKp30_isoform_c   91.94   93.22  100.00   92.11   90.68  100.00
4: NKp30_isoform_d   92.76  100.00   92.11  100.00   92.76   92.11
5: NKp30_isoform_e  100.00   92.76   90.68   92.76  100.00   90.68
6: NKp30_isoform_f   90.68   92.11  100.00   92.11   90.68  100.00
```

Figure S1. Sequence alignment of NKp30 isoforms. (A) Multiple sequence alignment (created by Clustal Omega) of NKp30 isoforms a-f from *H. sapiens*. (*) positions which have a single, fully conserved residue; (:) conservation between groups of strongly similar properties. (B) Percent identity matrix of NKp30 isoforms (created by Clustal2.1).

Human NKp46 (isoform a-d)

A

```
NKp46_isoform_a      MSSTLPALLCVGLCLSQRISAQQQTLPKPFIWAEPHFMVPKEKQVTICCQGNYGAVEYQL   60
NKp46_isoform_b      MSSTLPALLCVGLCLSQRISAQQQTLPKPFIWAEPHFMVPKEKQVTICCQGNYGAVEYQL   60
NKp46_isoform_c      MSSTLPALLCVGLCLSQRISAQQ-------------------------------------   23
NKp46_isoform_d      MSSTLPALLCVGLCLSQRISAQQ-------------------------------------   23
                     ************************

NKp46_isoform_a      HFEGSLFAVDRPKPPERINKVKFYIPDMNSRMAGQYSCIYRVGELWSEPSNLLDLVVTEM   120
NKp46_isoform_b      HFEGSLFAVDRPKPPERINKVKFYIPDMNSRMAGQYSCIYRVGELWSEPSNLLDLVVTEM   120
NKp46_isoform_c      ------------------------------------------------------------QM   25
NKp46_isoform_d      ------------------------------------------------------------QM   25
                                                                                 :*

NKp46_isoform_a      YDTPTLSVHPGPEVISGEKVTFYCRLDTATSMFLLLKEGRSSHVQRGYGKVQAEFPLGPV   180
NKp46_isoform_b      YDTPTLSVHPGPEVISGEKVTFYCRLDTATSMFLLLKEGRSSHVQRGYGKVQAEFPLGPV   180
NKp46_isoform_c      YDTPTLSVHPGPEVISGEKVTFYCRLDTATSMFLLLKEGRSSHVQRGYGKVQAEFPLGPV   85
NKp46_isoform_d      YDTPTLSVHPGPEVISGEKVTFYCRLDTATSMFLLLKEGRSSHVQRGYGKVQAEFPLGPV   85
                     ************************************************************

NKp46_isoform_a      TTAHRGTYRCFGSYNNHAWSFPSEPVKLLVTGDIENTSLAPEDPTFPADTWGTYLLTTET   240
NKp46_isoform_b      TTAHRGTYRCFGSYNNHAWSFPSEPVKLLVTGDIENTSLAPEDPTFP-------------   227
NKp46_isoform_c      TTAHRGTYRCFGSYNNHAWSFPSEPVKLLVTGDIENTSLAPEDPTFPADTWGTYLLTTET   145
NKp46_isoform_d      TTAHRGTYRCFGSYNNHAWSFPSEPVKLLVTGDIENTSLAPEDPTFP-------------   132
                     ***********************************************

NKp46_isoform_a      GLQKDHALWDHTAQNLLRMGLAFLVLVALVWFLVEDWLSRKRTRERASRASTWEGRRRLN   300
NKp46_isoform_b      ----DHALWDHTAQNLLRMGLAFLVLVALVWFLVEDWLSRKRTRERASRASTWEGRRRLN   283
NKp46_isoform_c      GLQKDHALWDHTAQNLLRMGLAFLVLVALVWFLVEDWLSRKRTRERASRASTWEGRRRLN   205
NKp46_isoform_d      ----DHALWDHTAQNLLRMGLAFLVLVALVWFLVEDWLSRKRTRERASRASTWEGRRRLN   188
                         ********************************************************

NKp46_isoform_a      TQTL           304
NKp46_isoform_b      TQTL           287
NKp46_isoform_c      TQTL           209
NKp46_isoform_d      TQTL           192
                     ****
```

B

```
Percent Identity Matrix

1: NKp46_isoform_a  100.00  100.00   99.52   99.48
2: NKp46_isoform_b  100.00  100.00   99.48   99.48
3: NKp46_isoform_c   99.52   99.48  100.00  100.00
4: NKp46_isoform_d   99.48   99.48  100.00  100.00
```

Figure S2. Sequence alignment of NKp46 isoforms. (A) Multiple sequence alignment (created by Clustal Omega) of NKp46 isoforms a-d from *H. sapiens*. (*) positions which have a single, fully conserved residue; (:) conservation between groups of strongly similar properties. (B) Percent identity matrix of NKp46 isoforms (created by Clustal2.1).

Human and mouse (engineered) NKp30

A

```
hNKp30_isoform_a      MAWMLLLILIMVHPGSCALWVSQPPEIRTLEGSSAFLPCSFNASQGRLAIGSVTWFRDEV  60
mNKp30                MAKVLLVIFIMVYPGSCALWVSQPPEIRVQEGTTASLPCSFNAIRGKPATGSVTWYQDKV  60
mNKp30-glyco          MAKVLLVIFIMVYPGSCALWVSQPPEIRVQEGTTASLPCSFNASRGKPATGSVTWYQDKV  60
                      ** :**:*:***:***************. **::* ******* :*: * *****::*:*
hNKp30_isoform_a      VPGKEVRNGTPEFRGRLAPLASSRFLHDHQAELHIRDVRGHDASIYVCRVEVLGLGVGTG  120
mNKp30                TLGMELSKVTPGFRGRLVSFSVSQFIRDHKAGLLIQDTQSYDAGIYVCRVEVLGLGVRMG  120
mNKp30-glyco          TLGMELSNVTPGFRGRLVSFSVSQFIRDHKAGLLIQDTQSYDAGIYVCRVEVLGLGVRMG  120
                      . * *: : ** *****. :: *:*::**:* * *:*.:.:**.*************  *
hNKp30_isoform_a      NGTRLVVEKEHPQLG------AGTVLLLRAGFYAVSFLSVAVGSTVYYQGKCLTWKGPRR  174
mNKp30                DRTRLLVEKGPPQQASNTEQEAHTSLLLRAGFYALSFLSVATGSTIYYQGKFLLGPCHME  180
mNKp30-glyco          NRTRLLVEKGPPQQASNTEQEAHTSLLLRAGFYALSFLSVATGSTIYYQGKFLLGPCHME  180
                      : ***:***  ** .      * * *********:******.***:***** *      .
hNKp30_isoform_a      QLPAVVPAPLPPPCGSSAHLLPPVPGG           201
mNKp30                IM-------DTPPAASEK---------           191
mNKp30-glyco          IM-------DTPPAASEK---------           191
                       :         **..*.
```

B

```
Percent Identity  Matrix

1: hNKp30_isoform_a  100.00   60.54   62.16
2: mNKp30             60.54  100.00   98.43
3: mNKp30-glyco       62.16   98.43  100.00
```

Figure S3. Sequence alignment of hNKp30 and mNKp30 forms. (A) Multiple sequence alignment (created by Clustal Omega) of NKp30 isoform a from *H. sapiens* (hNKp30_isoform_a), NKp30 from *M. musculus* without premature stop codons (mNKp30), and mNKp30 with repaired N-Glycosylation sites (mNKp30-glyco). (*) positions which have a single, fully conserved residue; (:) conservation between groups of strongly similar properties; (.) conservation between groups of weakly similar properties. (B) Percent identity matrix of NKp30 proteins (created by Clustal2.1).

6.3 Comparison of NKp30 and NKp46 Stalk Domains

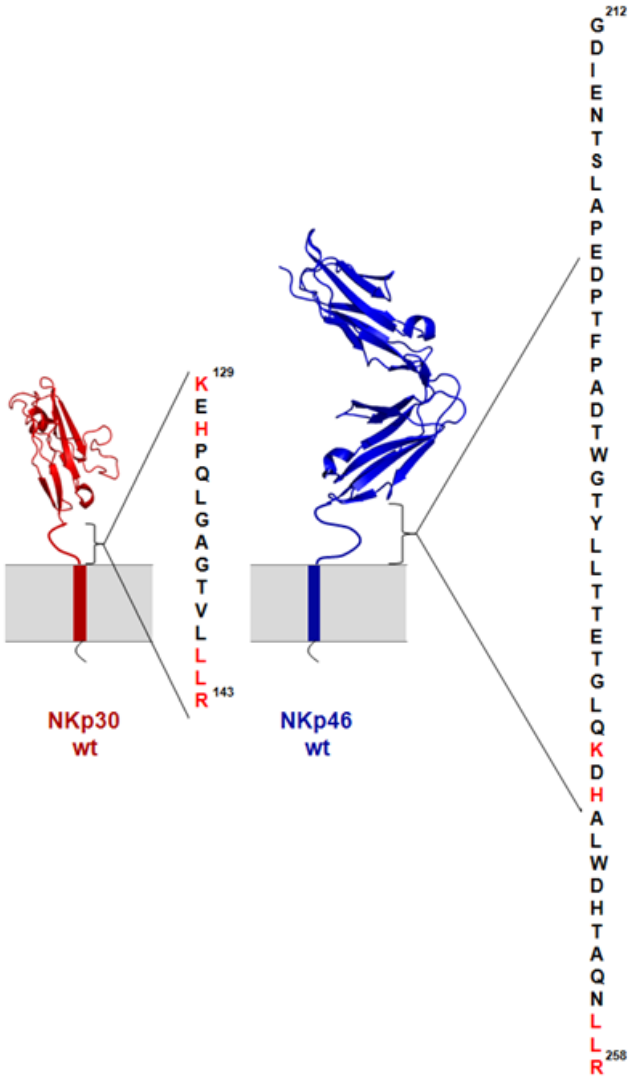

Figure S4. Stalk sequences of NKp30 and NKp46. Schematic representation of NKp30 wildtype (wt) (red, PDB: 3NOI) and NKp46 wt (blue, PDB: 1P6F). Stalk sequences are indicated, sequence identities are shown in red.

6.4 SPR Data

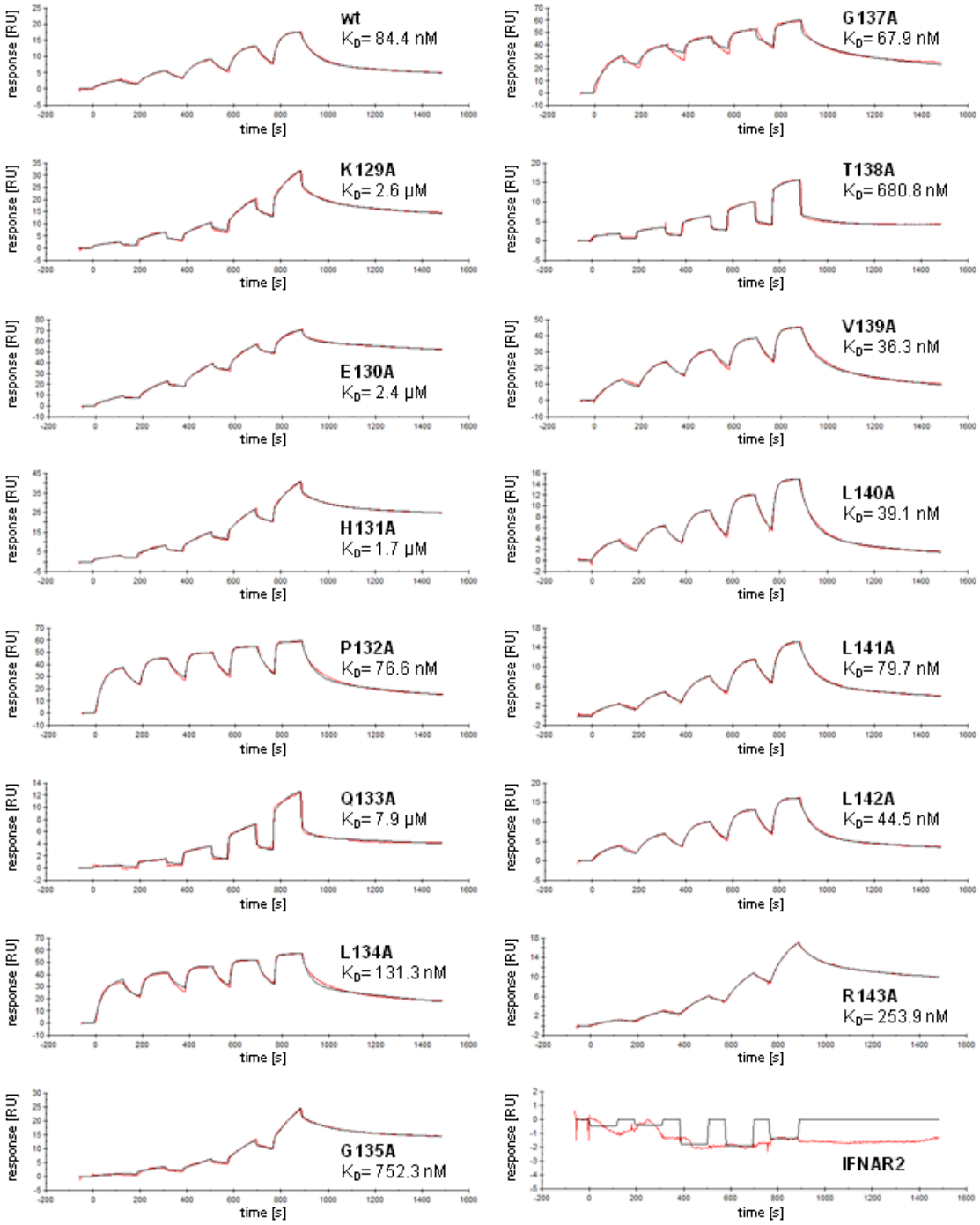

Figure S5. Equilibrium binding of NKp30 variants to B7-H6. SPR sensograms of NKp30-Fc and IFNAR2-Fc fusion proteins (negative control). For construction of NKp30 alanine mutants, each individual amino acid of the stalk (position 129-143) was exchanged except for the alanine on position 136 in the NKp30 wt receptor. Binding to immobilized biotinylated B7-H6-Fc fusion proteins was analyzed. Data was corrected for blank surface reference and fitted with the bivalent analyte model to determine the kinetic parameters and equilibrium dissociation constants. One representative out of at least three independent experiments is shown. Red: SPR sensogram, black: bivalent analyte fit.

6.5 NKp44 Ligand and NKp46 Ligand Candidate Genes from the shRNA Screening

Table S1: Candidate list of putative NKp44 ligands. FPKM: fragments per kilobase of exon per million fragments mapped.

Nr.	UniProt entry	Accession numbers	Gene names	Protein name	Expression (FPKM) screening cell line	Chromosome	Localization/type	Relation to	
								cancer	immunity
1	NHRF3_HUMAN (Q5T2W1)	NM_001201325, NM_001201326, NM_002614	PDZK1_CAP70_NHERF3 _PDZD1	Na(+)/H(+) exchange regulatory cofactor NHE-RF3	Mel-JuSo (na)	1	Cell membrane, cytoplasm/ Peripheral membrane protein	+	-
2	KPCD_HUMAN (Q05655)	NM_006254, NM_212539 NM_001316327	PRKCD	Protein kinase C delta type	Mel-JuSo (65)	3	Cytoplasm. Cytoplasm, perinuclear region. Nucleus. Endoplasmic reticulum. Mitochondrion. Cell membrane/ Peripheral membrane protein	+	+
3	N2DL1_HUMAN (Q9BZM6)	NM_025218	ULBP1_N2DL1_RAET1I	NKG2D ligand 1, ULBP1	293T (2-27.8)	6	Cell membrane/ GPI-anchor	+	+
4	TNR6_HUMAN (P25445)	NM_000043, NM_152871, NM_152872	FAS_APT1_FAS1_TNFR SF6 CD95	Tumor necrosis factor receptor superfamily member 6	DU145(3)	10	Isoform 1: Cell membrane, type-I-transmembrane protein, Isoform 2-6: Secreted	-	+

Table S2: Candidate list of putative NKp46 ligands. FPKM: fragments per kilobase of exon per million fragments mapped.

Nr.	UniProt entry	Accession numbers	Gene names	Protein name	Expression (FPKM) screening cell line	Chromosome	Localization/type	Relation to	
								cancer	immunity
1	CXB5_HUMAN (O95377)	NM_005268	GJB5	Gap junction beta-5 protein	Mel-JuSo (na)	1	Cell membrane/ Multi-pass membrane protein	+	-
2	CRIM1_HUMAN (Q9NZV1)	NM_016441	CRIM1_S52_UNQ1886/P RO4330	Cysteine-rich motor neuron 1 protein	Mel-JuSo(35), 293T (6-34.2)	2	Cell membrane/ Single-pass type I membrane protein	-	-
3	CD68_HUMAN (P34810)	NM_001040059, NM_001251	CD68	Macrosialin	Mel-JuSo (na)	17	Cell membrane, Endosome membrane/ Single-pass type I membrane protein	-	+
4	MUC16_HUMAN (Q8WXI7)	NM_024690	MUC16_CA125	Mucin-16	Mel-JuSo (na)	19	cell membrane/ Single-pass type I membrane protein	+	+
5	CD302_HUMAN (Q8IX05)	NM_001198763, NM_014880	CD302_CLEC13A_DCL1 _KIAA0022	CD302 antigen	DU145 (0.4)	2	Membrane, Single-pass type I membrane protein	+	-
6	CEAM5_HUMAN (P06731)	NM_001291484, NM_001308398, NM_004363	CEACAM5_CEA CD66e	Carcinoembryonic antigen-related cell adhesion molecule 5	293T (0-29.7)	19	Cell membrane lipid-anchor	+	-
7	CLD8_HUMAN (P56748)	NM_199328	CLDN8_UNQ779/PRO15 73	Claudin-8	293T (0-13.3)	21	Cell junction, tight junction. Cell membrane/ Multi-pass membrane protein	+	-
8	LIN7A_HUMAN (O14910)	NM_004664 CHIP A	LIN7A_MALS1_VELI1	Protein lin-7 homolog A	293T (5-13)	12	Cell membrane/ Peripheral membrane protein	-	-
9	ABCG2_HUMAN (Q9UNQ0)	NM_001257386, NM_004827	ABCG2_ABCP_BCRP_B CRP1_MXR CD338	ATP-binding cassette sub-family G member 2	293T (2-27.1)	4	Cell membrane, Mitochondrion membrane/ Multi-pass membrane protein	+	-
10	CEAM1_HUMAN (P13688)	NM_001024912, NM_001184813, NM_001184815, NM_001184816, NM_001205344, NM_001712	CEACAM1_BGP_BGP1 CD66a	Carcinoembryonic antigen-related cell adhesion molecule 1	293T (0-43.4)	19	Isoform 1, 5-8: Cell membrane, Isoform 2-4: Secreted/ Single-pass type I membrane protein.	+	+
11	HG2A_HUMAN (P04233)	NM_001025158, NM_001025159, NM_004355	CD74_DHLAG	HLA class II histocompatibility antigen gamma chain	293T (0-13.1)	5	Cell membrane, Endoplasmic reticulum membrane. Golgi apparatus, trans-Golgi network. Endosome. Lysosome/ Single-pass type II membrane protein	-	+

Table S3: Validation of putative NKp44 ligands.

Candidate	Population [%]		Amount of NKp44 ligand$^+$ cells [%]		MFI ratio NKp44-Fc/IFNAR2-Fc	
	Flag$^+$	Flag$^-$	Flag$^+$	Flag$^-$	Flag$^+$	Flag$^-$
PRKCD	3.4	96.6	32.2	8.1	3.9	3.4
FAS	14.4	85.6	6.2	1.8	3.1	3.1
PDZK1	2.0	98.0	13.5	2.3	2.8	2.9

The putative NKp44 ligand ULBP1 was validated using SPR measurements. No interaction with NKp44 could be confirmed (Data not shown).

Table S4: Validation of putative NKp46 ligands.

Candidate	Population [%]		Amount of NKp46 ligand$^+$ cells [%]		MFI ratio NKp46-Fc/IFNAR2-Fc	
	Flag$^+$	Flag$^-$	Flag$^+$	Flag$^-$	Flag$^+$	Flag$^-$
CD68	24.5	75.5	3.1	1.5	1.3	1.3
CD74	6.4	93.6	0.6	0.7	1.0	1.2
CD302	43.0	57.0	2.1	1.4	1.3	1.4
GJB5	6.1	93.9	3.1	7.1	1.2	1.4
LIN7A	5.8	94.2	10.7	18.1	1.3	1.3
ABCG2	4.4	95.6	38.1	39.6	1.7	1.7
CLDN8	4.8	95.2	1.8	1.1	1.4	1.5

Expression of the putative NKp46 ligands CRIM1, CEACAM1 and CEACAM5 was too low for flow cytometric analysis.
The putative NKp46 ligand MUC16 was validated unsing shRNA knockdown. No interaction with NKp46 could be confirmed (Data not shown).

Publications and Presentations

Publications

Weil S., **Memmer S.**, Lechner A., Huppert V., Giannattasio A., Becker T., Müller-Runte A., Lampe K., Beutner D., Quaas A., Schubert R., Herrmann E., Steinle A., Koehl U., Walter L., von Bergwelt-Baildon M., Koch J.: NKG2D ligand depletion reconstitutes NK cell immunosurveillance of head and neck squamous cell carcinoma. *Front. Immunol.* **2017** (accepted)

Memmer S.*, Weil S.*, Beyer S., Zöller T., Peters E., Hartmann J., Steinle A., Koch J.: The stalk domain of NKp30 contributes to ligand binding and signaling of a pre-assembled NKp30/CD3ζ complex. *J. Biol. Chem.* **2016**; 291 (49):25427-25438 (*both authors contributed equally)

Oral Presentations

"The stalk domain of NKp30 is important for ligand binding and intracellular signaling."
NK Cell Symposium of the German Society for Immunology, **2015**, Göttingen, Germany

Poster Presentations

"Cytotoxocity and infiltration of human NK cells in in vivo-like tumor spheroids."
15th Meeting of the Society for Natural Immunity, **2015**, Montebello, Canada

"The stalk domain of NKp30 drives receptor oligomerization and ligand binding."
NK Cell Symposium of the German Society for Immunology, **2014**, Hannover, Germany

Curriculum Vitae

Lebenslauf

Name:	Stefanie Memmer
Geburtsdatum:	08.02.1985
Geburtsort:	Darmstadt
Staatsangehörigkeit:	deutsch

Akademischer Werdegang:

08/2013- 03/2017	Promotion, Georg-Speyer-Haus Frankfurt, Arbeitsgruppe „NK Cell Biology“ unter der Leitung von Prof. Dr. Joachim Koch
seit 03/2016	am Institut für Medizinische Mikrobiologie und Hygiene, Universitätsmedizin Mainz, Arbeitsgruppe „Immunobiology of Natural Killer Cells“ unter der Leitung von Prof. Dr. Joachim Koch Titel der Dissertation: „Ligand binding and transmembranal signaling of the activating natural killer cell receptor NKp30“
10/2011-07/2013	Studium Molekulare Biowissenschaften, Goethe Universität Frankfurt a. M., Abschlussarbeit Arbeitskreis Prof. Entian (Abschluss: Master of Science, Titel der Abschlussarbeit: „Untersuchung der Lantibiotika-Immunitätsproteine EriI, EtnI und NisI“, Abschlussnote: 1,6)
09/2008-10/2011	Biotechnologie-Studium, Hochschule Darmstadt, Abschlussarbeit: Paul-Ehrlich-Institut, Langen (Abschluss: Bachelor of Science, Titel der Abschlussarbeit: „Entwicklung von CD20- oder CD105-spezifischen SIVsmmPBj-Targeting-Vektoren“, Abschlussnote: 1,9)
09/2005-02/2008	PTA-Lehranstalt Stiftung Collegium Pharmazeuticum Frankfurt a. M./ Post-Apotheke, Darmstadt-Eberstadt (schulische Ausbildung zur Pharmazeutisch-Technischen Assistentin mit anschließendem 6-monatigem Apotheken-Praktikum, Abschluss-note 1,75)

03/2005-08/2005	Pharmazie-Studium, Goethe Universität Frankfurt a. M.
10/2004-02/2005	Studium Angewandte Geowissenschaften, TU Darmstadt
07/2004	Schulabschluss Allgemeine Hochschulreife, Albrecht-Dürer-Schule Weiterstadt

Berufliche Tätigkeiten:

02/2012-03/2012	Werkstudentin Prozessentwicklung Biotechnologie, Sanofi Deutschland GmbH (Pharmaindustrie)
03/2008-09/2008	Laborassistentin Getränke-Entwicklung, DöhlerGruppe, Darmstadt (Lebensmittelindustrie)

Praktika:

03/2011-05/2011	Paul-Ehrlich-Institut, Langen, Abteilung Medizinische Biotechnologie, Fachgebiet: Nicht-virale Gentransfer-Arzneimittel

Acknowledgement

Danksagung

An dieser Stelle möchte ich mich bei all denen bedanken, die mich bei der Erstellung dieser Arbeit unterstützt haben.

Mein besonderer Dank gilt Prof. Dr. Joachim Koch für das interessante Thema meiner Arbeit, die spannende und lehrreiche Zeit in seiner Arbeitsgruppe und vor allem für seine engagierte Betreuung und Diskussionsbereitschaft.

Ich bedanke mich ebenso bei Prof. Dr. Beatrix Süß und Prof. Dr. Bodo Laube für die freundliche Betreuung und Unterstützung seitens der TU Darmstadt.

Zusätzlich danke ich allen Mitgliedern der AG Diefenbach für ihre Hilfe während und nach dem Wechsel an die Unimedizin Mainz.

Allen Mitarbeitern des Georg-Speyer-Hauses danke ich für das angenehme Arbeitsklima und die hilfreichen fachlichen Diskussionen. Mein besonderer Dank gilt hierbei Dr. Stefan Stein für seine zahlreichen Ratschläge und seine Unterstützung.

Ebenso bedanke ich mich bei all meinen Kooperationspartnern, die entscheidend zum Erfolg dieser Arbeit beigetragen haben. Insbesondere möchte ich mich bei Dr. Csaba Miskey für seine große Hilfe bei der Datenauswertung des shRNA Screenings bedanken. Mein Dank geht ebenso an alle Mitglieder der Arbeitsgruppe von Dr. Zoltán Ivics am Paul-Ehrlich-Institut in Langen für die Gastfreundschaft und die lustige Zeit im Büro.

Herzlich bedanken möchte ich mich zusätzlich bei Sandra Weil und Steffen Beyer, den besten Arbeitskollegen der Welt, für die tolle Zeit im Labor, ihre Hilfsbereitschaft und Freundschaft und für die Steak Night.

Ein großer Dank gilt ebenso meinen Eltern Christel und Gerhard für ihre Unterstützung, nicht nur im Rahmen meines Studiums, sondern in allen Lebenslagen, und ganz besonders meinem Freund Stephan: Danke dass du bei mir bist!

Declaration and Affidavit

Ehrenwörtliche Erklärung

Ich erkläre hiermit ehrenwörtlich, dass ich die vorliegende Arbeit entsprechend den Regeln guter wissenschaftlicher Praxis selbstständig und ohne unzulässige Hilfe Dritter angefertigt habe.

Sämtliche aus fremden Quellen direkt oder indirekt übernommenen Gedanken sowie sämtliche von Anderen direkt oder indirekt übernommenen Daten, Techniken und Materialien sind als solche kenntlich gemacht. Die Arbeit wurde bisher bei keiner anderen Hochschule zu Prüfungszwecken eingereicht.

Darmstadt, den 21.03.2017

_____

Stefanie Memmer